ELECTROCHEMICAL STUDIES OF METAL-LIGAND INTERACTIONS AND OF METAL BINDING PROTEINS

A thesis submitted in fulfilment of the requirements for the degree of

DOCTOR OF PHILOSOPHY

of

RHODES UNIVERSITY

by

JANICE LEIGH LIMSON

October 1998

Dedicated to Elaine

and the memory of Ralph and Joey

ACKNOWLEDGEMENTS

My sincerest thanks to Professor Tebello Nyokong, for the outstanding supervision of my PhD. My gratitude is also extended to her for fostering scientific principles and encouraging dynamic research at the highest level. Over the years, Prof Nyokong has often gone beyond the call of duty to listen, encourage and advise me in my professional and personal development.

Professor Daya, who has co-supervised my PhD, I thank for initiating research that has been both exciting and stimulating. His infectious enthusiasm for research has propelled my research efforts into the fascinating realm of the neurosciences. I am immensely grateful to both supervisors for their collaborative efforts during the course of my PhD.

I acknowledge the following organisations for bursaries and scholarships:

The Foundation for Research and Development in South Africa.
The German DAAD Institute
The British Council
Algorax (Pty) LTD
Rhodes University

My appreciation is extended to the following people:

My mother, Elaine, whom I deeply respect and admire for her tenacity and many sacrifices in ensuring that I received the best education possible. Her joy and pleasure in furthering my education has without doubt been a driving force. Hildegard for teaching me the alphabet, Aunt Cynthia for patient match-stick arithmetic, Uncle Peter for heavy metals, and my brother, Jonathan, for always providing the spark. My father, Ralph, who taught me the difference between wisdom and knowledge.

The staff of the Chemistry Department for their support. Margie Kent and Benita Tarr for their kindness. Joyce Sewry, for Chemistry tutorials in my first year of study. Andre Adriaan, whose skill at creating specialised glassware was of immeausurable value. My research group for kindness, friendship, sharing of ideas and support throughout. Clinton Boyd for many fruitful and enlightening discussions on biochemistry.

Graham (PC Support), Shirley (EM Unit) and Brian (Electronic Services) for generously giving of their time and expertise. Rodney, Paula and Guy, I thank for their time and valuable suggestions, while proof-reading sections of this thesis.

To the friends who have encouraged, supported and beared with me throughout this thesis, my heartfelt thanks. Courtney Dähler for caring. To Ilya Eigenbrot: Spasibo. I am especially indebted to Guy Nelson, for helping me climb yet another tree, for gourmet cooking and a relaxed, happy environment in which to write this thesis.

ABSTRACT

Electrochemical methods were researched for the analysis of metals, proteins and the identification of metal binding proteins.

Adsorptive cathodic stripping voltammetry for metal analysis combines the inherent sensitivity of electrochemical techniques with the specificity of ligands for the non-faradaic preconcentration of analytes at the electrode. The utility of catechol, resorcinol, 4-methylcatechol and 4-t-butylcatechol as ligands was explored for the sensitive analysis of copper, bismuth, cadmium and lead on a mercury film glassy carbon electrode. Metal complexes of lead, copper and bismuth with resorcinol showed the largest increase in current with increase in metal concentration, whereas complexes of these metals with 4-t-butylcatechol showed the lowest current response. Cadmium showed the highest current responses with 4-methylcatechol. The four metals could be determined simultaneously in the presence of resorcinol, although considerable interference was observed between bismuth and copper.

The electroanalysis of cysteine and cysteine containing proteins at carbon electrodes are impaired by slow electron transfer rates at carbon electrodes, exhibiting high overpotentials, greater than 1 V *vs* Ag/AgCl. Metallophthalocyanines have been shown to promote the electrocatalysis of cysteine at lowered potentials. Chemical modification of electrodes with appropriate modifiers is a means of incorporating specificity into electroanalysis, with applications in electrocatalysis. A glassy carbon electrode was modified by electrodeposition of cobalt (II) tetrasulphophthalocyanine $[Co(II)TSPc]^{4-}$ to produce a chemically modified glassy carbon electrode (CMGCE). The CoTSPc-CMGCE catalysed the oxidation of cysteine in the pH range 1 to 10. The significance of this electrode is an application for analysis of proteins at biological pH's. A biscyanoruthenium(II) phthalocyanine CMGCE catalysed the oxidation of cysteine at 0.43 V *vs* Ag/AgCl a significant lowering in the overpotential for the oxidation of cysteine.

Metallothionein, a metal binding protein, is believed to be involved in metal homeostasis and detoxification in the peripheral organs of living systems. A method for the quantitative determination of this protein utilising its high cysteine content was presented. At pH 8.4 Tris-HCl buffer, and using a CoTSPc-CMGCE modified by electrodeposition of the modifier, the anodic peaks for the oxidation of metallothionein was observed at 0.90 V vs Ag/AgCl.

Ferredoxin is a simple iron-sulphur protein. One tenth of its residues are cysteine. Ferredoxin is involved in simple electron transfer processes during photosynthesis and

respiration. Electrochemical studies of spinach ferredoxin were conducted at a CoTSPc-CMGCE. Anodic currents for the oxidation of the cysteine fragment of ferredoxin was observed at 0.85 V *vs* Ag/AgCl in HEPES buffer at pH 7.4, representing a new method for analysis of this protein. Voltammetric studies of its ferric/ferrous transition have shown quasi-reversible waves at $E_{1/2}$ -0.62 V *vs* Ag/AgCl only in the presence of promoters. At a CoTSPc-CMGCE, a cathodic wave attributed to the reduction of Fe(III)/Fe(II) was observed at E_{pc} -0.34 V *vs* Ag/AgCl. This represents an alternative method for voltammetric studies of the ferric/ferrous transition at significantly lowered potentials.

Melatonin, a pineal gland hormone functions in setting and entraining circadian rhythms and in neuroprotection as a free radical scavenger and general antioxidant. Using adsorptive cathodic stripping voltammetry, the binding affinities of melatonin, serotonin and tryptophan for metals, were measured. The results showed that the following metal complexes were formed: aluminium with melatonin, serotonin and tryptophan; cadmium with melatonin and tryptophan; copper with melatonin and serotonin; iron (III) with melatonin and serotonin; lead with melatonin, tryptophan and serotonin, zinc with melatonin and tryptophan and iron (II) with tryptophan. The studies suggest a further role for melatonin in the reduction of free radical generation and in metal detoxification and may explain the accumulation of aluminium in Alzheimer's disease.

TABLE OF CONTENTS

LIST OF ABBREVIATIONS

·OH	Hydroxyl free radical
5-HT	5-hydroxytryptophan
A	Amps
AAS	Atomic absorption spectrophotometry
AAS	Atomic absorption spectroscopy
AD	Alzheimer's disease
AdCSV	Adsorptive cathodic stripping voltammetry
Ads	Adsorbed
Ag/AgCl	Silver/silver chloride electrode
ALAD	γ-Aminolevulinic acid dehydrogenase
ASV	Anodic stripping voltammetry
ATP	Adenosine triphosphate
BAS	Bio-analytical services
BBB	Blood brain barrier
C	Catalytic
cAMP	Cyclic adenosine monophosphate
CAT	Catechol
Chl_a,	Chlorophyll a
CME	Chemically modified electrode
CMGCE	Chemically modified glassy carbon electrode
CNS	Central nervous system
CPE	Carbon paste electrode
CSV	Cathodic stripping voltammetry
CV	Cyclic voltammetry
Cyt*f*	Cytochrome *f*
Dep	Deposition
DMF	N,N-dimethylformamide
DMTD	2,5-dimercapto-1,3,4-thiadiazole
DNA	Deoxyribonucleic acid
DPP	Differential pulse polarography
E	Electrode
EDTA	Ethylene diamine tetraacetate
emf	Electromotive force
EP	Electropolymerised
ESR	Electron spin resonance spectroscopy

FTIR	Fourier transform infrared spectroscopy
GABA	γ-Aminobutyric acid
GCE	Glassy carbon electrode
GSH-Px	Glutathione peroxidase
HIOMT	Hydroxy-indole-O-methyltransferase
HiPIP	High-potential iron-sulphur protein
HMDE	Hanging mercury drop electrode
HSAB	Hard soft acid base rule
I	Current
IHP	Inner Helmholtz plane
IR	Infrared spectroscopy
L	Ligand
L-Dopa	3,4-dihydroxyphenylalanine
LSSV	Linear sweep stripping voltammetry
M	Metal
MB9	Mordant blue 9
MFGCE	Mercury film glassy carbon electrode
M-L	Metal-ligand complex
MLCT	Metal to ligand charge transfer
MPAQ	5 - [(p-methylphenyl)azo]-quinoline
MPc	Metallophthalocyanine
MT	Metallothionein
MTSPc	Tetrasulphonated metallophthalocyanine
NAD^+	Nicotinamide adenine dinucleotide, oxidised
NADH	Nicotinamide adenine dinucleotide, reduced
$NADP^+$	Nicotinamide adenine dinucleotide phosphate
NAT	N-acetyltransferase
NE	Norepinephrine
NMR	Nuclear magnetic resonance spectroscopy
OHP	Outer Helmholtz plane
PADNm	1-(2-pyridylazo) 2.7-dihydroxynaphthalene
pH	Hydrogen ion concentration
PUFA	Polyunsaturated fatty acid
Q_A, Q_B	quinone A, quinone B
R	Reduction
RSH	Cysteine
RSSR	Cystine
SCN	Suprachiasmatic nucleotide

SEM	Scanning electron microscopy
SHE	Standard hydrogen electrode
SOD	Superoxidase dismutase
SVRS	Solochrome violet RS
TAPc	Tetraaminophthalocyanine
TEAP	Tetraethylammonium perchlorate
UV-Vis	Ultraviolet-visible spectroscopy
V	Volt

LIST OF FIGURES

LIST OF TABLES

LIST OF SCHEMES

Chapter One

Overall Introduction

The rich chemistry of metals with a diverse range of ligands is an active area of research, with applications in catalysis, environmental monitoring of metals and the study of metal ions in biological systems.

Living organisms have specific requirements for metals, and the proteins and enzymes which bind, transport and facilitate their uptake and release[1,2]. Proteins and enzymes have specific metal requirements for structural and catalytic purposes. There exists thus an interdependence between metals and proteins. This creates an intricate, detailed network of biochemical events, the homeostasis of which is an absolute requirement for efficient functioning.

The interaction between a metal and a protein is best described as the formation of a metal-ligand co-ordination complex. The formation of such a co-ordination complex is formed by the interaction of an empty orbital of a metal with the filled orbital of a molecule (ligand).[3]

Of the elements thus far isolated, at least 28 are known to be of specific physiological function to life systems, and most of these are metals[1,2]. These metals show preference for certain types of ligands. The most common types of ligands are the amino acids, especially cysteine and the porphyrins, Fig.1.1. The main function of the porphyrins[4] is to bind metal atoms which act as centres for significant biochemical events.

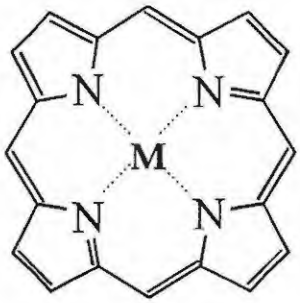

M = Metal

Figure 1.1 Structural representation of a Metalloporphyrin.

There are two approaches to understanding this metal-ligand chemistry: how the metal affects the ligand and how the ligand affects the metal in a metal-ligand complex[3].

Changing the ligand in a metal-protein complex affects its biological role. For example, iron at the centre of a simple protein, such as ferredoxin and bound to cysteine, is involved in simple electron transfer. Iron at the centre of a more complex ligand, a porphyrin, such as haemoglobin, functions in the transport and binding of oxygen[5,6]. Similarly, different metals at the centre of a porphyrin ligand, alters the function of the metalloporphyrin. For example, vitamin B_{12} (containing cobalt) and chlorophyll (containing magnesium) have a similar porphyrin based structure, but their diverse physiological roles are due to different metal centres. Biological ligands typically function by providing a protected environment for the catalytic metal centre, a pathway for electron transfer to the metal, or in storage and transport of the metal. Alternatively, the ligand may be bound to the metal for purposes such as homeostatic control, or metal detoxification in, for example, metallothionein.

The type and feasibility of metal-ligand interactions can be associated with the chemistry of the metals as defined by the periodic table of the elements, their redox potentials and as Lewis acids or bases. Metals and ligands may each be divided into three groups: hard, intermediate and soft, acids and bases, respectively. Table 1.1 shows this classification for selected metals and ligands. According to the Hard Soft Acid Base (HSAB) Rule[7,8], hard

acids show a preference for binding hard bases; soft acids for soft bases and the borderline acids and bases show preference for either groups.

Table 1.1 A select group of metals and ligands and their classification according to the HSAB Rule.[7,8]

Acids			Bases		
Hard	**Borderline**	**Soft**	**Hard**	**Borderline**	**Soft**
Fe^{3+}, Co^{3+} Al^{3+}	Fe^{2+}, Co^{2+} Ni^{2+}, Cu^{2+} Zn^{2+}, Ru^{3+}, Pb^{2+}, Bi^{3+}	Cu^{+}, Cd^{2+} Hg^{2+}	NH_3, OH^- O^{2-}, ROH RO^-	CH_3, CO, O^-, CO_3^{2-} $C_6H_5^-$, NH_2	C_6H_6, CO^- RSH, RS^-

Much of the research on metals has been sparked by the known toxicity of heavy metals [9,10]. Table 1.1 shows that soft acids such as cadmium and mercury have a predilection for soft ligands, such as the thiol groups of proteins. Catastrophes such as the Minamata disease (mercury poisoning) and the Japanese affliction the 'itai itai' disease (cadmium poisoning) are significant examples of the toxicity of heavy metals[11,12,13]. Metal toxicity, however, may also occur during instances of essential metal imbalances. Examples include, copper toxicosis in livestock[14] and vision impairment[1,15], associated with zinc deficiencies. These imbalances may have a dietary origin but are often an early indication of diseased states due to poor metabolism. Metal metabolism consists of delivering the correct metal ion to act where it is needed. Uptake, transport, buffering, storage and excretion must ensure that physiologically necessary metals are made available, though not in excess[16]. As metal homeostasis is reliant on proteins and enzymes involved in these metabolic processes, metal imbalances may be due to deficiencies in amino acids or malfunctioning metal-protein transport systems.

Much effort has thus been centred on the development of fast, efficient and sensitive techniques for the analysis of metals and proteins as early indicators of diseased states. Quantitative and qualitative assessments of metals and proteins support research into the role of metals in biological systems. Studies on the interaction of metals with biological

ligands, are also important in elucidating pathways for metal metabolism, homeostasis and detoxification. This thesis is largely concerned with the development of these techniques fundamental to which is the metal-ligand interaction.

Metal-ligand reactions essentially involve the uptake or release of electrons, making an electrochemical approach to analysis highly feasible. Electroanalytical chemistry offers a means of both analysing and quantifying metals and proteins. Electroanalysis is a relatively young analytical tool with much research being devoted to the development and design of techniques.

A brief overview of the principles and techniques of electrochemistry and electroanalysis follows this introductory chapter. Chapter 3 examines the application of synthetic ligands for electroanalysis of metals. The catalytic activity of metal centres in porphyrins, so well utilised in living systems, is used as a model for the design of metallophthalocyanine chemically modified electrodes (CME's). The design and application of these electrodes are explored for their quantitative analysis of the amino acid, cysteine, in chapter 4. This application is extended for analysis and voltammetric studies of the metalloproteins, metallothionein (chapter 5) and ferredoxin (chapter 6). In chapter 7, the techniques established are used to explore and define metal-ligand interactions in living systems. In each chapter other means of analysis are introduced, offering alternative and/or improved electrochemical methods for their analysis based on the findings of the research.

Chapter Two

Electrochemical Principles and Techniques

2.1 BASIC PRINCIPLES OF ELECTROCHEMISTRY

Faraday's discovery of the one to one equivalence that exists between chemistry and electricity provides the basis for all electroanalytical techniques.[17]

Much of the current understanding of electrode processes and the reactions occurring at an electrode has its basis in the theoretical understanding of phase differences and the expected solution dynamics. An electrode in solution creates a phase boundary between solutes close to the electrode and those in the bulk solution.[17]

2.1.1 Electrode Solution Interphase

Fig. 2.1 illustrates the widely accepted model of the electrode solution interphase. It developed from the Helmholtz model of the interphase which ,proposed a simple electrostatic model based on charge separation across a constant distance. The interphase between an electrolyte solution and electrode is referred to as the electrical double layer. Helmholtz observed that the interphase behaves like a capacitor in its ability to store charge. The model was unable to account for the potential and ionic strength dependence of the capacitance. The Gouy-Chapman theory explained the interphase as a Boltzmann distribution of ions.[18]

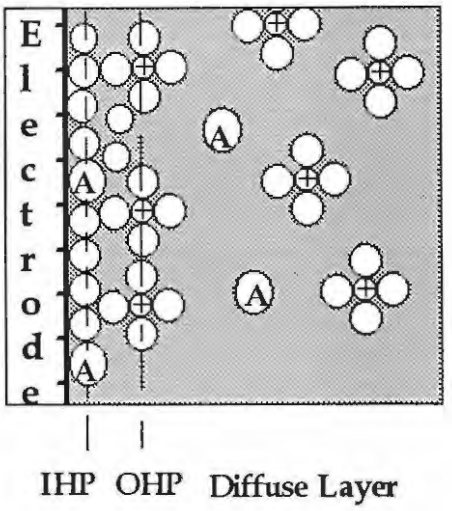

Figure 2.1 Model of the electrode-solution interphase.[17,18]

Fig. 2.1 shows the electrode behaviour for solute A in solvent (water) at an electrode. The electrode is sheathed by oriented water molecules, and those adsorbed anions or molecules, A, which interact directly with the electrode and are not fully solvated. The plane passing through this layer is known as the inner Helmholtz plane (IHP). The next layer contains molecules with a primary hydration shell separated by a monolayer of oriented solvent molecules. This is a separate plane and is termed the outer Helmholtz plane (OHP). Beyond this plane is the Boltzmann distribution of ions. These are determined by the electrostatic interaction between the ions and the potential at the OHP, and the random movement of ions and solvent molecules. This is referred to as the diffuse layer. In the diffuse layer there are two forces interplaying with each other: the random motion of the ions tending towards even distribution through the solution, and electrostatic forces of attraction or repulsion from the surface. These two forces result in a nonuniform distribution of ions near the electrode surface. There is, in effect, a potential difference, the gradient of which is dependant on the ionic strength of the analytes. The potential diminishes exponentially with the distance from the electrode, and this gradient would be sharper, according to the Debye Huckle theory of point charges, at high ionic strength. So ions in the homogeneous bulk solution, away from the electrode, do not experience this potential difference and hence do not "feel the presence of the electrode".[18]

Electrochemical reduction or oxidation occurs at the electrode-solution interphase of the working electrode where the electric field is greatest. Analytical electrochemistry thus involves the perturbation of only a minute fraction of the analyte, that at the electrode-solution interphase.

2.1.2 Transport to the Electrode

Reactants are transported to the working electrode from the bulk solution via diffusion, migration and convection, Fig 2.2. Collectively these are termed as mass transport.

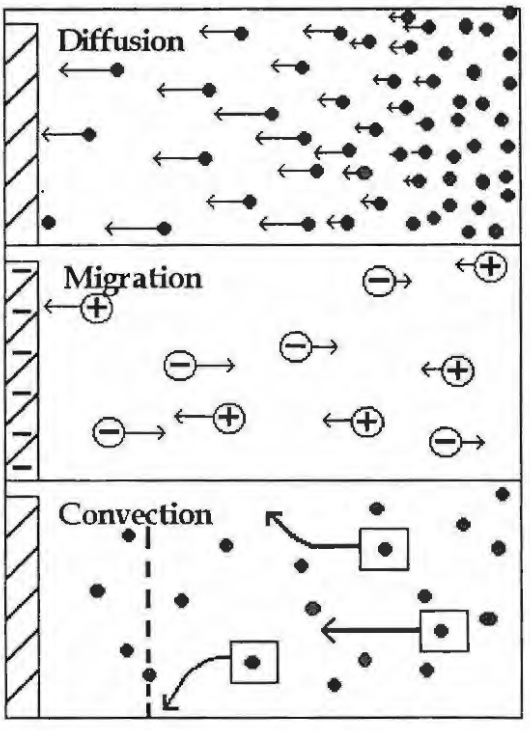

Figure 2.2 The three modes of mass transport.[19]

- Diffusion is the natural tendency of ions or molecules to move from a concentrated region to a more dilute region to reach uniformity.
- Migration is the process by which charged particles such as ions move towards the electrode under the influence of an electric field, such as that which exists in the vicinity of the electrode. Supporting electrolytes in solution with the analyte are

necessary to decrease the field strength near the electrode to minimise the effect of migration. Electrolytes also minimise the resistance to charge flow through the cell.

- Convection is the movement of reactants via mechanical means such as stirring, rotating the electrode or by flowing the solution through the cell. Reactants are transported to the electrode and electrogenerated product transported away.

When three modes of transport are involved, the current response equation is rather complex. Contributions due to convection and migration are minimised by using quiescent solutions and strong electrolytes, respectively.[18,19]

2.1.3 Definition of Electroanalytical techniques

Electroanalytical techniques may be defined as static or dynamic, Fig. 2.3. The static system involves measurement of potential difference at zero current, without any interference of the solid-solution interphase. Here, equilibrium conditions are maintained exhibiting a Nernstian response.[17]

In contrast, dynamic electrochemistry entails intentionally disturbing a system from equilibrium by excitation signals such as varying potential, time and current and then monitoring the excitation response, e.g. current. Most electroanalytical techniques are based on dynamic electrochemistry. The non-equilibrium behaviour of dynamic electrochemical techniques is largely controlled by diffusion.[18]

Dynamic electrochemical techniques are divided into small amplitude and large amplitude techniques, according to the magnitude of the excitation signal. These are further categorised and often named according to the nature of the excitation signal and the monitored response. For example, voltammetry refers to a controlled potential technique (volt) with the response measured being the current (ammetry).[17]

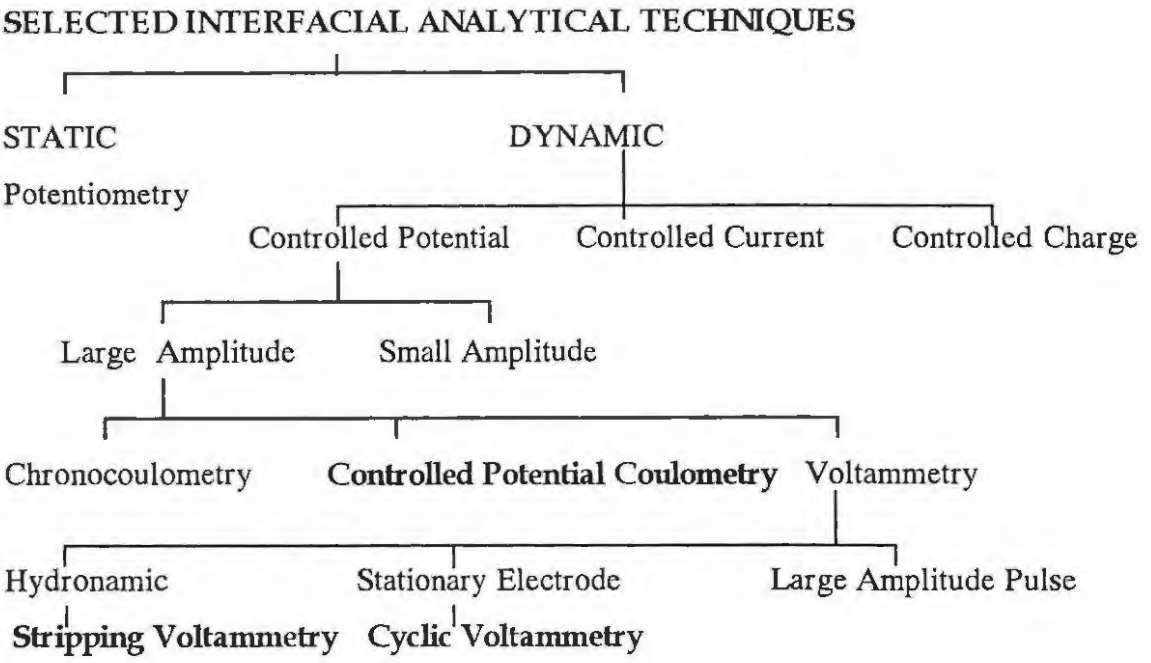

Figure 2.3 Tree of electroanalytical techniques, highlighting the dynamic techniques, used in the thesis and elaborated on further. Adapted from Reference 17.

2.1.4 Electrode Reaction

In controlled potential techniques, for example, the role of the electrode is to monitor the current response, which is related to the concentration of the analyte. This is achieved by monitoring the transfer of electrons during the redox process:

$$O + ne^- \underset{k_r}{\overset{k_f}{\leftrightarrow}} R \qquad \text{Equation 2-1}$$

O refers to the oxidised species, e^- the electron and R the species in reduced form on acceptance of the electron. k_f and k_r, are the formal rate constants for the forward and reverse reactions, respectively.

The conversion of O to R by reduction results in a cathodic current, i_c. Oxidation of R to O results in an anodic current, i_a. The observed current resulting in a change of oxidation state is the faradaic current. The faradaic current is a direct measure of the rate of the redox reaction. The resulting current potential plot is the voltammogram.

For reversible systems, the net current, $i_{net} = 0$ and $k_f = k_r$. Systems such as these are controlled by the laws of thermodynamics, and the Nernst equation applies:[17]

Nernst Equation: $\mathbf{E_{eq} = E^{0'} + 2.303(RT/nF) \log C_0/C_R}$ Equation 2-2

E_{eq} = potential applied to cell, $E_{eq} = 0$ at equilbrium

$E^{0'}$ = formal reduction potential of couple *vs* standard hydrogen electrode

n = number of electrons transferred per molecule, eq/mol

C_0 = concentration of O, $mol.cm^{-3}$

C_R = concentration of R, $mol.cm^{-3}$

The overall rate of the reaction and the current observed is in general affected by the rates of mass transfer of reactant and product; electron transfer at the electrode surface; chemical reactions preceding or following electron transfer; and other surface reactions such as adsorption, desorption or electrodeposition. When any of these steps are rate limiting, the potential applied to the system will no longer be the same as the thermodynamically determined value at equilibrium. This is due to overpotential or overvoltage, the sum of the different overpotential terms associated with the different reaction steps.[20] Overpotential is thus the difference between the equilibrium (reversible) potential of an electrode and the voltage which must be applied in order for current to flow. Alternatively, overpotential may be viewed as an activation barrier[21] to the reaction. The total potential applied (V) is then given by:[20]

$\mathbf{V = -E + RI + \eta}$ Equation 2-3

where E (V) is the reversible thermodynamic electromotive force (emf),

R (Ω) is the sum of ohmic resistance in the circuit,

I (A) is the total current passed and

η (V) is the overpotential.

Ohmic resistances are introduced by voltage drops across the electrical leads, electrodes and electrolyte in the circuit, and may be reduced by improved conductivity of the electrolyte or reducing the distance between the electrodes. [20]

When the overall reaction rate is controlled solely by mass transport, a Nernstian response, obeying thermodynamic relationships, applies. Here k_f and k_r are sufficiently fast and are equivalent. Overpotentials due to mass transport can be simplified by controlling the contribution of convection and migration, so that diffusion is the limiting factor. The current response is thus a function of diffusion. [19]

When mass transport is sufficiently fast, the reaction may be limited by the reaction rate at the electrode, this being the significant contribution to the observed overpotential. Here $k_f \neq k_r$ and the current response is thus a function of the rate of electron transfer.[20]

Characterising electrode reactions and obtaining both quantitative and qualitative information is described further in the discussion on cyclic voltammetry, Section 2.2.

2.1.5 The Three Electrode, Electrochemical Cell

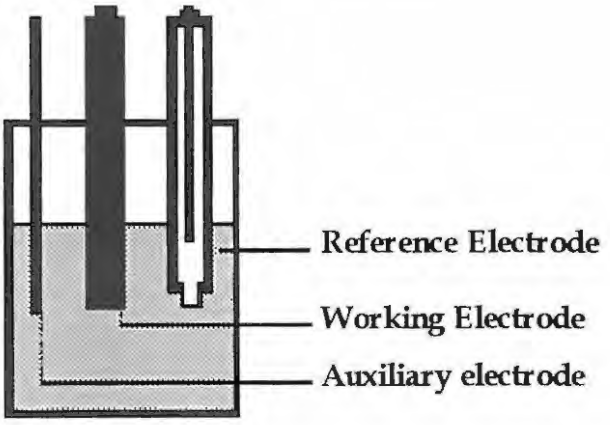

Figure 2.4 Simple diagram of the three electrode, electrochemical cell.

Most dynamic electrochemistry utilises the classic three electrode system depicted in Fig. 2.4. This comprises the working electrode, a reference and an auxiliary electrode. The electron transfer reactions occur at the surface of the working electrode. These reactions are monitored in relation to a reference electrode, which maintains a constant potential. The current passes between the working electrode and the auxiliary electrode, the latter serving to complete the circuit.[20]

- The auxiliary electrode is usually constructed of an inert substance such as platinum, either as a wire, a loop or a foil. This electrode is not usually isolated from the solution while the reference electrode is.[21,22]

- The standard hydrogen electrode (SHE) is the universal reference electrode for reporting half-cell potentials and these have been determined for many oxidation reduction reactions in reference to the hydrogen electrode potential. Associated with the use of the hydrogen electrode is the hazardous stream of gas required in its operation. This, together with the preparation and maintenance of its platinised surface, makes it undesirable for routine use. Secondary reference electrodes are

preferred, such as the saturated calomel electrode and silver/silver chloride electrode. The saturated calomel electrode (saturated with KCl) and the silver/silver chloride electrode (saturated with both KCl and AgCl), for example, have potentials of 0.244 V and 0.199 V respectively, *vs* SHE at 25°C. The silver/silver chloride (Ag/AgCl) electrode consists of a silver wire anodised with silver chloride in a glass tube. The wire is in direct contact with saturated or concentrated solutions of AgCl and either KCl or NaCl. The electrode is protected from the solution by a semi-permeable salt bridge.[21,22]

- The most utilised working electrodes are those of metallic origin. The basic requirements of the selected material are: that it provides a large potential range; that it is non-destructible under a variety of solution conditions; that it has a low electrical resistance; and that it has an easily reproducible surface. Platinum, gold, mercury and carbon electrodes have been of most use, with carbon electrodes the material of choice for many electrochemical applications. Mercury electrodes have varied designs: static, the hanging mercury drop electrode (HMDE); dropping, where reaction is monitored at a new surface by releasing a fresh drop of mercury; or a mercury film on a support such as carbon. Benefits of the mercury drop electrodes, include a renewable electrode surface and a high cathodic potential window while the limited anodic range and toxicity are a disadvantage. Among the most utilised of the solid carbon electrodes are carbon paste electrodes, pyrolitic graphite (ordinary or stress-annealed) and glassy carbon electrodes. Carbon paste electrodes are constructed by mixing graphite powder with a liquid, e.g. nujol into a glass tube. The other two electrodes are commercially available. Glassy carbon has excellent mechanical and electrical properties, a wide potential window and is chemically inert, exhibiting reproducible performance. Electron transfer rates at carbon electrodes are, however, slower than at metal electrodes. Electrode pre-treatment procedures can increase the electron-transfer rates.[19]

Present at carbon electrode surfaces, are surface confined species, hydroxyl and carboxyl groups, which are presumed to be involved in electrode processes. These surface functionalities[23] provide a means of chemically modifying glassy carbon

electrodes by binding redox active reagents at these sites, creating new electrode surfaces, the concept and application of which is discussed in detail in Section 2.6.

At the electrode surface, the reactions are monitored via a range of electrochemical techniques. Briefly, electrochemistry, or rather voltammetry, comprises of a group of electrochemical procedures based on the potential-current behaviour of a polarizable electrode in a supporting electrolyte. Theoretically, any species can be analysed if it undergoes oxidation or reduction within the working potential range of the electrode system employed. The redox reaction taking place at the electrode is therefore controlled by variation in the applied electrode potential.[24]

The dynamic electrochemical techniques used: stripping voltammetry and cyclic voltammetry are discussed in terms of their application and the reactions so monitored, occurring at the electrode.

2.2 CYCLIC VOLTAMMETRY

Cyclic Voltammetry is commonly used as the initial electrochemical technique to characterise a redox system. The redox couples are typically located by potential scans encompassing the entire accessible potential window of the electrode. For example, the forward scan (positive potentials) generates the oxidised species and the reverse scan the reduced species. A typical cyclic voltammogram (CV) provides information on the reversibility, kinetics, and formal reduction potential of the reaction, and information required for qualitative and quantitative definition of the reaction mechanism.[19,25] Fig. 2.5 shows a typical CV.

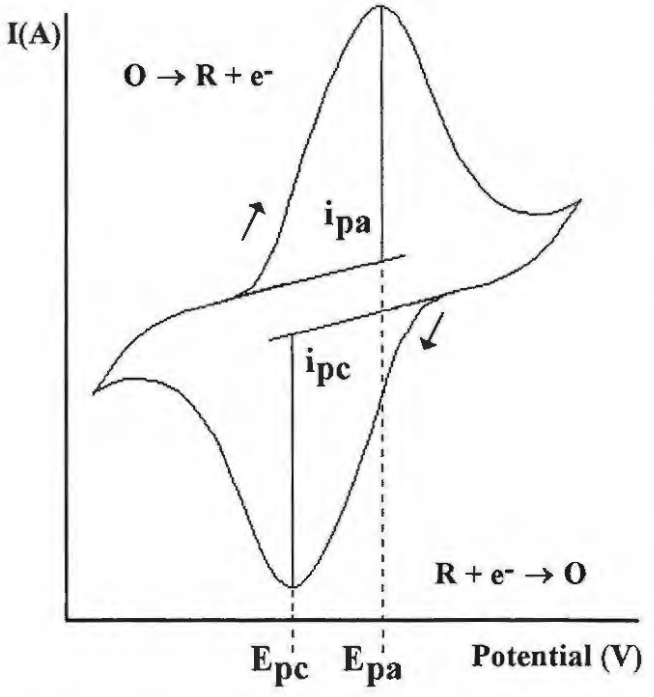

Figure 2.5 A typical cyclic voltammogram (for illustrative purposes only).

Information obtained from the CV is i_{pa}, the anodic peak current produced by scanning positively until the electrode becomes a sufficiently strong oxidant to oxidise the analyte. The current peak decays when all species at the electrode are oxidised. Scanning

negatively permits reduction of this species, producing i_{pc}, the cathodic peak current. Extrapolating the baselines of these peaks yields the magnitude of the currents. The anodic peak potential, E_{pa} and cathodic peak potential, E_{pc} are easily read from the voltammogram and the following information may be determined. [19,25,26]

The formal reduction potential, $E^{0'}$, of a redox couple is obtained as follows:

$$\mathbf{E^{0'} = (E_{pa} + E_{pc})/2} \qquad \text{Equation 2-4}$$

$E^{0'}$ = formal reduction potential, or half-wave potential ($E_{1/2}$)

E_{pa} = anodic peak potential

E_{pc} = cathodic peak potential

The number of electrons transferred in the electrode reaction are given by:

$$\mathbf{\Delta E_p = E_{pa} - E_{pc} = RT/nF} \qquad \text{Equation 2-5}$$

R = the gas constant, 8.314 J K^{-1} mol^{-1}

T = temperature in Kelvin

n = number of electrons

F = Faraday's constant = 96,485 C

At 25°C, RT/nF = 0.059 V/n

For a reversible one electron redox process, ΔE_p = 0.059 V

2.2.1 Reversibility

An electrochemically reversible couple is one in which both species rapidly exchange electrons with the working electrode, regenerating the starting reagent. Figure 2.5 showed a typical reversible cyclic voltammogram, with the forward wave having a corresponding reverse wave. The peak separation value of 0.059/n is independent of scan rate.[25]

For reversible couples: $i_{pa}/i_{pc} = 1$ with no kinetic complications and $k_f = k_r$.[19,25,26]
The current is defined by the Ilkovic equation:

$$\mathbf{i_p = 2.69 \times 10^5 n^{3/2} A D^{1/2} C \nu^{1/2}} \qquad \text{Equation 2-6}$$

i_p = peak current, A
n = number of electrons
A = electrode area, cm^2
D = diffusion coefficient
C = concentration, mol cm^{-3}
ν = scan rate, volts/second.

For reversible couples, Equation 2-6, current is directly proportional to concentration and i_p is proportional to $\nu^{1/2}$. At greater scan rates where current is no longer proportional to the square root of the scan rate, the peak separation becomes greater than 58/n mV. According to Ohm's law, E = iR so a change in peak separation is indicative of iR drop. This is caused by resistance (faradaic resistance) between the working and reference electrode. The iR drop may be compensated for by using an electrolyte of high ionic strength.[25]

2.2.2 Irreversibility

Cyclic voltammograms of irreversible couples often show a single oxidation, or reduction wave, with either a weaker return, or no return wave.

Irreversibility for a redox couple is caused by slow electron exchange of the redox species or is coupled with a chemical reaction at the working electrode. When $k_f > k_r$ or $k_r > k_f$, $i_{pa}/i_{pc} \neq 1$, and $\Delta E_p > 0.058/n$ volts (when iR drop is compensated for) electrochemical irreversibility is indicated. These are reactions controlled by the rate of electron transfer.

Totally irreversible systems exhibit a shift in peak potentials with changing scan rate. At increasing scan rates, the peak potential separation becomes greater and the electron transfer rate, the rate constant, decreases. The reaction thus becomes kinetically limiting. The peak current ratio is also affected; i_{pc} becomes smaller with the smaller rate constant. The rate constants for the forward and reverse reactions are also no longer equal.[25]

At increasing scan rates i_{pc} may be measured to determine the scan rate range in which the reaction is controlled by diffusion i.e. no other chemical processes limit the current. A linear plot of i *vs* $\nu^{1/2}$ indicates a diffusion controlled process at these scan rates.

The formal reduction potential cannot be defined as above for the reversible couple (Equation 2-6) and the Nernst equation no longer applies. The potential of the cathodic and anodic couples become dependant on the rate of electron transfer and is dependant on scan rate, so the following equation is used to define E_{pc}.[20]

$$\mathbf{E_{pc} = E^0 - (RT/\alpha\, nF)[0.780 + \ln(D^{1/2}/k_0 + \tfrac{1}{2} \ln \nu]} \qquad \text{Equation 2-7}$$

α = transfer coefficient
k_0 = rate constant
F = Faraday's Constant, 96 485 C/mole
and others as defined before in Equations 2-4 and 2-6.

A plot of E_{pc} *vs* ln ν (scan rate) will be linear and the slope equals $\frac{1}{2}RT/\alpha nF$. The value for α, determined from Equation 2-7, may be used in Equation 2.8 to determine D, the diffusion coefficient.

$$\mathbf{I_{pc} = -2.99 \times 10^5 n(\alpha\, n)^{1/2} A D^{1/2} C_o \nu^{1/2}} \qquad \text{Equation 2-8}$$

D = diffusion coefficient

C_o = the bulk concentration of the analyte in solution

Here i_{pc} is still proportional to the bulk concentration but will be lower in height. Once D is known then the rate constant k_0 for the reaction may be determined.

2.2.3 Quasi-reversibility

Similar information may be obtained for CV's of redox couples exhibiting quasi-reversibility. A quasi-reversible system is one in which $i_{pa} <> i_{pc}$. Cyclic voltammograms of quasi-reversible systems have a larger peak potential separation than reversible systems, tending to look more drawn out. The current is controlled by mass transport of reactant and product, and by charge transfer. [19]

Here the following equation applies:[21,27,28]

$$\psi = k_s/(\pi\, D_0 \times nF\nu/RT)^{1/2} \qquad \text{Equation 2-9}$$

ψ is a dimensionless parameter with given values for $n\Delta E$.

k_s = standard rate constant when $E = E^0$

In this equation, the value for the transfer coefficient, α, is assumed to be 0.5 when the anodic and cathodic current peaks are of the same height. k_s may be determined if D_o is known.

The current for quasi-reversible systems is defined by Equation 2-10.

$$i = nFA\, C_0\, D_0^{1/2} (nF/RT)^{1/2}\, \psi\, \nu^{1/2} \qquad \text{Equation 2-10}$$

Slopes of the plot of i_{pc} *vs* $\nu^{1/2}$ will give D_o and k_s may then be determined using Equation 2-9 once D_o is known.

CV's may thus be used to determine whether a redox process is reversible, quasi-reversible or irreversible. For truly reversible systems, no kinetic information such as rate constants, may be obtained. For both quasi-reversible and irreversible systems, rate constants may be obtained.[25]

2.2.4 Reaction Mechanisms

Fig. 2.5 showed an idealised situation for reversible one-electron transfer. A consecutive multi-electron reversible process will similarly yield several distinct peaks from which the reaction mechanism is easily interpreted. When the heterogeneous electrode transfer at the solution interphase is coupled with homogeneous chemical reactions, the shape, current response and peak potentials will be more complex, but useful in elucidating the reaction pathway.

Some common mechanisms have been identified, for example, the EC Mechanism. This is known as a following chemical reaction in which E is the heterogeneous electron-transfer reaction (Electrode reaction) and C is the subsequent homogenous electron transfer reaction (Chemical reaction), hence the term, EC.

$$\mathbf{O + e \overset{E}{\leftrightarrow} R \overset{C}{\rightarrow} Z} \qquad \text{Equation 2-11}$$

In the EC mechanism, R, the electrogenerated species, reacts to form product Z, affecting the reversibility of reaction E. This may be observed by a decrease in cathodic peak so that $i_{pc}/i_{pa} < 1$. The peak ratio may be used to estimate the rate constant of the chemical step. When no return peak is observed in the reverse scan, it implies that all of R reacted very fast to produce Z.

The next example shows the catalytic regeneration of reactant O during the C step, a variation of the EC mechanism:

$$\mathbf{O + ne \overset{E}{\leftrightarrow} R + A \overset{C}{\rightarrow} O} \qquad \text{Equation 2-12}$$

In Equation 2-12, the product of the E mechanism, R is reduced by analyte A placed into the solution back to O. This exhibits a peak ratio of unity.[19]

2.3 CONTROLLED POTENTIAL ELECTROLYSIS

This technique is also known as bulk electrolysis or controlled potential coulometry. It involves the determination of the quantity of material electrolysed from the amount of charge passed through the electrochemical cell during the electrolysis. Electrolysis is achieved by applying a fixed potential to the electrode. When the electrolysis is 100% complete, the current is indistinguishable from the residual current. The total charge, Q, passed during the electrolysis is obtained by integrating the current, i, as a function of time, t, Equation 2-13.

$$\mathbf{Q = it} \qquad \text{Equation 2-13}$$

The amount of chemical change during electrolysis is proportional to the charge passed, according to Faraday's Law. The total charge is then used to calculate the amount of material electrolysed, Equation 2-14.

$$\mathbf{Q = nFN} \qquad \text{Equation 2-14}$$

Q = charge
n = number of electrons transferred per molecule, Eq/mol
N = number of moles of substance electrolysed
F = Faraday's constant which is the electric charge carried by one mole of electrons and has a value of 96485 coulombs per mole of electrons.

The residual charge is subtracted from the total charge to obtain the Faradaic charge. The experiment is usually carried out on an electrode with a large surface area to reduce the time required to achieve full electrolysis.[25,26]

2.4 STRIPPING VOLTAMMETRY

Stripping voltammetry (or analysis) is a remarkably sensitive electrochemical technique for measuring trace metals.

Metal ions in solution are able to accept and donate electrons. This electroactive nature makes both qualitative and quantitative analysis possible. For trace metal ions in solution it is necessary to employ a preconcentration step, which has a 2-fold purpose: enrichment, and isolation, of the analyte from the complex matrix. The best known technique employing such an electrolytic preconcentration step at the working electrode, is stripping voltammetry. Two versions of this technique commonly employed, are: anodic and cathodic stripping voltammetry (ASV and CSV, respectively).[19,26]

ASV has been utilised with much success in the analysis of a range of toxic heavy metals in flowing solutions, soil samples and biological samples. The simultaneous determination of zinc, cadmium, lead and copper in the urine of patients with Blackfoot Disease[29] is an example of its application to biological samples. ASV has been used for environmental assessment[30] and comparison of metal content of drinking water from the Mississippi, the Rhine and the Nile by differential pulse stripping voltammetry. The advantage of ASV over atomic absorption spectroscopy and other non-electrochemical methods is the high sensitivity, typically (10^{-9}ppm to 10^{-12} ppm) and the simultaneous determination of certain metals it affords. In stripping voltammetry the most commonly employed electrode is the HMDE. A mercury film electrode may also be used, where the mercury film is formed on glassy carbon either by preliminary deposition or plating, from a mercury electrolyte in solution.

Metal ions present in a stirred solution with a mercury electrolyte are electrolytically extracted from solution by controlled potential electrolysis for a controlled time. In this step the metals reach the electrode by diffusion and convection. The analytes are reduced to the metallic state at potentials more negative than the reduction potential of the metal of

interest and form an amalgam with mercury at the electrode, Equation 2-15. In other words, the analytes are preconcentrated at the electrode. Bonding with mercury is essential in preventing the reduced metal ions from leaching back in to solution. The potential is then scanned in a positive going scan corresponding to the anodic dissolution and oxidation of the amalgam (at potentials unique to the metal species) releasing metal ions back into solution, Equation 2-16. Electrons evolved during this step generate a current which is recorded as a function of potential. The current is proportional to the concentration of the metal. Measurement of the current at increasing concentrations of metal are used to produce standard curves of current versus concentration, facilitating the quantitative determination of samples, while the peak potentials serve to identify the metals in the sample.[19,29]

Reduction	$\mathbf{M^{n+} + ne^- + Hg^{2+} \rightarrow M(Hg)}$	Preconcentration	Equation 2-15
Oxidation	$\mathbf{M(Hg) \rightarrow M^{n+} + Hg^{2+} + ne^-}$	Stripping	Equation 2-16

A typical ASV is shown below for metal, M, Fig. 2.6

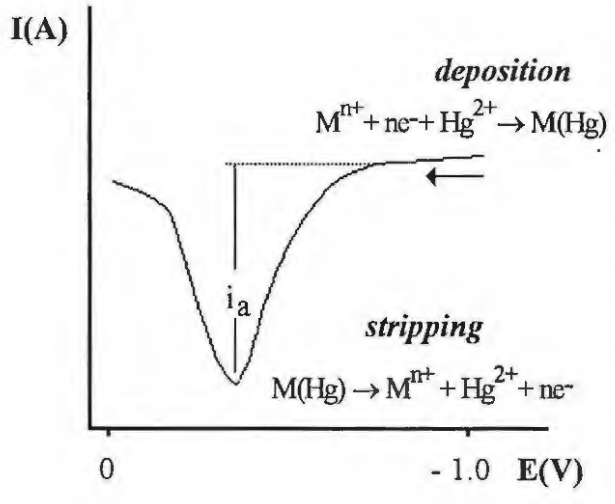

Figure 2.6 Schematic representation of a typical anodic stripping voltammogram (for illustrative purposes only).

Conversely, CSV undergoes an oxidation step during preconcentration and reduction during the stripping step and is thus used in analysis of negatively charged species such as Cl^- ions.

From the description above it can be noted that there are a few criteria which need to be met in order for a metal to be analysed using this technique:

1. The metal must be sufficiently soluble to form an amalgam with mercury at the electrode (otherwise the reoxidation step is electrochemically irreversible).
2. The reduction potential of the metal must be more positive than that of hydrogen ions or than that of any major reducible ion in the electrolyte (otherwise the reoxidation current is masked by that of hydrogen or the major reducible ion).
3. The reduction potential must be more negative than that of mercury.[29]

Based on these criteria (at a mercury electrode), theoretically only metals which have a reduction potential to the metallic state between 0 V and 0.8 V *vs* SHE may be analysed by ASV. However, mercury electrodes have a high hydrogen overvoltage, which extends the lower limit from 0 V to almost -1.0 V *vs* SHE.

Fig 2.7 gives a representation of the reduction potentials (to the metallic state) of a number of metals. The metals falling within the limits indicated by the dotted lines in Fig 2.7 may be analysed by ASV.

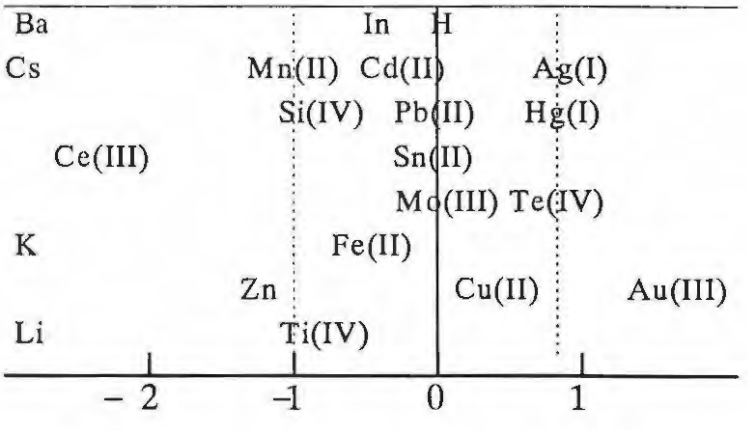

Figure 2.7 Reduction potentials vs SHE, to the metallic state of a number of metals in non-complexing and acidic conditions. Adapted from Reference 29.

Not all of the metals falling within this range can be analysed using the described voltammetric procedure. Eliminated are: iron, silicon, molybdenum, telluride and titanium as they are not sufficiently soluble in mercury. Furthermore, some of the reduction potentials of the remaining metals are very close together and interfere if they are present at similar concentrations. An example is the tin, lead, thallium, indium and cadmium group. Efficient schemes for simultaneous analysis are possible, e.g. Cu, Pb, Cd and Zn can be simultaneously determined by ASV.[29]

The interference effects of one metal over another can be minimised by masking agents, for example, thallium can be detected by masking lead and cadmium with EDTA (ethylenediaminetetraacetate). Sb can be analysed by shifting the potential of copper with chloride.[29] With the development of ideas such as these, researchers started looking beyond the boundaries as discussed above, and not only to the metals excluded by conventional stripping voltammetry, but also non-metals, metalloids and organic compounds.

A major step forward was the development of techniques for the non-faradaic deposition of analytes. One of the major shortcomings of ASV is that it involves a faradaic accumulation or preconcentration of the analytes at the working electrode surface. Therefore, the technique does not afford the voltammetric analysis of most organic compounds, as these cannot be electrodeposited. The natural tendency of analytes to adsorb onto the electrode in a simple diffusion step was utilised as the primary approach towards non-electrolytic preconcentration[31]. Two such techniques have emerged: specific reactions at chemically modified electrodes and adsorptive deposition (preconcentration) at ordinary electrodes[32]. The latter will be discussed first.

2.5 ADSORPTIVE CATHODIC STRIPPING VOLTAMMETRY FOR DETERMINATION OF METALS

Adsorptive stripping voltammetry exploits the spontaneous adsorptive tendencies of analytes at a stationary electrode as an effective preconcentration step for voltammetric measurements of trace analytes[32]. Preconcentration at the electrode is solely by interfacial deposition. The fundamental difference from ASV then, is that the preconcentration step does not involve any electrolytic (faradaic) process[32] extending the scope of stripping voltammetry to those species which cannot be electrolytically deposited such as organic compounds[29,31-42].

A few advantages of adsorptive stripping voltammetry over ASV in metal analysis are evident. Using adsorptive stripping voltammetry, any oxidation state can be collected rather than only the metallic state, thus facilitating analysis to any element with a reduction potential falling within the stability range of hydrogen and mercury. The material is collected as a monomolecular layer on the electrode surface, so all the material is instantly accessible to reduction or oxidation. The reduction current is independent of diffusion of the reactive species, meaning that very fast potential scanning techniques can be employed, producing larger currents.[29]

2.5.1 Theory of Adsorption

Adsorption occurs at the electrode/electrolyte interphase. This interphase exhibits properties which differ from that in the bulk solution. It is here at the electrode interface where adsorption occurs in what can be described as a displacement process: a molecule of analyte displaces a molecule of solvent as in Fig. 2.8.

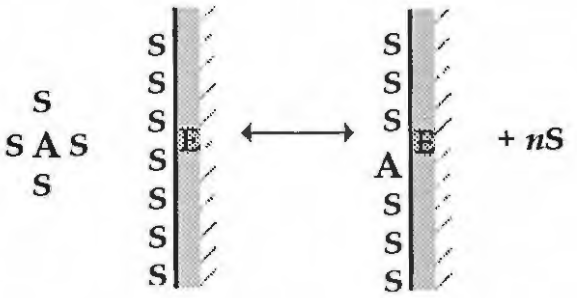

A = adsorbate, S = solvent molecules, E = electrode, n = number of solvent molecules

Figure 2.8 The adsorption equilbrium according to Anson.[17]

Assuming monolayer-coverage, the amount of adsorbate depends on the size of the electrode surface, the orientation of the adsorbed species, the hydrophobicity of the analyte (as smaller solubilities promote strong adsorption)[38]. These are the most important considerations, but other factors contribute to the amount of adsorption. These include: electrostatic interaction (between an ionic adsorbate and a charged electrode), field-dipole interaction (between the electrode double-layer and functional groups of organic reactants), and chemisorption (of certain electron or atomic groups on metallic electrodes) [32].

The voltammetric response is a function of the amount of adsorbate. The amount of adsorbate is related to the bulk concentration of the analyte. The relation between the bulk concentration and the adsorbed species is described by adsorption isotherms, such as the Langmuir adsorption isotherm. The Langmuir isotherm, assuming a maximum monolayer of coverage, describes a linear relationship between adsorbed species and bulk concentration of analyte at low adsorbate concentrations. This model assumes no interaction between surface-confined species. As the amount of adsorbate increases, approaching monolayer coverage, deviation from this linear relationship is to be expected as interactions between the adsorbed species at the electrode become a factor.[32]

The linearity of the current response is likewise affected at high adsorbate concentrations, with increased interaction between the adsorbates. This is depicted in Fig. 2.9, showing deviation from linearity at high adsorbate concentrations.

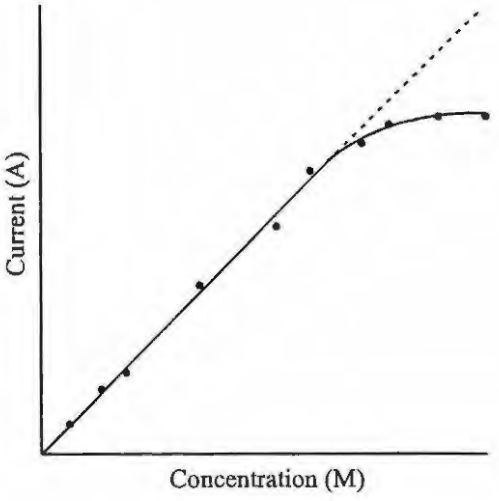

Figure 2.9 Deviation from linear current response at high analyte concentration

2.5.2 Metal-ligand Complexes

Early studies in trace metal analysis showed significant enhancements in the voltammetric response for several metals in the presence of different ligands. Suitable ligands bind the metal and adsorb to the electrode as a metal-ligand complex. These observations led directly to the use of ligands capable of forming complexes with the metal analytes, to enhance the non-faradaic deposition of the analyte at electrodes.[31,42]

The technique is described for the analysis of a metal via complex formation with a suitable ligand:

To a solution of the metal analyte and electrolyte, a sufficient amount of the chelating ligand of choice is added. Under nitrogen flow (to prevent oxidation of the species), and while stirring, the metal and ligand are allowed time to form a metal-ligand complex. During this accumulation time, metal-ligand complexes have already begun the simple adsorption process at the electrode surface by diffusion from the bulk solution. To

optimise adsorption, the electrode potential is held at a fixed potential (deposition potential) and for a controlled time (deposition time), while the solution is stirred at a fixed convection rate. This potential is usually 200-300 mV less negative than the actual reduction potential of the metal. The adsorbed complex is reduced during a negative going potential scan (the stripping step) and both the metal and ligand are released back into solution. These steps are depicted in Fig. 2.10. Peak current measurements provide for both quantitative analysis (due to the linear relation between current, adsorbate and bulk concentration) and qualitative analysis (as reduction occurs at a potential unique to the metal in the metal-ligand complex).[32]

Effectively, this is a cathodic stripping technique, involving reduction of the adsorbed complex. Only in exceptional cases has the stripping step involved oxidation of the adsorbed species. For this reason, the technique is referred to as adsorptive cathodic stripping voltammetry (AdCSV) in this text.

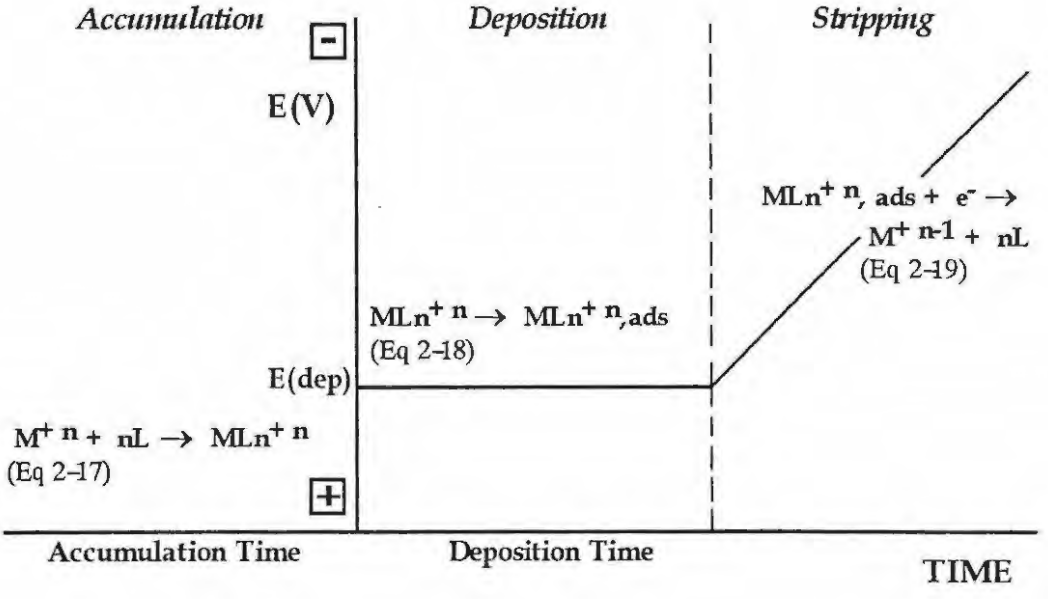

Figure 2.10 Steps in the accumulation of a metal (M) with ligand (L); the adsorptive deposition (dep.) of ML onto electrode and reduction (stripping) of the surface active complex. Equation numbers shown in brackets. Figure adapted from Reference 32.

For most metal-ligand complexes, the observed current response on stripping of the adsorbed metal-ligand complex is usually that of the reduction of the metal, the reduction

potential thus being specific to the metal. For metals with very negative reduction potentials, the reduction of the ligand may be utilised as a measure of the metal concentration, e.g. gallium with solochrome violet RS.[32] In both these cases the reduction potential of the metal-ligand complex is less negative than that of either the metal or the ligand, but this is not strictly the norm. In certain instances the catalytically accelerated reduction of the adsorbed metal-ligand complex by dissolved reactants is used to quantify the adsorbed material, e.g. platinum-formazone[29], catalysed by hydrogen ions.

The metal-ligand approach to stripping voltammetry, apart from extending the scope of metals analysed, also provides an alternative and often improved means of analysis for metals which can also be determined by conventional anodic stripping procedures, such as nickel, manganese, gallium, copper, cobalt and tin. With conventional anodic stripping procedures, the analysis of these metals is hampered by interferences such as the formation of intermetallic compounds or poor selectivity.[32,42]

Ligands for metal analysis may be selected from a wide range, based on research of the interactions of metal-ligand complexes via adsorptive stripping voltammetry. Table 2.1 shows a small selection of suitable ligands. The selectivity of the complex formation step in this technique provides for a measure of selectivity if a metal-specific ligand is chosen, while certain ligands may bind a range of metals specifically. In certain instances the ligand may bind strongly to a redox state of a metal, offering the possibility of speciation selectivity.[29]

The use of chelating ligands in metal analysis thus offers the following advantages:

- Extending the scope of metals analysed by stripping voltammetry.
- Improved sensitivity for metals which can be analysed by ASV.
- Measure of selectivity from a range of metal-specific chelating ligands.
- Speciation selectivity.
- Analysis of metals with highly negative reduction potentials using ligands (the reduction potential of the adsorbed complex is used as a sensitive measure of the metal).

- ASV measures the labile metal fraction (the fraction plated at the electrode) whereas AdCSV measures the concentration of metal in the metal-ligand complex, hence, when an excess of a strong ligand is used, the total metal content may be determined.[32]

The technique also allows for the simultaneous analysis of a group of metals. It has found ready application in simultaneous analysis in environmental and biological samples e.g. arsenic, nickel and selenium in oyster tissue;[31] copper, nickel, cobalt, lead and cadmium in human hair samples;[34] and nickel and cobalt in natural waters[37]. Using dihydroxyazo dyes, Wang[42] showed the possibility of simultaneous analysis of metals including indium and iron, zinc and nickel, thorium and iron.

Table 2.1 Metals analysed by AdCSV and the ligands employed

METAL	ASV*	AdCSV			LIGANDS	
		M	L	C		REF.
Aluminium			X		SVRS, dihydroxyanthraquinone sulphonic acid, DMTD	[32,29,31]
Antimony		X			Catechol	[29]
Arsenic		X			Copper, DMTD	[29,31]
Beryllium		X			Thorin	[40]
Bismuth	X					[29]
Cadmium	X	X			8-hydroxyquinoline, PADN, DMTD	[29,34,31]
Cerium			X		O - Cresolphthaleinthalexone	[32]
Chromium			X	X	Diethylenetriaminepentaacetic acid	[29+32]
Cobalt		X			Dimethylglyoxime, Br-PADN, nioxime, PADN	[29,39,29,34]
Copper	X	X			[29]-hydroxyquinoline, PADN, Catechol	[29,34,29]
Gallium			X		Solochrome violet RS	[32]
Germanium		X			Catechol	[29]
Indium	X					
Iodide		X			Copper, Mercury	[29,29]
Iron	X	X			Catechol, SVRS, 1-nitroso-2-naphtol	[29,32,29]
Lanthanide			X		Cresolphthalexon	[32]
Lead	X	X			PADN, O-cresolphthalexon, 8-hydroxyquinoline	[34,36,29]
Mercury	X					
Manganese	X		X		Eriochrome Black T	[32]
Molybdenum		X			8-hydroxyquinoline, oxime,	[29,32]
			X	X	Tropolone	[29]
Nickel		X			Dimethylglyoxime, PADN, MPAQ, Bipyridine, DMTD	[29,34,38,29] [31]

...Table 2.1 continued

METAL	ASV*	AdCSV			LIGANDS	
		M	L	C		REF.
Palladium		X			Dimethylglyoxime	[32]
Platinum				X	Formazone	[32]
Praseodymium			X		O-cresolphthaleinthalexone	[32]
Selenium		X			Copper, DMTD	[29,31]
Silicon			X		Molybdate	[29]
Silver	X					
Sulphur	X					
Technetium		X			Thiocyanate	[32+29]
Telluride		X			Copper	[29]
Thallium	X					
Tin		X			Catechol [Sn0, SnII], Tropolone	[37,32+29]
Titanium			X		SVRS	[32]
		X		X	Cupferron (M) Mandelic Acid (M and C)	[29]
Thorium			X		Mordant Blue T	[32]
Uranium		X			Catechol, Oxime, 8-hydroxyquinoline.	[29,32,29]
			X		Mordant Blue	[32]
Vanadium		X			Catechol	[32,29]
Yttrium			X		SVRS	[32]
Zinc	X	X			Amnonium pyrrolidine dithiocarbamate, DMTD	[29,31]
Zirconium			X		SVRS	[32]

AdCSV analysis via, Metal (M) or ligand (L) reduction or via Catalytic (C) process. DMTD = 2,5-dimercapto-1,3,4-thiadiazole, MPAQ = 5 - [(*p*-methylphenyl)azo]-quinoline, PADN = 1-(2-pyridylazo) 2.7-dihydroxynaphthalene, Br-PADNm = 4-[2-(5-bromopyridyl)azo] 1,3-dihydroxynaphthalene, SVRS = solochrome violet RS. * All ASV from Reference [19].

2.5.3 Practical Considerations

Many factors need to be considered when developing and optimising adsorptive stripping schemes for single or multi-element analysis. All of the steps as outlined above need to be carefully controlled. The parameters and variables involved include concentration of the ligand, concentration of the metal (when doing simultaneous measurements), pH and buffer concentration, accumulation time, deposition potential and scan rate.[31,34,37,42] These will be discussed in more detail.

2.5.3.1 Concentration of Ligand

Generally, increases in ligand concentration lead to the formation of more metal-ligand complexes and hence an increase in adsorption. This is then reflected by an increased current response. There is, however, a point where further increase in ligand concentration brings about a levelling off, or a decrease, in current response as free ligand in solution competes for metal-ligand sites at the electrode.[37,42]

2.5.3.2 Buffer Concentration and pH

Buffer concentration affects buffering capacity and hence the sensitivity of the measurements. High buffer concentrations may lead to irreproducibility of the current response. The pH of the solution is equally important as the electrode process is pH dependant. For example, it has been observed that at low pH's the ligand, catechol, when protonated, was unable to form complexes with the metal, tin, while at very high pH's the tin ions hydrolysed[37]. Highly basic or highly acidic pH's have been shown to increase the background current[31]. Determining the optimum pH is thus important as it affects the overall hydrogen evolution[32] and hence current response.

2.5.3.3 Deposition Time

During deposition, sufficient time is required for equilibrium to be reached between adsorbed species, and species in the bulk solution. This is optimum preconcentration time, but the chosen time is a judicious choice between sensitivity and speed. Longer preconcentration times bring about greater adsorption and hence increased current response. Once saturation of the electrode has been reached, no further increase in current response, with increase in deposition time, is observed. This also serves to confirm that adsorption is involved in the electrode process.[37]

For analytes present in high concentrations, shorter preconcentration times than for weaker analyte solutions are preferred, as equilibrium between the amount of adsorbate and the bulk concentration is reached faster.

For such high concentrations of analyte, as the adsorption approaches a maximum, co-adsorption effects and interactions between adsorbed species will affect the current response negatively, bringing about a deviation from the Langmuir current-concentration linearity. So, to extend the linear range for current responses at high concentrations, shorter preconcentration times become feasible.[37]

2.5.3.4 Deposition Potential

The choice of deposition potential is critical for the adsorptive deposition of the metal-ligand on the electrode surface. Optimum potentials are generally 300-400 mV less negative than the characteristic reduction potential of the analyte. Again, this potential needs to be optimised for each system. In addition, judicious choice of the deposition potential will permit only the reduction and analysis of the metal species of choice. [37]

2.5.3.5 Simultaneous Analysis

For simultaneous analysis of trace metals, the same rules apply as for single-element analysis but here additional factors are considered. The primary consideration is that there is adequate separation between potential peaks. Reduction potentials are affected by experimental variables such as scan rate, deposition potential, pH and ligand concentration. These variables differ for each metal-ligand complex. Also of importance is: the competition between the metals for the ligand; competition of metal-ligand complexes for sites at the electrode; and the interaction between metal-ligand complexes and other co-adsorbed species (such as free ligand), at the electrode.[42]

i) *Concentration of analytes*:

A large concentration of one metal may lead to the depression of the reduction peak of another by competition for the ligand and sites at the electrode[26,34,42]. This need not necessarily apply to all systems: co-adsorption effects[42] have been observed where the reduction of one metal-ligand chelate enhances the current response of a neighbouring metal-chelate.

ii) *Rate at which equilibrium is reached*:

For simultaneous analysis the choice of deposition time must be optimised for the system as a whole. Metal-ligand complexes travel at different rates from the bulk solution to the electrode. They thus have different equilibrium constants depending on their hydrophobicity (which promotes strong and faster adsorption), their bulkiness (which retards rate of equilibrium) and also the electrostatic affinity of the complex for sites at the electrode[32]. Wang[42] showed that a nickel-mordant blue 9 (MB9) metal-complex, exhibited an increasing current response which was linear with increases in deposition time, of up to 180 seconds, while in the same solution a levelling off appeared for thorium-MB9 after only 30 seconds. It can be assumed that the thorium-MB9 complex attains a faster adsorptive equilibrium.

iii) *Scan rate*:

Gradual broadening of the peak currents may occur on increasing scan rates. This may lead to overlapping peaks in simultaneous analysis.[42]

So, for simultaneous measurements factors affecting single-element analysis apply and must be optimised accordingly for such a system.

2.5.3.6 Choice of Ligand

Looking at the function of the ligand in adsorptive stripping analysis, the most important considerations are clear. Firstly, the ligand must bind to the metal to form a metal-ligand complex, adsorb to the electrode in a non-faradaic step and then freely release the metal back into solution when the metal-ligand complex is stripped from the electrode[32]. This may be related to the structure of the ligand in terms of binding affinity and tendency to adsorb to the electrode surface[34]. Ligands suitable for adsorptive stripping schemes are characterised by the presence of aromatic rings as these readily adsorb to the electrode surface. The synthesis and design of ligands with these functional groups are a focus for enhanced sensitivity of the technique[39].

2.5.3.7 Determining the suitability of a ligand.

It must be shown that addition of the ligand brings about an enhancement in the metal current response. This not only serves as a test for the utility of the ligand but also to show the *in situ* formation and deposition of the metal-chelate complex at the electrode surface.[37]

A potential shift over either the metal or ligand reduction, is commonly observed on reduction of the metal-ligand complex. This potential shift is different for each metal with the same ligand. This shift, again, is indicative of the *in situ* formation of a metal-ligand complex. Many theories have been postulated for the potential shifts but one of the more accepted is that the shift is indicative of bond strength. The shift to more negative potentials of the metal-chelate from the ligand or the metal itself, shows that more energy is required to strip the complex than the ligand or metal alone. [37,42]

Various factors control the formation of a metal-ligand complex and its utility for adsorptive stripping schemes. These factors include steric hindrance, bond-strengths, bulkiness of the complex, stability constants, and appropriate bonding sites at the ligand. This is advantageous in simultaneous AdCSV analysis as it provides for a degree of selectivity.

Computer modelling of the possible bonding sites may be of value in pre-determining these values.

AdCSV permits the analysis of a broad range of metals and elements, organic compounds and molecules of pharmaceutical and biological interest, many of which cannot be electrolytically deposited. Of relevance then, are questions pertaining to methods for molecular recognition of these analytes and electrocatalysis of analytes which have slow electron transfer rates. These pertinent questions, are the subject matter of the field of chemically modified electrodes, the second of the techniques designed for the non-faradaic deposition of analytes.

2.6 CHEMICALLY MODIFIED ELECTRODES

The basic concept of chemically modified electrodes (CME's) is to perform the desired chemistry at the surface of the electrode via a judicious choice of reagents for the non-faradaic preconcentration of various electrolytes. A range of reagents are deliberately attached to the surface of the electrode via a number of methods with the aim of modifying the electrode to adopt the binding properties of the attached reagents, producing a chemically modified electrode. Through a judicious choice of modifiers, a few major advantages have been realised in this direction:[32]

- electrodes modified with a selectively accessible surface for improved selectivity of detection; (where the appropriate modifier may "recognise" and thus preconcentrate a specific molecule from a solution)
- improvements in sensitivity as the techniques involves preconcentration of the analyte at the electrode
- improvements in stability (using electrodes coated with polymeric layers)
- preferential deposition of analytes onto bound surface functionalities
- electrodes modified with electrocatalytic moieties and redox mediators to promote reactions which otherwise have slow electron transfer kinetics
- lowering of overpotential
- minimisation of interferences[32,43]

Preconcentration of the analyte of choice is usually via forced convection to facilitate mass transport. Similar to adsorptive stripping voltammetry, preconcentration of the analyte at the electrode surface is via non-faradaic deposition. This means that the technique is also open to analytes which cannot be electrolytically deposited. Depending on the reactivity of the modifying group, the analytes are held at the modifier by complexation, electrostatic attraction and covalent linkages.[32]

Quantitation of the analyte is subsequently carried out in the same solution or in an electrolyte solution possessing more ideal background character (also known as "medium

exchange"). The usual voltammetric waveforms, where current response is a measure of the amount of analyte preconcentrated at the modified electrode, are then produced.[32] The most common electrochemical technique employed is cyclic voltammetry.

Using cyclic voltammetry as discussed before, Section 2.2, the following information may be obtained:

- quantitative analysis, as current response is proportional to the amount of analyte preconcentrated
- establishing the mode of electron transfer and obtaining kinetic information
- qualitative analysis using specific modifiers
- determination of the amount of modifier at the electrode, as well as the amount corresponding to full surface coverage

Chemically modified electrodes add a powerful new dimension to preconcentration/voltammetric schemes. The requirements and mechanisms of such schemes outlined above, will be discussed in more detail.

The choice of modifier is perhaps the primary consideration. The affinity of the modifier for the analyte, its selectivity for that analyte from others in solution, and its ability to successfully chemically modify the electrode surface, needs to be assessed.[32]

2.6.1 Chemically Modifying the Electrode

Chemical modification of the electrode surfaces has usually been achieved by attaching appropriate reagents to conventional electrode substrates. Attachment of modifiers has been achieved via direct deposition and held at the surface by chemisorption, covalent bonding and adsorption,[44] or by electrodeposition of species onto the electrode[32,45]. An alternative approach involves mixing an appropriate reagent with the conductive particles of a carbon paste electrode or as part of an appropriate polymeric coating[44]. Variations on these methods have been reported. The variations are usually subtle improvements on

these methods and are modified to suit the particular application of the technique, under different conditions.

2.6.1.1 Chemisorption

Chemisorption is an adsorptive interaction between a molecule and a surface in which electron density is shared by the adsorbed molecule and the surface. For example, aromatic compounds are held at the electrode surface by sharing of the pi-electron density between the electrode and the adsorbate molecule. Chemisorption requires direct contact between the chemisorbed molecule and the electrode surface and so the highest coverage achieved is a monolayer. A downside is that the chemisorbed molecules tend to leach back into the solution. An example is the derivitisation of gold electrodes with thiols. Dipping the electrode into the modifier-thiol solution produces monolayers of derivatised thiols at the surface of the electrode. This technique utilises the high affinity of gold atoms for thiol groups.[45] Fig 2.11 shows how the modifier is attached to the surface of a gold electrode via the thiol groups.

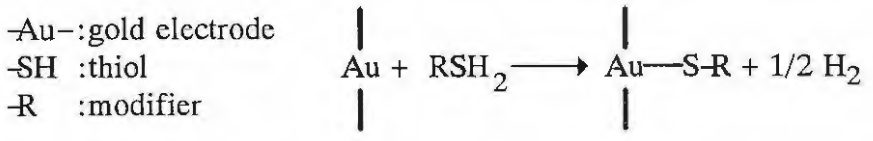

Figure 2.11 Model of chemisorption of a derivatised thiol onto a gold electrode. Figure adapted from reference 45.

2.6.1.2 Covalent bond formation

This method utilises the specific functional groups on unmodified electrodes such as COOH and OH groups on "bare" carbon electrodes. Unmodified carbon electrodes are thus not really bare due to these surface functionalities. An example is the attachment of silane to the hydroxyl groups on carbon electrodes, Fig 2.12. The silane incorporates the desired modifier and together they form a multi-molecular layer of modifier at the surface of the electrode.[45]

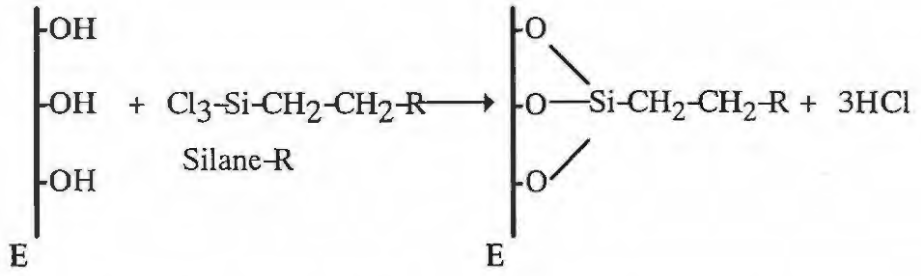

OH is hydroxyl group on electrode (E), R = the modifier attached to silane.

Figure 2.12 Model of covalent bond formation of derivatised silane onto carbon electrode. Figure adapted from reference 45.

2.6.1.3 Polymer films

Another popular route for chemical modification is incorporation of the modifier into the backbone of a polymer such as polystyrene. The derivatised polymer readily forms a film which is held at the electrode by a combination of chemisorptive and solubility effects. Multilayered, dynamic, polymer coatings provide a three-dimensional reaction zone at the electrode surface, increasing the flux of reactions occurring there, and hence increasing sensitivity. An extra dimension is added as the range of functional groups on the polymer surface present a basis for further chemical derivitisation. [32]

Polymeric films are easily prepared, with high stability and no loss of material from the electrode. The film structure and thickness have a pronounced effect on analytical performance. To achieve high sensitivity for analyte preconcentration, the polymer should permit efficient charge and mass transport, hence the film thickness must be carefully controlled[32]. The high stability of the film may be countered by a decrease in sensitivity as opposed to direct deposition of the modifier onto the electrode, as in chemisorption and covalent attachment schemes.

A range of chemical processes including ion exchange, complexation, precipitation and enzyme reactions can be carried out at polymer surfaces.[44] There are three categories:

1. redox polymers which contain the electroactive functionalities inside the main polymer chain or side groups, for example, polypyrrole.
2. ion-exchange and co-ordination polymers, containing electroactive molecules such as metals and counterions bound by co-ordination and ion-exchange reactions to the polymer, respectively, for example, Nafion®.
3. electronically conductive polymers, where the chain itself is redox active, for example, polypyrrole[46]. The polymers can be attached by dip-coating, drop-drying, spin-coating or electrodeposition[45].

2.6.1.4 Inorganic materials

Inorganic materials such as clays and zeolites are useful modifiers of electrode surfaces as they are ion-exchangers with well-defined microstructures. An advantage is that unlike the organic polymers, they can withstand high temperatures and highly oxidising solution environments. An example here is the hexacyanometallates which, when functionalised with transition metal of different formal oxidation numbers, provide catalytic properties. These materials form inorganic polymers coated as thin films on electrode surfaces. Some exhibit electrochromism, the ability to change colour on oxidation change.[45]

2.6.2 Methods of Attachment of the Modifiers

Direct deposition of the modifier can proceed via spin-coating, drop-dry or dip-coating. Dip-coating involves simply dipping the electrode surface into the modifier solution, removing and allowing the solvent to evaporate. This method is problematic as it is difficult to control the amount of modifier. The drop-dry method involves placing a measured drop of the modifier onto the surface of the electrode and allowing this to dry. This method overcomes the reproducibility deficiency of the dip-coat method. Spin-coating of the modifier onto the electrode is similar to the dip-coat method but here the electrode is mechanically spun in the solution, producing films of uniform thickness, The electrode is removed from solution and allowed to dry.

While these methods are simple and sensitive, they may be of little analytical utility if the film leaches back into solution. This may be prevented by attaching the modifier onto the electrode by means of a polymeric support. However, it has been noted that while the polymer provides a support for the modifier, preventing it from leaching back into the solution, the increase in stability is countered by a decrease in sensitivity.[47]

Carbon paste electrodes[47] are constructed by mixing the modifier with carbon paste and an oil, and incorporating this mixture into a tube to form the matrix of the electrode. Numerous agents can be inserted into the paste with no need to devise individual attachment schemes for each modifier. This is quite a versatile technique with reports of high stability, control of surface coverage, reproducibility over long periods and the availability of chemical regeneration steps to produce analyte-free surfaces after voltammetry. A further requirement of this method, is that the solubility of the modifier incorporated in the carbon paste matrix, be sufficiently low in the solvents employed, so as to prevent leaching off of the modifier[32]. While this technique affords the product of robust, polishable, chemically modified electrodes for use under harsh conditions,[43] the loss of sensitivity is quite an important consideration for highly sensitive analyses.

The attachment scheme which is the subject of much research effort is that of electrochemical deposition. The various methods of attachment of polymeric films onto electrodes have been well-characterised[44]. These studies[44] showed that significant advantages are offered when polymeric films are attached by electrodeposition. Polymeric films may be electropolymerised directly onto electrode surfaces by either repetitive cycling of the polymer or the monomer to produce the electrodeposited polymer.

Electrodeposition, to form electropolymerised films, is a simple, clean and efficient route to polymer synthesis. Using electrochemical methods, the rate and extent of the polymerisation process, as well as the chemical and physical properties of the resulting polymer, can be carefully controlled[48]. Monomers which have been attached via electrodeposition include a wide range of heteroaromatics, styrene, phenol and the

phthalocyanines[45]. The technique has found application for analysis of metals, electroinactive species and biological molecules[44].

Mechanism of Electrodeposition

Repetitive CV's of a monomer at a glassy carbon electrode produces both anodic and cathodic peak currents. Gradual increases in Faradaic current for both the forward and reverse scan with each successive cycle is indicative of its oxidative electrodeposition. Peak heights, and hence the film thickness, increase steadily initially, then gradually slow down before reaching a point without any further increase. At this point, when no further increases in peak current are observed, electrodeposition is complete, indicating that the electrode is fully coated. The film stops growing because, as the thickness of the film increases, the electronic migration rate through the film decreases, limiting further electrodeposition of the monomer.[48]

The thickness of the films formed can be controlled by controlling the number of cycles. This also provides for a measure of reproducibility for subsequent studies. The film thickness can be determined as described in Section 2.6.4.

2.6.3 Practical Considerations

2.6.3.1 Electrodes

A conventional 3-electrode system is generally used consisting of a working electrode, a reference and an auxiliary electrode. For electrodeposition, the positioning of these in the solution should be a symmetrical arrangement, to ensure even coatings. A Faraday cage usually functions better than a conventional platinum wire as an auxiliary electrode, by ensuring even coatings. A disadvantage is that large volumes of modifier are required to cover the bottom of the Faraday Cage.[44]

A range of electrode surfaces have been employed to produce CME's. The most commonly employed are glassy carbon, platinum and gold surfaces. Less commonly used

are titanium, aluminium, mild steel, brass, mercury, gold-coated plastic films, tin oxide or silver.

Glassy carbon electrodes appear to be the best in terms of a large electrochemical working range and the ease of formation of strongly adherent films, an advantage when the mode of attachment is electrodeposition.[44]

One of the requirements is that the chemically modified surface not be easily saturated with the analyte. As with adsorptive stripping voltammetry, current response may deviate from linearity at high modifier concentrations. The chemically modified surface must also be easily regenerated for further analytical measurements and not be destroyed in the reaction.[32]

2.6.3.2 Solvent and Electrolyte

Solvent:

Choice of solvent from which the modifier is deposited at the electrode, is critical. The solvent affects the morphology, conductivity and electrochemical activity of the chemically modified electrode produced. Strong bonding, for example, between the solvent molecules and the modifier will hinder the interaction between the modifier and the analyte, thus lowering the catalytic activity of the electrode. For electrodeposition of the modifier, non-nucleophilic solvents, such as acetonitrile, produce films with good conductivity. Nucleophilic species in solution tend to competitively inhibit the growth of the film.[44]

pH of solvent:

An important consideration for ensuring reproducibility and stability is the pH of the solvent as redox processes are pH dependant. Different voltammetric responses observed over the entire pH range using chemically modified electrodes may also suggest a difference in the structure of the adsorbed layers[49].

Furthermore, aggregation of the modifier at certain pH's, may affect the catalytic ability for the analyte of choice[50].

Electrolyte:

With aqueous solvents, a large number of electrolytes are available. The phosphate buffers are a popular choice. For non-nucleophilic solvents, care must be taken to choose an electrolyte that does not interfere with film formation at the electrode.[44]

2.6.4 Characterising Chemically Modified Electrodes

Cyclic voltammetry, while being the waveform of choice for analysis of the redox behaviour and quantitative determination of the species, may also be used to characterise the amount of modifier preconcentrated at the electrode surface.

For example, during electrodeposition, the area under the reduction or oxidation wave of the species coated at the electrode, represents the charge associated with the reduction or oxidation of the adsorbed species[20] according to:

$$\mathbf{Q = nFA\Gamma} \qquad \text{Equation 2-20}$$

Q = charge, C

n = number of moles of electrons transferred

F = Faraday's constant, 96 485 C/mole

A = the area of the electrode, cm^2

Γ = surface coverage, mol cm^{-2}

Q then equals the integral of the faradaic current determined from the area under the oxidation or reduction wave, depicted in Fig 2.13. Surface coverage Γ can thus be

calculated. Full surface coverage is calculated by measuring the area under the largest peak once the film stops growing.

Similarly, by repetitive cycling of the analyte at the chemically modified electrode, until no increase in cathodic or anodic waves are observed, the area under this peak can be used to determine the amount of analyte that relates to a monolayer of preconcentrated analyte.[43]

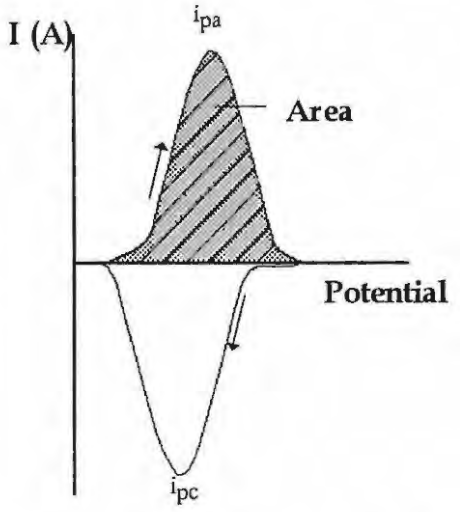

Figure 2.13 Cyclic voltammogram showing the area under the anodic wave (shaded) used to determine surface coverage.

The current response observed is thus a function of the amount of modifier at the electrode. At low scan rates and fast electron transfers, Equations 2-21 and 2-22 for current and potential, apply.[51]

$$\mathbf{I_p = 0.496\ FAC_0 D^{1/2} v^{1/2} (F/RT)^{1/2}} \qquad \text{Equation 2-21}$$

$$\mathbf{E_p = E^0 - 0.78\ (RT/F) + (RT/F) + \ln[\mathit{k}\ \mathit{l}\ \Gamma D^{1/2}\ (Fv/RT)^{1/2}]} \qquad \text{Equation 2-22}$$

with symbols as defined before in Equations 2-4, 2-5, 2-6, 2-7, 2-8 and 2-20.

2.6.5 Applications of Chemically Modified Electrodes

The chemical modification of electrodes with appropriate modifiers has found a range of applications, in electrocatalysis, in electroanalysis, electrosynthesis and energy conversion.

A useful application has been in electroanalysis of metals, using modifiers possessing specificity for the metal. The preconcentration step thus involves complex formation between the metal in solution and the ligand immobilised at the electrode. Various ligands and modification strategies have been explored for selective preconcentration of metal ions, with clear benefits for increased sensitivity. Speciation studies have benefited with this technique, utilising modifiers with a high affinity for particular metal oxidation states. An example is the ligand, sulphonated 2,9-dimethylbatho-phenanthroline for selective measurements of copper in the presence of iron. The two methyl groups of the modifier sterically hinder complex formation with iron, but not with copper. These methods have found much application for use in environmental sensors. Examples include the selective accumulation and analysis of uranium(VI) in sea water;[42] modified carbon paste electrodes for simultaneous analysis of zinc, cadmium, lead, copper and mercury using chelating resins;[52] and self-assembled monolayers of ω-mercaptocarboxylic acid on thin mercury film electrodes for cadmium analysis in the presence of organic and ionic interferences in seawater[53]. Self-assembled monolayers of thiol groups as modifiers have been incorporated with copper phthalocyanine on gold electrodes, forming stable films for selective copper analysis[54].

Chemical sensors have found wide application in determining biochemical analytes in what is known as *in vivo* voltammetry, initially introduced in 1976,[55] to monitor catecholamines. *In vivo* voltammetry is an active area of research in which miniaturised electrodes repeatedly monitor organic analytes in tissue fluid of either anaesthetised or conscious animals, circumventing the need of radiolabelled transmitter stores or killing of the animal[56]. A pertinent application for CME's is the electrochemical detection of amine-based neurotransmitters such as electroactive dopamine. This involves the surgical

implantation of electrodes into the cerebrospinal fluid of the living organism. The detection of dopamine is, however, hampered by the presence of ascorbate. Ascorbate oxidises at potentials close to that of dopamine, interfering with its *in vivo* electrochemical analysis. Since dopamine is a cation at physiological pH's and ascorbate is an anion, the problem was solved by using the cation exchange polymer, Nafion®. Nafion® coated at the electrode transports dopamine and rejects ascorbate and other acidic metabolites. Electrodes modified with Nafion® for *in vivo* analysis of dopamine and other cationic neurotransmitters, have become standard procedure for these investigations,[45,57] aimed at understanding the process of neurotransmission in the brain. Design of appropriately modified electrodes for electrochemical pre-treatment offers greater sensitivity, selectivity and minimisation of interferences, research areas of importance in the development of *in vivo* voltammetry[56,57].

Electrodes modified with deoxyribonucleic acid (DNA) have been used as sensors for DNA and haem-containing proteins such as myoglobin and haemoglobin. The DNA reportedly promotes faster electron transfer rates at the electrode surface[58]. Polypyrrole modified electrodes have been designed as sensors for proteins such as ovalbumin and myoglobin[59].

Electrocatalysis is an important application of CME's, directed at lowering overpotentials and increasing the rate of sluggish chemical reactions. Electrocatalysis may be monitored with the catalyst in solution with the analyte, known as solution-phase catalysis. Deposition of the catalyst onto electrodes to produce chemically modified electrodes are advantageous, as the method eliminates the problems associated with the introduction of solution-phase electron shuttles[60]. The use of CME's is desirable for the analysis of amino acids, proteins and small biological molecules as many of these have slow electron transfer kinetics and characteristically exhibit high overpotentials at unmodified electrodes[61].

Electron transfer between the analyte and the electrode is thus facilitated by the modifier which acts as a mediator to the reaction. These reactions may be represented by Equations 2-23 and 2-24 with M, the mediator or catalyst, and A, the analyte.

$$\mathbf{M_{ox} + ne^- \rightarrow M_{red}} \qquad \text{Equation 2-23}$$

$$\mathbf{M_{red} + A_{ox} \rightarrow M_{ox} + A_{red}} \qquad \text{Equation 2-24}$$

In Fig. 2.14 below, electron transfer occurs between the mediator immobilised at the electrode surface and an analyte with slow electron transfer kinetics. The analyte, for example, may be an enzyme which can convert a substrate into a product. The reaction between the enzyme and the substrate may be monitored at the electrode, indirectly, through electron transfer with the mediator.

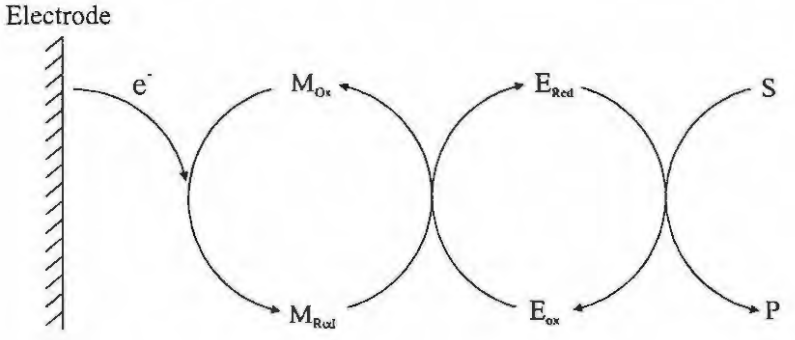

Figure 2.14 Mediated electron transfer where, M = mediator, E = enzyme, S = substrate and P, = product.

One such example of an application for biological chemical sensors is the use of enzyme based sensors which will recognise and catalyse a specific analyte, facilitating its electrochemical analysis. Glucose sensors, commercially available are designed on this premise. The design utilises the natural catalysis of glucose by the enzyme glucose oxidase, glucose oxidase being the modifier at the electrode[44,45].

Designing chemically modified electrodes for sensitive and selective analysis of biological molecules is an active area of research. Much research in this area has focused on

identifying and characterising modifiers for enhancing selectivity and sensitivity of analysis by careful attention to practicalities. These include the method of attachment of the modifier onto the electrode; its chemical state; and interaction with the analyte, solvents, electrolytes and buffers.

This research has led to new chemically modified electrodes for specific analysis with improvements over earlier methods. This level of research activity may be exemplified using the glucose sensor as an example. The use of a porphyrin modifier, chemically polymerised manganese tetrakis (*o*-aminophenyl) porphyrin,[62] has recently been shown to offer improved performance for the glucose electrode. Glucose oxidase is introduced into the polymeric porphyrin film electropolymerised onto the electrode. The polymeric porphyrin film acts as host for the enzyme and catalyses its electro-oxidation. This enhances the catalysis of glucose oxidation by glucose oxidase, extending the concentration range of the glucose sensor over that previously mentioned. Other mediators for the electron transfer between glucose oxidase and the electrode include ferrocene derivatives and benzoquinone.[63]

Metalloporphyrin modified electrodes have found wider application, as sensors for anions such as nitrites,[64] iodide and chloride;[65] in oxygen electroreduction;[66,67] for analysis of nitric oxide;[68] as pH sensors;[69] the detection of sulphide ions;[70] in solution-phase electro-oxidation of a range of molecules such as cystine, cysteine, mercaptoethanol, thioacetamide,[71] and hydrazine;[72] in electroreduction of cystine[73] and other disulphur compounds;[74] and in solution reaction with nucleic acids as means for analysis of DNA.[75] These modifiers have also found application in organic electrosynthesis in, for example, polymerisation of methacrylic esters by aluminium porphyrins.[76] Metalloporphyrins as mentioned before, have important roles in nature: in oxygen transport, storage, transfer and in respiration. They are therefore of interest as biomimetic models for enzymes, for example, catalase peroxidase[77] and are appropriate modifiers for the design of CME's geared towards understanding their natural redox and electrocatalytic mechanisms[71].

A modifier which has found much application is the metallophthalocyanines, structural analogs of the porphyrins. Indeed, the phthalocyanines have found application in designing glucose sensors, as they have been shown to catalyse the electro-oxidation of glucose oxidase. A design based on a new mediator, cobalt octaethoxyphthalocyanine, has shown high stability in this application, offering the possibility of renewable electrode surfaces. Here the mediator was incorporated into a carbon paste matrix with a polyethylene glycol modified glucose oxidase[63].

A wide range of phthalocyanines incorporating different metal centres have been the subject matter of much research. Their catalytic activity for a host of molecules of biological interest and their natural tendencies to adsorb onto electrode surfaces[48], predisposed their utility as modifiers at electrode surfaces. The phthalocyanines and their role in electrocatalysis of small biological molecules are discussed in relation to their application towards chemically modified electrodes in chapter 4. Chapter 4 examines the utility of the phthalocyanines as modifiers for analysis of cysteine.

Chemical modification of electrodes thus provides a different approach to obtaining both quantitative and qualitative information about electroactive species. Much research effort is thus involved in practical applications of this field of electrochemistry, particularly as sensors for analytes of environmental and biological interest such as proteins and amino acids. Design of CME's is an important field in electrochemistry; the development of which has clear benefits for both the biological and physical sciences.

Chapter Three

Heavy Metal Analysis via Adsorptive Stripping Voltammetry

3.1 INTRODUCTION

Metals and inorganic salts have been used medicinally for centuries. The Egyptians are believed to have used copper to sterilise water around 3000 B.C. By the Renaissance, mercurous chloride was used as a diuretic, arsenic for the treatment of syphilis and gold cyanide for tuberculosis. Many of these ancient inorganic drugs are still in use today but fortunately their toxicity is appreciated and accounted for. Electrochemical and spectroscopic techniques such as multinuclear nuclear magnetic resonance (NMR) spectroscopy are used in conjunction with modern medicine to identify target sites and ligands in an effort to understand the biological action of useful but potentially harmful inorganic drugs and to control their fate within the body. Examples of modern drugs containing a metal or inorganic salt as the active ingredient include Auranofin (containing gold) for treatment of arthritis, Denol (bismuth) as an antacid, Cisplatin (platinum) in tumour therapy and various preparations containing lithium for the treatment of manic depression.[6]

Adsorptive cathodic stripping voltammetry (AdCSV), as described in Section 2.5, provides a technique for metal analysis and can also provide information on the type of ligand which such metals bind. An example where this type of information about metal-ligand interaction may be of medicinal value is in the administration of EDTA, used to chelate overdoses of iron (III).

The development of adsorptive stripping schemes for metals has focused on the design and utilisation of synthetic ligands for the quantitative determination of metals which present problems in other analytical techniques. Common techniques such as atomic absorption spectroscopy (AAS), which has dominated the field of metal analysis, NMR, neutron activation, and electrochemical techniques such as anodic stripping voltammetry (ASV), all have limitations with particular metals. For example, arsenic, antimony, bismuth and gold are difficult to study in solution by NMR, as none of them have observable isotopes. However, as the above are redox active analytes,[6] electrochemical methods can be used for their study, and AdCSV has been found particularly effective in this respect.

3.1.1 Overview of Non-Electrochemical Methods for Elemental Analysis

Atomic absorption spectroscopy is used for the quantitative and qualitative analysis of about 70 elements. There are different types of AAS based on the excitation source employed, e.g. a flame or graphite furnace. AAS utilises single element hollow cathode lamps for the determination of a range of toxic heavy metals. AAS has been the technique of choice in the past for the environmental analysis of heavy metals, for example in slaughter animals as indicators of environmental overload.[10,78,79] While the technique is useful for the quantitative and qualitative determination of a wide range of elements, it excludes metals which cannot be reduced to an atomic vapour, e.g. tungsten, elements emitting in a vacuum, and artificial elements.

A major advantage of AAS is the amount of research that has gone into optimising the technique, so that problems that do exist have been well characterised and may be controlled.

The sensitivity of flame AAS is impaired at concentrations below the mg/ml range, where the precision becomes lower. For analysis at lower concentrations, furnace AAS is often chosen, with sensitivities in the mg/l range. In furnace AAS, better control of the amount of analyte transferred to the flame by the nebuliser is offered, as the entire analyte is converted into an atomic vapour. Furnace AAS has a major disadvantage in being

essentially a single element technique and may therefore be time-consuming, as each determination requires two to four minutes.[80] For multielement analysis[81], inductively coupled plasma emission spectroscopy is the technique of choice. It is often more rapid than furnace AAS but is more expensive and requires higher operator skill.

Another popular technique for heavy metal analysis is neutron activation. In neutron activation, samples and standards are irradiated with thermal neutrons produced in a nuclear reactor. Characteristic gamma and X-rays are emitted by the radioactive isotopes which are produced and these are characterised by number and energy to determine the concentration of the element of interest. It has an advantage in biomedical multi-trace element analysis as no pre-treatment of sample is necessary. A disadvantage is the cost of the sophisticated equipment required for irradiation and analysis. Time is also a constraint as there is often a long delay in analysis, especially of elements with long half-lives, where delays of up to two weeks may be experienced.[82]

The developing field of electroanalytical chemistry circumvents many of the shortcomings of non-electrochemical methods, offering many advantages, as discussed further.

3.1.2 Electrochemical Methods in Analysis

The electrochemical technique, stripping voltammetry, has developed into a useful analytical tool for elemental analysis. The current signal in electrochemistry is very sensitive, meaning that analyte concentrations as low as the picomolar range can be detected. Highly sensitive quantitative analysis is possible as the current response is proportional to analyte concentration. The quantitative relationship between current and concentration, especially when diffusion controlled, may be calculated simply from first principles and is generally not affected by minor changes in experimental conditions. In addition, by measuring current as a function of potential, qualitative information about the analytes may be obtained. This allows for analysis of unidentified substances. One major advantage is that the amount of charge passed and hence the amount of material converted in a typical voltammetric experiment is so small, that it is a non-destructive technique.

The various forms of stripping voltammetry, cathodic stripping voltammetry (CSV), ASV and AdCSV provide a technique for sensitive analysis of at least 36 trace elements, as shown in Table 2.1. These techniques, discussed in Sections 2.4 and 2.5, provide additional information over AAS. These include oxidation state discrimination of the analytes, selective analysis in the presence of other elements and the study of analyte interactions with various ligands.

Voltammetry is essentially a multielement technique. It is thus of particular benefit in heavy metal studies.[83]

Stripping analysis offers elemental analysis for a range of samples sources of environmental,[29,33] industrial and pharmaceutical origin, in foodstuffs and even in gunshot residues[19]. With such a broad scope of sample sources, it is advantageous that the technique requires little sample pre-treatment. For example, for research in lead analysis in petrol[84], voltammetric procedures showed improvements in terms of the reduced sample pre-treatment required, as opposed to techniques such as AAS.

Electrochemical sensors based on stripping potentiometry have been designed for field study, the advantages over AAS being on-site monitoring, for example, in groundwater tests for heavy metal pollutants (Hg, Pb, Se, Cu). Data obtained from on-site analyses provide sensitive, reliable results, uncomplicated by both the time delay and possibility of sample decay, during transport for laboratory analysis of samples[85]. An apparent advantage is the low cost of this technique over the expense of traditional AAS laboratory analysis. New designs have produced disposable screen-printed carbon strip electrodes for analysis of blood lead and mercury, offering remote, simplified, low-cost, sensitive elemental analyses[36,86].

A major interlaboratory study ranked stripping analysis above spectroscopic methods for blood lead analysis in terms of overall reliability[36]. AAS analysis of lead in biological tissue was shown to suffer interference from cadmium and bismuth due to competitive

binding with the chelator[87]. Simultaneous ASV and AdCSV methods may overcome these interferences[34].

Stripping voltammetry has subsequently been recognised by the United States government as a useful tool for trace metal analysis.

The many advantages of AdCSV over conventional ASV have been discussed in terms of sensitivity and the degree of selectivity in trace metal analysis. Much research in metal speciation is prompted by environmental concerns and the need for highly sensitive, selective and efficient systems. There has thus been a need to develop ligands that may increase the sensitivity and selectivity of metal ion determination[34,39]. AdCSV is showing much progress in this field[88] and is the electrochemical tool of choice for this research.

3.2 AIM OF RESEARCH

The aim of this research was to examine a) the utility of catechols as ligands for a group of metals in their analysis via AdCSV and b) the utility of the catechol ligands for the development of simultaneous metal analysis schemes. Catechol (1,2-dihydroxybenzene) has been used successfully in the adsorptive stripping determination of many metals including Cu, Ge, Sb, Fe, U, V and Sn[29,37]. Here the use of the catechol ligand via AdCSV provided improved copper analysis over conventional stripping schemes, where the copper oxidation wave suffered interference from mercury[89].

Catechols are a versatile electroactive species. Recently, their polymerisation onto electrode surfaces have been shown to be effective electrode modifiers for mediating electron transfer between the oxidised and reduced forms of nicotinamide adenine dinucleotide (NAD^+ and NADH, respectively). Further functionalisation of the polycatechol films with amines or enzymes is possible, making these films useful as redox mediators for other enzyme catalysed reactions[90]. The catechol groups of naturally occurring siderophores such as enterobactin are known to sequester and scavenge iron(III) ion. Analogues of the catechol units have been designed with a view to use as iron-sequestering agents in human iron overload owing to their high kinetic stability[91].

Physiologically important polyhydroxyaromatics include the catecholamines, 3,4-dihydroxyphenylalanine (Dopa) and dopamine and the catechol-estrogens. Polyhydroxyaromatic compounds such as catechol and 1,4 hydroquinone auto-oxidise to generate the oxygen free radical which induces DNA strand breaks. This effect is promoted in the presence of transition metals such as Cu^{2+}which are known to induce DNA damage by the Fenton reaction. Nitric oxide may synergistically enhance the DNA damage caused by these polyhydroxyaromatic compounds and hence tissue damage, contributing to neurodegenerative diseases such as Parkinson's Disease. In these studies[92] it was shown that the polyhdroxyaromatic compounds, guaicol (O-

methylcatechol) and resorcinol (1,3-dihydroxybenzene) which do not generate the dioxygen radical, do not induce DNA strand breakages. It was also shown that nitric oxide dose-dependently inhibits the strand breakages mediated by the polyhdroxyaromatic compound and copper or by the Fenton reaction.[92]

Catechols are of further interest in biochemistry in their ability to bind copper. Cu^{2+} catalyses the oxidation of low or high density lipoproteins. Catechol estrogens have recently been shown to be more potent antioxidants than estrogens for this Cu^{2+} catalysed oxidation[93]. Catecholamines also reportedly enhance the inactivation of the enzyme dihydrolipoamide dehydrogenase, offering protection as a copper chelator[94].

In these studies, the effect of different ring substituents on catechol were examined for their role in promoting the utility of catechol as a ligand for metal analysis. Comparisons were thus made between catechol, 4-methylcatechol, 4-t-butylcatechol and resorcinol as ligands. Structural representation of these ligands, Fig. 3.1, show this structural similarity, but with different ring substituents.

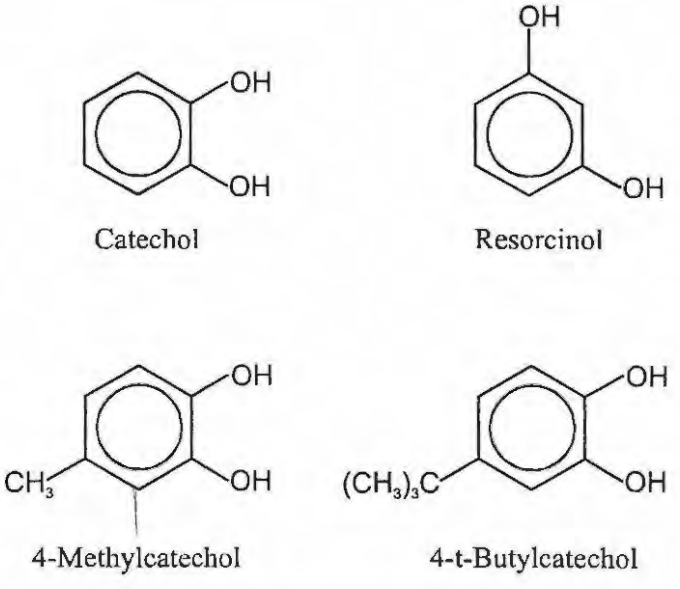

Figure 3.1 Structural representation of the catechols.

The metals chosen for analysis via this adsorptive stripping scheme were lead, copper, cadmium and bismuth. Lead, cadmium and bismuth are all classified as toxic metals while

copper is an essential element, only toxic when its concentrations in living organisms are unbalanced. They are of biological interest due to their possible binding to thiolate ligands to form metal-thiolate clusters[95]. They have all been studied via both anodic stripping and adsorptive stripping schemes as shown in Table 2.1. The exception is bismuth where studies have concentrated on its anodic stripping analysis in the presence of HCl[96]. These researchers[96] experienced problems with the overlap between bismuth and copper, making the simultaneous ASV analysis of these two metals unsuitable. No AdCSV schemes have been shown for simultaneous analysis of bismuth and copper. The simultaneous analysis of not only copper and bismuth, but lead and cadmium, are explored in this research.

In these studies bismuth was examined for the first time in the presence of ligands containing aromatic rings. No research to date shows the use of the substituted catechol derivatives as chelating ligands for adsorptive stripping schemes for any of these metals.

The use of a mercury film glassy carbon electrode (MFGCE) as the working electrode for adsorptive stripping measurements was also explored in this work. The HMDE is the electrode of choice in most AdCSV experimental work as it offers the possibility of renewing the surface of the electrode, allowing repetitive measurements at fresh surfaces. The HMDE has the disadvantage of cost and blockages of the capillary. Rotating mercury coated electrodes have been used successfully in AdCSV.[19,37] The use of the MFGCE is not common. Previous experimental work showed MFGCEs coated with Nafion®, incorporating suitable chelating agents for the detection of metals such as lead [97]. A rotating MFGCE has also been previously described for analysis of tin by adsorption with catechol. These researchers[42] commented that the use of a HMDE is unfavourable for on-site work in flowing solutions as the electrode is not convection stable. A MFGCE was thus a better option and comparative studies utilising the HMDE showed the former to provide enhanced sensitivity[42]. Mercury film on glassy carbon strips have been used for on-site monitoring of lead by adsorptive stripping voltammetry with 0-cresolphthalexin, the advantage being the low-cost (indeed, it is disposable), ease of preparation and the added advantage of decentralised testing. Examining further the utility of MFGCE is of

benefit towards related testing for on- site analysis[36]. The main disadvantage of MFGCE is that the electrode activity is affected by deposited complexes that may not have been removed during the stripping step. Immersion of the electrode surface after each scan, in acid, will readily remove some complexes[97]. Glassy carbon electrodes were readily available and the use of MFGCE was further explored in this research, in developing AdCSV schemes for metal analysis.

3.3 EXPERIMENTAL

3.3.1 Reagents

Triply distilled deionised water was used in the preparation of all solutions. Sodium acetate (0.1M) buffer solution of pH 4.4 was used for all electrochemical measurements. This was prepared from stock solutions of 0.2M acetic acid and 0.2M sodium acetate.

A stock mercury solution (1000μg /ml), used as an electrolyte in electrochemical measurements, was prepared by dissolving 1g $HgCl_2$ (PAL chemicals) in 0.1M HCl and then made up to volume with water. All stock metal solutions prepared were 500ppm. Solutions of $CuSO_4$ (PAL Chemicals) and $CdSO_4$ (Merck) were prepared by dissolving 0.5g of each salt in 50ml of 0.5M HCl before being made up to volume with water. HCl (32% assay) was required as a solvent as it prevents the metals from precipitating. $Pb(NO_3)_2$ (NT Chemicals) was only sparingly soluble at this concentration of HCl, so was subsequently dissolved in 100ml of 1% HNO_3. BiI_3 (Merck) presented the most difficulty in dissolving as it was only sparingly soluble in a range of acids at different concentrations of HCl, HNO_3, and H_2SO_4. The best solvent appeared to be 50ml of 0.5M HCl used for $CuSO_4$ and $CdSO_4$. Most BiI_3 precipitated out of solution. The dissolved portion was filtered and separated from the bulk solution and its concentration determined by titration with EDTA (Holpro). A xylenol orange/KNO_3 indicator was used, according to standard procedures[98]. The concentration was found to be 9.58×10^{-5}M.

0.1M solutions of the chelating ligands were prepared fresh daily and kept in the dark until required. Appropriate amounts of catechol, 4-t-butylcatechol, resorcinol (all from Aldrich Chemicals) and 4-methylcatechol (Fluka Chemicals) were dissolved in and made up to 10ml volumes with water.

3.3.2 Apparatus

Stripping voltammograms were obtained with the Bio Analytical Systems (BAS) CV-50W voltammetric analyser. All electrochemical measurements were carried out under an inert nitrogen atmosphere in a C2 cell stand. Nitrogen gas was dried by passing it over anhydrous copper sulphate. Forced convection when required during experiments, was achieved through a magnetic stirring bar controlled by the stirring function of the C2 cell stand. Electronic spectra were recorded with a Cary 1E ultraviolet-visible (UV-Vis) spectrophotometer.

A conventional 3-electrode system was utilised. A glassy carbon electrode (GCE) with a 3mm diameter filmed with mercury *in situ*, was used as the working electrode, a platinum wire as the auxiliary electrode and a Ag/AgCl electrode ([KCl = 3M]) as the reference electrode.

All glassware was thoroughly washed in hot soapy water, rinsed with copious amounts of deionised water and allowed to soak in a dilute HCl acid solution to free the glassware of adsorbed metals. The glassware was rendered acid free by rinsing and soaking in deionised water.

Stringent methods were also employed for cleaning of the electrodes. The glassy carbon electrode was first rinsed in distilled deionised water, its surface scrubbed on an alumina polishing pad and soaked in a dilute HCl solution followed by thorough rinsing with water and the buffer solution. The last three steps were adequate for cleaning the GCE between experiments. The platinum wire, after rinsing in water was also soaked in the acid solution and thoroughly rinsed with water. The acid sensitive membrane of the Ag/AgCl electrode was subjected to thorough rinsing in water and when required, the KCl solution inside replaced. This was particularly important in between experiments where different metals were used.

3.3.3 Methods

The required volume of metal solution was placed in a glass cell containing 10ml of pH 4.4 acetate buffer, 100µl of 1000µg/ml $HgCl_2$ solution and at least 100µl of the chelating ligand (optimum ligand concentrations determined separately). The whole solution was deaerated for 5 minutes by bubbling nitrogen through slowly. The metal-ligand complexes are expected to form during this time, hence the deaeration time is called the accumulation time.

For the technique used, adsorptive stripping voltammetry, the wave-form of choice linear sweep stripping voltammetry (LSSV), was selected. The appropriate parameters: deposition time, deposition potential, scan rate and potential range are selected accordingly. A scan rate of 100 mV s^{-1} was used throughout. The other parameters, once optimised for each of the metals, were then applied.

The solution was stirred, for a set time (deposition time) and a set potential (deposition potential) allowing for the formation of the mercury film onto the GCE and the adsorption of the metal-ligand complex onto the mercury film. Instead of bubbling with nitrogen gas, the solution was blanketed with a nitrogen flow during the deposition. Following a 15 second rest period allowing for the solution to settle, the voltammogram was recorded from the deposition potential to -1.0 V *vs* Ag/AgCl at 100 mV s^{-1} during the stripping step. Electrons produced as the metal-ligand is stripped from the electrode generates current, recorded as a function of potential by the computer. In order to ensure that all of the metal-ligand complex was removed from the glassy carbon electrode before the next AdCSV scan, the MFGCE was immersed in 2 mol dm^{-3} HCl for 30 sec then rinsed in the acetate buffer. This procedure was adequate for the removal of any deposit on the electrode, and resulted in good reproducibility (within 5% standard deviation) of the voltammetric responses for each solution.

In obtaining standard curves of current response versus concentration for each metal, a standard approach was used. To ensure cleanliness of the solutions and to determine

background interference due to contamination, baseline measurements were first taken of a) the buffer solution, b) buffer solution plus mercury electrolyte and c) buffer solution, electrolyte and chelating ligand. Furthermore, to prove the utility of the ligand, current measurements with all other reagents in solution, including the metal of interest, are taken before addition of the ligand. An enhancement in current response of the metal peak and or a shift in potential should be observed on addition of the ligand.

At increasing metal concentrations, standard curves of metal concentration versus current were produced for each metal in the concentration range 5 to 30 μg/ml with each of the ligands chosen. From these standard curves, comparisons of the utility of the different metal-ligand interactions could be made. The best ligand for each of the metals could be gauged, and at the same time the comparisons of the utility of the ligands themselves could be made.

For simultaneous metal analyses, optimum conditions for this system: accumulation time, deposition potential, deposition time and ligand concentration were determined by keeping all other conditions constant and only varying the parameter to be optimised.

3.4 RESULTS AND DISCUSSION*

3.4.1 Optimisation of Parameters

Accumulation time, deposition time and deposition potential were optimised for the adsorptive cathodic stripping voltammetry of Cu^{2+}, Pb^{2+}, Bi^{3+} and Cd^{2+} with each of the ligands. The concentrations of the various ligands for each metal and of the metals for each ligand were also optimised.

The deposition potentials were determined for each metal by keeping constant all the other variables such as the concentrations of the ligand (0.001 mol dm^{-3}), metal (5 ppm) and $HgCl_2$ (10ppm), and the deposition and accumulation time, while varying the potential. The highest current response versus potential applied was used as the measure of assessment of the optimum deposition potential. The deposition time and ligand concentration were optimised similarly, by keeping the other variables constant. Optimum deposition time chosen was a compromise between current response and speed.

Fig. 3.2 a) shows the optimisation for the deposition potential of the Pb-resorcinol complex. The optimum deposition potential of -0.10 V *vs* Ag/AgCl was obtained for lead, being the potential at which the highest current response for lead was observed. The optimum deposition potentials for copper, cadmium and bismuth, were 0.20 V, 0.40 V and -0.10 V, respectively, also shown in Fig. 3.2. These deposition potentials were then used for subsequent measurements.

---

* The following publication resulted from this work. For the sake of continuity, it is not referred to further in this chapter. J.Limson and T.Nyokong, Substituted catechols as complexing agents for the determination of bismuth, lead, copper and cadmium by adsorptive stripping voltammetry, *Analytica Chimica Acta*, **1997**, *344*, 87-95.

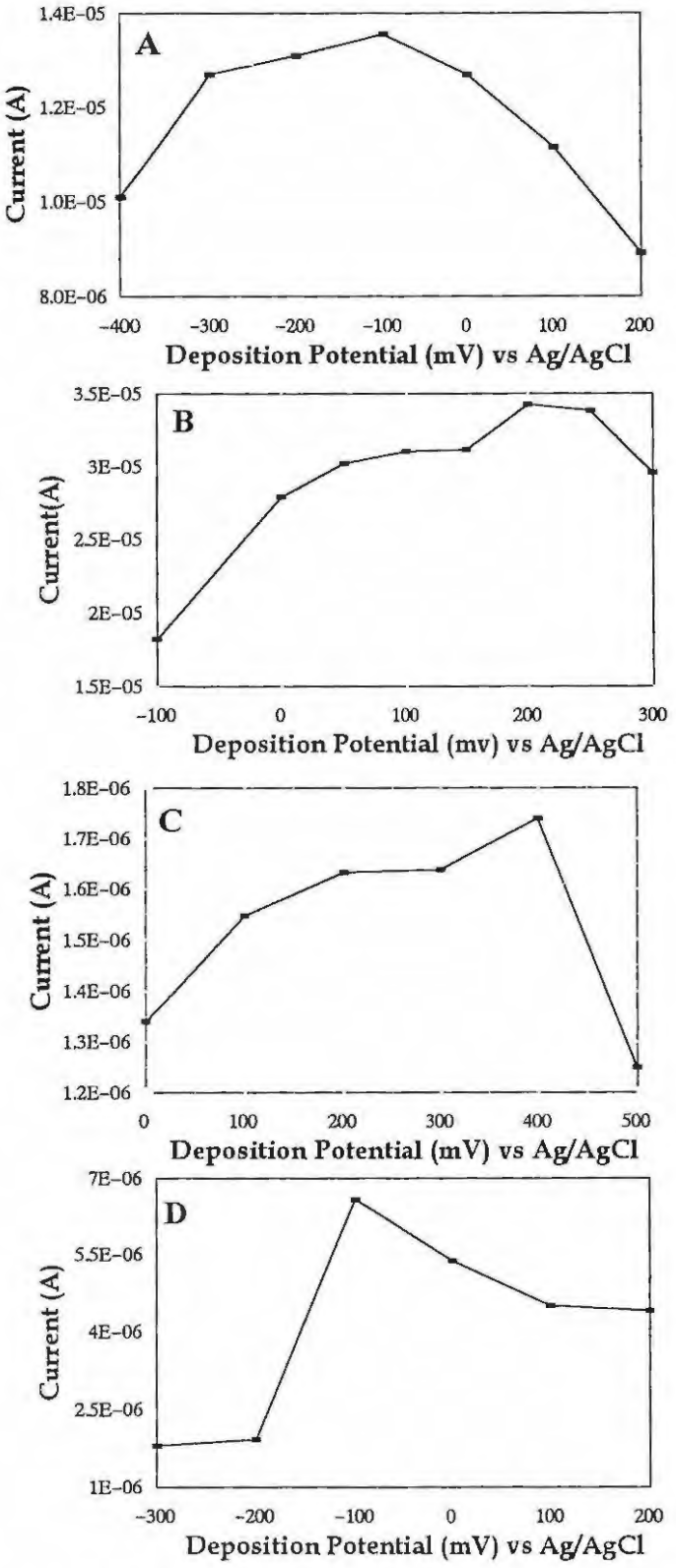

Figure 3.2 The dependence of AdCSV peak currents on the deposition potential for a) Pb^{2+} (5ppm) with resorcinol (0.001 mol/), b) Cu^{2+} (20ppm) with 4-methylcatechol (0.001 mol dm^{-3}), c) Cd^{2+} with 4-t-butylcatechol (0.001 mol dm^{-3}) and d) Bi^{3+} (4.8 ppm) with resorcinol (0.001 mol dm^{-3}). Scan rate = 100 mV s^{-1}.

The time required for the deposition of the metal-chelate complex onto the electrode depends on the concentration of the complex, with less time required for higher concentrations and longer times for lower concentrations. Ligand concentrations that are higher than required may cause inhibition of the metal-chelate adsorption by a competitive coverage of the free ligand[42].

A rapid increase in the stripping peak current with deposition time was observed for all the metal-ligand complexes. The increase was nearly linear at low deposition times. As is expected for adsorption processes, the dependence of the peak current on the deposition time is limited by the saturation of the electrode, resulting in the current reaching a plateau at high deposition times as shown in Fig. 3.3 a) for the Cu-resorcinol complex. When resorcinol was employed as a ligand, a levelling of current was observed at deposition times greater than 200 sec, for all the metals. On the basis of this observation, a deposition time of 180 sec was employed for all subsequent adsorptive stripping voltammetry measurements. Fig. 3.3 b), c) and d) is representative of the current response with deposition time for other metal-ligand complexes.

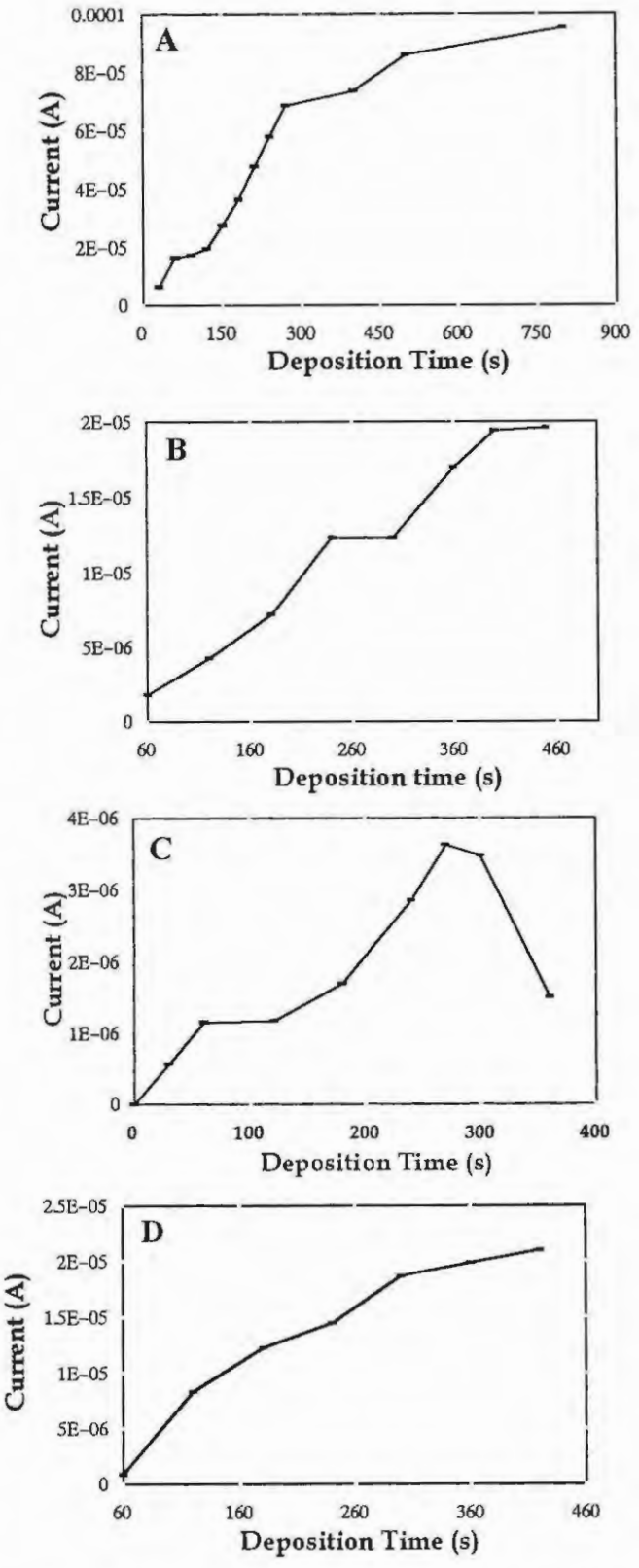

Figure 3.3 The dependence of AdCSV peak currents on the deposition time for a) Cu^{2+}(25 ppm) and 0.005 mol dm^{-3} resorcinol, b) Pb^{2+} (5ppm) and 0.001 mol dm^{-3} 4-methylcatechol, c) Cd^{2+} and 0.001 mol dm^{-3} 4-t-butylcatechol and d) Bi^{3+} and catechol. Scan rate = 100 mV s^{-1}.

Optimisation of the accumulation time was carried out similarly. As with the deposition time, long accumulation times bring about the formation of more metal-ligand complexes, and hence higher current responses. Shorter accumulation times are preferred at high analyte concentrations, so that the electrode is not easily saturated, while longer times are preferred at low analyte concentrations to enhance sensitivity. In terms of sensitivity and speed, an accumulation time of 5 minutes was the optimum time determined and used in all analyses.

3.4.2 Adsorptive Cathodic Stripping Voltammetry of Individual Metals.

Figures 3.4 (a-d) show the adsorptive cathodic stripping voltammogram of Pb^{2+}, Cu^{2+}, Cd^{2+}, and Bi^{3+}, respectively, obtained in the absence and presence of the ligands, catechol, 4-methylcatechol, 4-t-butylcatechol and resorcinol. No voltammograms were obtained for the ligands alone in the absence of the metals. As Figures 3.4 (a-d) show, addition of the ligands to solutions of Cu^{2+}, Bi^{3+}, Pb^{2+} and Cd^{2+}, result in the enhancement of the reduction peaks. This enhancement of the metal reduction peak is an indication of the *in situ* formation and deposition of metal-ligand complexes at the electrode. The voltammetric response of surface confined species is directly related to their surface concentration and at low adsorbate concentrations, the surface concentration is directly proportional to the bulk concentration[42]. For uncomplexed and complexed bismuth, voltammograms showed two cathodic peaks. The more intense peak located at more negative potentials, was used for the determination of peak potentials. The origin of the second peak is not known. This peak may be due to some impurities in the Bi^{3+} solution. Bi^{3+} ion is known to undergo a one-step, three electron reduction to the metal.

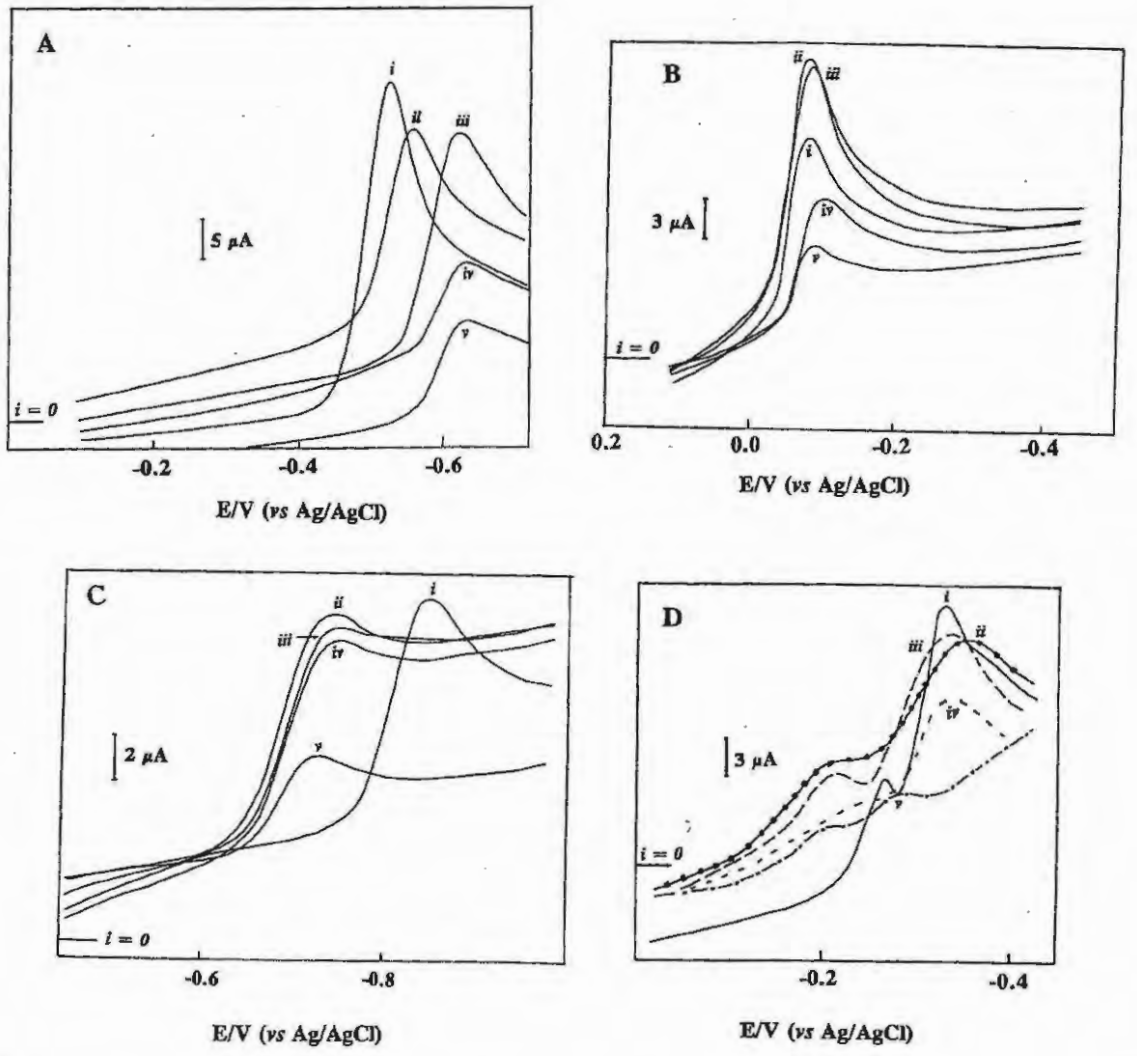

Figure 3.4 Adsorptive cathodic stripping voltammograms obtained on GCE for (a) Pb^{2+}, (b) Cu^{2+}, (c) Cd^{2+} and (d) Bi^{3+} in the presence of (i) resorcinol, (ii) catechol, (iii) 4-methylcatechol and (iv) 4-*tert*-butylcatechol. Curve (v) is the adsorptive cathodic stripping voltammogram of the metals in the absence of ligands. Concentration of metal solutions, 5 ppm and ligands, 0.001 mol dm^{-3}. Scan rate = 100 mV s^{-1}.

3.4.3 Potential Shifts

Table 3.1 lists the shifts in the peak potentials for the reduction of the metals, ΔE_p, on addition of ligands. The magnitude of ΔE_p is expected to depend on the stability of the metal-ligand complexes.

Table 3.1 Parameters obtained for adsorptive cathodic stripping voltammetry of copper, lead, cadmium and bismuth.

Metal	Ligand	Slope[a] ($\mu A/\mu g ml^{-1}$)	E_p (V) vs Ag/AgCl	ΔE_p[b]
Copper	None		- 0.084	0.00
	Catechol	1.93	- 0.076	+ 0.08
	Resorcinol	2.28	- 0.075	+ 0.09
	4-methylcatechol	1.98	- 0.080	+ 0.04
	4-tert-butylcatechol	1.22	- 0.098	-0.14
Lead	None		- 0.62	0.00
	Catechol	2.30	- 0.56	+ 0.06
	Resorcinol	3.35	- 0.52	+ 0.10
	4-methylcatechol	1.11	- 0.62	0.00
	4-tert -butylcatechol	0.51	- 0.63	- 0.01
Bismuth	None		- 0.29	0.00
	Catechol	2.13	- 0.35	- 0.06
	Resorcinol	5.03	- 0.32	- 0.03
	4-methylcatechol	2.59	- 0.33	- 0.04
	4-tert -butylcatechol	4.22	- 0.31	- 0.02
Cadmium	None		- 0.72	0.00
	Catechol	0.82	- 0.72	0.00
	Resorcinol	0.93	- 0.84	- 0.12
	4-methylcatechol	1.32	- 0.73	- 0.01
	4-tert -butylcatechol	0.40	- 0.73	- 0.01

[a] Slope of the plot of adsorptive cathodic stripping voltammetry currents (in μA) versus concentration of the metal in $\mu g\ ml^{-1}$. [b] The difference between the peak potentials of the uncoordinated metal and metal-ligand complexes.

Table 3.1 shows that for copper, the complex with 4-*tert*-butylcatechol gave the largest ΔE_p, hence implying that this complex is the most stable of all the Cu-ligand complexes under discussion. The ΔE_p values for the other copper complexes were relatively smaller than that for the 4-*tert*-butylcatechol complex. There was, however, spectroscopic evidence for the formation of a Cu-resorcinol complex, while there was no spectroscopic evidence for the formation of Cu-4-*tert*-butylcatechol, Cu-catechol or Cu-4-methylcatechol complexes. When Cu^{2+} was added to solutions of resorcinol in pH = 4.4 acetate buffer, slight shifts in the electronic absorption spectra of the ligand were observed, Fig. 3.5. Such shifts in the spectra are associated with the formation of a complex between copper and resorcinol. Addition of Cu^{2+} to catechol, 4-methylcatechol or 4-*tert*-butylcatechol resulted only in the decrease in the absorption peak due to the ligand with no significant wavelength shift.

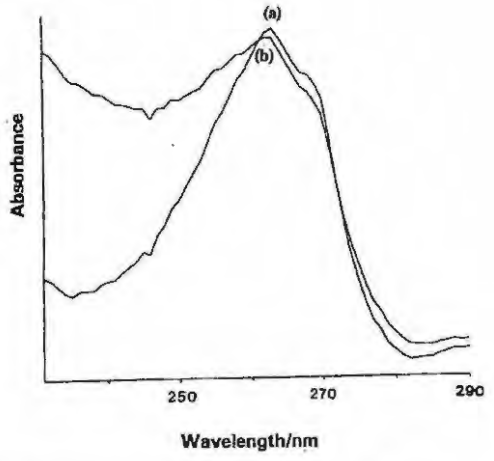

Figure 3.5 The electronic absorption spectral changes observed when Cu^{2+} (5 ppm) was added to solutions of resorcinol (0.001 mol dm^{-3}) in pH 4.4 acetate buffer; (a) spectra of resorcinol and (b) spectra after addition of Cu^{2+} to (a).

The electron-donating ability of the methyl groups of 4-*tert*-butylcatechol are expected to increase the electron density on the ligand compared to the catechol ligand. This would increase the ligand to metal charge transfer, resulting in a stronger metal-ligand bond. The resulting complex requires greater energy to reduce and to free the metal.

The large negative shift in the reduction potential on co-ordination of 4-*tert*-butylcatechol is thus indicative of a strong bond with copper, reflecting the difficulty in reducing the

complex as compared to the reduction of the free metal. It was mentioned before, Section 2.5.3.6, that an appropriate ligand, while binding to the metal freely in solution, should also free the metal easily during the reduction step. 4-*tert*-butylcatechol would thus be unsuitable under these criteria. It may, however, be of benefit in complexing and analysing copper competitively in media where natural ligands are present. A positive ΔE_p indicates the ease of reduction of the other Cu-ligand complexes as compared to the 4-*tert*-butylcatechol complex. As shown in Table 3.1, the most positive ΔE_p for copper-ligand complexes, was with resorcinol and catechol, followed by 4-methylcatechol and a negative shift with 4-*tert*-butylcatechol. This order may be explained by the relative bond strengths of the Cu-ligand complexes, as resorcinol $\cong$ catechol<4-methylcatechol and<4-t-butylcatechol. This is in keeping with the theory of a stronger bond between metal and increasingly negatively polarised ligands. This order also applies for lead-ligand complexes except that the complex with 4-t-butylcatechol with lead is not as stable as that for copper-4-t-butylcatechol, as indicated by the potential shifts.

The Cd^{2+} resorcinol complex showed a large negative ΔE_p value compared to the other Cd-ligand complexes, Table 3.1, implying that Cd^{2+} forms a relatively stable complex with resorcinol. Comparatively small ΔE_p values were observed for all the Bi-ligand complexes, making the comparison of the relative stability of the complexes difficult.

Table 3.1 also gives the slopes of the plots of the dependence of AdCSV currents on metal concentration, discussed further in Section 3.4.4. The slopes are representative of the sensitivity of the ligands to the various metals. In general, bismuth-ligand complexes produced the largest slopes of the metal-ligand complexes. Cadmium-ligand complexes showed the lowest slopes, indicating that cadmium has a lower affinity for these ligands than the other metals. This may be accounted for by the HSAB theory. From Table 1.1, page 3, copper, bismuth and lead are classified as borderline acids with a preference for either hard or soft bases. Cadmium is a soft acid and as such, a preference for borderline or soft bases is expected. The hydroxyl group, where the metal-ligand interaction is expected to occur on the ligands, is a hard base. This may explain the lower slopes observed for cadmium with these ligands. For Bi^{3+}, Pb^{2+} and Cu^{2+}, the resorcinol

complexes showed higher slopes than the other ligands. Using the slopes as criteria for the sensitivity of the ligands for metal detection, it is concluded that resorcinol is more sensitive than the other ligands for the detection of Bi^{3+}, Pb^{2+} and Cu^{2+}, whereas, 4-methylcatechol is more appropriate for the detection of Cd^{2+}.

Based on the current responses and the slopes of the standard curves for the metals, Table 3.2 gives a simple representation of the order of preference for each of the metals with the ligands.

Table 3.2 Respective metal preference for ligands.

	catechol	**resorcinol**	**4-methylcatechol**	**4-t-butylcatechol**
cadmium	3	2	1	4
copper	2	1	2	3
bismuth	2	1	2	3
lead	2	1	3	4

Decreasing order from 1 to 4. A repeated number means a similar preference.

3.4.4 Current *vs* Metal Concentration

Adsorptive stripping voltammograms were obtained for copper, lead, cadmium and bismuth at increasing concentrations for each of the chelating ligands: catechol, resorcinol, 4-methylcatechol and 4-*t*-butylcatechol. Fig. 3.6 shows the adsorptive cathodic stripping voltammograms obtained at increasing concentrations of copper with 4-methylcatechol. The current responses measured at each concentration was used to create a plot of current *vs* concentration for each of the metal-ligand complexes.

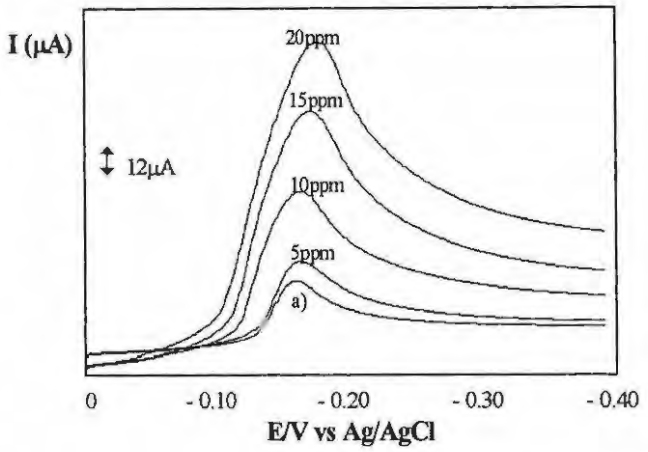

Figure 3.6 AdCSV obtained on GCE for increasing concentrations of copper with 0.001 mol dm^{-3} of 4-methylcatechol. [Cu^{2+}], 5 to 20ppm; a) 5ppm Cu^{2+}, no 4-methylcatechol. Scan rate = 100 mV s^{-1}.

The plots of metal concentration against current response for the four ligands (kept at constant concentration of 0.001 mol dm^{-3}) were linear for all the metals as shown in Figures 3.7 (a-d) for Pb^{2+}, Cu^{2+}, Cd^{2+}, and Bi^{3+}, respectively. However, clear deviations from linearity were observed for the complex of bismuth with 4-*tert*-butylcatechol, Fig. 3.7 (d). This may be explained in terms of adsorption isotherms. Current response is linear to the amount of adsorbate at the electrode. At high adsorbate concentrations, approaching full coverage of the electrode, current deviates from linearity. This is due to increased competition for adsorption sites and increased interactions between the adsorbates. These interactions are mostly electrostatic in origin. The deviation from linearity observed for bismuth with 4-*tert*-butylcatechol thus reflects an approach to complete coverage of the electrode at concentrations of Bi^{3+} greater than 7 ppm. This is a relatively low metal concentration. The deviation from linearity was not observed for the other bismuth-ligand complexes at this concentration, indicating that the ligand is the limiting factor. 4-*tert*-butylcatechol is bulkier than the other ligands and Bi^{3+} is larger than the other metals. The Bi-4-*tert*-butylcatechol complex is thus expected to occupy the available space on the electrode at lower concentrations than the other metal-ligand complexes.

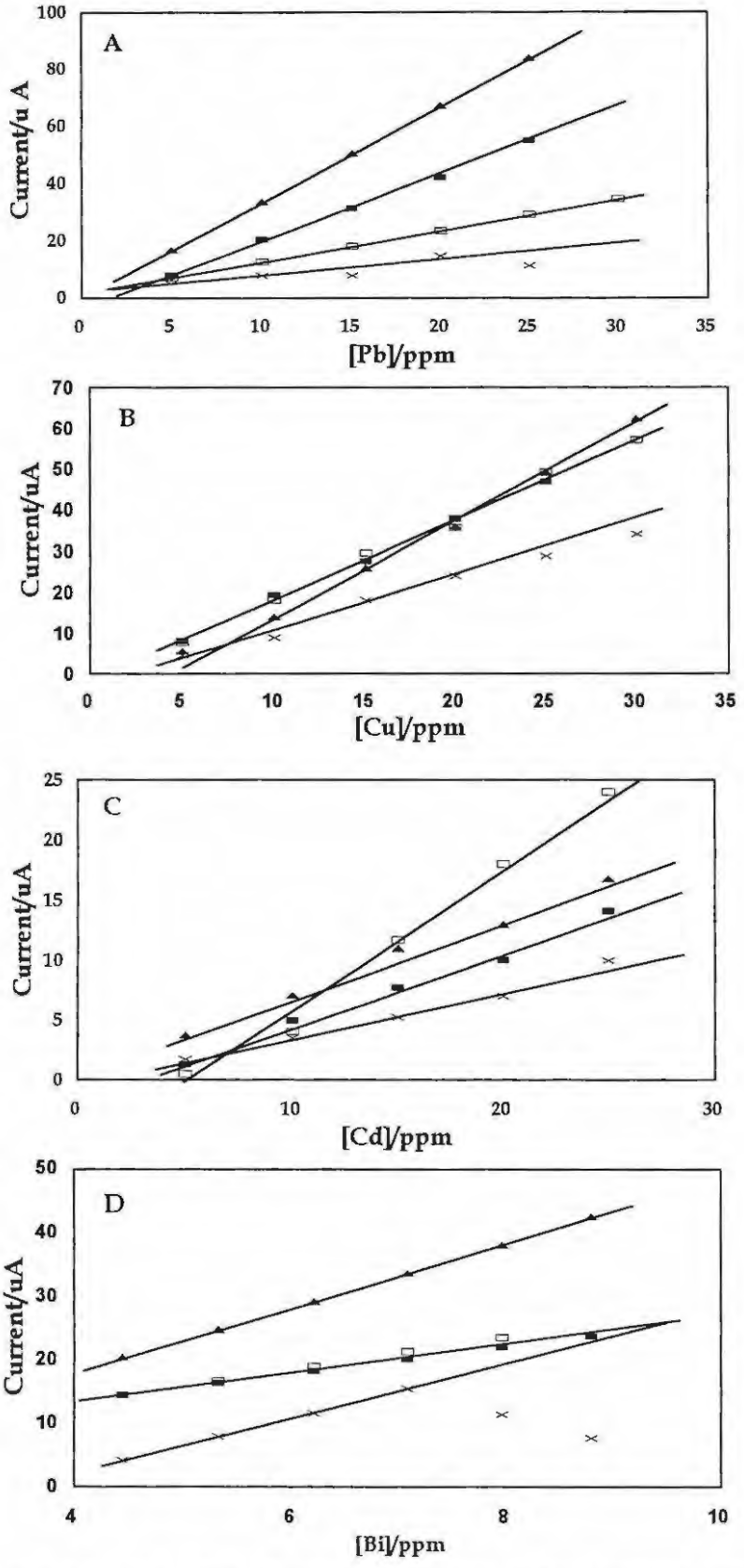

Figure 3.7 The effect of metal concentration on the adsorptive cathodic stripping currents of (a) Pb^{2+}, (b) Cu^{2+}, (c) Cd^{2+} and (d) Bi^{3+}, in the presence of 0.001 mol dm^{-3} of (a) resorcinol (▲), catechol (■), 4-methylcatechol (□) and 4-*tert*-butylcatechol (×). Scan rate = 100 mV s^{-1}.

Considering the same metal and ligand concentrations, metal-4-*tert*-butylcatechol complexes showed the smallest current responses for all the metals under consideration. These observations may also be explained from a perspective of size. The metal-4-*tert*-butylcatechol complexes are larger than the other metal-ligand complexes, resulting in a lower number of sites that these complexes occupy on the electrode. Furthermore, in the time allowed for adsorption, bulkier ligands travel at a slower rate towards the electrode. These factors may explain the smaller AdCSV currents observed for the metal-4-*tert*-butylcatechol complexes.

The lower current response observed may also be related to the ease of reduction at the electrode during the stripping step. Cu^{2+} and Pb^{2+} formed the strongest bonds with 4-*t*-butylcatechol than the other ligands and this may explain the slower release of these metals during stripping, hence the reduced electron evolution and current response observed.

The complexes of Bi^{3+} and Pb^{2+} with resorcinol showed higher AdCSV currents than the other Bi-ligand and Pb-ligand complexes, Fig. 3.7 a) and 3.7 d). For cadmium, Fig. 3.7 c), the resorcinol complexes showed higher currents at metal concentrations lower than 10 ppm. Above this concentration, the 4-methylcatechol complex gave higher currents than the other Cd-ligand complexes, whereas for Cu^{2+}, Fig. 3.7 b), resorcinol showed higher currents only at high metal concentrations. In terms of the size factor, metal-4-methylcatechol complexes are expected to show smaller reduction currents than the metal-resorcinol or metal-catechol complexes. This trend was observed only for Pb^{2+}, Fig. 3.7 a), at all concentrations, where the strength of current response, resorcinol> catechol> 4-methylcatechol> 4-t-butylcatechol is reflected by an increase in ligand-complex size. This trend is also reflected by the potential shift values for lead complexes with the ligands (Table 3.1), where the more positive the ΔE_p values, the higher the current response observed. So for lead, the ease of reduction of the metal-ligand parallels the size constraint in explaining the higher current responses observed.

The observed current responses for the other metals with the ligands cannot be explained as simply as for lead. This suggests that apart from size there are other factors which

affect the adsorption of the metal-ligand complexes onto the electrode and ultimately the observed current response. These factors include the relative affinities of the metals for the ligand, relative solubilities and hydrophobicity of the metal-ligand complex. The hydrophobicity of a complex promotes stronger interaction at the electrode.

3.4.5 Effects of Ligand Concentration on Current Response

For constant metal concentration, the AdCSV currents increased with increase in the concentration of the ligands at low concentrations, as shown in Fig. 3.8 a) to d) for the metal-ligand complexes represented.

Fig 3.8 a) for example, shows the Cu-resorcinol complex, where at high ligand concentrations, the current response decreases as the concentration of the ligand increases. The implication is that the activity of the electrode decreases at high ligand concentrations due to the full coverage of the electrode. This is caused by excess free ligand which may compete with the metal-ligand complex for free sites on the electrode. Optimum concentrations for the ligand in solution with 5ppm of the metal showed the highest current response at near or equal to equimolar concentrations of metal and ligand for all the metals-ligand complexes. For cadmium, lead, bismuth and copper, with resorcinol the ratios were: 1:1, 1:1.2, 1:1 and 1:1.25, respectively.

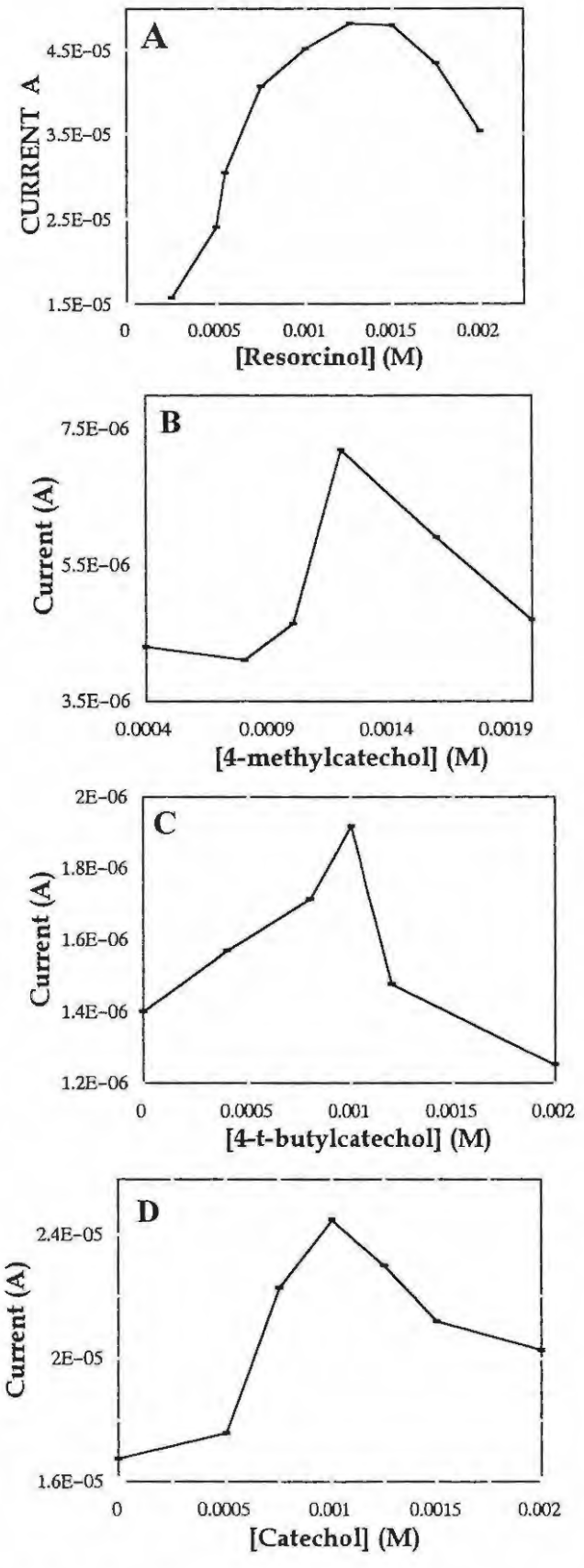

Figure 3.8 The influence of ligand concentration on the adsorptive cathodic stripping current of 5 ppm a) Cu^{2+}, b) Pb^{2+} , c) Cd^{2+} and d) Cu^{2+} for resorcinol, 4-methylcatechol, 4-t-butylcatechol and catechol, respectively. Scan rate = 100 mV s^{-1}.

3.4.6 Role of Structure and Chemistry in Metal-Ligand Current Response

It is assumed that structural differences and hence the chemical reactivity of the four chosen ligands affects their roles in the adsorptive stripping process and hence their utility as effective chelating ligands in metal analysis. As can be seen in Fig. 3.1, catechol and resorcinol have two hydroxyl groups. NMR studies have shown that the hydrogens are deprotonated in solution giving the catechol ligands an overall -2 charge[99]. Bonding with the metals is expected to occur at the negatively charged oxygens of the hydroxyl groups.

Hydroxyl groups are mildly electron-withdrawing via inductive effects. The inductive effects are due to the intrinsic electronegativity of atoms and bond polarity in functional groups. Oxygen is more electronegative than carbon and so the hydroxyl groups withdraw electrons through these sigma bonds. For the hydroxyls, the resonance effect is also involved. Resonance effects operate by donating or withdrawing electrons through pi bonds when the substituent is connected to the aromatic ring by an atom that has a p-orbital. The aromatic ring is connected to the hydroxyl group through p-orbital overlap with oxygen, hence the pi electrons on the oxygen are delocalised onto the ring. The resonance electron-donating effect of the hydroxyl group through pi bonds is stronger than its electron-withdrawing effect through sigma orbitals, hence there is a net electron-donating effect onto the aromatic ring. The electron density on the ring is expected to be even more pronounced when more electron-donating groups are attached to the ring, as with two hydroxyl groups on catechol.

Phenols are weak acids as they can dissociate in aqueous solution to produce the phenoxide anion. The phenoxide anion is resonance stabilised by the aromatic ring and the free energy of this dissociation is low. The effect of substituents on the acidity of the phenols depends on the substituent. An electron-donating substituent results in a phenol with less acidity as these substituents destabilise the phenoxide anion by concentrating the charge.

Functional groups such as the methyl group are electron-donating through inductive effects via sigma bonds with the aromatic ring. These electrons are delocalised through the aromatic ring. Larger alkyl groups such as t-butyl are more electron-donating than the methyl substituent.

The four ligands studied can be ranked in order of decreasing acidity: phenol (included as a measure), catechol, 4-methylcatcehol and 4-t-butylcatechol. The acidity of resorcinol and catechol are expected to be the same. A lowered acidity means that the hydrogen on the hydroxyl group is less likely to dissociate. This may be one of the factors involved in the lowered current response behaviour of the methyl and t-butyl substituted catechols.

The behaviour observed for resorcinol and catechol cannot be explained by this argument as they have the same functional groups, molecular mass, bulk and acidity. The difference is in the positions of their hydroxyl groups relative to each other, with catechol being a 1,2 disubstituted and resorcinol a 1,3 disubstituted benzene. The effect of introducing a metal at the hydroxyl group, creates steric hindrance with other substituents on the ring. As the substituents on catechol are closer together on the ring, this steric hindrance is greater than for resorcinol, so metal substitution may be more favourable at resorcinol. For lead and bismuth this effect is more noticeably pronounced in their higher current responses with resorcinol than with any of the other ligands and indeed, with catechol. Lead and bismuth are the largest of the four metals studied, and so the steric hindrance on binding to a hydroxyl group on catechol will be greater than for the other metals. It may furthermore be suggested that lead and bismuth are large enough to have formed bonds with both hydroxyl groups on resorcinol. This may not have been possible with catechol as the distance between the two hydroxyl groups would have been too small. These theories may explain why lead and bismuth showed a greater affinity for resorcinol.

3.4.7 Simultaneous Adsorptive Cathodic Stripping Voltammetry of the Metals

Using appropriate choices of concentration, Cu^{2+}, Pb^{2+}, Bi^{3+} and Cd^{2+} could be determined simultaneously in the presence of each of the ligands, as shown in Fig. 3.9 for resorcinol. Here optimum current response for all four metals simultaneously was reached with a ratio of 1:1:2:2 for copper, lead, bismuth and cadmium respectively. Simultaneous detection of metals requires careful attention to the concentration ratios at which the metals are present. Even slight increases or decreases in the concentration of one metal may affect the current responses of the others due to intermetallic effects, competition for the complexing ligand and the available surface on the electrode. Interference between metal ions are often encountered in simultaneous analysis of metals. For example, zinc and copper are known to form amalgams, resulting in the increase in the reduction currents due to copper and a decrease in the currents due to zinc[52].

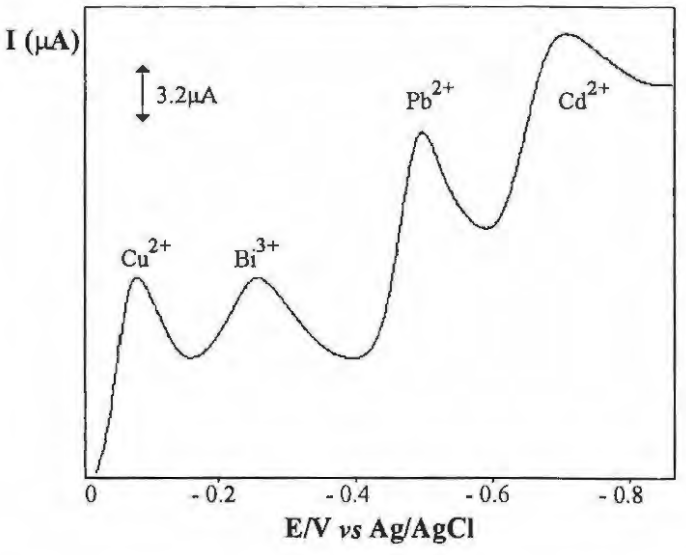

Figure 3.9 Simultaneous adsorptive stripping voltammograms of Cu^{2+}(5ppm), Pb^{2+}(5ppm), Cd^{2+} (10ppm) and Bi^{3+} (10ppm) in the presence 0.002 mol dm^{-3} of resorcinol. Scan rate = 100 mV s^{-1}.

Ligand Concentration

The concentration of the ligand in these studies was also an important factor. Increases in ligand concentration led to increases in current responses for the metals. However, twice the concentration of resorcinol was used for the simultaneous analysis as would be used for the same amount of a single metal. This is because of the increased competition for ligand caused by the presence of more than one type of metal in solution. So for 5ppm copper and lead and 10ppm bismuth and cadmium, 0.002 mol.dm^{-3} of resorcinol was used. Too much resorcinol would create further competition at the electrode as free ligand would also adsorb to the electrode, taking up sites otherwise occupied by metal-ligand complexes.

As an example Fig. 3.10 shows the effect of increasing the resorcinol concentration on metal reduction currents. Curve 1 shows weak reduction potentials for the four metals at the concentration ratios indicated. Increasing the ligand concentration as shown by curve 2, increased the current responses significantly for Bi^{3+}, Pb^{2+} and Cd^{2+}. The lowered Cu^{2+} and increased Bi^{3+}, Pb^{2+} and Cd^{2+} current responses in curve 2, serve as an example of the competition between Cu^{2+} and the other metals for sites at the electrode.

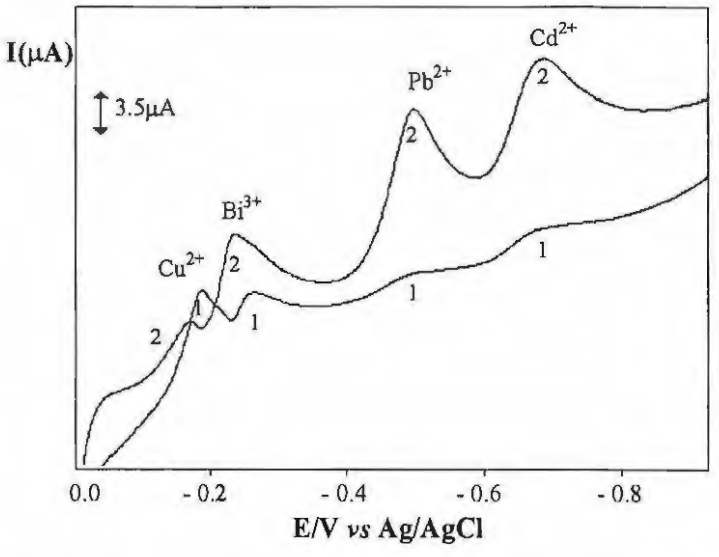

Figure 3.10 Simultaneous adsorptive stripping voltammograms of Cu^{2+} (5ppm), Pb^{2+} (5ppm), Cd^{2+} (5ppm) and Bi^{3+} (25ppm), showing effect of resorcinol concentration, curve 1 = 0.001 mol dm^{-3} and curve 2 = 0.002 mol dm^{-3}, on metal current response. 5ppm $HgCl_2$, scan rate = 100 mV s^{-1}.

Fig. 3.11 shows the effect of increasing $HgCl_2$ concentration on the AdCSV currents of the metals studied. Keeping the metal concentrations constant, curve 1 shows the AdCSV obtained for 5ppm $HgCl_2$ and curve 2 for 10 ppm $HgCl_2$. Significant increases for Cd^{2+} and Cu^{2+}, a slight increase for Pb^{2+} and a slight lowering for Bi^{3+} current responses are shown on increasing the $HgCl_2$ concentration. This was not observed for single-metal analysis. So, whereas usually 10ppm of $HgCl_2$ was employed, 20ppm showed a significant improvement on metal current responses.

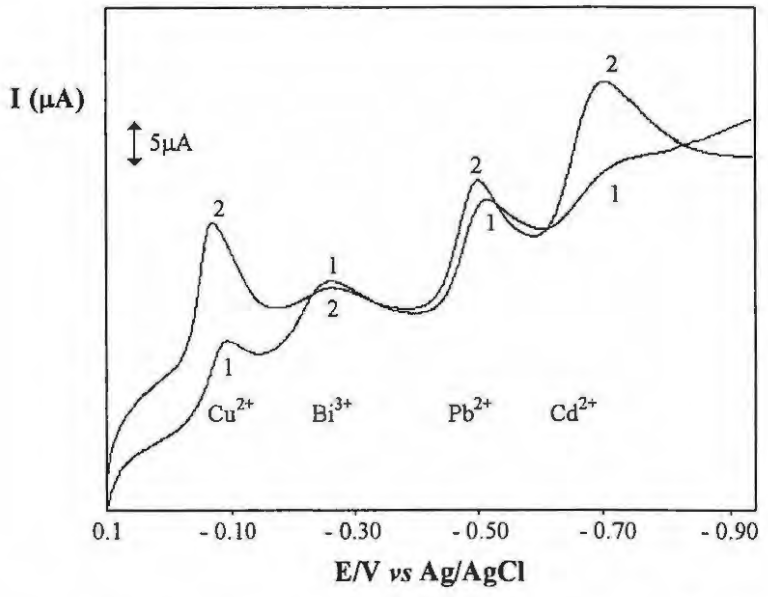

Figure 3.11 Simultaneous adsorptive stripping voltammograms of Cu^{2+}(5ppm), Pb^{2+} (5ppm), Cd^{2+} (7.25ppm) and Bi^{3+} (7.25ppm) in the presence of resoreinol (0.002 mol dm^{-3}). $HgCl_2$ coneentration for curve 1 = 10ppm and curve 2 = 20ppm. Sean rate = 100 mV s^{-1}.

Interference between Metal ions

The interference between metal ions were studied more closely for the resorcinol complexes of bismuth, lead, copper and cadmium, since resorcinol generally showed higher current responses than the other ligands. Simultaneous AdCSV of Pb^{2+} and Cu^{2+} at equimolar concentrations showed that Cu^{2+} complexes exhibited higher current responses than Pb^{2+} complexes. Addition of an equal concentration of Cd^{2+} to a solution containing equimolar concentrations of Cu^{2+} and Pb^{2+} in the presence of resorcinol, resulted in

insignificant changes in the magnitudes of these AdCSV peaks. The cadmium current response was lower than for lead, and that of lead lower than for copper. This may be related to the relative electronegativity of the metals. Copper has the highest electronegativity of 1.75 with lead and cadmium electronegativities of 1.55 and 1.46, respectively. Copper thus has a greater affinity for the ligand, explaining its higher current response in terms of competition with lead and cadmium.

However, when equimolar concentrations of Bi^{3+} were added to solutions containing Cu^{2+}, Pb^{2+} and Cd^{2+}, a significant decrease in the peak current due to Cu^{2+} was observed, while Cd^{2+} and Pb^{2+} were not affected. Less than equimolar concentrations of bismuth still decreased the copper current response. The intermetallic effects between Bi^{3+} and Cu^{2+} were examined more closely. Figure 3.12 shows how the addition of Bi^{3+} reduces the Cu^{2+} current response, while the Bi^{3+} current response increases with increasing concentration.

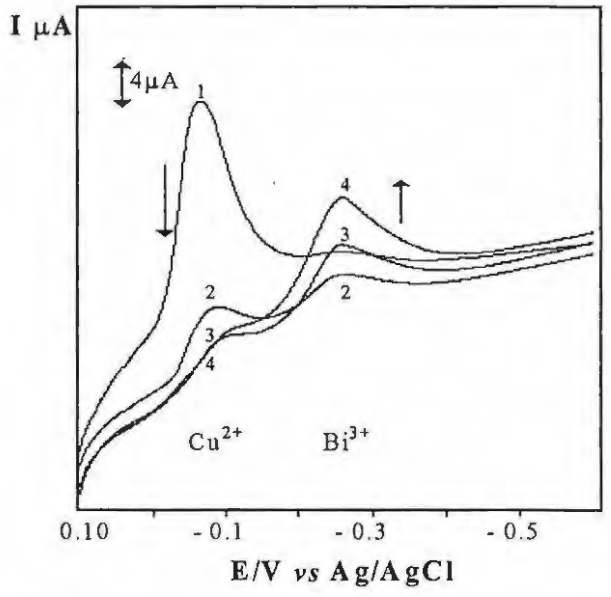

Figure 3.12 AdCSV on MFGCE, showing effects of increasing bismuth concentration on copper reduction current. $[Cu^{2+}]$ = 5ppm. $[Bi^{3+}]$, curve 1 = 2.5ppm, curve 2 = 5ppm, curve 3 = 7.5 ppm and curve 4 = 10ppm. [Resorcinol] = 0.001 mol dm^{-3}. Scan rate = 100 mV s^{-1}.

Bismuth has an electronegativity of 1.67, closer to that of copper, which may explain this competition. The competition may also be related to the strong binding affinity of bismuth for two hydroxyls of resorcinol as discussed in Section 3.4.6. Since the Bi-resorcinol complex gave a much higher current responses than the rest of the metal-resorcinol complexes considering similar metal ion concentrations, the observed interference between bismuth and copper could be due to the competition of these metals for the ligand. So, for simultaneous analysis of Bi and Cu, careful attention to concentration ratios is required.

While masking of Cu^{2+} by bismuth was observed, Pb^{2+} current responses remained mostly unaffected by the intermetallic effects caused by slight decreases or increases in the concentration of the other metals.

Potential differences

Probably the most important factor in simultaneous metal analysis, is that the reduction potentials are sufficiently resolved to prevent overlap. Potential separations between the peaks for the simultaneous reduction of the metals in the presence of similar ligands ranged from 0.17 to 0.3 V. Such separations are enough to allow for the efficient simultaneous determination of the metals[42].

There is thus a delicate balance controlled by concentration of the analytes which will lead to the enhancement or reduction of the current responses. Naturally, when the difference in reduction potential between adjacent metals is small, then competition at the electrode will be greater than between metal reductions with a larger potential difference. This is the case with copper and bismuth, a potential difference of at least 170 mV. When neither bismuth nor copper are completely masked in simultaneous analysis as, for example, in Fig. 3.9, the difference between their reduction potentials is at least 200 mV. This indicates that at least 200 mV potential separation is adequate for simultaneous analysis of these metals. Even at low concentrations, bismuth can almost completely mask the reduction of copper; remembering that in the absence of bismuth, copper produces the highest current response.

The potential difference between lead and bismuth is at least 250 mV, which may explain why lead is least affected by competition from bismuth. A potential difference of at least 200 mV was observed between cadmium and lead at equimolar concentrations. In the absence of bismuth, there is not an appreciable amount of competition between lead and cadmium, although lead produces a slightly higher current response. However, addition of bismuth creates competition between the two metals, where the cadmium current response is significantly lowered over that of lead. Slight excess of cadmium on the other hand, enhances not only the cadmium response but that of lead and copper, at the expense of bismuth which can be completely masked. Increases such as these may be explained in terms of co-adsorption effects, where the reduction of a metal species such as cadmium above, enhances the reduction of other metal species co-adsorbed at the electrode.

Table 3.3 The potential separation between metals with adjacent reduction waves.

	Resorcinol	Catechol	4-Methylcatechol	4-t-butylcatechol
Cu - Bi	0.244 V	0.274 V	0.254 V	0.234 V
Bi - Pb	0.21 V	0.21 V	0.29 V	0.32 V
Cd - Pb	0.32 V	0.14 V	0.11 V	0.10 V

Table 3.1 noted the shifting potentials of the metals in being complexed to different ligands. Table 3.3 shows the potential difference between metals with reduction peaks adjacent to each other (as in Fig 3.9) and calculated from Table 3.1 for each of the ligands. While the values do not hold true during simultaneous analysis as discussed above, it provides a useful indication of which ligand will provide adequate separation between the reduction potentials of metals analysed. Resorcinol already provides early indication of its utility for simultaneous metal analysis, as peak separation is at least 0.21 V between each of the metals, compared with the lowest peak separation of 0.14 V for catechol. A table such as this may be useful for defining the best ligand in simultaneous analysis of at least two metals.

Affinity of metal for ligand

The individual affinities of the four metals for the ligand is perhaps a deciding factor. The current response of each metal with resorcinol shows that over a range of concentrations, lead produces the highest current response, followed by copper, cadmium and then bismuth. For simultaneous metal analysis it is evident that this still holds true, as far as lead and cadmium are concerned, while copper is subjected to additional competition from bismuth.

3.5 CONCLUSIONS

The formation and deposition onto the electrode, of the metal-ligand complexes may be represented by Equations 3-1 to 3-3[37].

$$M^{+n} + xCat_{aq} \rightarrow M(Cat)_x^{+n},aq \qquad \text{Equation 3-1}$$

$$M(Cat)_x^{+n},aq \rightarrow M(Cat)_x^{+n},ads \qquad \text{Equation 3-2}$$

$$M(Cat)_x^{+n},ads + e^- \rightarrow M^{+n-1} + xCat_{aq} \qquad \text{Equation 3-3}$$

Where cat = catechol, resorcinol, 4-methylcatechol and 4-*tert*-butylcatechol; M = Cu^{2+}, Pb^{2+}, Cd^{2+}, Bi^{3+}; x represent the number of complexing ligands; n is the charge on the metal ion.

AdCSV schemes for analysis of Cu^{2+}, Pb^{2+}, Cd^{2+}, Bi^{3+} with the catechol ligands, catechol, resorcinol, 4-methylcatechol and 4-t-butylcatechol are presented in this work. Ring substituents on the catechols affected the sensitivity of the analysis, as shown. Resorcinol showed the largest sensitivity for the determination of bismuth, copper and lead, 4-methylcatechol for copper, while 4-*tert*-butylcatechol showed the lowest sensitivity for the detection of all the metals except bismuth. These affinities were explained by the differing electronegativity and size of the metals, cumulative bulk of the metal-ligand complexes, bond strength and relative stabilities.

By careful attention to the concentration ratios of bismuth and copper, simultaneous analysis of these two metals are possible with the ligand, resorcinol. The technique offers an improved method for the analysis of bismuth and for the simultaneous analysis of bismuth, lead, cadmium and copper. The method employed in this work whereby MFGCE was employed as a working electrode for AdCSV may not have some of the advantages that are possessed by the HMDE. However, the utility of this electrode for metal analysis was justified by the reproducible and sensitive AdCSV currents obtained.

The advantage of this method then, is that it may be used for decentralised and simultaneous analysis of these metals, utilising the benefit of an electrode which has a low cost and is of simple construction.

Chapter Four

Chemically Modified Electrodes for Analysis of Cysteine

4.1 INTRODUCTION

There exists an extremely wide variety of proteins in nature, where subtle differences in chemical structure is associated with major differences in physiological function. A knowledge of the chemistry of amino acids and proteins and their composition is essential in understanding the way in which biological activity is conferred on the protein.

Cysteine **(RSH)** and cystine **(RSSR)**, its oxidised form, are two of the most important amino acids. They have an important role in biological systems and have been used widely in the medicinal and food industries[100]. The thiol group, $^{-}$SH of cysteine forms an integral part of proteins such as metallothionein, glutathione and ferredoxin where its function in electron transfer facilitates the biochemical role of these proteins. The thiol group is also known as the sulphydryl or mercapto group, the latter term derived from its ability to "seize" mercury[101]. Cysteine is also a structural requirement for glutathione synthesis. Glutathione is known to protect cells from oxidative stress. Many electron carrier proteins working in the energy metabolism of most cellular life have cys-X1-X2-cys sequences as their functional sites, where cys is cysteine and X is a bridging ligand. For example, the two cysteine side chains are binding sites to haem in cytochrome c, the iron clusters in ferredoxin, and are the redox sites for the formation of disulphide bonds in thioredoxin[102]. Several enzymes have been demonstrated to contain the essential element selenium in the form of selenocysteine, including the mammalian glutathione peroxidase which protects tissue from oxidative damage[103]. The development of detection methods

of thiols in proteins is not only important for effective utilisation of its industrial application[104] but also for understanding the biological function of these proteins.

Quantitative determination of cysteine is of benefit in analysis of proteins in which there is a high cysteine content, such as metallothionein. In this chapter, the quantification and analysis of cysteine is explored and used for further studies in analysis of metallothionein, Chapter 5.

4.1.1 Cysteine Analysis

Techniques for Cysteine Analysis

Thiols do not have strong chromophores in the UV-Vis range, meaning that pre- or post-column derivitisation is a pre-requisite for spectrometric detection[47]. Using this technique, the reactions of thiol species such as cysteine, may only be monitored indirectly in the presence of a catalyst. Suitable catalysts were sought in nature.

Cobalamin or Vitamin B_{12}, a member of the porphyrin family, participates in redox reactions where its main function is to activate sulphydryl and disulphide groups. Vitamin B_{12} and its derivatives are active in the biological oxidation of cysteine, glutathione and 2-mercaptopropanol. Kundo and Keier[104] reported on the similarity of structure between the transition metal phthalocyanines (MPc's), and vitamin B_{12}. The phthalocyanines can be seen as the synthetic counterpart of the naturally occurring porphyrins. It was thus not surprising that the metal phthalocyanines, in particular the cobalt derivative (CoPc), were shown to be effective catalysts for the autoxidation of cysteine to cystine. It was suggested[104] that CoPc and its substituent, cobalt tetrasulphonated phthalocyanine $[CoTSPc]^{4-}$, Fig 4.1, followed a reaction mechanism similar to vitamin B_{12} in their autocatalytic oxidation of cysteine. The phthalocyanines have an intense colour, making possible the spectrophotometric monitoring of reactions with cysteine.

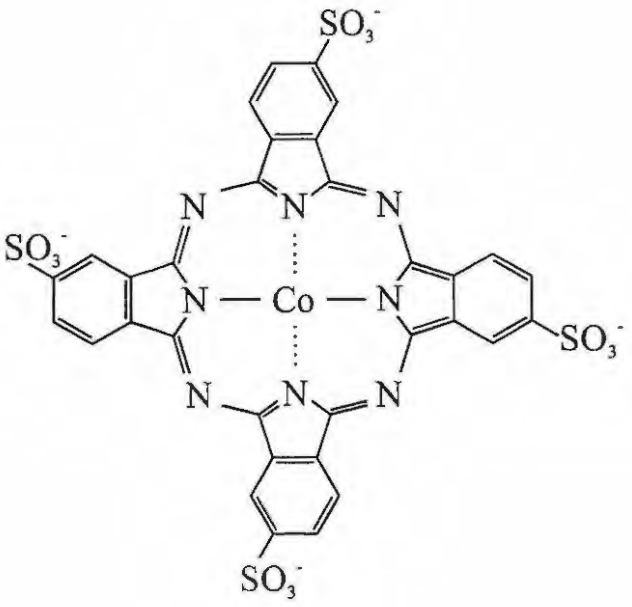

Figure 4.1 Electronic structure of $[Co(II)TSPc]^{4-}$.

The nature of the intermediates formed during the autocatalytic oxidation of cysteine in the presence of $[CoTSPc]^{4-}$, were elaborated on by Cookson[105] using electron spin resonance spectroscopy (ESR). ESR is a tool in the study of changes occurring as a result of redox reactions. These authors corroborated the findings of Kundo and Keier[104] and postulated the following mechanism for the autoxidation of cysteine to cystine by $[CoTSPc]^{4-}$:

$$\mathbf{RSH \leftrightarrow RS^- + H^+} \qquad \text{Equation 4-1}$$

$$\mathbf{[Co(II)TSPc]^{4-} + RS^- \rightarrow [Co(I)TSPc]^{5-} + RS^{\cdot}} \qquad \text{Equation 4-2}$$

$$\mathbf{[Co(I)TSPc]^{5-} + O_2 \rightarrow [Co(II)TSPc]^{4-}} \qquad \text{Equation 4-3}$$

$$\mathbf{RS^{\cdot} + RS^{\cdot} \rightarrow RSSR} \qquad \text{Equation 4-4}$$

These authors reported that the autoxidation of cysteine only occurs in the pH range 4.0 to 9.0, the rate increasing with pH. They further reported that cystine precipitated out at pH> 4. [105]

In the pH range 9.5 to 12.0, $[Co(II)TSPc]^{4-}$ catalyses the reduction of cystine to cysteine, Equation 4-5. Cystine redissolves at pH 9.5 and the dominating reaction with $[Co(II)TSPc]^{4-}$ becomes oxygenation, Equation 4-6[105].

$$[Co(I)TSPc]^{5-} + RSSR \rightarrow [Co(II)TSPc]^{4-} + RSH \qquad \text{Equation 4-5}$$

$$[Co(II)TSPc]^{4-} + O_2 \rightarrow [Co(III)TSPc(O_2)]^{3-} \qquad \text{Equation 4-6}$$

The lack of adequate quantitation methods for cysteine also prompted investigation into its redox reactions and subsequently its electrochemical analysis. Electrochemical detection of sulphydryls has usually been performed at mercury or mercury amalgam electrodes[106,107]. At these electrodes, the oxidation of cysteine occurs at potentials where mercury is oxidised. Cysteine oxidation proceeds by forming a complex with the oxidised mercury. The reversible mercury sulphide species $[Hg\text{-}(RS)_2]$ with a half wave potential of -0.50 V *vs* SHE, is formed and adsorbs to the electrode[53,108]. Similar observations were reported for the oxidation of glutathione[109]. The electro-oxidation of these thiols is thus observed indirectly, dependant on the oxidation of mercury. The use of the Hg electrode for monitoring direct electro-oxidation of thiols is limited, because the oxidation of thiols proceeds at highly positive potentials, out of the working potential range of mercury electrodes.

Direct electro-oxidation of thiols is possible at electrodes with more positive working potential ranges. Electro-oxidation of cysteine has been observed on gold and platinum electrodes at potentials between 0.7 V and 1.45 V vs SHE.[107] The electro-catalytic oxidation of the thiols is due to the strong interaction of the sulphur group with active sites on noble electrode surfaces.

The use of more conventional electrodes such as carbon in thiol detection is hampered by the sluggish electrode kinetics of these groups. The slow electron exchange is caused by the weak interaction between thiols and carbon electrode surfaces. Oxidation of the thiol groups exhibit high overvoltages at unmodified carbon electrodes (oxidation of cysteine

occurs at potentials greater than 1 V *vs* Ag/AgCl)[106]. Extremely positive potentials are thus required to monitor the redox reaction. At these potentials and in aqueous solvents, the cysteine oxidation wave may be masked by that of hydrogen.

It became clear that catalysts were required for the electrochemical oxidation and subsequent analysis of cysteine to reduce the high overpotential. The catalytic oxidation of cysteine by metallophthalocyanines was the approach utilised.

4.1.2 Metallophthalocyanines (MPc's)

Because of their intense colour, redox activity and high thermal stability, MPc's have found many applications. These include photoconductive surfaces, optical information storage media and, electrochromic devices, to name but a few. It is the redox properties of the MPc's which defines their utility in these applications.[110]

Phthalocyanines are composed of a ring system made up of four isoindole units, at the centre of which various metals can be inserted, Fig. 4.2.

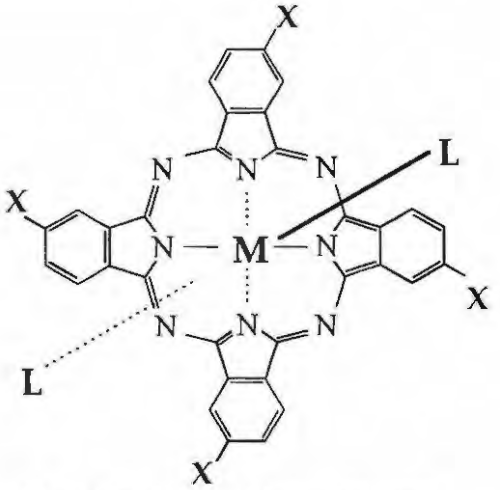

M = Metal, X = Ring substituent,
L = Axial ligand

Figure 4.2 A metallophthalocyanine, showing the sites for binding by a variety of metals, axial ligands and the site for attachment of ring substituents.

The MPc unit itself is an 18 pi electron system carrying two negative charges, and is capable of both oxidation or reduction. The central metal ion, usually a transition element, may undergo reduction or oxidation at potentials comparable to the MPc ring process. Oxidation or reduction may thus occur at the central metal or the ring, depending on the nature of the central metal ion. Many MPc's bind one or two axial ligands, the feature utilised in its catalytic reactions.

The redox reactions of a transition MPc is markedly dependent on the ability of the central metal ion to bind extraplanar ligands (to occupy co-ordination sites on the axis perpendicular to the ligand plane) and on the total oxidation state of the MPc[105]. Owing to a strong ligand field of the tetrasulphophthalocyanine anion, copper and nickel tetrasulphophthalocyanines have minimum tendency to bind further ligands to form octahedral complexes. Comparisons of the ease of oxidation of a group of tetra-sulphonated MPc's show a dependence on the central metal ion, in decreasing order, for the following metals: Co(II), Cu(II) and Ni(II) [110].

Ring unsubstituted MPc's have very limited solubility in most solvents, limiting their solution-phase redox measurements and catalysis. This is related to the nature of the central metal ion. Those MPc's preferring a 6-coordinate rather than 4-coordinate bond scheme, such as iron and cobalt phthalocyanine, will dissolve in donor solvents through axial interaction between metal and donor solvents. Their solubility is, however, provisional on the donor solvent co-ordinating to the central metal ion.[110]

Improvements in the solubility are achieved to an extent by the introduction of functional groups through ring substitution, for example, the sulphonate groups in $[CoTSPc]^{4-}$, shown in Figure 4.1 and represented as 'X' in Fig 4.2. These functional groups influence the resultant chemistry of the MPc when adsorbed at the electrode. They can also affect the electroactivity, the potential at which the MPc is oxidised or reduced and the rate of reaction[44]. Different axial ligands also influence the redox properties of the MPc's[110]. Another factor which may affect the redox activity of the MPc's is the nature of the supporting electrolyte anions.

The metal phthalocyanines show two distinctive electronic transitions in the UV-Vis spectral region, namely the Soret band in the UV region and the Q band in the 600-750nm region. Fig.4.3 shows these bands typical for the UV-Vis spectra of a metallophthalocyanine. The Soret bands are not very sensitive to the valence state of the central metal in MPc's whereas the Q bands are sensitive to the central metal ion, their valence states and the solvent. Reduction or oxidation of the MPc's are monitored by observing spectral changes. The resulting metal to ligand charge transfer (MLCT) bands are observed in the spectral region between the Soret and Q bands.[111]

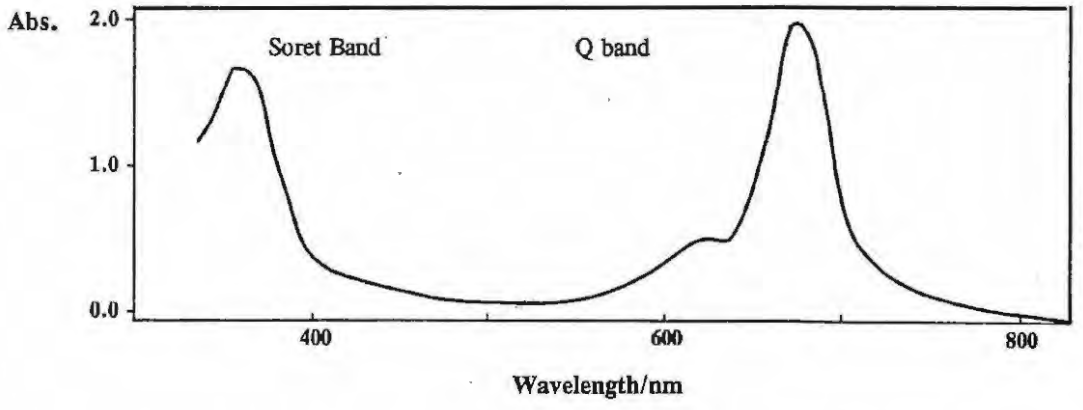

Figure 4.3 UV-Vis Spectra of a MPc (for illustrative purposes only).

4.1.3 Electroanalytical Scope of the MPc's

The MPc's, incorporating different metal centres, including $[CoTSPc]^{4-}$, have been shown to promote the electrocatalytic oxidation of cysteine. Utilisation of this approach has led to a spate of research geared towards electroanalysis of thiols and cysteine at modified electrodes. This work[112] pioneered further research and developments for the MPc catalysis of a number of molecules (hydrazine and oxygen by $[CoTSPc]^{4-}$).

Table 4.1 shows just some of the analytes electrocatalysed by metallophthalocyanines together with the mode of attachment of these modifiers onto the electrodes.

Table 4.1 Some analytes electrochemically analysed by MPc's

Analyte	MPc	Technique	Reference
Co_2 (R)	CoPc	Ads	[113]
Cysteine	CoPc	Ads, CPE	[107,43]
H_2O	Ni, Co, FePc	Ads	[114]
Hydrazine,	CoTAPc CoPc	EP CPE	[61] [43]
Nitrite Ions	Cu, Fe, Ni, Co, Mn, Zn	Ads	[115]
Oxalic Acid	CoPc	EP, CPE	[60, 43]
Oxygen	$[CoTSPc]^{4-}$	EP	[116, 100]
Penicillamine	CoPc	CPE.	[43]
Phenols	CoPc	Ads	[117]
T-butylhydroxyanisole	NiTAPc	EP	[48]

MPc, metallophthalocyanine; TAPc, tetraaminophthalocyanine; CPE, carbon paste electrode; Ads, adsorption; EP, electroploymerisation; R, electroreduction.

One of the most important observations was the natural tendency of the MPc's to adsorb to electrode surfaces, producing effectively, a chemically modified electrode at which catalytic oxidation could occur at lowered potentials[100,118]. Studies on the modification of electrodes with MPc complexes have been focused at CoPc and its derivatives[50,60,61,63,70,107,116,119].

MPc's have been modified at electrodes as part of the matrix of carbon paste electrodes[107], held at the surface of graphite and carbon electrodes by direct deposition[47], incorporated into polymer modified electrodes[120], electrodeposited[70] and electropolymerised in the presence of coadsorbates.[48,49] Deposition of polymeric metallophthalocyanines allows the formation of films or microcrystalline deposits, with

enhanced electrochemical sensitivity, chemical and mechanical stability, in both aqueous and non-aqueous solvents[48].

Each MPc complex exhibits slightly different voltammetric responses related to its mode of interaction with the electrode and the substrate[47].

4.1.4 How the MPc Binds to the Electrode

The mode of interaction of the MPc with the electrode varies for each method of attachment, varying also according to its metal centre, axial ligands and the surface of the electrode. From reflectance spectra of adsorbed tetrasulphonated MPc's, it was concluded that adsorbed MPc's are lined up at the electrode with their macrocyclic ring perpendicular to the electrode surface.[111]

Comparison of CoPc with FePc at platinum and carbon electrodes surfaces showed variation in the way the molecule was aligned. These differences were based on the variations in the metal centre and the surface itself. This in turn affected their catalytic response in the presence of oxygen. From UV spectral studies[111], and Penning Ionisation Electron spectroscopy[121], it was concluded that π electron orbitals of planar MPc's interact with π electron clouds at carbon surfaces. This interaction is maximised for the MPc interacting with the plane parallel to the benzene rings on the graphite surface. There is a greater tendency for this type of interaction than with carbonyl or hydroxyl groups present on the carbon electrodes. It has been shown that tetra-sulphonated MPc's interact with solid surfaces through the sulphonate group.[111]

MPc's as Electrocatalysts for Cysteine Analysis

The use of the metallophthalocyanines has dominated the field of cysteine electrocatalysis. Electrocatalysis of cysteine oxidation has been observed with the MPc species in solution or immobilised at the electrode[100]. The use of chemically modified electrodes for cysteine analysis is an active area of research. This research has been directed at lowering the

potential of the cysteine oxidation for effective analysis, increasing sensitivity of the catalysis, reproducibility and hardiness under harsh flowing conditions[47].

The central metal ion plays an important role in the catalytic ability of the MPc towards sulphydryls. ESR studies of $[CoTSPc]^{4-}$ solutions have shown that cysteine interacts with $[CoTSPc]^{4-}$. It is likely that the interaction occurs via the sulphur atom in the cysteine and a dz^2 orbital in the metal chelate[105]. Comparative studies with different transition metal tetrasulphonated phthalocyanines, $[MTSPc]^{4-}$ for M = Zn, Mn, Fe, Co and Cr, showed Co to be the best in terms of solution-phase electrocatalysis of cysteine[100]. This is related to the tendency of the cobalt ion to form octahedral complexes[105] and its ease of reduction[104].

$[CoTSPc]^{4-}$ has been shown to catalyse the electro-oxidation of cysteine in solution-phase catalysis, via direct deposition or indirectly at carbon paste electrodes or electrodeposited in the presence of coadsorbates such as polymers.

4.1.5 Catalytic Mechanism

In biological systems cysteine, RSH, dissociates to RS^- in aqueous solution at slightly alkaline pH. The RS^- then co-ordinates to vitamin B_{12} from one axial co-ordination site and oxygen on the opposite site, the sixth axial ligand. Next, an electron transfer from RS^- to oxygen via the central metal ion of the ternary complex occurs and results in the formation of radical RS· and superoxide oxygen. Two free radical RS· groups couple to form cystine, the reduced form of cysteine, while the superoxide oxygen ion decomposes to oxygen and water via a catalase-like reaction.[110]

It is believed that for metal MPc's adsorbed at electrodes, a similar pathway for the catalysis of cysteine is followed. Cysteine binds to the metal as a fifth axial ligand, while the sixth axial ligand, is adsorbed to the electrode surface. The 2-step electrocatalytic

process begins with the oxidation of M(II)Pc(-2) to M(III)Pc(-2)[49,100], where M is an electroactive metal. In the presence of cysteine or sulphydryls, enhancement of this anodic current corresponding to the oxidation of cysteine, has been observed[47,107].

4.1.6 Practical Considerations

MPc complexes tend to aggregate in solution. This is due to intermolecular interactions and the lability of axial ligand for water molecules.

Only in alkaline solution is it believed that an equilibrium exists between monomeric and dimeric forms of $[Co(III)TSPc(-2)]^{3-}$. This is dependent on the concentration of $[CoTSPc]^{4-}$, its ionic strength and temperature of the solution[49]. The dimeric form dominates over the monomeric form at low pH's, and is believed to be a better catalyst than the monomeric form[122]. The phthalocyanines may also undergo oligomerisation or dimerisation when adsorbed onto carbon surfaces, and less readily at platinum surfaces. Polymeric forms of the first row transition metals are better catalysts than their monomeric counterparts and so adsorption at carbon electrodes leading to polymerisation improves their catalytic activity[111]. Previous research from pH studies of $[CoTSPc]^{4-}$ adsorbed at GCE showed that higher polymerisation occurs at low pH, high concentrations and ionic strength[49].

In order to obtain well-defined voltammetric peaks, aggregation effects as a function of pH, are important considerations, and more so because these two factors may affect the catalytic ability of the aggregated species[116]. The effects of pH on the ionisation states of analytes such as amino acids is an additional practical consideration.

4.2 AIM OF RESEARCH

Essentially, the field of electrocatalysis is directed at lowering the overpotential and increasing the rate of certain electrochemical reactions so that a more sensitive or selective detection can be achieved. The sluggish electrode reaction of thiols at unmodified electrodes and its high overpotential is diminished in the presence of MPc's[47].

The design of chemically modified electrodes is a growing field of research in the field of electrocatalysis. Modification of the electrode by electrodeposition has the benefit of reproducibility, sensitivity and the control over the amount of modifier deposited at the electrode. Research on the electrodeposition of the phthalocyanines at electrodes have reported on the good mechanical and chemical stability of the chemically modified electrodes[48]. CoPc has been electrodeposited at solid electrodes in the presence of supports such as pyrrole[116]. While these methods offer stability, they are countered by the loss of sensitivity on electrodeposition of the MPc in the presence of a support. Incorporation of the catalyst into a polymer or as part of a carbon paste matrix, reduces the sensitivity, while direct electrodeposition of the catalyst onto the electrode offers greater sensitivity, with the added advantage of utility in aqueous and non-aqueous solvents. Electrodes modified with polymeric supports containing the modifier are not suitable for use under alkaline conditions as the film conductivity in such solutions is weak or non-conductive[116]. No research has shown the direct electrodeposition of $[CoTSPc]^{4-}$ onto GCE, in the absence of supports, for electrocatalysis of cysteine.

$[CoTSPc]^{4-}$ has been shown to catalyse the oxidation of cysteine with overpotentials at about 0.77 V *vs* Ag/AgCl[107]. Thus far all studies for cysteine analysis at CME has been conducted at low pH. This is owing to the favourable hydrogen evolution at the electrode at these pH's. No studies have shown the use of a CME for cysteine analysis at higher pH's. One of the aims of this research is to design electrodes for analysis of cysteine containing proteins. Low pH's are not feasible as this would involve decomposition of the analytes.

In this thesis a method for direct electrodeposition of the modifier onto the electrode for cysteine analysis is examined. The aim is to produce an electrode surface which is reproducible, sensitive and stable, while reducing the overpotentials associated with the electroanalysis of thiols. The design of a glassy carbon electrode modified by direct electrodeposition of $[CoTSPc]^{4-}$ onto GCE for cysteine analysis at acidic and alkaline conditions is presented in this research.

The role of the MPc in catalysis is markedly dependent on the nature of the central metal ion. It is thus explored whether this holds true for electrocatalysis of cysteine, at electrodes modified by electrodeposition of phthalocyanine complexes of cobalt(II) iron(II), nickel(II) and molybdenum(II).

Ring substitution of MPc complexes such as the attachment of sulphate groups on Co(II)Pc to produce water soluble $[CoTSPc]^{4-}$ increases the solubility of MPc's in aqueous solvents. The presence of ring substituents such as the sulphate groups leads to aggregation in solution which may complicate their electrochemistry.

Biscyanoruthenium(II) phthalocyanine is soluble in water at pH's greater than 5 and does not show aggregation effects common with the tetrasulphonated MPc's. The electrodeposition of this modifier for electrocatalysis of cysteine is presented in this work for the first time.

4.3 EXPERIMENTAL

4.3.1 Reagents

4.3.1.1 Solvents

Various solvents were tested for both their ability to dissolve the MPc complexes and also their utility as solvents from which the MPc would readily be electrodeposited at the electrode. Pyridine, acetonitrile, dichloromethane and dimethylformamide (DMF) (all from Saarchem) were the organic solvents tested. All organic solvents were distilled before used.

4.3.1.2 Electrolytes and buffers

When organic solvents were employed, the electrolyte used was tetraethylammonium perchlorate (TEAP). TEAP was prepared by mixing equal volumes of hot solutions of tetraethylammonium chloride (1 mol dm^{-3}) and sodium perchlorate (1 mol dm^{-3}). The mixture was refluxed for one hour and allowed to cool. The precipitate formed was filtered and washed with ice cold ethanol. The white powder-like crystals of TEAP were obtained by recrystallisation from hot absolute ethanol. Ferrocene, used as an internal standard for non-aqueous experiments employing a Ag wire pseudo-reference electrode, was recrystallised from absolute ethanol before use.

Triply distilled deionised water was used in all aqueous solution experiments. For pH 8.4 electrochemical experiments, Tris buffer was employed. The pH of this buffer was adjusted to 8.4 by addition of HCl (0.2 mol dm^{-3}). For electrochemical experiments at pH<4, H_2SO_4 (0.05 mol dm^{-3}) was employed as the electrolyte. A pH 9 buffer solution containing boric acid, potassium chloride and sodium hydroxide was prepared from pH 9 sachets (BDH) and was employed for solutions of $K_2[(CN)_2RuPc]$ in water. A pH 2.5 sodium phosphate buffer (0.1 mol dm^{-3}), prepared from sodium dihydrogen phosphate

(Eltec) and sodium phosphate (Saarchem) was also used for cysteine analysis with $K_2[(CN)_2RuPc]$, OMo(V)(OH)Pc and $[OMo(OH)TSPc]^{4-}$.

4.3.1.3 Cysteine

Cysteine was obtained from Sigma chemicals and used without further purification. Cysteine solutions were prepared daily in 0.05 mol dm^{-3} H_2SO_4 , in pH = 8.4 Tris-HCl buffer (0.2 mol dm^{-3}), or in pH 2.5 sodium phosphate buffer (0.1 mol dm^{-3}). These were deaerated with nitrogen (dried over anhydrous copper sulphate) for 10 minutes before cyclic voltammetric experiments were run.

4.3.1.4 MPc complexes

The MPc complexes of cobalt(II) tetrasulphophthalocyanine ($Na_4[CoTSPc].2H_2O$), biscyanoruthenium(II) phthalocyanine ($K_2[(CN)_2RuPc]$, oxomolybdenum (V) tetrasulphophthalocyanine ($Na_4[OMo(V)OH)TSPc]\cdot 5H_2O$) and oxomolybdenum (V) phthalocyanine (OMo(V)(OH)Pc), were synthesised according to the published procedures detailed in Section 4.3.2. MPc complexes of iron (FePc), cobalt (CoPc), and nickel (NiPc) were purchased from Eastman Kodak or Aldrich and used without further purification.

4.3.2. Preparation of the MPc Complexes

4.3.2.1 Tetrasodium salt of cobalt(II) tetrasulphophthalocyanine $Na_4[CoTSPc].2H_2O$

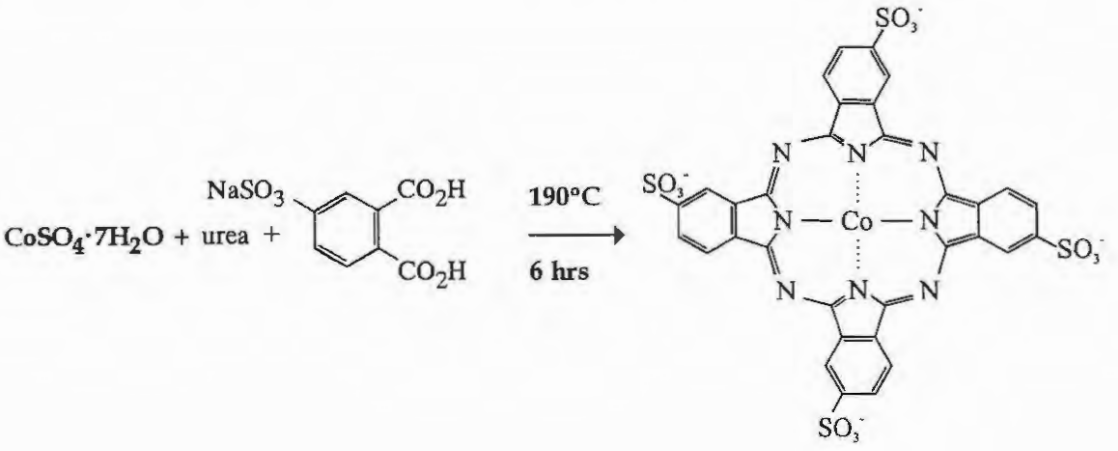

***Scheme 1**: A simplified synthetic route for $[CoTSPc]^{4-}$*

Na_4[Co(II)TSPc] was prepared according to the methods of Weber[123] and Busch. The monosodium salt of 4-sulphophthalic acid (4.32g), ammonium chloride (4.7g), urea (5.8g), ammonium molybdate (0.068g), and cobalt(II) sulphate 7-hydrate (1.36g), were ground together until homogeneous.

10ml of nitrobenzene was added to a 150ml two-necked flask fitted with a condenser and a thermometer and slowly heated to 180°C. At this point the solid mixture was slowly added while keeping the temperature between 160°C and 180°C. The heterogeneous mixture was then heated for 6 hours at 180°C. The crude product formed a solid blue cake which was washed with methanol until the odour of nitrobenzene could no longer be detected. The solid remaining was added to 110ml of 1M HCl saturated with NaCl. This step ensures removal of excess cobalt(II) sulphate from the product. The solution and undissolved material was briefly heated to boiling, cooled to room temperature, and filtered. The resulting solid was dissolved in 70ml of 0.1M NaOH and after heating to 80°C, insoluble impurities were removed by filtration. 27g of NaCl was added to this solution, initiating the precipitation of some of the solid product. This slurry was heated

to 80°C and stirred at this temperature until ammonia evolution stopped. The product was obtained by filtration and the initial reprecipitation process repeated two additional times. It was necessary to extract the filtrate by centrifugation, to prevent loss of product.

The solid obtained after filtration was washed with absolute ethanol until the filtrate was chloride free. This was ensured by testing for the presence of chloride ions in the filtrate with a 0.1M $AgNO_3$ solution. It was necessary here to obtain the filtrate by centrifugation. The product was refluxed for 4 hours in 20ml of absolute ethanol, and the blue product filtered and dried overnight. Three further washings in absolute ethanol ensured the purity of the product.

4.3.2.2 Tetrasodium pentahydrate oxomolybdenum (V) tetrasulphonated phthalocyanine- $Na_4[OMo(V)OH)TSPc]\cdot 5H_2O$

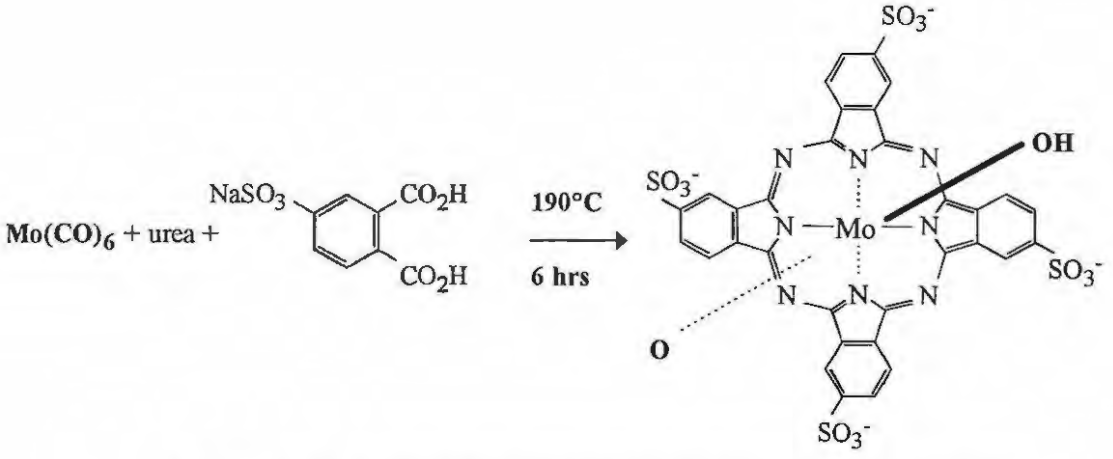

***Scheme 2**: A simplified synthetic route for $[OMo(OH)TSPc]^{4-}$*

$[OMo(V)(OH)TSPc]^{4-}$ was prepared by the procedure as outlined for synthesis of cobalt (II) tetrasulphonated phthalocyanine (Section 4.3.2.1), except that molybdenum hexacarbonyl was used instead of cobalt sulphate.

4.3.2.3 *Dipotassium biscyanoruthenium(II) phthalocyanine* $K_2[(CN)_2RuPc]$

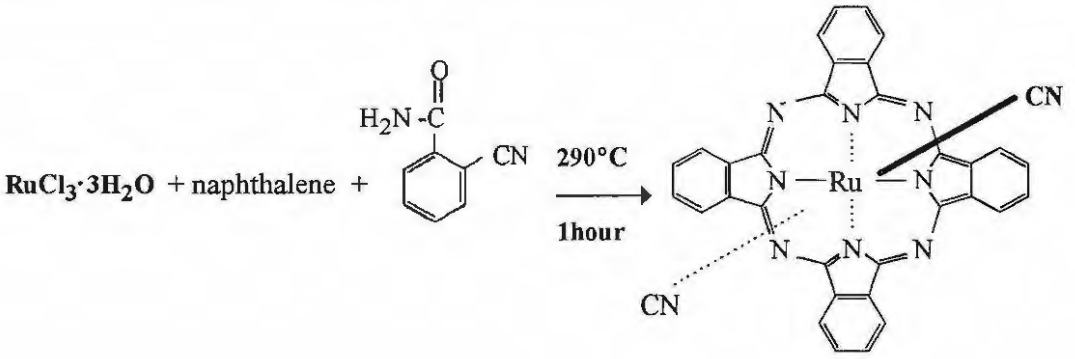

***Scheme 3**: A simplified synthetic route for $[(CN)_2RuPc]^{2-}$*

a) Crude RuPc

Crude RuPc was prepared according to the method used by Farrell[124]. $RuCl_3.3H_2O$, O-cyanobenzamide and naphthalene were mixed in a ratio of 1: 12.6: 5.06, respectively, in a round bottomed flask and heated for 1 hour at 290°C. The mixture was cooled, washed with ethanol and filtered. The dried residues were Soxhlet-extracted with glacial acetic acid until the washings were colourless. The remaining greenish-black solid was dried in vacuo, in order to remove excess acetic acid. The crude RuPc formed was used further as a precursor for the preparation of the cyanated RuPc.

b) O-cyanobenzamide

O-cyanobenzamide was prepared by dissolving 16.4g of phthalamide in 54.6ml of acetic anhydride, heating the mixture as fast as possible to the boiling point and then refluxing the solution (using a water condenser) for 3 hours. After cooling the solution, white needle shaped crystals were formed which were washed with cold alcohol and dried at 100°C overnight. Its melting point range was 170-190°C as expected.

c) Phthalamide

The phthalamide used was prepared by adding 20g of phthalimide to 60ml of ammonia and stirred for 24 hours. The resulting solution was filtered and the white crystals formed were

dried at 100°C for 2 hours. M.P. 218-224°C as expected.

d) $K_2[RuPc(CN)_2]$

Crude RuPc (0.05g, 0.08mmol) and KCN (0.05g, 0.77mmol) were suspended in absolute ethanol ($10cm^3$). The mixture was refluxed for 3 hours (using a water condenser), yielding a blue solution. The solution was filtered to remove insoluble RuPc and the filtrate evaporated to dryness. The purple-coloured solid formed was washed repeatedly with absolute ethanol to remove excess cyanide and then finally recrystallized from ethanol. The final product, $K_2[RuPc(CN)_2]$ was characterised via infrared spectroscopy and cyclic voltammetry to ensure its purity.

4.3.2.4 Oxomolybdenum (V) phthalocyanine complex- (OMo(V)(OH)Pc)

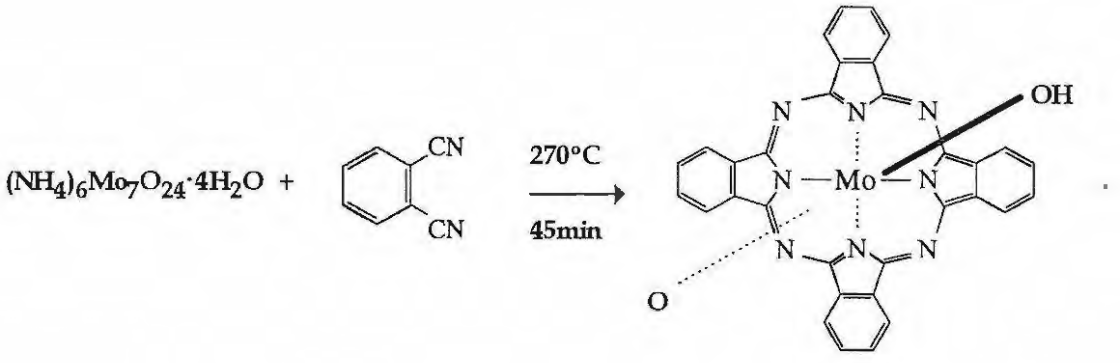

***Scheme 4**: A simplified synthetic route for (OMo(V)(OH)Pc)*

OMo(V)(OH)Pc was synthesised by the procedure of Edmondson and Mitchell[125]. Ammonium molybdate and phthalodinitrile were mixed in a ratio of 1:4, respectively. The mixture was ground until homogeneous and heated in air at 270°C for 45 minutes. The blue solid formed was purified by Soxhlet-extraction with butanone for 6 hours. The product was then washed with 0.1 mol dm^{-3} sodium hydroxide and water to remove any unreacted molybdate, molybdenum oxide or phthalamide. The product was then further washed with ethanol and acetone until the washings were colourless.

4.3.3 Apparatus

Electrochemical data were collected with the computerised Bio Analytical Systems (BAS) CV-50W voltammetric analyser, equipped with a C2 cell stand. For electrochemical experiments employing phthalocyanine complexes of ruthenium and molybdenum, a BAS Model CV 27 voltammograph equipped with a C2 cell stand, was employed. When the BAS CV 27 was used, CV data were collected on a Hewlett-Packard 7047A X-Y plotter. A three-electrode system was employed for all electrochemical measurements. This consisted of a glassy carbon working electrode of 1.5mm radius and a platinum wire auxiliary electrode. For aqueous solutions, silver/silver chloride (Ag/AgCl, 3M KCl) was employed as the reference electrode.

A silver wire electrode coated with silver chloride was employed as a pseudo reference electrode in electrochemical studies in organic solutions. In these instances ferrocene was added to the solution as an internal standard and the $E_{1/2}$ value versus the ferrocenium/ferrocene (fc^+/fc) couple determined. Potentials were referenced to fc^+/fc by subtracting $E_{1/2}$ fc^+/fc from potentials measured at Ag wire. The $E_{1/2}$ of fc^+/fc has been determined in DMF to be 0.45 V *vs* saturated calomel electrode (SCE). [126,127]. Potentials vs fc^+/fc were thus referenced to the SCE by adding 0.45 V to these values. Potential values were then referenced to Ag/AgCl, 3M KCl by adding 0.05V to these values. All potential values reported are *vs* Ag/AgCl. The glassy carbon electrode of 1.5mm radius when modified by anodic deposition with $[CoTSPc]^{4-}$] is referred to as the CoTSPc-CMGCE.

Electronic absorption spectra were recorded with a Cary IE UV-Vis spectrophotometer in the ultraviolet-visible range. Spectrophotometric cells of 1cm pathlength were used. Concentrations of both the $[CoTSPc]^{4-}$ and $[(CN)_2RuPc]^{2-}$ solutions were determined from absorbance measurements and an extinction coefficient of 58,000 $dm^3mol^{-1}cm^{-1}$ and 60,000 $dm^3mol^{-1}cm^{-1}$ [122], respectively.

Infrared (IR) spectra using potassium bromide discs of the purified MPc complexes were collected with a Perkin-Elmer Model 180 IR, or Fourier Tranform (FTIR) 2000 IR spectrometer.

4.3.4 Electrochemical Methods

As explained in Section 3.3, all glassware was thoroughly washed in hot soapy water, rinsed in deionised water and soaked in dilute acid solutions before being rinsed thoroughly with deionised water.

The glassy carbon working electrode was modified by anodic electrodeposition from a 10^{-3} mol dm^{-3} solution of the MPc complexes, $[CoTSPc]^{4-}$, Fe(II)Pc and Ni(II)Pc, in DMF, containing 0.1 mol dm^{-3} tetraethylammonium perchlorate. For anodic electrodeposition of $[(CN)_2RuPc]^{2-}$ the solvent used was pH 9 buffer. The MPc solution was bubbled with nitrogen for 10 minutes.

The cyclic voltammogram waveform was chosen. Unless otherwise stated, electrodeposition was performed by scanning the carbon working electrode continuously in the potential range of -0.2 V to 1.0 V at a scan rate of 100 mV s^{-1}. By choosing the multi-run option in the CV50 programme, the number of runs can be controlled. Twenty scans were continuously cycled and this number used each time to ensure reproducibility of the modified electrode surface.

The working electrode, once modified, was rinsed in the solvent to free the electrode of contaminating MPc not electrodeposited. A fresh surface of the electrode was obtained by cleaning the electrode using alumina, followed by soaking in dilute acid and rinsing of the electrode in water, acetone (only when organic solvents were used) and then in the solvent to be used for electrodeposition.

CoPc and OMo(OH)Pc were attached to the electrode by the drop-dry method for adsorption of the MPc onto the electrode. A concentrated solution of the MPc (~1 x 10^{-3} mol dm^{-3}) in an organic solvent was bubbled with nitrogen for 10 minutes. 4µl of this solution was placed on the GCE surface and allowed to dry under a gentle flow of nitrogen gas. The electrode was then rinsed in the solvent to free the electrode surface of unadsorbed MPc.

Voltammetric measurements were conducted at a) MPc-CMGCE in solutions containing no cysteine, b) solutions containing cysteine, and c) at unmodified GCE in cysteine-containing solutions.

Electrochemical experiments with $[OMo(OH)TSPc]^{4-}$ was conducted with the MPc dissolved in pH 2 phosphate buffer. Voltammetric measurements were conducted in this solution in the absence and presence of cysteine.

Concentrations of the MPc were of the order of 10^{-5} to 10^{-6} mol dm^{-3} for electronic absorption spectral studies and 10^{-3} mol dm^{-3} for cyclic voltammetry.

4.4 RESULTS AND DISCUSSION

Voltammetric Studies on Dipotassium Biscyanoruthenium(II) Phthalocyanine ($K_2[(CN)_2RuPc)]$

4.4.1 Characterisation of $K_2[(CN)_2RuPc]$

4.4.1.1 Absorption Spectroscopy

Absorption spectra of $[(CN)_2RuPc]^{2-}$ in acetonitrile are shown in Fig 4.4. In the visible region, intense absorption maxima were observed at 620 nm with a weaker band at 565 nm, characteristic of the Q band spectra of metallophthalocyanines. Characteristic absorption in the Soret region was observed at 345nm[128,129].

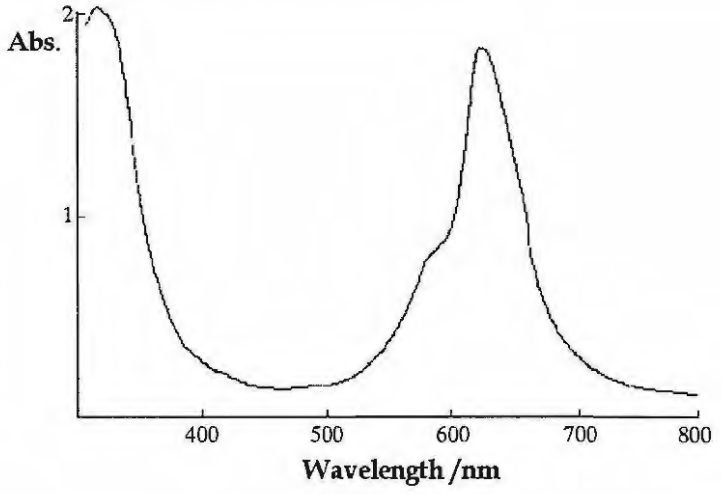

Figure 4.4 Electronic Absorption Spectra for $[(CN)_2RuPc]^{2-}$ in acetonitrile.

4.4.1.2 Infra-Red Spectroscopy

Figure 4.5 shows the IR spectra of $[(CN)_2RuPc]^{2-}$. IR spectral analysis show bands typical of MPc complexes and of Ru-CN bands at 2067 cm^{-1} [128,129]. Appendix 1 tabulates this information.

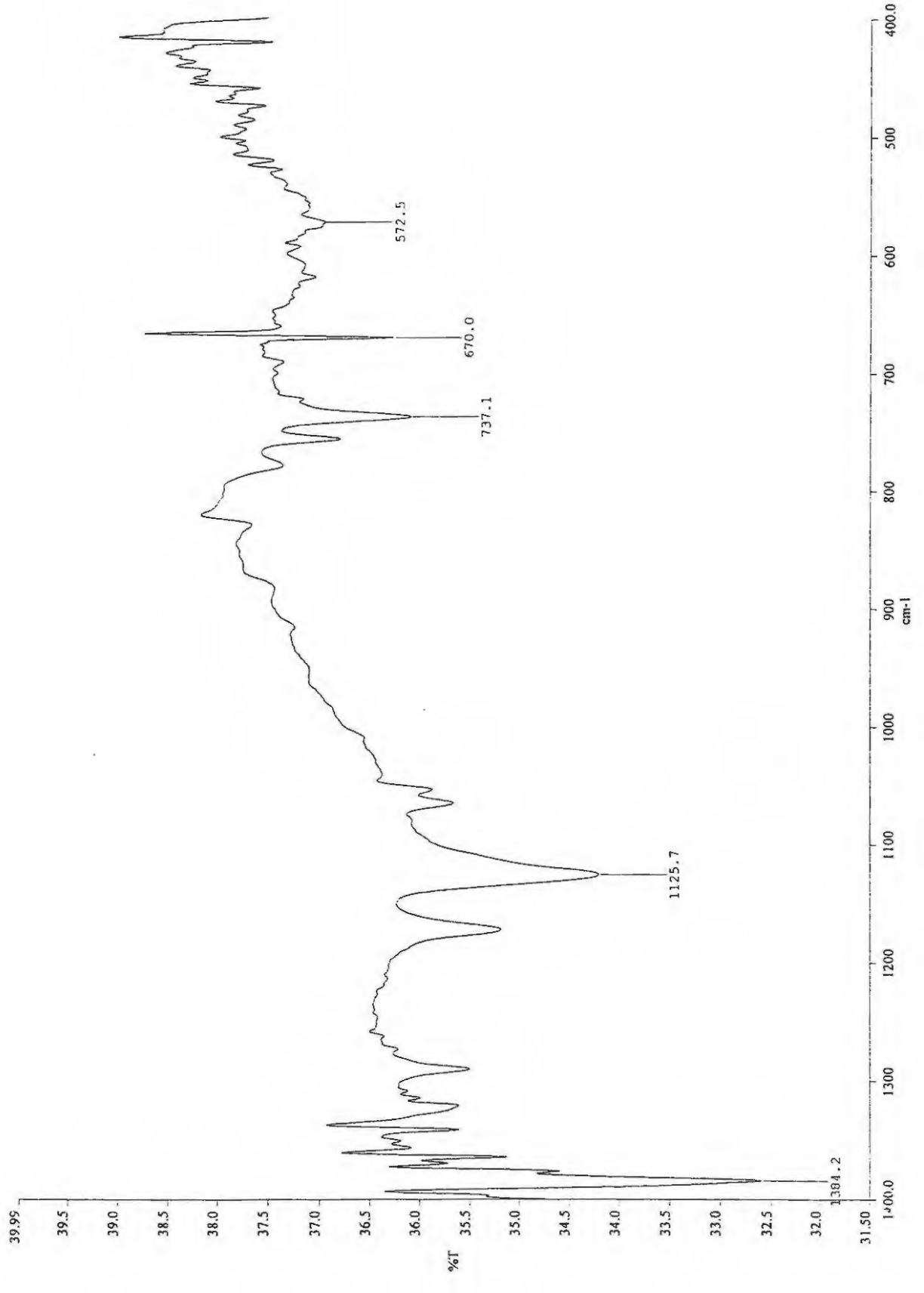

Figure 4.5 Infrared spectra for $K_2[(CN)_2RuPc]$ (KBr discs)

4.4.1.3 Cyclic Voltammetry

Figure 4.6 shows the CV obtained for $[(CN)_2RuPc]^{2-}$ in pH 9 buffer. The redox couple, E_{pa} = 0.33 V and E_{pc} = 0.19 V, with $E_{½}$ = 0.26 V *vs* Ag/AgCl, is quasi-reversible with ΔE_p = 140 mV. This oxidation couple is consistent with the oxidation of the phthalocyanine ring in $[(CN)_2RuPc]^{2-}$ [129]. For $[(CN)_2RuPc]^{2-}$, two successive ring oxidations are observed in RuPc, Equations 4-7 and 4-8[128].

$$[(CN)_2RuPc\ (-2)]^{2-} \rightarrow [(CN)_2RuPc\ (-1)]^{-} + e^{-} \qquad \text{Equation 4-7}$$

$$[(CN)_2RuPc\ (-1)]^{-} \rightarrow [(CN)_2RuPc\ (O)]^{0} + e^{-} \qquad \text{Equation 4-8}$$

The couple shown in Figure 4.6 corresponds to the first ring oxidation, Equation 4-7.

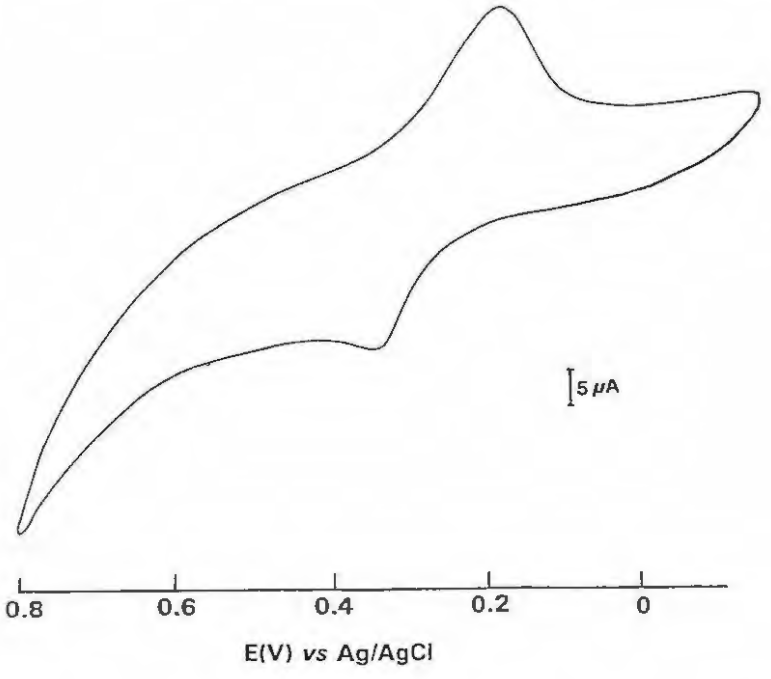

Figure 4.6 Cyclic Voltammogram of $[(CN)_2RuPc]^{2-}$ in pH 9 buffer. Scan rate: 200 mV s^{-1}.

4.4.2 Chemical Modification of GCE

Figure 4.7 shows repetitive CV's scanned from -0.2 V to 0.8 V for $[(CN)_2RuPc]^{2-}$ in pH 9 buffer. The peak currents for the oxidation of $[(CN)_2RuPc]^{2-}$ increased with each successive potential scan, then began to decrease. The decrease in peak currents generally began after the seventh cycle. The increase in anodic and cathodic waves is consistent with the formation of a conductive phthalocyanine film. A purple film was observed on the electrode surface after removing the electrode from the $[(CN)_2RuPc]^{2-}$ solution. When the CMGCE was placed in a pH 9 buffer solution, the CV of the $[(CN)_2RuPc]^{2-}$ species was observed. No significant dissolution of the $[(CN)_2RuPc]^{2-}$ occurred. The electro-oxidised form of $[(CN)_2RuPc]^{2-}$ is insoluble in water at pH 9. Cyanide is known to act as a bridging ligand in MPc complexes[130]. The electro-oxidation of $[(CN)_2RuPc]^{2-}$ during the forward scan to produce the π cation radicals, is probably followed by the polymerisation of the radical to form CN^- linked polymers at the electrode. It is thus likely that it is the polymerised species that is reduced during the reverse scan.

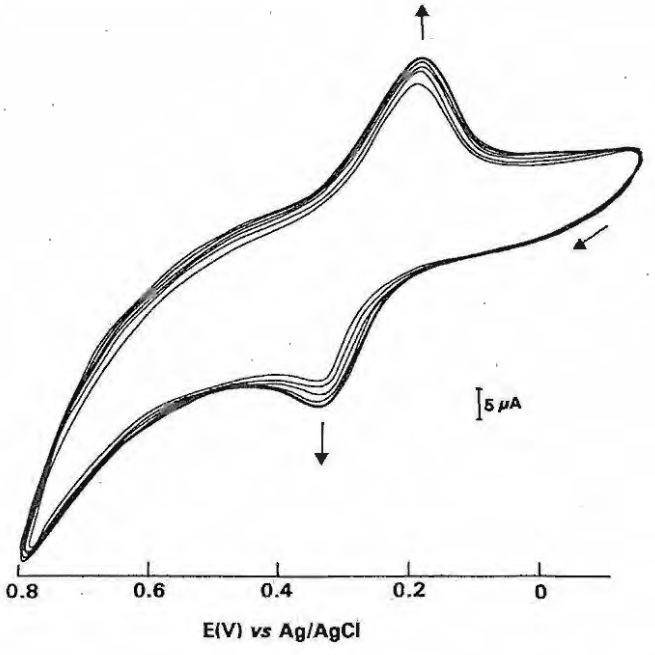

Figure 4.7 Successive CV's of $[(CN)_2RuPc]^{2-}$ in pH 9 buffer. Scan rate: 200 mV s^{-1}.

4.4.3 $[(CN)_2RuPc]^{2-}$ in Electro-oxidation of Cysteine

When the RuPc-CMGCE was placed into pH 9 buffer solutions containing cysteine, the CV shown in Fig. 4.8 a) was observed. The last scan of electropolymerisation of $[(CN)_2RuPc]^2$ from Fig 4.7 is shown as the dotted line. The principal change then is the marked increase in the anodic current associated with the first ring oxidation of $[(CN)_2RuPc]^{2-}$ with a potential shift from 0.33 V to 0.43 V *vs* Ag/AgCl. This indicates the electrocatalytic oxidation of cysteine by this species. These changes were not observed in the absence of cysteine and no anodic waves associated with the oxidation of cysteine were observed at an unmodified GCE. No return peak is observed following oxidation (Fig 4.8 a) consistent with the irreversible oxidation of cysteine[107]. On subsequent scans, the anodic currents decreased in intensity, as represented by Fig. 4.8 b) and c). This is consistent with the depletion of cysteine near the electrode surface after the first scan or the poisoning of the electrode by the oxidation products. The anodic current on the first scan was found to be directly proportional to the cysteine concentration.

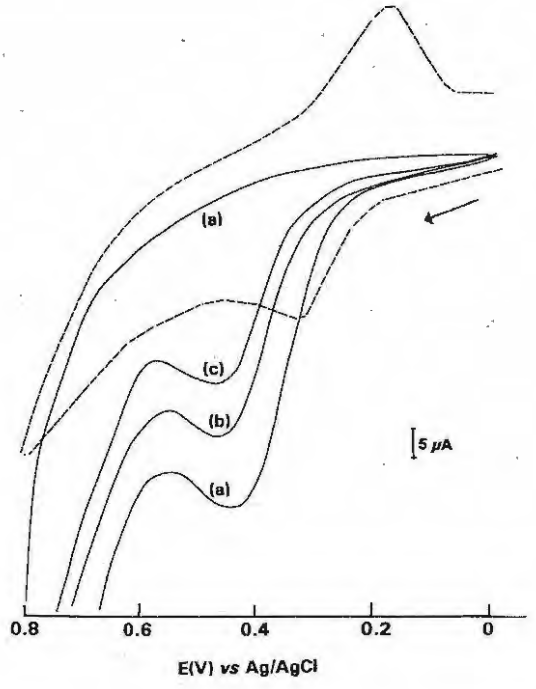

Figure 4.8 CV of 1 x 10^{-2} M cysteine at RuPc-CMGCE. a) First, b) second and c) third scans. Electrolyte: pH 2.5 buffer. Scan rate; 200 mV s^{-1}. Dotted line is the CV of $[(CN)_2RuPc]^{2-}$ corresponding to the last scan in Fig. 4.7.

The potential difference of 100 mV in the anodic potential of $[(CN)_2RuPc]^{2-}$ before and after addition of cysteine, may indicate that a different species from $[(CN)_2RuPc]^{2-}$ is oxidised in the presence of cysteine. This may be due to the prior formation of a cysteine compound with $[(CN)_2RuPc]^{2-}$ before the electron transfer, Equation 4-9 below.

The RuPc-CMGCE could be regenerated (greater than 70%) by electrolysing the electrode at -1.0 V. The extent of the regeneration was determined by comparison of the intensities of the anodic currents on freshly coated electrode and on regenerated electrode.

The proposed reaction mechanism for the electrocatalytic oxidation of cysteine at RuPc-CMGCE is represented by Equations 4-9 to 4-12. The electrocatalytic process is initiated by the electrochemical oxidation of [RuPc(-2)] to $[RuPc(-1)]^+$. This step catalyses the transfer of an electron from cysteine to $[RuPc(-1)]^+$, to regenerate [RuPc(-2)].

RuPc(-2) + RSH	$\rightarrow$	**RuPc(-2)RSH**	Equation 4-9
RuPc(-2)RSH	$\rightarrow$	**$[RuPc(-1)]^+ \cdot RSH + e^-$**	Equation 4-10
$[RuPc(-1)]^+ \cdot RSH$	$\rightarrow$	**$RuPc(-2)RS\cdot + H^+$**	Equation 4-11
2RuPc(-2)RS•	$\rightarrow$	**2RuPc(-2) + RSSR**	Equation 4-12

Where RSH = cysteine and RSSR = cystine.

The interaction of cysteine with MPc's such as CoPc occurs via the interaction of the sulphur atom of the cysteine to the d orbital of the Co central metal[100]. For metal-free porphyrins, interaction occurs between cysteine and the MPc ring[71]. Based on the observations of ring based oxidation processes it is suggested, in this work, that the cysteine interacts with the phthalocyanine ring rather than the metal during electron transfer.

Using RuPc-CMGCE a catalytic oxidation wave of 0.43 V vs Ag/AgCl for cysteine electro-oxidation presents a significant lowering in the overpotential. At CoPc adsorbed on GCE, this wave was reported at 0.77 V vs Ag/AgCl[107].

Solvents for electrodeposition

Different solvents were tested for the efficiency in electrodeposition of $[(CN)_2RuPc]^{2-}$ onto GCE as described above for pH 9 buffer. These CMGCE were then tested for catalysis of cysteine under the same conditions described. So for $[(CN)_2RuPc]^{2-}$ dissolved in the following solvents with TEAP as electrolyte for organic solvents, the results were as follows:

Pyridine: Increasing cathodic and anodic waves on repetitive cycling of the modifier showed the formation of a conductive phthalocyanine film onto the GCE. A purple film was observed on the GCE. The RuPc-CMGCE showed catalytic efficiency for cysteine oxidation. On subsequent scans the cysteine anodic wave was irreproducible.

DMF: No increases in the anodic and cathodic wave observed on repetitive cycling and no film was observed at the GCE, indicating that the GCE was not chemically modified. In keeping with this result, this GCE showed no catalytic efficiency for cysteine oxidation.

Water (KNO_3 electrolyte): Slight increases in the anodic and cathodic waves were observed. A purple film was observed on the RuPc-CMGCE. This electrode showed a weak and irreproducible catalytic oxidation for cysteine.

The results indicate that the pH 9 buffer was the best solvent for the electrodeposition of $[(CN)_2RuPc]^{2-}$ to produce a RuPc-CMGCE. The catalytic efficiency of this electrode for cysteine is dependent on the growth of a conductive film at the GCE during repetitive cycling. This is evidenced by the lack of catalytic efficiency towards cysteine when deposited via the drop-dry method. These findings furthermore suggest that the catalysis of cysteine is dependent on the electro-oxidation of the [RuPc(-2)] to $[RuPc(-1)]^{+}$ species during the forward scan of electrodeposition.

Voltammetric Studies on Tetrasodium Cobalt(II) Tetrasulphophthalocyanine ($Na_4[CoTSPc].2H_2O$)*

4.4.4 Characterisation of $[CoTSPc]^{4-}$

Electronic absorption spectra of $[CoTSPc]^{4-}$ showed an intense absorption at 627nm and a less intense absorption at 660nm, as shown in Fig. 4.9. These two absorption maxima are typical of the aggregation of $[CoTSPc]^{4-}$ in aqueous solutions. In highly acidic media, the dimeric species, the Q band at 627nm, dominates over the monomeric species at 660nm.

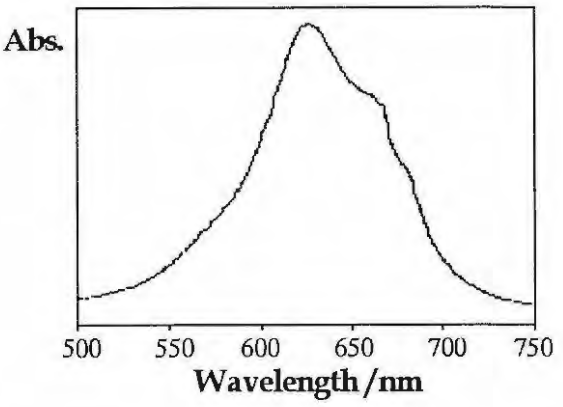

Figure 4.9 Electronic absorption spectra of $[CoTSPc]^{4-}$ in 0.005 M H_2SO_4.

The IR spectra of $[CoTSPc]^{4-}$ is shown in Fig. 4.10. Characteristic infrared spectra of the metallophthalocyanines were exhibited. This data is tabulated in Appendix 1.

---

* The following publication resulted from the research on the interaction of $[CoTSPc]^{4-}$ with cysteine. For the sake of continuity, it is not further referenced in this chapter: Janice Limson and Tebello Nyokong, Voltammetric behaviour of Cysteine and Metallothionein on cobalt(II) tetrasulphonated modified glassy carbon electrodes, *Electroanalysis*, **1997**, *9* (3), 255-259.

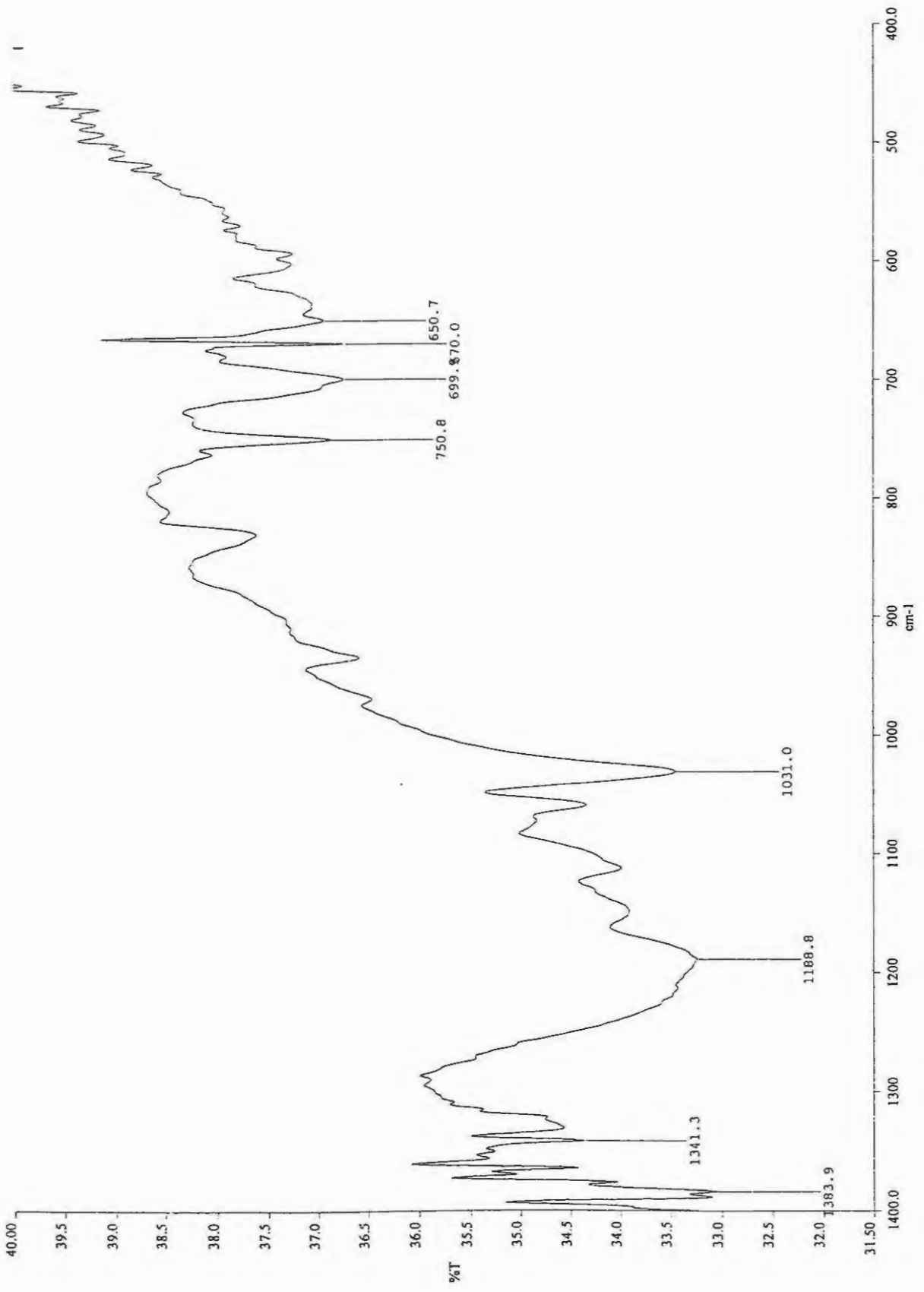

Figure 4.10 IR spectra of $[CoTSPc]^{4-}$ (KBr disks)

Cyclic voltammetry of $[CoTSPc]^{4-}$ in DMF gave the redox couples shown in Fig. 4.11. Scanning a potential window from -1.4 V to +1.4 V showed four couples. Two quasi-reversible reduction couples were observed at -0.28 V and -1.31 V *vs* Ag/AgCl. In donor solvents such as DMF, the first reduction is known to occur at the metal in CoPc complexes[110]. Thus, the reduction couples observed at -0.28 V and -1.31 V correspond to the reduction of $[Co(II)TSPc(-2)]^{4-}$ to $[Co(I)TSPc(-2)]^{5-}$ and of further reduction of $[Co(I)TSPc(-2)]^{5-}$ to $[Co(I)TSPc(-3)]^{6-}$, respectively. The first oxidation shows only a weak cathodic return peak. It has been reported before that the first oxidation of $[CoTSPc]^{4-}$ is irreversible in DMF [110]. The anodic peak for the first oxidation is observed at 0.70 V and it corresponds to the oxidation of $[Co(II)TSPc(-2)]^{4-}$ to $[Co(III)TSPc(-2)]^{3-}$. The second oxidation couple, observed at 1.19 V, was quasi-reversible, this couple corresponds to ring oxidation of $[Co(III)TSPc(-2)]^{3-}$ to $[Co(III)TSPc(-1)]^{2-}$.

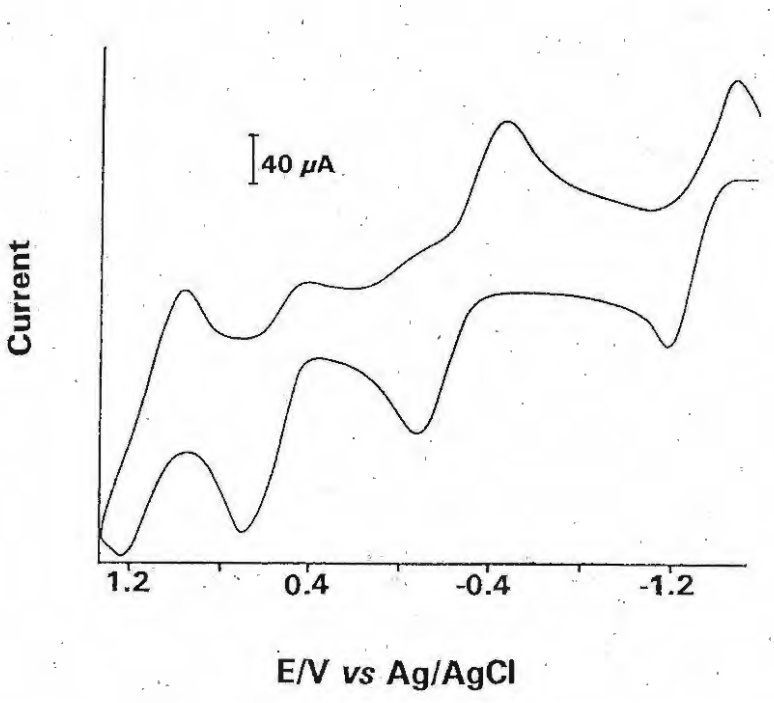

Figure 4.11 Cyclic voltammogram (*vs* Ag/AgCl (KCl saturated)) of $[Co(II)TSPc]^{4-}$ in DMF containing 0.1 mol dm^{-3} TEAP. Scan rate 100 mV s^{-1}.

4.4.5 Chemical Modification of GCE

The first oxidation of $[Co(II)TSPc]^{4-}$ to $[Co(III)TSPc]^{3-}$ is believed to be the transition which catalyses the oxidation of cysteine[107]. The potential window to effect electrodeposition of the electroactive species was optimised. As mentioned in the Section 4.3.4, a potential window of -0.2 V to 1.0 V was selected to effect electrodeposition of the $[CoTSPc]^{4-}$ species. The lower potential limit was optimised in terms of efficient electrodeposition and the catalytic efficiency for cysteine oxidation. Exceeding the upper limit of 1.0 V brought about the formation of electrodeposited species with no catalytic efficiency for cysteine oxidation.

Repetitive scanning between -0.2 and 1.0 V *vs* Ag/AgCl at 100 mV s^{-1} of a 1 x 10^{-3} mol dm^{-3} solution of $[CoTSPc]^{4-}$ showed a gradual increase in the faradaic current of the first oxidation of $[CoTSPc]^{4-}$, Fig. 4.12, indicating the formation of a conductive phthalocyanine film by electrodeposition of $[CoTSPc]^{4-}$ onto the glassy carbon electrode. Increases in both the anodic and cathodic wave are required for effective electrodeposition. The coating increased steadily and then slowed down. After 20 cycles, the electrode was removed from solution. A purple film was observed on the electrode surface. Excess $[CoTSPc]^{4-}$ was rinsed off in water. The surface coverage after 20 cycles was calculated from the charge under the anodic curve to be = 8.5 x 10^{-8} mol cm^{-2}, as described in Section 2.6.4, Equation 2-20 , $Q = nFA\Gamma$.

The electrode covered by the electrodeposited film of $[CoTSPc]^{4-}$ showed stability when left in water for several hours, under nitrogen atmosphere. Its reproducibility in terms of catalytic efficiency for cysteine oxidation is discussed further.

Electrodeposition of the $[CoTSPc]^{4-}$ film was also attempted with acetonitrile and pyridine. As discussed, the nature of the solvent is critical for film growth. Using acetonitrile and pyridine as solvents did not show the increases in both anodic and cathodic currents expected for electrodeposition of the $[CoTSPc]^{4-}$ onto the electrode. For

pyridine, increases in the anodic currents were observed, but these were not strongly adherent and did not show reproducibility for cysteine analysis. Electrodeposition in which a strongly adherent film was produced, proceeded best from DMF, with careful attention to cleanliness of the electrodes, purity of the solvent and electrolyte and positioning of the electrodes equidistant from each other .

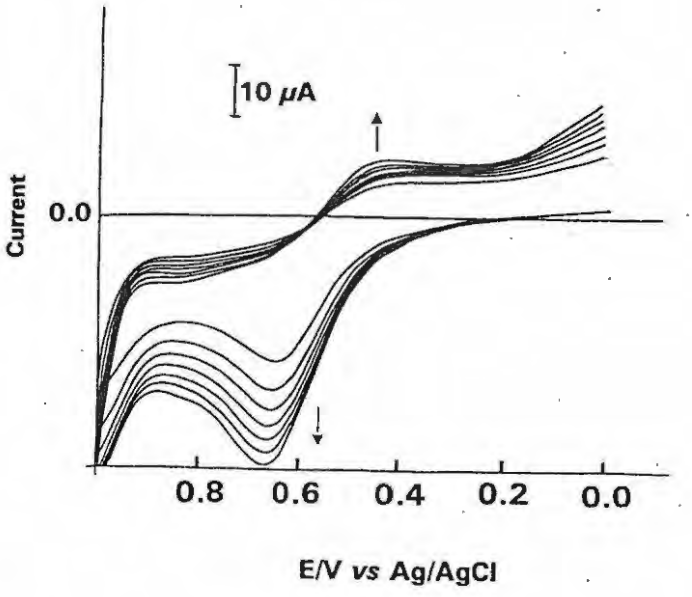

Figure 4.12 Electrodeposition of $[Co(II)TSPc]^{4-}$, dissolved in DMF containing 0.1 mol dm^{-3} TEAP, onto a glassy carbon electrode. Scan rate = 100 mV s^{-1}.

4.4.6 Catalysis of Cysteine

The glassy carbon electrode chemically modified by electrodeposition of $[CoTSPc]^{4-}$ was tested for its catalytic efficiency for cysteine oxidation at various pH's.

Fig. 4.13 a) shows the cyclic voltammogram obtained for 0.01 mol dm^{-3} cysteine, dissolved in 0.05 mol dm^{-3} H_2SO_4, at an unmodified glassy carbon electrode. No cysteine oxidation currents were observed at the unmodified electrode. Fig. 4.13 b) shows the CV of the same solution on CoTSPc-CMGCE. At the CoTSPc-CMGCE, a strong anodic peak was observed at 0.82 V. The reverse scan showed an irregular shape with an anodic

dip in current. The formation of an anodic dip on cathodic return scans has been observed before for $[CoTSPc]^{4-}$-catalysed oxidation of thiols and was attributed to the involvement of a complexation step during catalysis by $[CoTSPc]^{4-}$ species[107].

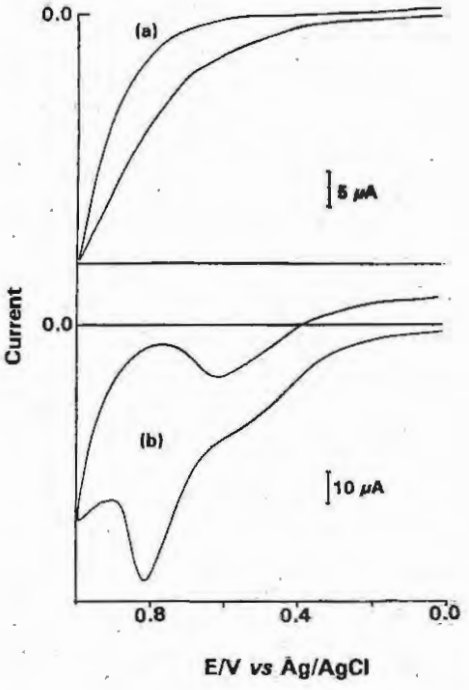

Figure 4.13 Cyclic voltammetry of 0.01 mol dm^{-3} cysteine on (a) unmodified glassy carbon electrode and (b) CoTSPc-CMGCE. Electrolyte = 0.05 mol dm^{-3} H_2SO_4. Scan rate = 100 mV s^{-1}.

Fig. 4.14 (1) shows the 20th scan from the electrodeposition of $[Co(II)TSPc]^{4-}$and Fig. 4.14 (2) shows the enhancement in the wave attributed to the oxidation of $[Co(II)TSPc(-2)]^{4-}$ to $[Co(III)TSPc(-2)]^{3-}$ during electrocatalysis of cysteine. This indicates that it is the oxidation of $[Co(II)TSPc(-2)]^{4-}$ to $[Co(III)TSPc(-2)]^{3-}$ which catalyses the oxidation of cysteine. A broad ill-defined pre-anodic wave at lower potentials than the oxidation of cysteine is observed in Fig 4.13 b) and 4.14 (2). This wave is more noticeable at less acidic pH's and has been observed before[47]. This oxidation is not believed to be involved in the catalysis of cysteine. It is suggested here that it is due to the presence of some monomeric $[Co(II)TSPc]^{4-}$ species in solution.

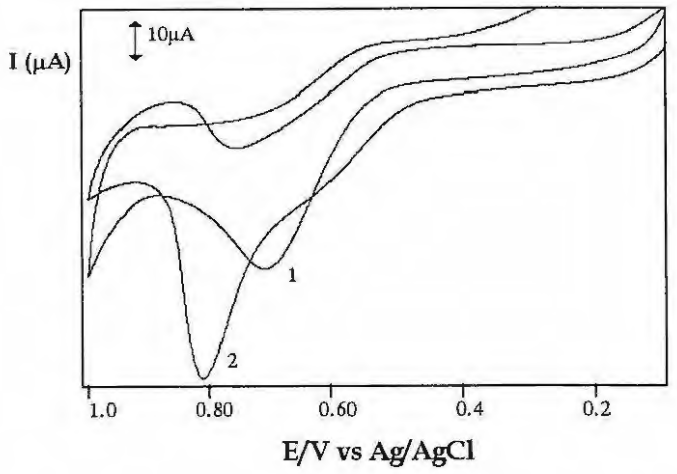

Figure 4.14 Cyclic voltammetry showing the peak due to the electrodeposition of $[Co(II)TSPc]^{4-}$ from DMF (1), which is the final scan in Figure 4-12; and the enhancement of this peak at CoTSPc-CMGCE in the presence of 0.005 mol dm^{-3} cysteine (2) after cysteine oxidation. Electrolyte: 0.05 mol dm^{-3} H_2SO_4. Scan rate = 100 mV s^{-1}.

At pH 1 the cysteine is unionised and fully protonated. According to Halbert[107] the oxidation of cysteine is catalysed by the $[Co(III)TSPc]^{3-}$ species generated by the oxidation of $[Co(II)TSPc]^{4-}$ in the forward voltammetric scan, Equations 4-13 and 4-14. Figure 4.15 shows a schematic representation of these reactions.

$$[Co(II)TSPc]^{4-} \rightarrow [Co(III)TSPc]^{3-} + e^- \qquad \text{Equation 4-13}$$

$$2[Co(III)TSPc]^{3-} + 2RSH \rightarrow 2[Co(II)TSPc]^{4-} + RSSR \qquad \text{Equation 4-14}$$

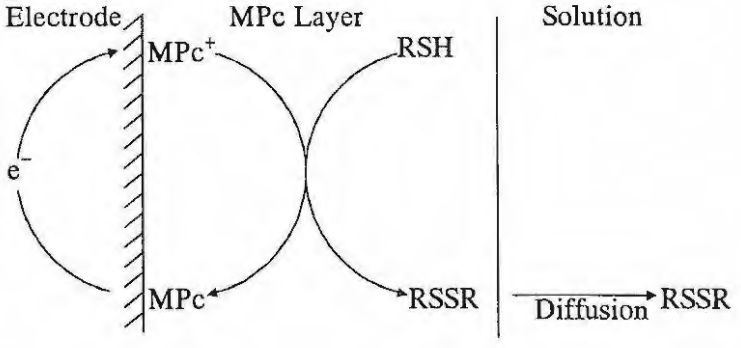

Figure 4.15 Schematic representation of electron transfer between CoTSPc-CMGCE and cysteine.

Studies have shown that addition of cysteine to $[OMo(V)(OH)TSPc]^{4-}$ solutions resulted in a shift to higher energies of the spectra of $[OMo(V)(OH)TSPc]^{4-}$ in 0.05 M H_2SO_4 [131]. These spectral changes were associated with the co-ordination of cysteine to $[OMo(V)(OH)TSPc]^{4-}$ prior to the electron transfer reactions. It is also quite likely that a complex is formed between cysteine and $[Co(II)TSPc]^{4-}$ prior to the electrocatalytic oxidation reaction. At these low pH's this is electrostatically feasible taking the positive charge on the cysteine into account.

The enhancement of the anodic currents observed in Fig. 4.13 b) on addition of cysteine is a consequence of electron transfers by Equations 4-13 and 4-14. $[Co(II)TSPc]^{4-}$ is regenerated after electron transfer to the cysteine, a feature of an efficient catalyst. At these low pH's, the cystine formed as the product of the oxidation of cysteine remains in solution and does not contaminate the CoTSPc-CMGCE. For this reason the anodic currents shown in Fig. 4.13 b) were reproducible, and the chemically modified electrode did not suffer loss of catalytic efficiency. This was proven by reproducibility of current response after repeated measurements in a cysteine solution.

Furthermore, the catalytic wave at 0.82 V associated with cysteine oxidation increased with the increase in cysteine concentration, Fig. 4.16. A plot of the variation of peak current, i_p, with cysteine concentration, Fig. 4.17, was linear only at low concentration ($< 10^{-3}$ mol dm^{-3}). At higher concentrations of cysteine, deviations from linearity for plots of i_p *vs* cysteine concentration are expected. This may be due to the interactions between cysteine molecules at the electrode with increased competition for sites at the electrode as these become limited with increased cysteine concentration.

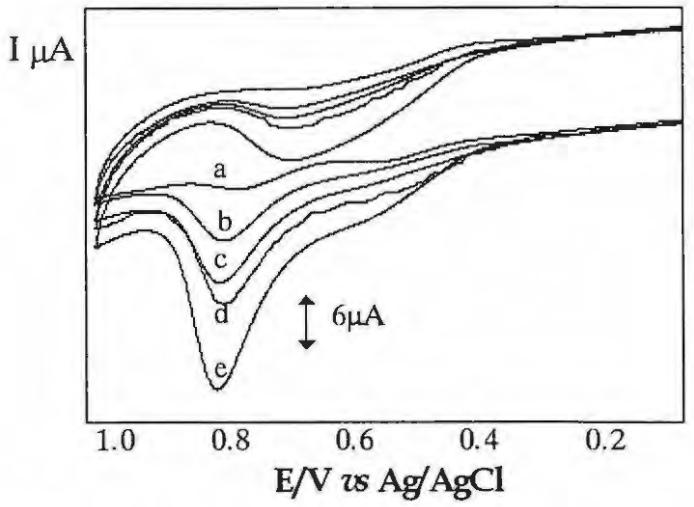

Figure 4.16 Cyclic voltammograms of cysteine on CoTSPc-CMGCE. Cysteine concentrations shown, a) to e) between $1x10^{-7}$mol dm^{-3} and $5x10^{-4}$ mol dm^{-3}. Electrolyte = 0.05 mol dm^{-3} H_2SO_4. Scan rate = 100 mV s^{-1}.

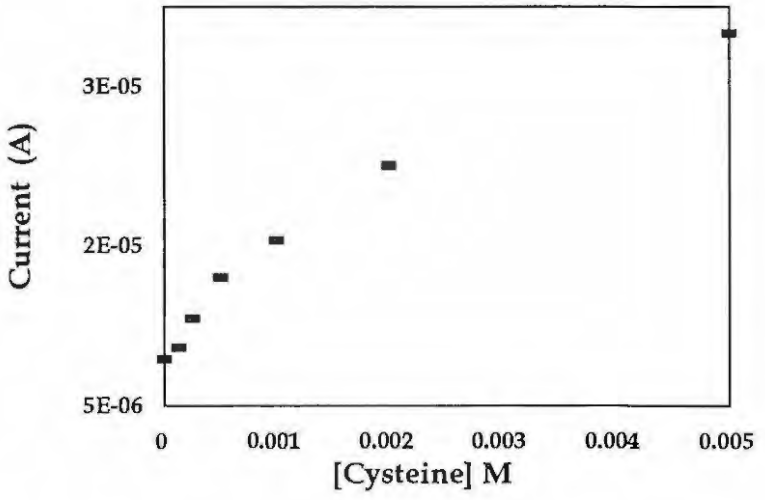

Figure 4.17 The variation of cysteine concentration with the anodic currents for the oxidation of cysteine on CoTSPc-CMGCE. Electrolyte = 0.05 mol dm^{-3} H_2SO_4. Scan rate = 100 mV s^{-1}.

The lowest cysteine concentration that was detected using CV and CoTSPc-CMGCE was near 1 x 10^{-8} mol dm^{-3}, a value slightly higher than that observed for the detection of cysteine on CoPc[126] carbon paste electrodes.

The mode of mass transfer of cysteine to the electrode was determined by measuring the anodic current at increasing scan rates, Fig 4.18. These values were plotted against the square root of the scan rate in the range 100 to 800 mV s^{-1}, Fig. 4.19. The linear relation found indicated a diffusion controlled cysteine oxidation.

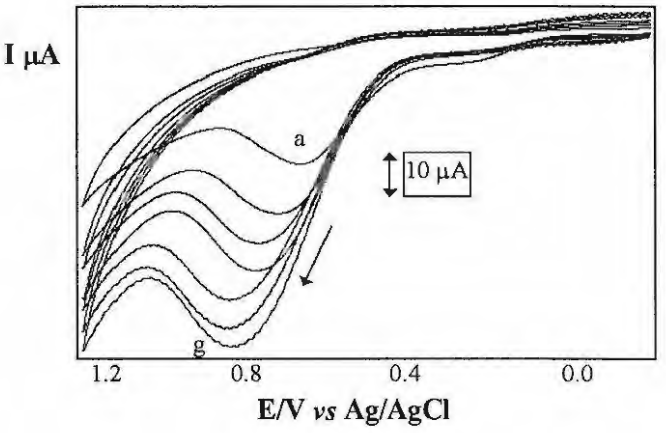

Figure 4.18 Cyclic voltammograms on CoTSPc-CMGCE for the oxidation of 0.01 mol dm^{-3} cysteine in 0.05 mol dm^{-3} H_2SO_4, at scan rates a) to g) between 100 and 800 mV s^{-1}.

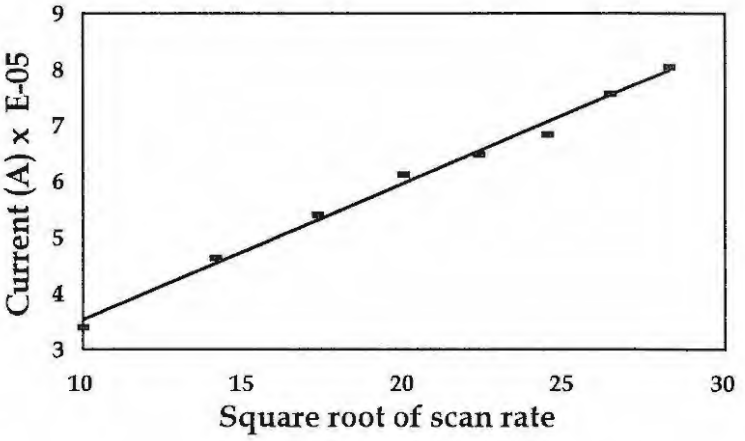

Figure 4.19 Peak current versus the square root of scan rate ($v^{1/2}$) for the oxidation of 0.01 mol dm^{-3} cysteine in 0.05 mol dm^{-3} H_2SO_4 on CoTSPc-CMGCE.

Solution-phase catalysis of cysteine was also observed at this low pH. Voltammograms similar to those shown in Fig. 4.13 b) could also be obtained for catalytic oxidation of cysteine by $[Co(II)TSPc]^{4-}$ in 0.05M H_2SO_4 and using unmodified glassy carbon electrodes. In this case, the anodic currents associated with cysteine were observed at

0.77 V as has been observed before[107]. The anodic current response for the solution-phase catalysis of cysteine was reproducible only after bubbling with nitrogen in between repeated scans. It is believed that this convection action will remove oxidised species at the electrode-solution interphase.

The oxidation of cysteine occurs at a relatively low potential when acidic solutions of $[Co(II)TSPc]^{4-}$ are employed in catalysis, E_p = 0.77 V [107]. The potentials obtained during the catalytic oxidation of cysteine with metallophthalocyanine complexes are a function of the oxidation potentials of the catalysts [131]. The differences between the potentials obtained for the catalytic oxidation of cysteine on CoTSPc-CMGCE and those obtained for solution catalysis employing the same catalyst, may reflect the higher oxidation potential for the surface bound $[Co(II)TSPc]^{4-}$ relative to the potentials of this species in solution. Catalysts that result in a larger lowering of the oxidation potential for sulphydryl compounds are preferred since they make the electrochemical determination of the species more feasible. While this slightly lower oxidation potential is observed during solution-phase catalysis, it is countered by a slight loss in current response over catalysis at a chemically modified electrode. A further advantage of the use of the chemically modified electrode is that the sample, in this case cysteine, may be used for further analytical experiments as it remains uncontaminated by the $[CoTSPc]^{4-}$. Any leaching of the $[CoTSPc]^{4-}$ from the electrode which could cause contamination of the cysteine and the loss of activity of the electrode, would be clearly visible as the solution would become discoloured. No leaching was observed for electrodeposited $[CoTSPc]^{4-}$ GCE.

4.4.7 Voltammetric Response of Cysteine at pH = 8.4

As electrochemical studies of amino acids and proteins are commonly conducted at slightly basic conditions, a more detailed electrode behaviour of cysteine at a pH of 8.4 was investigated. At this pH, solutions of $[Co(II)TSPc]^{4-}$ auto-oxidises cysteine to cystine[104,105] as shown in Equations 4-2 and 4-3. It is thus not surprising that no anodic

currents were observed when CV's of solutions containing cysteine and $[Co(II)TSPc]^{4-}$ at pH = 8.4 were recorded on unmodified glassy carbon electrodes. At the unmodified GCE in pH 8.4 Tris-HCl and in the absence of cysteine, the $[CoTSPc]^{4-}$ did not show clear anodic or cathodic waves associated with the redox couples. On the addition of cysteine a colour change from blue to green was observed. This is in keeping with what has previously been observed in the pH range 5 to 9[105]. In this report,[105] ESR studies showed that cystine precipitated at pH's greater than 4, redissolving at pH 9.5 where the blue colour was restored. No colour change was observed for the same experiment at pH 1.

However, when CoTSPc-CMGCE's were employed for recording the voltammograms of solutions containing cysteine in Tris buffer at pH 8.4, CV's shown in Fig. 4.20 were observed. The peak for the oxidation of cysteine at this pH was observed at 0.85 V. There was thus no significant shift in potentials for cysteine oxidation on going from acidic to basic media.

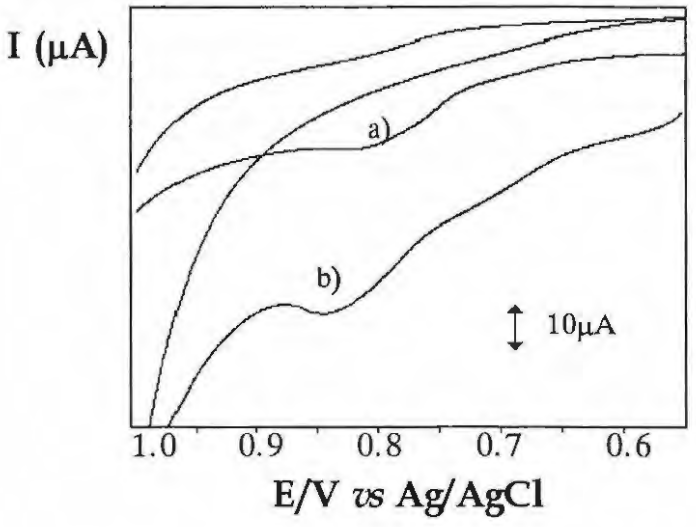

Figure 4.20 Cyclic voltammetry of (a) CoTSPc-CMGCE in buffer solution in the absence of cysteine and (b). CoTSPc-CMGCE in 0.005 mol dm^{-3} cysteine. Electrolyte = 0.2 mol dm^{-3} Tris-HCl, pH 8.4. Scan rate = 100 mV s^{-1}.

The cystine formed by the oxidation of cysteine precipitates out at pH's greater than 4,[105] inhibiting the activity of the electrode. Thus, the anodic currents for the oxidation of

cysteine on CoTSPc-CMGCE could only be observed for the first scan at this pH. Attempts to regenerate the CoTSPc-CMGCE by suggested methods of scanning from -1.0 V; cleaning the electrode at this potential for 1 minute and dipping the surface into acid media[71], were unsuccessful in regenerating the activity of the electrodeposited film for cysteine catalysis. The contamination of the electrode by cystine may also be a contributing factor to the decrease in anodic current observed at pH's above 4 (discussed further in Section 4.4.8).

The fact that anodic currents are observed for the oxidation of cysteine on CoTSPc-CMGCE at pH = 8.4 but not for solution catalysis at the same pH, suggests that when $[Co(II)TSPc]^{4-}$ is electrodeposited onto the electrode, it is not involved in the autocatalysis of cysteine that is observed in solution, Equations 4-2 and 4-3. Autocatalytic oxidation of cysteine by solutions of $[Co(II)TSPc]^{4-}$ in basic media[105], depletes its concentration to an extent that no anodic currents due to the oxidation of cysteine are observed and hence cysteine cannot be detected electrochemically under these conditions.

The mode of interaction of the cysteine with the adsorbed $[CoTSPc]^{4-}$ species is thus different from solution-phase catalysis. Previous research[106] indicated that at $[CoTSPc]^{4-}$ adsorbed on graphite, reduction of the central metal from Co(II) to Co(I), associated with autocatalysis, does not occur.

As previously suggested[106], and depicted in Fig 4.21, at high pH's the proton is dissociated from the RSH group before the electron transfer. The electrocatalytic oxidation of cysteine on CoTSPc-CMGCE may thus be summarised by Equations 4-15 to 4-17:

$$\mathbf{RSH \rightarrow RS^- + H^+} \qquad \text{Equation 4-15}$$

$$\mathbf{[Co(III)TSPc]^{3-} + RS^- \rightarrow [Co(II)TSPc]^{4-} + RS\cdot} \qquad \text{Equation 4-16}$$

$$\mathbf{2\,RS\cdot \rightarrow RSSH} \qquad \text{Equation 4-17}$$

with the $[Co(III)TSPc]^{3-}$ being generated during the forward scan, according to Equation 4-13.

4.4.8 Cysteine Electrocatalysis at various pH's

The voltammetric response of the electrodeposited $[CoTSPc]^{4-}$ for cysteine catalysis was examined at various pH's and the faradaic current measured. The concentration of cysteine (0.005M) and other variables such as scan rate were kept constant. Current responses for the oxidation of cysteine increased with increasing pH up till pH 4 and then decreased with increasing pH. Only a very weak current response due to cysteine oxidation was observed at pH 9 and none at pH 10.

The oxidation state of cysteine changes with pH according to Fig. 4.21.

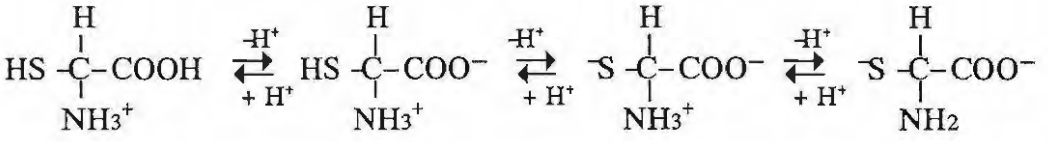

		pK_{a1}	pI	pK_{a2}		pK_{a3}	
pH:	0.71	1.71	5.02	8.33	9.55	10.78	11.78
Charge:	1	+ ½	0	-½	-1	-1½	-2

Figure 4.21 Oxidation state changes and change of cysteine with pH.

Fig. 4.21 takes into consideration the charge of the cysteine at these various pH's and the values for the charge are approximated. The current response may be a function of the charge on the cysteine. At low pH's, with a positive charge on the amino acid, higher current responses were observed. At these pH's the proton on the sulphydryl group has not yet dissociated. The proton on the carboxyl group is lost between pH 1 and 5, where the net charge on the amino acid becomes zero. The sulphydryl proton dissociates between pH 5 and 9.55, creating a net negative charge on the amino acid. Between pH 5 and 9, lower current response for cysteine oxidation were observed at the CoTSPc-

CMGCE. No current response was observed after pH 9 as the sulphydryl group is completely ionised.

This data may be compared to previous studies[132] on the vitamin B_{12} catalysed oxidation of cysteine. For vitamin B_{12} adsorbed on glassy carbon electrodes, increases in catalytic activity for cysteine oxidation were observed between pH 3 and 7 and decreases from pH 7 to 10. The decrease in catalytic currents may be associated with the unfavourable hydrogen evolution background at higher pH's.

Another explanation takes into account the increasing overall negative charge of the cysteine with increasing pH. When in solution, $[CoTSPc]^{4-}$ is expected to have four negative charges due to the sulphonate groups. $[CoTSPc]^{4-}$ is believed to adsorb to the electrode via the sulphonate groups. It is assumed that it is sterically impossible for all four groups to be involved in the adsorption and so those that are not would contribute a negative charge to the $[CoTSPc]^{4-}$. The overall positive charge on the cysteine at pH's below 4 could thus indicate a favourable electrostatic interaction at the CoTSPc-CMGCE electrode, while negative charges beyond pH 5 could be linked to unfavourable electrostatic interactions via repulsion of the negatively charged species and hence a reduced catalytic activity.

Another theory relates to the effects of aggregation of the MPc on catalytic function. At neutral pH, the Q band at 670nm, Fig. 4.22 b), associated with the monomeric species, became more resolved on addition of cysteine to a $[CoTSPc]^{4-}$ solution, showing that the interaction between cysteine and $[CoTSPc]^{4-}$ at this pH is with the monomeric species[133].

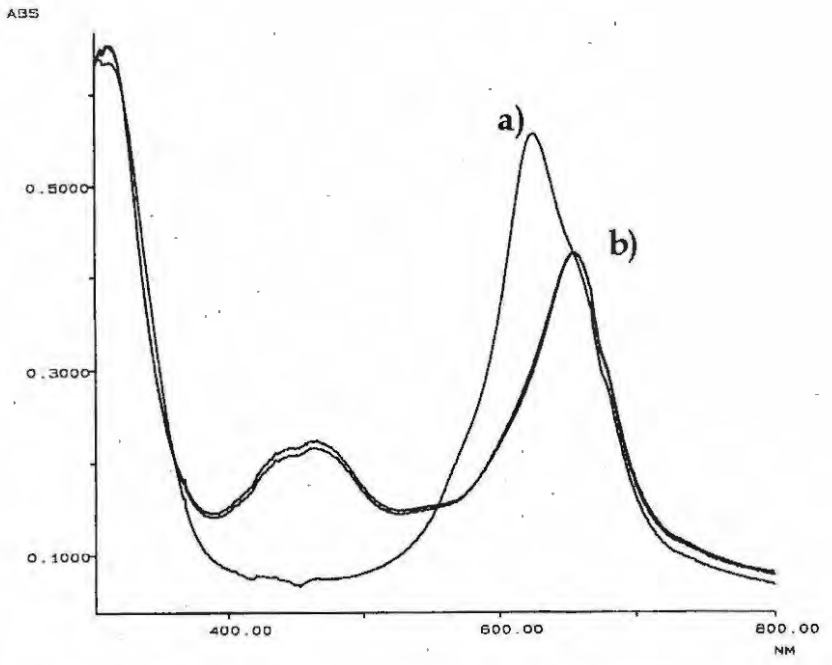

Figure 4.22 UV spectral changes on addition of cysteine b) to a solution of Co(II)TSPc a) in pH7 Tris-Buffer.

The difference in structure of $[CoTSPc]^{4-}$ in acidic and alkaline electrolytes has been discussed for $[CoTSPc]^{4-}$ adsorbed at an OPG electrode[49]. While an equilibrium exists between the monomeric and dimeric forms of the MPc's in alkaline solution, these authors suggested that, when adsorbed onto an electrode, $[CoTSPc]^{4-}$ may be dimeric in alkaline conditions, involving even higher aggregates at acidic conditions. If this situation is to be envisaged, then two waves should be seen in the case of the oxidation or reduction of a mixed valence dimer[49].

This may explain the appearance of two oxidation waves when a CoTSPc-CMGCE was placed into a cysteine solution of pH 4, shown in Fig 4.23 1 a) and 1 b). The peak denoted as 1 b) dominated over peak 1 a) at lower pH's, with the latter ill-defined and visible as a broad current response. If higher aggregates dominate at lower pH's as suggested for solution-phase studies of $[CoTSPc]^{4-}$ [122], then this may explain the dominance observed. Only at weakly acidic pH's as shown for pH 4, could both these waves be observed following electrocatalytic oxidation of cysteine. While the role of the peak at 0.84 V has been assigned to the catalytic oxidation of cysteine, evidenced for example by its cysteine dependent current response, the role of the peak at 0.61 V in catalysis of cysteine, is

unclear. It was suggested in Section 4.4.6 that this wave was due to monomeric species in solution. Peak 1 a) showed no dependence on cysteine concentration. Fig. 4.23 2 a) and 2 b) shows the current response observed on placing a CoTSPc-CMGCE into a pH 1 solution, containing no cysteine. Peak 2 b) is due to the oxidation of $[Co(II)TSPc(-2)]^{4-}$ to $[Co(III)TSPc(-2)]^{3-}$. Peak 2 a) may arise from the splitting due to stabilisation of $[Co(II)TSPc(-2)]^{4-}$mixed valence species, such as $[Co(III)TSPc(-2) \cdot Co(II)TSPc(-2)]^{7-}$ / $[Co(II)TSPc(-2)]_2^{8-}$ as suggested for Co(II)Pc[110] in solution.

Peak 2 a) and 2 b) as shown by overlapping of these CV's, may be linked with peak 1 a) and 1 b), respectively. There is almost no difference in the current response of peak 2 a) and 1 a), suggesting that peak 1 a) has no role in the electrocatalytic oxidation of cysteine at CMGCE's. The large difference between peak 2 b) and 1 b) in the presence of cysteine again corroborates the finding that this peak is associated with sulphydryl oxidation at the CMGCE.

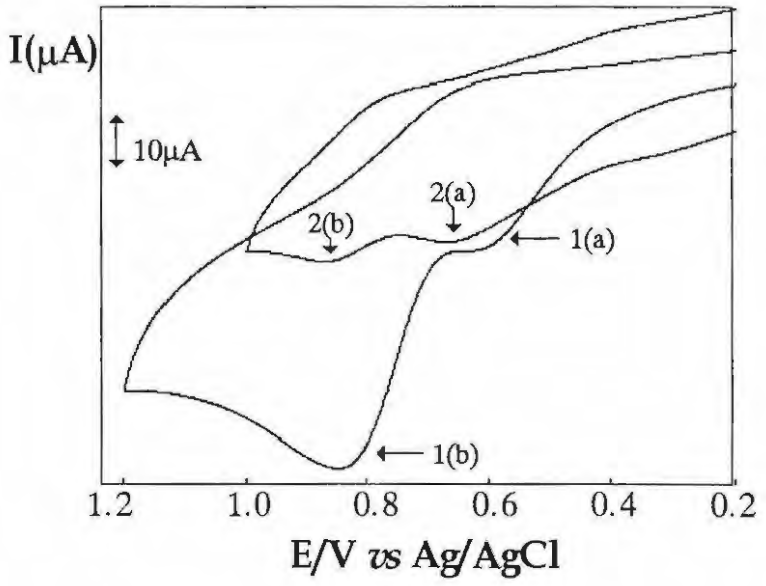

Figure 4.23 Cyclic voltammetry of 0.01 mol dm^{-3} cysteine on CoTSPc-CMGCE in pH 4 buffer solution (1) and (2) CV of CoTSPc-CMGCE in the absence of cysteine at pH 1, 0.005M H_2SO_4. Scan rate = 100 mV s^{-1}.

Dimers or aggregates of $[CoTSPc]^{4-}$ have been shown to be more active than the monomeric species for oxidation of mercaptoethanol[134]. If higher aggregation associated

with low pH's is assumed to result in better catalysis, this may explain the decrease in catalytic activity observed in these studies with increased pH. The anodic wave obtained at high pH of 9, of weaker current response, may be associated with the prevailing monomeric species in alkaline solution.

The catalysis of cysteine oxidation observed above differs from the autocatalytic oxidation of cysteine by $[CoTSPc]^{4-}$, monitored by ESR and ultraviolet spectroscopy[105]. Notably, the increase in autocatalytic oxidation of cysteine observed from pH 4 to 9 contrasts with the decrease observed in this research. The reaction when monitored electrochemically is fundamentally different. In addition, $[CoTSPc]^{4-}$ behaves differently in solution and when immobilised at the electrode.

However, solution-phase catalysis of cysteine, at an unmodified electrode by $[CoTSPc]^{4-}$ concurs with catalysis at a CoTSPc-CMGCE at pH's below 4.

4.4.9 CoPc at Chemically Modified Glassy Carbon Electrode

$[CoTSPc]^{4-}$ is the tetrasulphonated derivative of CoPc. The primary difference is that CoPc is insoluble in aqueous solutions, while $[CoTSPc]^{4-}$ is soluble in aqueous media at all pH's. Both are soluble in non-aqueous, organic media. Aqueous solution-phase catalysis is thus only possible with $[CoTSPc]^{4-}$. CoPc at chemically modified electrodes may offer an advantage in aqueous solutions as it is not expected to leach off into the solution. A glassy carbon electrode was modified by the drop-dry method, and by electrodeposition of CoPc, as explained for MPc complexes in Section 4.3.4. The efficiency of both methods in the catalytic oxidation of 0.0066 mol dm^{-3} cysteine were tested for cysteine solutions of pH 1 and pH 8.4.

Using the drop-dry method for deposition of CoPc onto the electrode, no catalytic wave due to cysteine oxidation at pH 8.4 was observed. However, this electrode showed catalytic activity for cysteine oxidation at pH 1.

The electrode modified by electrodeposition of CoPc showed no catalytic wave due to cysteine oxidation at pH 8.4. This electrode, however, showed a strong catalytic wave due to cysteine electro-oxidation at pH 1. The strength of the current response was larger than that observed for the electrode modified by the drop-dry method in the same cysteine solution at pH 1.

So, at pH 8.4, CoPc electrodes modified by both drop-dry and electrodeposition, showed no catalytic activity for cysteine oxidation. At pH 1, however, electrodes modified by both methods of preparation of the CoPc-CMGCE, catalysed the oxidation of cysteine. Previous research by Kok et al[47] showed that the drop-dry method, which results in direct adsorption, produced higher current responses than at a CoPc containing carbon paste electrode. The results above indicate that CoPc when electrodeposited at a GCE produces higher current responses than the drop-dry method.

Comparatively, $[CoTSPc]^{4-}$ showed a slightly higher current response for cysteine catalysis at pH 1 at GCE modified by electrodeposition than did CoPc.

The effects of the solvent used to dissolve the MPc complex prior to deposition onto the electrode were examined. When CoPc was dissolved in pyridine for the drop-dry method, no catalytic currents for cysteine oxidation were observed. Dissolving CoPc in DMF, however, facilitates the electrocatalytic oxidation of cysteine. This relates to the electron-donating and withdrawing effects of the solvent.

4.4.10 Scanning Electron Microscopy (SEM)

SEM photographs of $[CoTSPc]^{4-}$ drop dried and electrodeposited at glassy carbon electrodes are shown in Fig. 4.24 a) and b) respectively and magnified 5000 times. The drop-dried film of $[CoTSPc]^{4-}$ shows the film to be composed of tiny crystals.[135] For the electrodeposited film, Fig 4.24 b), these crystals are more evenly spread over the electrode and are smaller than those in Fig. 4.24 a).

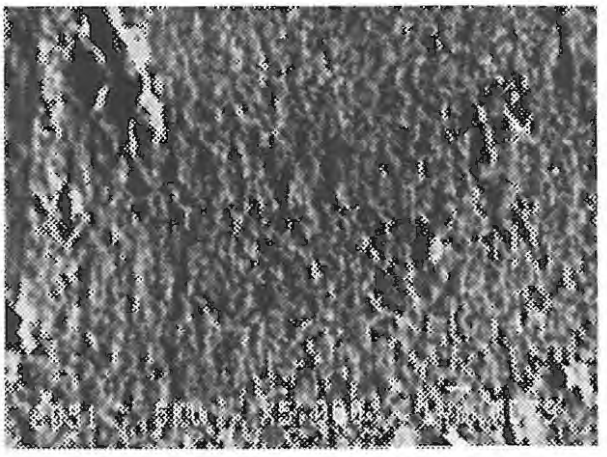

(A)

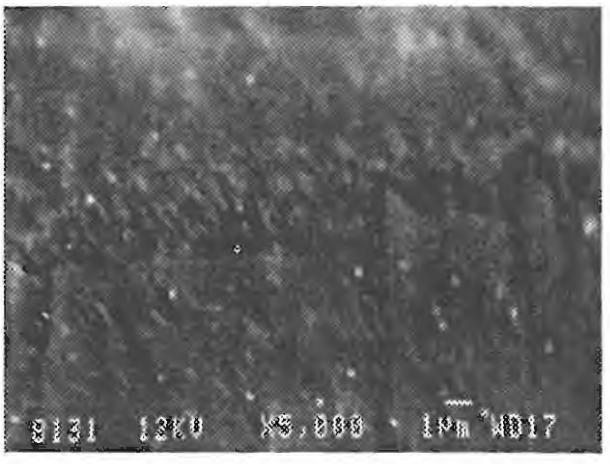

(B)

Figure 4.24 SEM photograph of a) CoTSPc-CMGCE, modified by the drop-dry method and b) CoTSPc-CMGCE, modified by electrodeposition. Magnification 5000 X.

Compounds deposited on carbon electrodes form a microcrystalline structure and not a thin film. Penning ionisation spectroscopy show that films of FePc deposited on graphite change structurally from a disordered layer, to a closely packed monolayer to an island.[121]

The CoTSPc-CMGCE thus shows structural variation dependant on the mode of attachment of the modifier onto the electrode surface. This may affect the differing current responses, reproducibility and stability observed using the two techniques.

4.4.11 Cysteine Analysis via other MPc Electrodeposited at GCE.

(i) Iron and Nickel MPc

Fe(II)Pc and Ni(II)Pc were electrodeposited at GCE as described in Section 4.3.4. Only Fe(II)Pc showed increases in the anodic and cathodic waves on repetitive cycling of the modifier at GCE, indicating the formation of a conductive phthalocyanine film, Fig. 4.25.

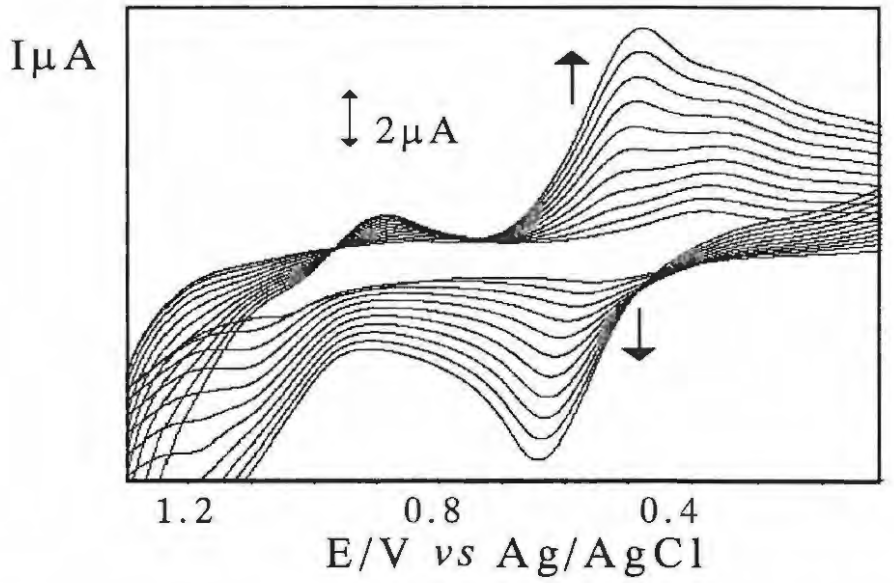

Figure 4.25 Electrodeposition of Fe(II)Pc dissolved in DMF containing 0.1 mol dm^{-3} TEAP, onto a glassy carbon electrode. Scan rate = 100 mV s^{-1}.

When these CMGCE's were placed into solutions of cysteine at low pH, anodic waves at 0.70 V *vs* Ag/AgCl corresponding to the catalytic oxidation of cysteine were observed for Fe(II)Pc (Fig. 4.26) and only very weakly for Ni(II)Pc. Nickel does not form axial ligands readily, while iron and cobalt do, explaining why metallophthalocyanines of cobalt and iron readily catalyse the oxidation of cysteine.

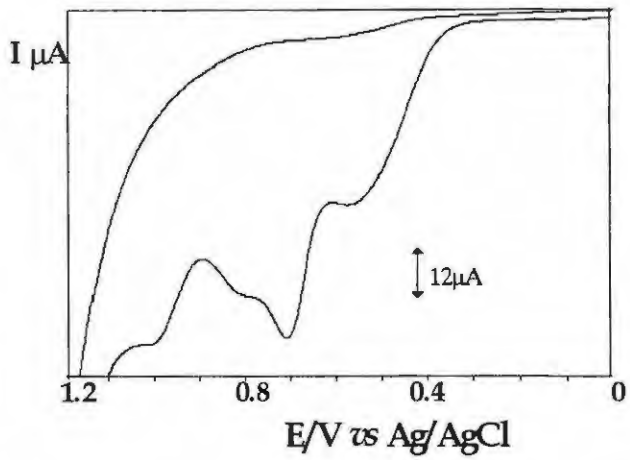

Figure 4.26 Fe(II)Pc-CMGCE in 0.016M cysteine solution. Electrolyte: 0.005M H_2SO_4. Scan rate: 100 mV s^{-1}.

At Fe(II)Pc-CMGCE, the cysteine oxidation wave decayed on the subsequent scan and after the third scan, no oxidation wave was observed. This indicated the decomposition of the CMGCE by the oxidation products of the cysteine oxidation. The activity of the electrode could not be restored by other means except for recoating with Fe(II)Pc.

ii) Molybdenum

$OMo^{(V)}$(OH)Pc did not form a conductive film at the GCE during repetitive cycling from pyridine. $OMo^{(V)}$(OH)Pc dissolved in pyridine was attached to the GCE by the drop-dry method explained in Section 4.3.4. When this CMGCE was placed into a cysteine solution of pH 2.5, only a weak anodic wave corresponding to cysteine oxidation was observed. However, $OMo^{(V)}$(OH)Pc chemically modified by incorporation into the matrix of carbon paste has been reported to catalyse the oxidation of cysteine at 0.33 V[131]. It may thus be inferred that the sensitivity of $OMo^{(V)}$(OH)Pc in the catalytic electro-oxidation of cysteine is dependent on the method of modifying the electrode.

$OMo^{(V)}$(OH)Pc is insoluble in aqueous solutions. To examine the solution-phase catalysis of cysteine by molybdenum MPc's, $[OMo(OH)TSPc]^{4-}$ was used. When cysteine was added to solutions of $[OMo(OH)TSPc]^{4-}$ in pH 2 buffer, an anodic wave was observed at 0.32 V *vs* Ag/AgCl. This wave increased with increasing concentrations of cysteine. The

$[OMo(OH)TSPc]^{4-}$ solution-phase catalysis of cysteine has been reported at 0.29 V *vs* Ag/AgCl in 0.05M H_2SO_4[131]. The significance of these findings is the marked lowering in the overpotential for cysteine electro-oxidation. The disadvantage is that only cysteine concentrations in excess of 0.01M brought about current responses. The CoTSPc-CMGCE produced was sensitive for cysteine oxidation at concentrations as low as 1×10^{-8} mol dm^{-3}, as reported in Section 4.4.6.

4.5 CONCLUSIONS

The following conclusions may be drawn from this work. A glassy carbon electrode modified by electrodeposition of $[(CN)_2RuPc]^{2-}$ showed catalytic activity for the oxidation of cysteine. Electrodeposition of a strongly adherent film proceeded best from a pH 9 buffer. The interaction with cysteine is believed to be mediated by a ring oxidation and not that of the central metal. The oxidation wave for cysteine catalysis was observed at a lowered potential of 0.43 V *vs* Ag/AgCl. This potential relates to the first oxidation of the MPc species at 0.33 V *vs* Ag/AgCl. Sensitivity for electrocatalysis of cysteine was in the millimolar range.

For those MPc complexes believed to interact with cysteine via the central metal, the electrocatalytic efficiency for cysteine oxidation was metal dependant. The sensitivity of the electrode for the catalytic oxidation of cysteine also showed a dependence on the formation of a conductive phthalocyanine film during electrodeposition. Ni(II)Pc and $OMo^{(V)}(OH)Pc$ did not readily form conductive phthalocyanine films. These electrodes showed poor sensitivity for the catalytic oxidation of cysteine. The solution-phase catalysis of cysteine by $[OMo(OH)TSPc]^{4-}$ was observed at 0.32 V *vs* Ag/AgCl. The low overpotential exhibited is countered by a low sensitivity for cysteine analysis. Fe(II)Pc readily formed a conductive phthalocyanine film during electrodeposition from DMF. This electrode catalysed the oxidation of cysteine at 0.70 V *vs* Ag/AgCl at low pH. The electrode activity, however, could not be readily regenerated.

$[Co(II)TSPc]^{4-}$ formed strongly adherent films during electrodeposition of this modifier onto GCE. The direct electrodeposition of CoTSPc onto a GCE showed good reproducibility and sensitivity for the catalytic oxidation of cysteine at pH's below 4 and cysteine concentrations in the micromolar range. The CoTSPC-CMGCE catalysed the oxidation of cysteine at 0.82 V *vs* Ag/AgCl at low pH. This technique is suitable for the quantitative analysis of cysteine analysis *ex situ*, offering the advantage over solution-phase

catalysis by not destroying the sample. At pH's greater than 4, $[Co(II)TSPc]^{4-}$ catalysed oxidation of cysteine is possible by electrodeposition and not by solution-phase catalysis. A limitation is the expected precipitation of cystine which irreversibly degrades the catalytic activity of the electrode, but analysis is still possible at higher pH's by renewed electrodeposition. Solution-phase catalysis is limited to low pH values. However, electrodes modified by adsorption and electrodeposition of $[Co(II)TSPc]^{4-}$ can be utilised in both acidic and alkaline media, making this technique and MPc more feasible for analysis of cysteine containing proteins.

Chapter Five

Voltammetric Studies of Metallothionein

5.1 INTRODUCTION

The quantification of cysteine provides a means for the quantification of cysteine-containing proteins. One such protein with a high cysteine content is metallothionein (MT).

Metallothioneins were first discovered in 1957 by researchers Margoshes and Vallee. These authors were searching for a tissue component responsible for the natural accumulation of cadmium in horse kidney cortex. This was named metallothionein.[136]

It was found to be a sulphur containing protein of low molecular weight (6000-7000 g/mol) usually containing 61 amino acids with an unusually high amount of cysteines, (at least 30%) and containing no aromatic compounds.[136,137,138,139] One of their most remarkable features, is the wide range of metals they bind. The cysteines, in the reduced form, are co-ordinated to the metal ions through mercaptide bonds[136]. The metals include the group 11 and 12 metals, cadmium(II), zinc(II), copper(I), mercury(II), gold(I), silver(I)[136] and cobalt(II), nickel(II), and bismuth (III)[95].

The primary sequence of metal-free metallothionein is that of a random chain containing no disulphide bonds but where all the cysteine amino acids are available for co-ordination to metals. This peptide chain is cross-linked by the formation of cys-metal-cys bonds forming a metal binding site (cluster) enclosed and protected by the hydrophilic envelope

of the peptide chain. The three dimensional structure shows cluster formation in mammalian peptides where metals are bound in one of two domains, termed as the alpha (the C-Terminal) and beta (N-terminal) metal binding domains. These consist of 20 cysteines containing 8 bridging thiolates and 12 terminal thiolates and are insulated from the environment except, for two deep crevices providing access to the metal-thiolate centres in each domain[95].

The ratio in which the metals bind the 20 cysteine amino acids of metallothionein is generally 7 for Co(II), Cd(II) and Zn(II); 12 for Cu(I) and Ag(I) and in isoforms of 7, 11 and 18 for Hg(II)[140]. These metals are bound to the thiolate ligands in the two domains. For example, for Zn_7(II) and Cd_7(II) (7 denoting the number of metal ions) the 7 metal ions are bound to the 20 cysteines as the M_3S_9 cluster in the beta domain and the M_4S_{11} cluster in the alpha domain[95]. M_x refers to the number of metal ions bound to the number of cysteine groups, S_x.

In mammals, at least two major isoforms of metallothionein have been isolated, referred to as MT1 and MT2. The isoforms differ slightly in amino acid composition and isoelectric point, with no spectroscopic evidence that that they differ in their metal binding properties[140]. A brain specific isomer, MT3, contains 68 amino acids as opposed to the 61-62 amino acids in MT1 and MT2[141].

MT's have been found not only in vertebrates but in invertebrates, plants, eukaryotic micro-organisms and some prokaryotes. It is thus believed that metallothioneins were produced by living systems very early in evolution. Three classes of metallothioneins have been identified to date.[136,95]

Class I proteins include the mammalian peptides, with 60-62 amino acids (1/3 cysteine), grouped as cys-x-cys and cys-x-x-cys units, where x represents a noncysteine amino acid and cys represents cysteine. Structural studies have relied on NMR (^{111}Cd, ^{113}Cd and ^{1}H) and on X-ray spectroscopic experiments. The class II proteins from yeasts and fungus, contain about half the number of cysteines of class I. They have a metal-thiolate cluster in

a single domain with an M_8S_{12} core. The class III peptides are the gamma-glutamyl cysteinyl isopeptides found in yeast and plants and these bind Zn(II) Cd(II) and Cu(I).[95]

While naturally occurring metallothioneins are generally isolated as Zn(II) and Cd(II) in class I, and as Cu(I) in class II, mixed-metal metallothioneins have also been isolated. These are generally Cd,Zn-MT and Cu,Zn-MT mostly found in class I MT, and Cu,Cd-MT found in class II MT's. For these mixed-metal clusters, there appears to be a preference in binding domain, with Cu(I) showing preference for the beta domain and Cd(II) for the alpha domain.[95]

5.1.1 Biological Role of MT

Almost forty years after their discovery, researchers are still unable to define a specific biological role for MT. This is because of the inducibility both *in vitro* and *in vivo* by a variety of agents and conditions. These include abundance of metal ions [137,142] (reaching toxic levels), certain hormones, cytokines, growth factors, tumour promoters, and physical and chemical stress.[143] Usually the form of the protein induced by these agents is either the zinc or copper containing metallothionein.

In mammalian systems, metallothionein has been found mainly in the liver and kidney. While MT has also been found in localised areas of the brain, MT appears to function mainly in the peripheral organs concerned with detoxification. In renal metallothionein, cadmium is the dominating metal while in metallothionein from the brain [144] and liver, zinc is the dominating metal[145]. The relationship between the tissue concentrations and toxicity of group 11 and 12 favours the role of metallothionein in limiting intracellular concentrations of reactive heavy metals and shielding cellular structures from the harmful influences of toxic metals[95]. However, as the form of MT isolated usually contains copper or zinc, MT may function in homeostatic control of these biologically essential metals[136].

MT has been detected in foetal tissue suggesting a prenatal and postnatal role and in nearly every tissue of the body, fostering ideas of a possible role in maintaining oxidation and reduction potential[139].

Considering the causative role played by cadmium in the Japanese affliction, the "itai itai" disease, the link between cadmium dietary intake and stimulated physiological levels of MT proposes a role in cadmium detoxification. However, while protecting the kidney from acute cadmium toxicity, the low molecular weight of Cd-MT causes it to accumulate in this organ, leading to chronic toxicity[145]. Wilson's and Menkes' diseases, which involve incorrect metabolism of copper, have been associated with metallothionein through its Cu(I) binding reactions. The liver and kidneys play an important role in the metabolism of copper in mammals and indeed the presence of metallothionein in livers of patients suffering from Wilson's disease, implies a corrective role[95,146]. It has been suggested that Cu overload may be due to compromised MT biosynthesis[146].

The range of metals that induce metallothionein is large and generally the MT form induced is either bound to the challenge metal (the metal administered to induce MT synthesis) or bound to Zn(II) or Cu(I).

Metallothionein production is controlled at a genetic level[95]. When metal accumulation in the liver reaches toxic levels, the apoform of MT, apo-MT or thionein production is stimulated by the 'switching on' of the gene coding for its production. The thionein produced binds to the metal which activated its synthesis, forming a metallothionein. More thionein gets produced if required and subsides when metal levels reach normal levels. This involves a feedback mechanism at the genetic level coding for thionein production. If the metal is an essential metal such as zinc or copper, the thionein acts as a transient storage site. The thionein releases the metal when their levels drop. If not required by the body, the MT gets excreted. The thionein may also act as a transport protein by moving metals in between tissues where they are needed e.g. in zinc-dependent processes in replication, transcription and translation of DNA.[24]

In vitro experiments show an even broader range of metals that bind metallothionein, including Pt(II), Tc(IV) and Fe(II). Metals bind readily to the apoform of metallothionein with the order of binding constants following the general order as exhibited by inorganic thiolates, Hg(II)>Ag(I)~Cu(I)>Cd(II)>Zn(II).

MT's inducibility by other factors have proposed a larger physiological function for metallothionein, implying that binding metals may not be its sole or primary role. The thiol groups on MT have been shown to bind the toxic hydroxyl radical as effectively as glutathione. The thiols are believed to be regenerated by glutathione. The mechanism involved is unclear but it may follow the same pathway as glutathione. Evidence of metal exchange with iron at sites where the iron induces free radicals has also been observed. This is conceivable considering the high affinity of iron for thiol ligands. The kinetic lability of the group II metals they bind and the chemistry of the nucleophilic thiol group indicates that the metallothioneins may offer protection against electrophiles, alkylating agents and radical species.[146] The recent detection of metal-free thionein in a range of tumour cells in mice and rats[95] raises obvious questions.

5.1.2 MT Analysis

5.1.2.1. Non-electrochemical methods

A major drawback in assigning function has been the lack of a measurable biological activity in analysis and quantification of MT. Researchers have been forced to consider unique structural aspects of MT to provide analytical procedures. Direct determination of the protein moiety by UV spectroscopy, immunological assays, or colour reaction by the Folin-Ciocalteu or Biuret reagent,[147] and indirect methods such as estimates of metal binding and sulphydryl content, provide the basis for MT analysis.[148]

Metallothionein contains no aromatic compounds, a feature utilised in absorption spectroscopic analyses of proteins. Its concentration may, however, be determined by the absorption of the apoprotein[92].

The immunological approach is an enzyme-linked immunoabsorbent assay. It affords the specificity inherent in antibodies and the sensitivity of either isotope counting or enzyme-catalysed reactions, offering analysis in most body fluids including plasma and urine. A disadvantage is that it may suffer from a lack of interspecies cross-reactivity by binding non-MT proteins as well. An important consideration in determining total MT content with this technique is that the presence of different isoforms in biological tissue do not differ in their specificities to the antibodies used.[148,149]

Other assay methods utilising the metal-binding characteristic of MT's rely on saturation of metal-binding ligands with group 11 and 12 heavy metals. When employed with radionuclides, this can be a very sensitive analytical tool, but can be time-consuming in terms of creating conditions where the radionuclide binds specifically to the MT[148]. In this technique the presence of non-MT proteins is of minor importance as these are generally of high molecular weight, and their interference easily removed by their heat or acid denaturation[149].

In selecting an analytical technique, the metals bound to the MT are of considerable importance as metal composition affects heat stability, sensitivity to oxidation and the pH dissociation of the metals. In immunological techniques the type of metals are of limited importance. However, with metal affinity assays the differing affinities for proteins is a concern. For chromatographic and photometric analysis of MT, the metal composition can affect the observed absorption spectrum. With chromatographic techniques, resolution is affected by high non-MT protein to MT protein ratios.[149]

5.1.2.2 Electrochemical Methods

The high content of cysteine has been utilised for electrochemical quantification, the analytical tool in which much progress has been made. Electrochemical methods overcome many of the shortcomings of alternate methods of detection. The advantage is that it is rapid, reproducible and species independent. Using differential pulse polarography (DPP), Brdicka[150] devised a technique for cysteine quantification. Further

explored by Palecek and Pechan,[147] it was only in 1973 that Kehr adopted the technique for MT analysis. The technique was also adopted for analysis of cysteine in haemoglobin[151]. The DPP method of analysis has subsequently been refined[138,152,153] and described in detail below.[148]

DPP Technique

At a dropping mercury electrode, the current difference between two time measurements is repetitively made at a renewed mercury droplet, while the polarographer scans a potential range.[148]

The basis of the Brdicka DPP assay for protein is the generation of catalytic double waves from SS/SH- containing proteins in a hexa-ammine cobalt chloride supporting electrolyte. The electrode process is unclear, but it was suggested that the cobalt from the electrolyte co-ordinates to the protein, from which hydrogen is catalytically released[147]. Electrodeposition of the cobalt complex onto the mercury electrode catalyses the reduction of the ionised sulphydryl groups. The sulphydryl groups are reduced by accepting hydrogen atoms from the supporting electrolyte, producing a cathodic current response. It was proposed that the cobalt-protein co-ordination bond is preserved upon electrodeposition, facilitating the proton reduction. The resulting cathodic wave height is then a function of the number of thiol groups adsorbed onto the electrode and is controlled by the recombination rate of ionised sulphydryl groups and protons. Wave potentials of the sulphydryl compounds so detected exhibited high overpotentials of -1.41 V *vs* Ag/AgCl for cysteine and -1.47 V *vs* Ag/AgCl for a crab Cd-MT at a stationary mercury drop electrode.[148]

In addition to the redox active mercaptide groups, the redox activity of the metal groups provides for further electrochemical analysis. If metallothioneins are decomposed in acid solution then the metals released may be quantified by stripping voltammetry. Electrochemistry may also be used for characterisation of the metal-mercaptide clusters.

To this end, there has been much research using DPP or cyclic voltammetry in an effort to characterise and identify common features between different types of metallothioneins.[154]

Studies using cyclic voltammetry at a stationary mercury electrode showed the two step reduction of MT, following electrolysis[154]:

$$\mathbf{MT \rightarrow MT^{-} \rightarrow MT^{2-}} \qquad \text{Equation 5-1}$$

Most electrochemical research on MT's have utilised mercury electrodes as the working electrode. It was noted that the adsorption of metallothionein and formation of mercury compounds (owing to the affinity of sulphur containing compounds for mercury surfaces) dominated over original MT peaks with time. Alternative MT analyses have been conducted at carbon composite and glassy carbon electrodes. At these electrodes apometallothionein (metal-free MT) could be distinguished from MT's, while slight differences in the voltammetric peaks of Cd-MT and Cd,Zn-MT, distinguished between the two types of MT's.[154]

For freshly prepared MT at carbon composite and mercury electrodes, no anodic waves were observed around +0.8 V (*vs* Ag/AgCl) (potential indicative of thiol oxidation). This is in support of the theory that metallothioneins contain neither free SH or SS groups. Only when oxidation of the MT occurred in the presence of air, or oxygen, or after decomposition of MT in stored solutions was any anodic oxidation at +0.8 V (vs Ag/AgCl) observed. This was related to the formation of metal-free thiolate ions.[154]

5.2 AIM OF RESEARCH

The development of techniques for the quantitative analysis of MT is of value for measurements during physiological experiments; in assigning its biological role; and for health reasons. Monitoring its concentrations in biological and environmental samples may be useful as early indicators of diseased states, such as heavy metal overload.

The advantages of the Brdicka[148] DPP method of MT analysis over non-electrochemical methods, is countered by the high overpotential exhibited. High overpotentials are not feasible in electrochemical analysis, as discussed in Section 4.1.1. It is thus important to develop techniques which reduce the overpotentials for the electroanalysis of MT.

However, as with cysteine, MT cannot be oxidised at unmodified carbon electrodes due to its large background current. The use of chemically modified electrodes have shown significant lowering of the overpotentials associated with sulphydryl oxidation. There has been no research on the behaviour of MT at chemically modified electrodes.

In this thesis a method for MT quantification at chemically modified electrodes, is proposed. The quantitative determination is based on the high concentration of cysteine. As MT comprises 1/3 cysteine, quantification of cysteine would provide estimates of MT concentration. The catalytic activity of metallophthalocyanines towards the sulphydryls, as discussed in Chapter 4 is examined as electrode modifiers for electrocatalytic oxidation of MT. MPc's studied are $[CoTSPc]^{4-}$, $[NiTSPc]^{4-}$, $[FeTSPc]^{4-}$and $[CuTSPc]^{4-}$.

Apart from this work, cysteine oxidation has only been observed following the decomposition of MT[154], as discussed before in Section 5.1.2.2. The technique proposed is aimed at the design and utilisation of chemically modified electrodes for analysis of undecomposed MT.

Comparisons will be made of the electrochemical behaviour of animal-MT isolated from the liver of a local farm animal and Cd,Zn-Metallothionein obtained from Sigma.

5.3 EXPERIMENTAL

5.3.1 Reagents and Analytes

Preparation of MT from animal liver

Triply distilled deionised water was used in all experimental work. NaCl, 0.9%, required for the sample preparation was prepared by dissolving 0.45g analytical grade NaCl in 50ml of distilled deionised water. For electrochemical measurements, a 0.2M Tris-HCl buffer was prepared weekly from a stock solution of 1M Tris solution. The pH was adjusted to 8.4 by the addition of 0.2M HCl.

Metallothionein was isolated using published procedures[148,153]. 200mg liver tissue was homogenised in 10ml of a 0.9% NaCl solution using a probe homogeniser. The sample was then centrifuged at 10,000g (11600rpm) at 4° for twenty minutes to remove excess tissue which can cause loss of metallothionein by coprecipitation in the saline. The supernatant was subjected to heat denaturation in a boiling water bath for five minutes at 90-95°C. This step denatures most proteins with cysteinyl residues (which may distort the cysteine reduction wave) but not the heat stable metallothionein. The flocculent material was removed by centrifugation at 10,000g at 4° for 20 minutes. The sample was kept at 4 °C in the dark until needed.

Standard MT

Standard rat Cd,Zn metallothionein (Cd,Zn-MT) was purchased from Sigma Chemicals and used without further purification.

Modifiers

Na_4[Co(II)TSPc] was synthesised and characterised as described before in Sections 4.3.2 and 4.4.4. Iron(II), nickel(II) and copper(II) tetrasulphophthalocyanine complexes, Na_4[Fe(II)TSPc], Na_4[Ni(II)TSPc] and Na_4[Cu(II)TSPc], were synthesised in a similar

manner as described for Na_4[Co(II)TSPc], except that the appropriate metal salt was substituted for that of the cobalt salt. These were $FeCl_3$ (Unilab), $NiCl_2$ (Aldrich) and $CuCl_2$ (Unilab), for iron(II), nickel(II) and copper(II) tetrasulphophthalocyanine complexes, respectively. IR spectra for Na_4[Fe(II)TSPc] and Na_4[Ni(II)TSPc] are shown in Appendix 2 and 3 and the data tabulated in Appendix 1.
Solutions of cysteine were prepared fresh daily in Tris-HCl buffer of pH 8.4.

5.3.2 Apparatus

The three electrode cell, voltammetric analyser and spectrophotometer as described in Section 4.3.3 was used for these studies. The glassy carbon electrode was chemically modified with $[MTSPc]^{4-}$, where M = Co, Fe, Ni or Cu, by electrodeposition as described before for cysteine analysis, Section 4.3.4.

A Beckman Model J2-21 centrifuge machine with a JA-28 Rotor was used in the preparation of the sheep liver sample.

All glassware was washed in hot soapy water; rinsed in water and soaked in 55% HNO_3 for 24 hours to free glassware of metal contamination. The glassware was then soaked for 12 hours in distilled deionised water and rinsed with copious amounts of distilled deionised water. Stringent methods for cleaning of electrodes were also conducted, as described in Section 4.3.4.

5.3.3 Electrochemical Methods

Animal Metallothionein

Metallothionein of known volume extracted from animal liver was placed directly into a glass cell with a known volume of Tris-HCl buffer. The solution was degassed for 5 minutes with nitrogen. A constant flow of nitrogen was held throughout the experiment.

The MPc-CMGCE was prepared as before in Section 4.3.4 by electrodeposition from a solution of the MPc in distilled DMF. Once modified, the electrodes were placed inside the cell and the working electrode scanned in the potential range of 0 to 1200 mV.

Standard metallothionein

Standard MT solutions were prepared by dissolving Cd,Zn-MT from Sigma in 0.1M Tris-HCl buffer. As with the animal liver metallothionein, a known mass of the MT solution was placed inside a glass cell with Tris-HCl buffer, pH 8.4 and degassed with nitrogen for 5 minutes. The MPc-CMGCE was scanned between the potential range 0 to 1200 mV, while the solution was deaerated with a constant flow of nitrogen gas. The working electrode was cleaned and chemically modified between voltammetric scans.

Cd,Zn-MT solutions of different concentrations, were prepared by dilution with Tris-HCl. These were scanned for sulphydryl content using a MPc-CMGCE in the potential range: 0 to 1200 mV. The glassy carbon working electrode was again cleaned and chemically modified between voltammetric determinations for each solution.

For voltammetric analysis of both standard and animal liver MT, comparisons were drawn of the analytical utility of different MPc's. Voltammetric measurements were conducted at the CMGCE in buffer solutions in the absence and presence of MT, and at unmodified GCE in solutions of MT.

Once scanned for sulphydryl content MT solutions were kept in a fridge overnight. These solutions were allowed to reach room temperature for 2 hours before voltammetric analysis. Cyclic voltammetric scans were repeated on these MT solutions under the same conditions as the previous day, in order to draw comparisons of sulphydryl content over prolonged periods.

5.4 RESULTS AND DISCUSSION*

5.4.1 Voltammetric Response of Rat Cd,Zn-Metallothionein

Fig. 5.1 shows the electrodeposition of $[CoTSPc]^{4-}$ onto the GCE. Increases in the anodic and cathodic waves on repetitive scans show the formation of a conductive phthalocyanine film, as explained in Section 4.4.5.

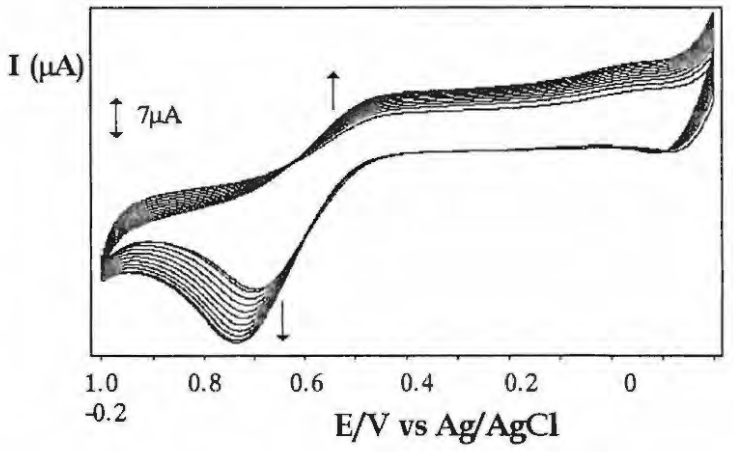

Figure 5.1 Electrodeposition of $[Co(II)TSPc]^{4-}$, dissolved in DMF containing 0.1 mol dm^{-3} TEAP, onto a glassy carbon electrode. Scan rate = 100 mV s^{-1}.

Fig. 5.2 shows the CV obtained, on unmodified glassy carbon electrode, for freshly prepared solutions of rat Cd,Zn-MT in Tris-HCl buffer at pH = 8.4. No peaks are observed under these conditions, as has been observed before [154]. When a CoTSPc-CMGCE was employed for the same solution of Cd,Zn-MT employed in Fig. 5.2, a sharp peak was obtained at 0.90 V *vs* Ag/AgCl, Fig. 5.3 a), implying that $[CoTSPc]^{4-}$ catalyses the oxidation of Cd,Zn-MT. The last scan of the electrodeposition of $[CoTSPc]^{4-}$ onto the GCE, Fig 5.1, is shown in Fig 5.3 b). Fig 5.3 b) shows the oxidation of $[Co(II)TSPc]^{4-}$ to $[Co(III)TSPc]^{3-}$ as explained in Section 4.4.5. The enhancement and potential shift of this

---

* This work has been published in the following paper and is not referred to further in this chapter: Janice Limson and Tebello Nyokong, Voltammetric behaviour of Cysteine and Metallothionein on cobalt(II) tetrasulphonated modified glassy carbon electrodes, *Electroanalysis*, **1997**, *9* (3), 255-259.

oxidation wave on placing the electrode into the Cd,Zn-MT solution, Fig 5.3 a), indicates that it is involved in the catalytic oxidation of MT.

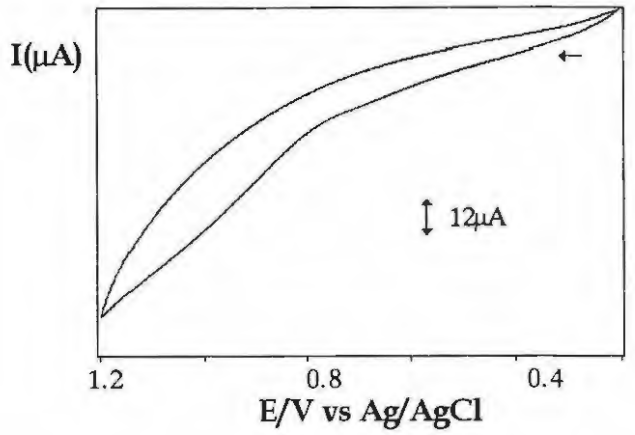

Figure 5.2 Cyclic voltammetry of rat Cd,Zn-MT (2 ppm) on unmodified glassy carbon electrode on CoTSPc-CMGCE. Electrolyte = pH = 8.4 Tris buffer. Scan rate = 100 mV s^{-1}.

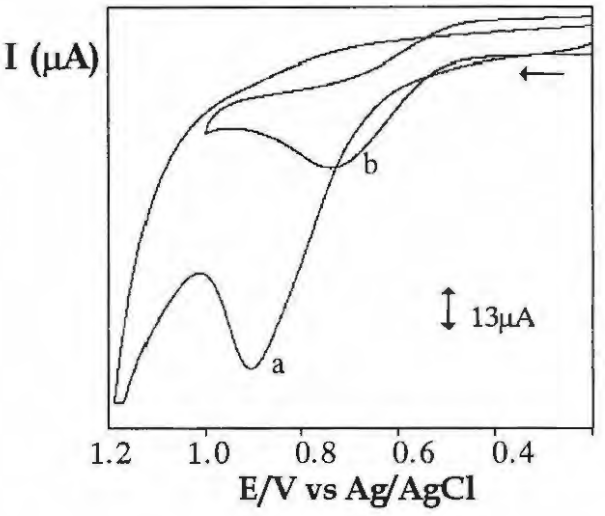

Figure 5.3 Cyclic voltammetry of (a) CoTSPc-CMGCE in absence of MT, (b) rat Cd,Zn-MT(2 ppm) on CoTSPc-CMGCE. Electrolyte = pH = 8.4 Tris buffer. Scan rate = 100 mV s^{-1}.

The electrochemistry of MT is influenced by the metal ions and by the mercaptide groups. The cyclic voltammetry peak near 0.80 V in MT solutions has been associated with the oxidation of thionein[154]. The peak observed at 0.90 V in Fig. 5.3 a) is thus assigned to the oxidation of the cysteine component of Cd,Zn-MT. The fact that this peak is observed at more positive potentials may be attributed to the effects of modifying the electrode with

the $[CoTSPc]^{4-}$ species. The potential of 0.90 V is slightly higher than the potential for free cysteine oxidation of 0.85 V observed in pH 8.4 buffer, Section 4.4.7. The higher oxidation potential for the oxidation of cysteine in Cd,Zn-MT is not surprising since free cysteine is expected to be easier to oxidise than bound cysteine. As observed for free cysteine, no cathodic waves corresponding to the anodic wave at 0.90 V were obtained on the return scan in Fig. 5.3 a), hence showing an irreversible oxidation of the cysteine component of metallothionein. This correlates with the irreversible oxidation of the thiol group of free cysteine.

A cathodic peak was observed at -0.90 V on scanning a potential window to -1.2 V following oxidation of Cd,Zn-MT shown in Fig. 5.3 a). This peak may be correlated with the subsequent reduction of the oxidation product of cysteine, cystine, as shown in Fig. 5.4. The origin of the cathodic peak at -0.61 V is not known but may be related to the oxidation products of the cysteine component of MT. Addition of zinc and cadmium to solutions containing Cd,Zn-MT, did not bring about increases in these cathodic peaks, indicating that the Cd,Zn-MT is not decomposed in this solution. Other researchers have commented on the presence of several smaller cathodic peaks on the return scan following cysteine oxidation (including the cystine reduction at -0.90 V) and attributed them to the history of the electrode and pH of the electrolyte solution.

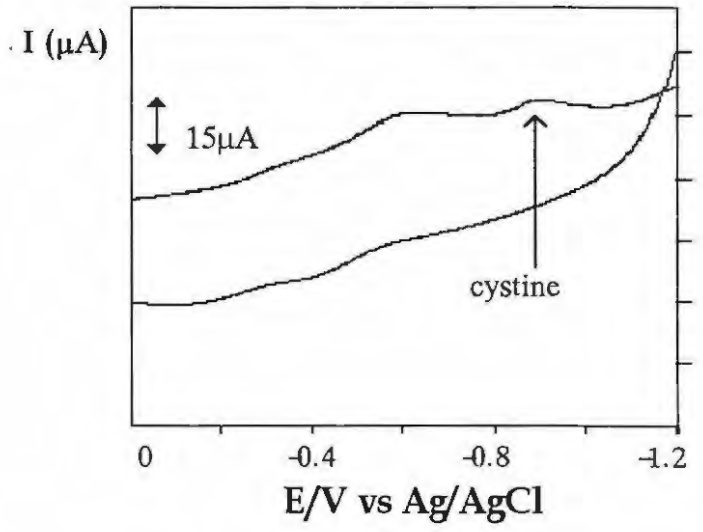

Figure 5.4 CV of rat Cd,Zn-MT (2 ppm) on CoTSPc-CMGCE showing the return scan upon cysteine oxidation, with two cathodic waves attributed to the reduction of the oxidation products. Electrolyte pH = 8.4 Tris buffer. Scan rate = 100 mV s^{-1}.

The activity of the CoTSPc-CMGCE decreased after the first scan suggesting the poisoning of the electrode by adsorption of the oxidation products. On freshly coated electrodes, the anodic currents for the oxidation of Cd,Zn-MT were reproducible. The magnitudes of the anodic currents were unchanged even for Cd,Zn-MT solutions, in pH = 8.4 Tris buffer, that had been stored at 4° C for 24 hours. When a freshly coated CoTSPc-CMGCE was employed for cyclic voltammetry scans of different concentrations of Cd,Zn-MT, an increase in current with Cd,Zn-MT concentration was observed, Fig. 5.5. Fig 5.6 shows a plot of the current response measured *vs* Cd,Zn-MT concentration. The lowest concentration of metallothionein that could be detected on CoTSPc-CMGCE was 0.01 ppm. The oxidation of Cd,Zn-MT on CoTSPc-CMGCE, following the electrochemical generation of $[Co(III)TSPc]^{3-}$ by Equation 5-2, may be represented by Equation 5-3:

$$[Co(II)TSPc]^{4-} \rightarrow [Co(III)TSPc]^{3-} + e^- \qquad \text{Equation 5-2}$$

$$[Co(III)TSPc]^{3-} + Cd,Zn\text{-}MT \rightarrow [Co(II)TSPc]^{4-} + Cd,Zn\text{-}MT^{+} \qquad \text{Equation 5-3}$$

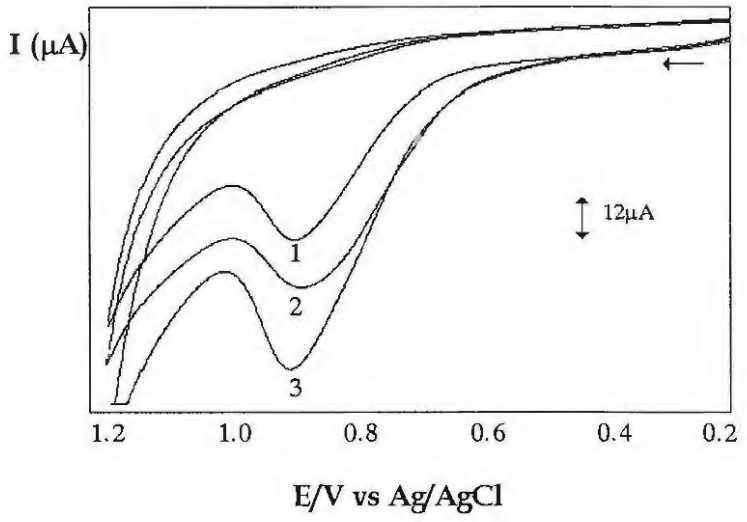

Figure 5.5 Cyclic voltammograms at CoTSPc-CMGCE showing the anodic current response for increasing concentrations of rat Cd,Zn-MT (1) 0.4 ppm; (2) 1.0 ppm and (3) 2.0 ppm. Electrolyte pH = 8.4 Tris buffer. Scan rate = 100 mV s^{-1}.

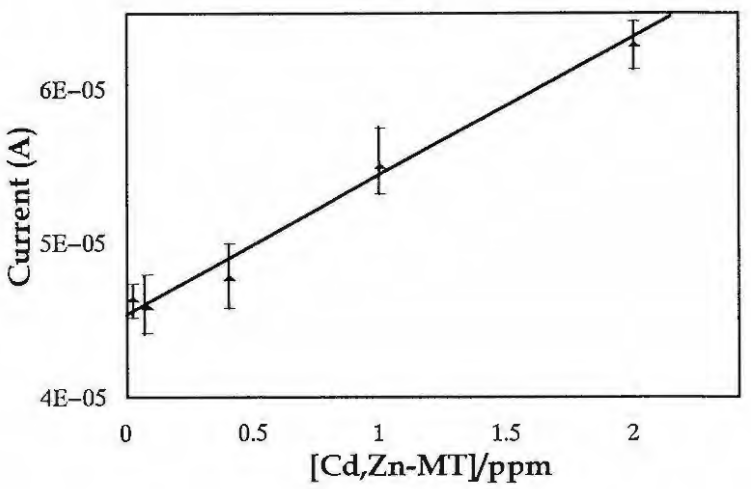

Figure 5.6 The variation of the concentration of Cd,Zn-MT with the anodic currents for the oxidation of the Cd,Zn-MT on CoTSPc-CMGCE. Electrolyte = pH 8.4 Tris buffer. Scan rate = 100 mV s^{-1}.

5.4.2 Voltammetric Response of Sheep Liver Metallothionein

At an unmodified GCE, no oxidation wave was observed for MT from sheep liver, as also observed for Cd,Zn-MT, shown in Fig. 5.2. Voltammograms shown in Fig. 5.7 a) were observed for the oxidation of MT isolated from sheep liver at CoTSPc-CMGCE. Fig 5.7 b) shows the last scan obtained on electrodeposition of the $[Co(II)TSPc]^{4-}$ species onto the GCE. The enhancement in the oxidation wave of $[Co(II)TSPc]^{4-}$, Fig 5.7 b), indicates its involvement in the catalytic oxidation of MT observed in Fig 5.7 a). No peaks were observed on the return scan, indicating an irreversible oxidation of the MT. Addition of free cysteine to solutions of MT from different sources resulted in the increase in these anodic currents.

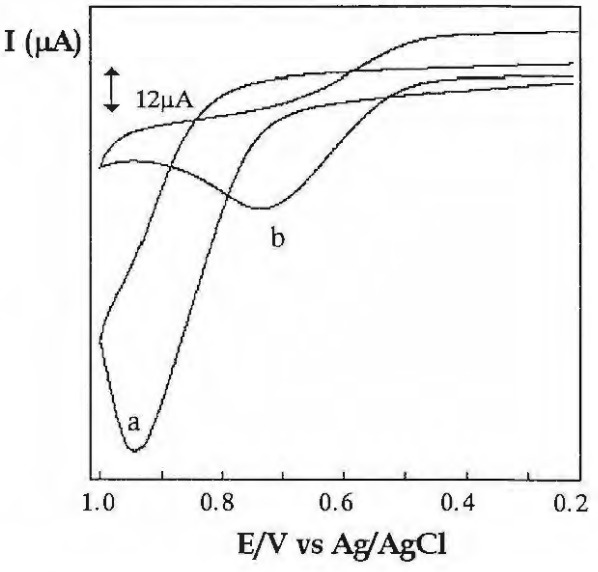

Figure 5.7 Cyclic voltammetry of (a) Sheep liver MT on CoTSPc-CMGCE and (b) CoTSPc-CMGCE in absence of MT. Electrolyte = pH 8.4 Tris buffer. Scan rate = 100 mV s^{-1}.

The anodic peak 5.7 a) was observed at a higher potential, E_p = 0.98 V, than for rat Cd,Zn-MT purchased from Sigma. The higher oxidation potential may be related to the difference in the origin of the MT samples. Fig. 5.8 shows the comparison of the oxidation potentials of a) rat Cd,Zn-MT at 0.90V, b) sheep liver MT at 0.98 V and c) cysteine at 0.82 V. The lowest potential was observed for free cysteine.

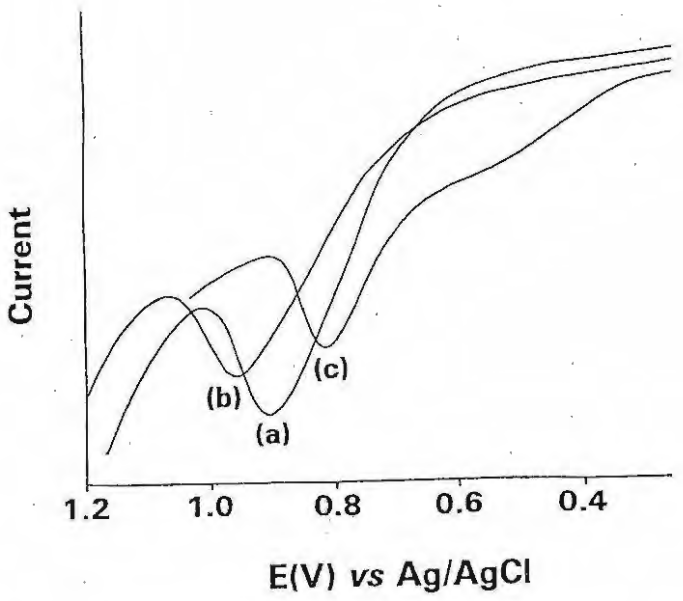

Figure 5.8 Comparison of cysteine oxidation potentials at CoTSPc-CMGCE for a) Cd,Zn-Metallothionein, b) Metallothionein isolated from sheep liver and c) free cysteine.

Since earlier studies have shown that peaks due to the -SH groups in MT were observed only in decomposed MT or following electrolysis, it was necessary to examine the possibility of the decomposition of Cd,Zn-MT under the conditions for electrochemical experiments discussed in this work. The anodic peaks for the oxidation of Cd,Zn-MT were observed for freshly prepared solutions. Peaks due to the reduction of free metals that are expected at -0.58 and -1.01 V for decomposed MT[155] were not observed for CV's of Cd,Zn-MT solutions at pH = 8.4, indicating that Cd,Zn-MT was not decomposed in solution.

CV's, on unmodified glassy carbon electrode, of solutions containing MT and $[Co(II)TSPc]^{4-}$ showed no anodic peaks, implying that $[Co(II)TSPc]^{4-}$ is not an effective catalyst in solution at pH = 8.4. This is in keeping with the data observed previously for free cysteine at this pH. When Cd,Zn-MT was added to solutions of $[Co(II)TSPc]^{4-}$ in pH = 8.4 Tris buffer, the spectroscopic changes observed showed a reduction in the intensity of the Q band spectra of the $[Co(II)TSPc]^{4-}$ species without any changes in the wavelengths. This implied that some decomposition of the $[Co(II)TSPc]^{4-}$ catalyst occurs

in the presence of MT. There was no spectroscopic evidence for the interaction of Cd,Zn-MT with $[Co(II)TSPc]^{4-}$.

$[Fe(II)TSPc]^{4-}$, $[Cu(II)TSPc]^{4-}$ and $[Ni(II)TSPc]^{4-}$ were also examined as catalysts for MT oxidation. These studies were conducted following the same procedures as described for the electrodeposition of $[Co(II)TSPc]^{4-}$ onto a GCE, Section 4.3.4. After electrodeposition onto the GCE $[Fe(II)TSPc]^{4-}$, $[Cu(II)TSPc]^{4-}$ and $[Ni(II)TSPc]^{4-}$ CMGCE, were tested for electrocatalytic oxidation of MT. When these MPc-CMGCE's were placed into solutions containing MT, no catalytic wave associated with the oxidation of MT was observed, indicating that they did not catalyse the oxidation of MT.

5.4.3 Voltammetric response of Metallothionein at low pH

CV's of Cd,Zn-MT in acid solutions (pH = 2 Tris solution) and on CoTSPc-CMGCE showed evidence of the presence of free Zn^{2+} and Cd^{2+}. The cathodic peaks observed at -0.45 V and -1.07 V, Fig. 5.9 are attributed to the reduction of the free Zn^{2+} and Cd^{2+} ions, respectively. The peaks at -0.45 V and -1.07 V were enhanced by the addition of the respective metal ions. Free Cd^{2+} and Zn^{2+} ions are reduced at -0.58 V and -1.01 V *vs* Ag/AgCl, respectively[156]. Metallothionein bound metal ions would be reduced at more negative potentials than free metals. The anodic peak observed at 0.82 V for acid solutions of Cd,Zn-MT, Fig. 5.9, is attributed to the oxidation of free cysteine. This peak was broader than that observed for the oxidation of cysteine in Cd,Zn-MT at pH = 8.4 and is shifted towards more negative potentials by 0.08 V. The observation of the cysteine oxidation peak at 0.82 V in acid solution is consistent with the presence of free cysteine in solution, observed at 0.82 V in Section 4.4.6. The free cysteine is produced by the decomposition of MT in acid solutions.

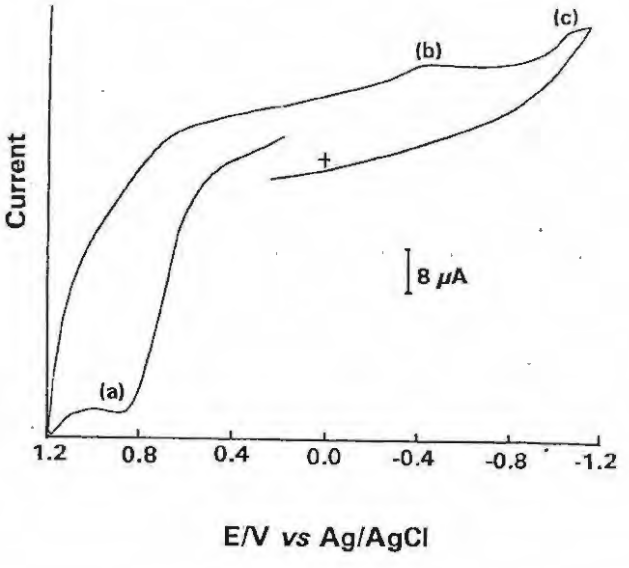

Figure 5.9 Cyclic voltammetry of rat Cd,Zn-MT dissolved in pH = 2 Tris buffer and on CoTSPc-CMGCE. (a) Cysteine oxidation (b) Cd^{2+} reduction and (c) Zn^{2+} reduction. Scan rate = 100 mV s^{-1}.

Solution-phase catalysis of Cd,Zn-MT by $[CoTSPc]^{4-}$ at pH1 showed catalysis of the cysteine component of the metallothionein, Fig. 5.10. This cysteine component is again due to the decomposition of the MT at these pH's. Here a significant shift in oxidation potential to 0.95 V is observed. Higher oxidation potential is unfavourable for electrochemical analysis. The decomposition of the metallothionein is also unfavourable from an analytical viewpoint as it involves destroying the sample, making solution-phase catalysis at this low pH unfeasible.

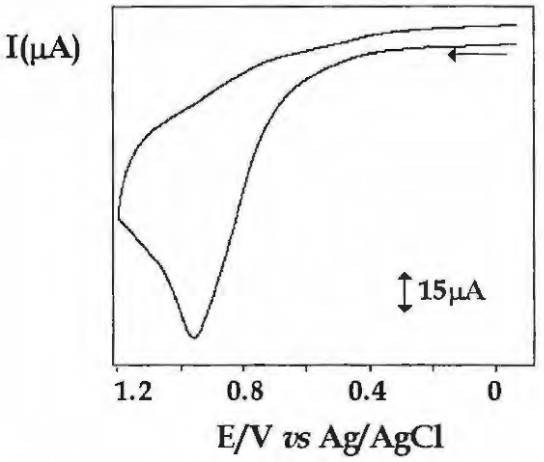

Figure 5.10 Cyclic voltammetry of rat Cd,Zn-MT dissolved in pH = 2 Tris solution on unmodified glassy carbon electrode in $[CoTSPc]^{4-}$ solution. Scan rate = 100 mV s^{-1}.

5.5 CONCLUSIONS

It was shown in this work, that electrodes modified by electrodeposition of $[CoTSPc]^{4-}$ catalyse the oxidation of the organic part of Cd,Zn-MT. The anodic peak associated with the oxidation of the cysteine component of Cd,Zn-MT is observed at 0.90 V at pH = 8.4 when $[CoTSPc]^{4-}$ modified glassy carbon electrodes are employed. There was no evidence for the decomposition of Cd,Zn-MT at pH = 8.4. Anodic peaks due to decomposed Cd,Zn-MT were observed at 0.82 V *vs* Ag/AgCl at pH = 2, and associated with the oxidation of the cysteine component of metal-free metallothionein. The CoTSPc-CMGCE catalysed the oxidation of the cysteine component of MT isolated from sheep liver at 0.98 V *vs* Ag/AgCl at pH = 8.4. The difference in oxidation potentials of the current responses observed were attributed to the different origins of the MT species.

It has been shown in this work that the adsorbed $[CoTSPc]^{4-}$ catalyses the oxidation of cysteine and MT at pH = 8.4, while there was no catalytic activity for solution-phase catalysis at this pH. Cysteine reduces the $[Co(II)TSPc]^{4-}$ catalyst to the $[Co(I)TSPc]^{5-}$ species in basic media, whereas in the presence of the metallothionein species, some decomposition of $[CoTSPc]^{4-}$ was observed in solution at pH = 8.4.

The anodic currents observed on oxidation of Cd,Zn-MT were linear with MT concentrations on freshly coated CoTSPc-CMGCE (pH 8.4). These currents could be used in the analysis of this protein since the cysteine component of MT is generally known to be one-third of the total amino acids in MT.

Chapter Six

Voltammetric Studies of Ferredoxin

6.1 INTRODUCTION

"One of the major assets of iron as a bioinorganic element is the fact that its ferric/ferrous, Fe^{3+}/Fe^{2+}, transition is conveniently fine-tuned through its co-ordination chemistry over the better part of the redox potential range available to life. This property is frequently used in iron-sulphur proteins which act in electron transfer." [157]

6.1.1 Iron-containing Proteins

Iron is the most abundant transition metal on earth and as such is found in many proteins and enzymes in nature. Iron is incorporated into proteins in 3 general groups: non-haem iron proteins, haem-containing proteins and enzymes, and the iron-sulphur proteins.

Non-haem iron:

These are proteins involved in oxygen transport and in mixed function oxidases; in electron transport and storage. An example is methane mono-oxygenase which converts methane into fuels [6, 158].

Haem-iron:

These are proteins which contain the haem prosthetic group: a porphyrin containing macrocyclic ligand that co-ordinates iron. The major functions of these include:

1. Transfer of electrons by redox proteins and enzymes e.g. cytochrome c
2. Transporting (myoglobin) and binding (haemoglobin) oxygen
3. Insertion of oxygen atoms or dioxygen into organic substrates e.g. cytochrome p450 in the respiratory chain
4. Catalysis of organic reactions e.g. catalase peroxidase catalyses the oxidation of hydrogen peroxide to harmless water.

Iron-Sulphur proteins:

These are proteins which contain iron strongly bound to sulphur atoms. The iron-sulphur proteins are widespread throughout the plant and animal kingdom and function typically in electron transfer sequences in storage and donation of electrons in photosynthesis, respiration, hydroxylation reactions and in nitrogen fixation. They have also been associated with three other functions namely: non-redox catalysis, regulation of gene expression, and (multi) electron pair associated redox catalysis.[157]

The iron-sulphur proteins have been classified according to the number of iron atoms: the rubredoxins found in anaerobic bacteria, containing one iron atom tetrahedrally complexed with the thiol sulphurs of four cysteine residues; the ferredoxins and the so-called high potential iron-sulphur proteins, both of which contain more than one iron atom.

6.1.2 Ferredoxin

Ferredoxin is one of the most important members of the iron-sulphur proteins. Ferredoxin was the name given to this class of proteins, so named after its discovery in 1962 as the previously unknown electron carrier in the pyruvate metabolism of *Clostridium Pasteurianum*[159]. Ferredoxins are low molecular weight proteins composed of a simple

amino acid sequence. These amino acids envelop the iron-sulphur active site. Unlike other iron-sulphur centres such as the cytochromes, with more elaborate active centres, the ferredoxins do not in principle require complicated enzyme-catalysed pathways for their biosynthesis. This corroborates the widely accepted proposal that ferredoxins are probably the most primitive of electron transfer proteins[103].

The ferredoxins consist of non-haem iron and sulphur complexed in three different ways:

1. 2Fe-2S : Two Fe atoms complexed with two cysteine residues and two inorganic sulphur atoms.
2. 3Fe-3S: Three Fe atoms complexed with three cysteine residues and three inorganic sulphur atoms.
3. 4Fe-4S: Four Fe atoms complexed with four cysteine residues and four inorganic sulphur atoms.

Figure 6.1 shows a structural representation of the simple iron-sulphur active sites at the centre of two types of iron-sulphur proteins.

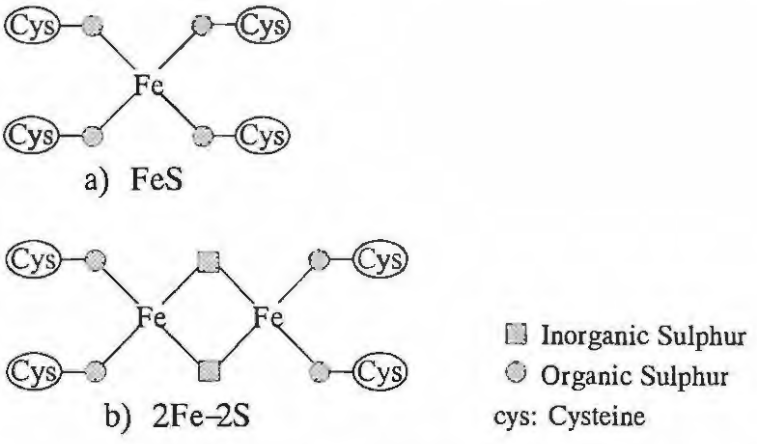

Figure 6.1 Molecular structure of iron(III)-sulphur clusters in , a) Rubredoxin represented as FeS and b) Ferredoxin represented as 2Fe-2S.

The type of co-ordination of the iron-sulphur centres in ferredoxins depends on its specific biological role. So, although general similarities in structure and function exist between all ferredoxins, each appears to be species and tissue specific[160].

In general, ferredoxins from plants, chloroplast-containing algae and blue green bacteria possess the 2Fe-2S active centre accepting one electron on reduction. Two 4Fe-4S active centres are found in most bacteria, including photosynthetic bacteria other than the blue-green bacteria, accepting two electrons on reduction. The exception is *Desulphovibrio Gigas*[161,162], a sulphate reducing bacteria which contains one 4Fe-4S active centre and accepting only one electron on reduction. Ferredoxin from plant non-photosynthetic tissues such as the root have been linked with nitrogen fixation by transfer of electrons to nitrite reductase[163].

Ferredoxin found in vertebrates, such as adrenodoxin, have a 2Fe-2S active centre. It functions at the inner adrenal mitochondrial membrane to transfer electrons from nicotinamide adenine dinucleotide phosphate (NADPH)-adrenodoxin reductase to cytochrome P-450[160]. Another example is hepatoredoxin, (also with a 2Fe-2S active centre) from bovine liver mitochondria which functions similarly in the mono-oxygenase system linked with cytochrome P-450[164].

Ferredoxins from cyanophyta, rhodophyta and chlorophyta are of interest as these may represent intermediate stages in evolution between the anaerobic photosynthetic bacteria and green plants. Studies therefore on ferredoxins may give insight into the biochemical evolution of photosynthesis[161]. As an example, amino acid sequences of ferredoxin from plants have been used to determine phylogenetic trees of related species[165].

Ferredoxin plays a role in plant and bacterial photosynthesis by transporting electrons from $NADP^+$ to water by the catalytic action of ferredoxin-$NADP^+$ reductase. This is shown in Figure 6.2 where Fe(III) on accepting an electron from $NADP^+$, is reduced to Fe(II). Fe(III) is recycled on transfer of this electron to Receptor 1. Interaction is believed to be electrostatic between the negatively charged ferredoxin and positive reductase. Electron transfer between reductase and the iron-sulphur centre is believed to be via electrostatic interaction of reductase with surface amino acids, attached to the iron-sulphur centre[166]. The cysteine groups complete the electron transfer process to the iron centre. In iron-

sulphur proteins, the distances between the cysteine groups differ depending on the specific role of the protein, for example, in co-factor binding or disulphide bond formation[102]. The relatively short distance between the cysteine groups in ferredoxin thus constitutes a role in simple electron transfer and storage.

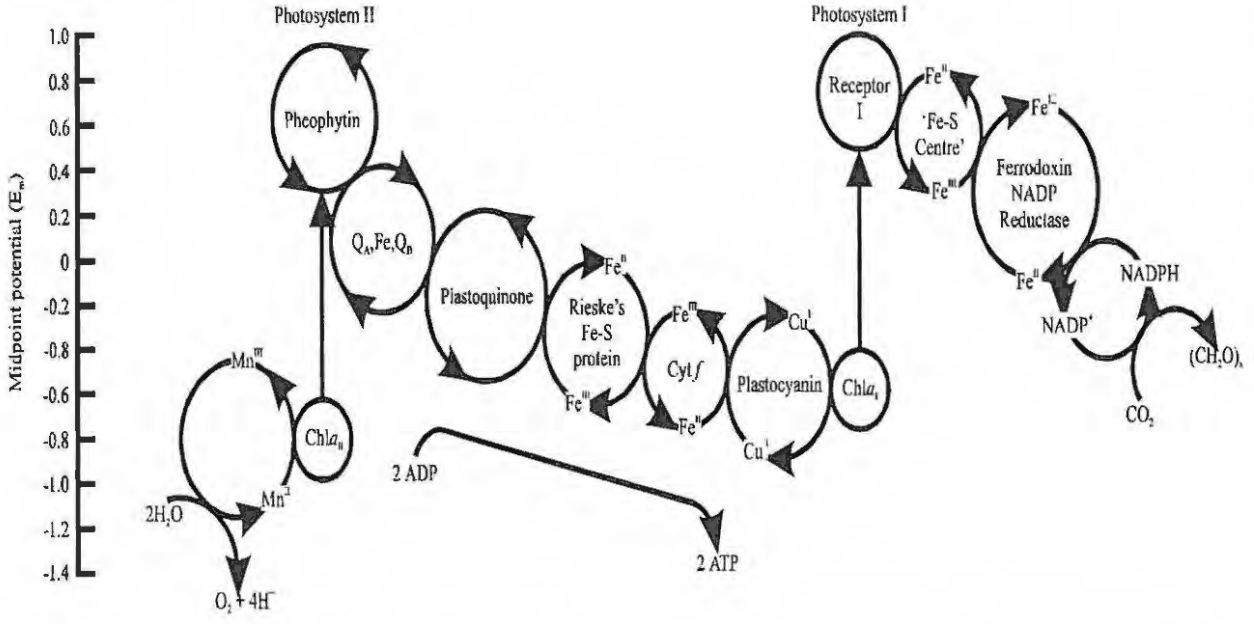

$Q_{A,B}$ = quinone $_A$, quinone $_B$, Chl*a* = chlorophyll, Cyt *f* = cytochrome *f*, NADP = nicotinamide adenine dinucleotide phosphate, E_m = midpoint potential.

Figure 6.2 The role of ferredoxins in the electron transport chain in photosynthesis.

Thermodynamic control of the redox potentials in metalloproteins is generated by a complex set of factors including the nature of the co-ordination sphere and the metal ion geometry, the nature of the surrounding protein lattice and the degree of exposure of the metal redox centre to the solvent. The redox potentials resulting from a combination of these factors have evolved to control the overall rates in biologically important electron transfer processes[5]. Iron-sulphur proteins such as the cytochromes and the ferredoxins demonstrate this in electron transfer chains in photosynthesis and respiration. Figure 6.2 shows the energetically feasible electron transport chain in photosynthesis and the role of the iron-sulphur proteins in electron transfer.

6.1.3 Methods for Analysis of Ferredoxin

Electron spin resonance spectroscopy (ESR), UV spectroscopy and electrochemistry are commonly used to characterise ferredoxins.

The cyclic oxidoreduction between the Fe^{3+} and Fe^{2+} states of the ferredoxins has been the focal point of ferredoxin analysis. Of interest in this research is the 2Fe-2S ferredoxin, often represented as $[2Fe\text{-}2S]^{n+}$. In the oxidised state, both irons atoms are Fe^{3+} and n is 2. Usually only one of the iron atoms are reduced[5], Equation 6-1, so that one Fe (III) and one Fe (II) atom is present, represented as $[2Fe\text{-}2S]^{+}$.

$$\mathbf{[2Fe\text{-}2S]^{2+} + e^- \leftrightarrow [2Fe\text{-}2S]^{+}} \qquad \text{Equation 6-1}$$

The two Fe atoms are located within 5Å of the accessible protein surface. Spectroscopic data indicate that the Fe atom nearest the surface (Fe_A) is reduced during electron transfer processes. The implication is that the E^0 value for the other iron is considerably more negative, out of the biological potential range feasible for life. The most likely route of electron transfer is a 3.49Å electron transfer through space between the aromatic ring of tyrosine, the carboxyl of cysteine, followed by four through bond electron transfers from cysteine to Fe_B over a total distance of 9.35 Å. This is followed by rapid electron transfer from the Fe_B to Fe_A. The distance travelled by the electron may be a deciding factor in determining electron transfer rates.[5] Electron transfer can take place at appreciable rates over distances in excess of 10 Å in proteins[167].

In the $[2Fe\text{-}2s]^{2+}$ cluster, the Fe-Fe distance is only 2.72 Å and the two formally high-spin (d^5) iron atoms have their magnetic moments so strongly coupled antiferromagnetically that the cluster is diamagnetic[103]. This coupling persists upon reduction and because it has only one unpaired electron, ESR detection of the reduced cluster is relatively easy[168].

Ferredoxins exhibit characteristic UV spectra with Fe-S charge transfer bands contributing around 300nm and 400nm[162]. Wavelength shifts indicate a reduced or oxidised state of the protein.

Electrochemical means of ferredoxin analysis has likewise also focused on the ferric/ferrous transition states[5]. Electrochemistry has evolved as a valuable tool for the study of small redox proteins such as the ferredoxins. In theory, for electron transfer to occur at the electrode surface, the metalloprotein diffuses towards the electrode surface until it is sufficiently close to the double layer region (discussed in Section 2.1.1) to accept or donate electrons. The product diffuses away from the electrode back into the bulk solution. Cyclic voltammetry has provided information on electron transfer potentials (usually close to the standard reduction potentials) and on kinetics of electron transfer in ferredoxins[5,157,169]. This information has an important application in characterising electron transfer pathways and defining the physiological role of these proteins. For example, electrochemical methods are being used to characterise the newly discovered *Azotobacter vinelandii*[170] ferredoxin from bacteria. Several studies on the dependence of the redox potentials and observed electron transfer rates of the ferredoxins on parameters such as temperature and pH have been conducted[157,171,172]. These studies revealed that different pH's brings about structural changes at sites either removed from the metal centre or at the metal centre, affecting measured electron transfer rates and hence redox behaviour[173].

The standard redox potential for the Fe^{3+}/Fe^{2+} state is reported at about -420 mV *vs* SHE[174]. Ferredoxin exhibits slow electron transfer kinetics, yielding highly irreversible voltammograms at unmodified electrodes. This makes the determination of redox potentials and kinetic information difficult. Direct electrochemistry of proteins such as ferredoxins has been monitored at electrodes which have been modified[175,176]. Quasi-reversible waves for the redox couple have been obtained in the presence of suitable promoters. A promoter is a species, either immobilised at the electrode or in solution, which brings the protein into closer contact with the electrode surface, facilitating electron

transport between the electrode and ferredoxin. The reversibility of the reduction couple of ferredoxin depends highly on the treatment of the glassy carbon electrode[157].

A requirement for direct electron transfer with the electrode is that the interaction with the electrode is electrostatically feasible[177]. As the ferredoxin from spinach has an overall negative charge, -18 in the oxidised and -19 in the reduced state,[175] a positively charged promoter is required. These include aminoglycosides such as neomycin and[157,166] polycations such as $Cr(NH_3)_6^{3+}$. The hypothesis here is that the $Cr(NH_3)_6^{3+}$ interacts with carboxylate groups at the electrode surface, changing the interface in such a way that the negatively charged ferredoxin is drawn in towards the surface and thus facilitating electron kinetics[178]. The charge density of the promoter facilitates its ability to promote electrocatalytic response e.g. $Cr(NH_3)_6^{3+} > Mg^{2+} \gg K^+$.[177] Addition of poly-L-lysine and other cationic polypeptides in solution was also effective for the rapid transfer of ferredoxins at Hg and In_2O_3 electrodes[179]. Polymyxin[170], a complex peptide containing amine groups, in solution with ferredoxin has also been shown to induce strong adsorption of negatively charged ferredoxin at the electrode surface.

Poly-L-lysine[180] and aminosilane were also shown to promote ferredoxin electron transfer, when drop-dried onto electrodes. This method produced a chemically modified electrode which yielded a quasi-reversible ferredoxin reduction couple[179]. Many advances have been made in achieving direct electrochemistry of redox proteins such as the ferredoxins, but there is much scope yet for characterisation of chemically modified electrode surfaces[177].

The electrochemistry of ferredoxin is highly pH dependant. This is due to the presence of ionisable amino acid substituents. Spinach ferredoxin, has an isoelectric point of 4.0[179]. The protein is positively charged below pH 4 and negatively charged at pH's greater than 4. The protein becomes increasingly negatively charged as the pH approaches that of the sulphydryl oxidation with pK_a 8.3. The positive charge (density) of the electrode thus

plays an important role for the rapid electron transfer of ferredoxin at neutral pH's, where ferredoxin has an overall negative charge.

Despite the two iron centres in most ferredoxin of plant and animal origin, only the reduction of one iron centre has been observed, as mentioned earlier in this chapter. This redox transition at -605 mV *vs* Ag/AgCl is pH independent in the pH range 5 - 10. Only in the 2Fe-2S Rieske protein from bovine heart has a second redox transition been observed[157]. This is of interest as it may suggest that the second iron in most other ferredoxins was involved in redox transitions at some point in evolution. In the Rieske protein, the reduction of the second iron centre has been observed at -1040 mV *vs* Ag/AgCl and is also pH independent in the pH range 5-10. The reduction of the first iron in the Rieske cluster, observed at 100 mV *vs* Ag/AgCl[181] is pH dependant[157].

Oxidation studies on the ferredoxins have been confined to the high-potential iron-sulphur proteins (HiPIP), from purple bacteria, containing $[4Fe\text{-}4S]^{2+/3+}$ clusters. The HiPIP readily undergo reversible one-electron oxidation from the $[4Fe\text{-}4S]^{2+}$ to $[4Fe\text{-}4S]^{3+}$ and only reduce under forcing conditions. Normal $[4Fe\text{-}4S]^{2+}$ type ferredoxins, however, do not undergo this oxidation but act similarly to the 2Fe-2S ferredoxins in their ready reduction from the $[4Fe\text{-}4S]^{2+}$ to $[4Fe\text{-}4S]^{+}$.[182] These transitions are represented in Equation 6-2.

$$\mathbf{[4\,Fe\text{-}4S]^{3+}} \underset{-\,e^-}{\overset{+e^-}{\rightleftharpoons}} \mathbf{[4Fe\text{-}4S]^{2+}} \qquad \mathbf{[4Fe\text{-}4S]^{2+}} \underset{-\,e^-}{\overset{+e^-}{\rightleftharpoons}} \mathbf{[4Fe\text{-}4S]^{+}} \qquad \text{Equation 6-2}$$

~ +350 mV	~ - 400 mV
HiPIP couple	Normal ferredoxin

This disparity has been linked to the presence of a higher number of hydrogen bonds surrounding protein NH groups to cysteinyl sulphur in ferredoxin (about twice as many) than in HiPIPs, predisposing the ferredoxins to reduction. Other theories suggest that the preferred oxidation in HiPIPS and reduction in ferredoxins are based on the preferred

protein conformations around the cluster[168]. It has also further been noted that the iron-sulphur cluster from HiPIPs are almost completely inaccessible to water and surrounded by hydrophobic residues, while the ferredoxin cluster is in a more hydrophilic environment and more accessible to reduction[182].

6.2 AIM OF RESEARCH

The focus in this research is shifted slightly from the well-characterised reduction of the iron-sulphur centre of ferredoxin, to the oxidation of its co-ordinating cysteine ligands. The use of the redox behaviour of the organic part of ferredoxin in analysis, has not been explored prior to this thesis.

The cysteine groups attached to the iron centres are electrochemically active and available for oxidation. The cysteine groups bound to the active Fe^{3+}centre, transport electrons from the protein environment to the iron centre and as discussed in Section 6.1, may be the pathway for transport of this electron from the reduced Fe^{2+} to the acceptor molecule[175].

Chapter 4 discussed the high overpotential of cysteine at unmodified electrodes and the need for catalysts to facilitate the kinetics of its electron transfer with the electrode. Chapter 4 showed the feasibility of electrodeposited $[CoTSPc]^{4-}$ as electrode modifier for cysteine analysis. Chapter 5 showed how the catalytic oxidation of cysteine in the protein metallothionein is a sensitive measure of the protein concentration. In ferredoxin, the cysteine groups comprise on average 11% of the mass of the protein[162]. Therefore, analysis of the cysteine fragment can be used as a quantitative measure of ferredoxin and probably other cysteine containing iron-sulphur proteins. As previously elucidated, bound cysteine is more difficult to oxidise than free cysteine, as evidenced by the comparison between the oxidation potentials of metallothionein and free cysteine. With ferredoxin, this catalytic oxidation is expected to require even more energy. This is because cysteine in ferredoxin acts as a ligand and cannot lose a proton ($RSH \rightarrow RS^-$), as is expected to occur in basic media.

The aim is thus to examine the oxidation of the cysteine component of spinach ferredoxin, by metal phthalocyanines, as a means of protein quantification. These studies may also provide a basis for further research into the role cysteine plays in electron transfer to the iron centres. Also investigated in this work, is the effect of the glassy carbon electrode

modification on the reduction of the $[2Fe\text{-}2S]^{2+}$ clusters in ferredoxin. It has been reported before[157] that the reversibility of the reduction couple of ferredoxin depends highly on the treatment of the glassy carbon electrode. The utility of the metal phthalocyanines as potential mediators for the reduction of ferredoxin is thus also explored.

Studies on the interaction of metallophthalocyanines and metalloproteins are of interest in characterising metalloenzyme models[77].

6.3 EXPERIMENTAL

6.3.1 Reagents

Cobalt(II), copper(II), iron(II), nickel(II) and oxomolybdenum(V) tetrasulphophthalocyanine complexes: Na_4[Co(II)TSPc], Na_4[Cu(II)TSPc], Na_4[Fe(II)TSPc], Na_4[Ni(II)TSPc], and Na_4[(OH)MoO(V)(II)TSPc] respectively, were synthesised and purified according to the method of Weber and Bush[123] as described in Section 4.3.2 for $[MTSPc]^{4-}$ complexes of Co(II) and Mo(II) and Section 5.3.1 for $[MTSPc]^{4-}$ complexes of Fe(II), Ni(II) and Cu(II). Cobalt(II), copper(II), iron(II) and nickel(II) phthalocyanines: Co(II)Pc, Cu(II)Pc, Fe(II)Pc and Ni(II)Pc, respectively, were purchased from Aldrich and used without further purification. Oxomolybdenum (V) phthalocyanine, OMo(V)(OH)Pc, was synthesised according to reported procedures[125] described in Section 4.3.2. Appendix 1 shows the results of the IR spectra of OMo(V)(OH)Pc and Na_4[(OH)MoO(V)(II)TSPc, typical of phthalocyanine complexes.

Ferredoxin used in these studies was spinach ferredoxin. The spinach ferredoxin, 2.2 mg/ml in 0.15 mol dm^{-3} Tris® buffer (pH 7.5), Sigma Chemicals, was kept below 0° C and used without further purification.

For electrochemical studies, ferredoxin was diluted to the desired concentration with either HEPES® (N-2-hydroxyethylpiperazine-N'-2-ethanesulfonic acid), or Tris® buffers. Unless otherwise stated, 0.01 mol dm^{-3} HEPES® buffered to pH = 7.4 was employed for electrochemical studies. 0.1 mol dm^{-3} KCl electrolyte was added to HEPES buffer. The pH of the buffer was adjusted by addition of 0.1 mol dm^{-3} NaOH. In certain experiments 0.1 mol dm^{-3} Tris® buffer was employed, the pH being adjusted by addition of 0.1 mol dm^{-3} NaOH and 0.1 mol dm^{-3} HCl.

In some experiments, 0.01M EDTA (ethylenediaminetetraacetate) containing 0.1M KNO_3 was used as the electrolyte. The concentration of the acids used, HNO_3, HCl and H_2SO_4 was 0.2M. Iron (III) and iron(II) solutions (1×10^{-3}M) were prepared by dissolving $FeCl_3$ in a 0.1M citrate buffer solution and $FeCl_2$ in Millipore water. Triply distilled Millipore water was used for all experimental work.

6.3.2 Apparatus

Electrochemical data were collected with the Bio Analytical Systems (BAS) CV-50W voltammetric analyser. Electronic absorption spectra were recorded with a Cary 1E UV-Vis spectrophotometer.

6.3.3 Methods

A three electrode cell consisting of a Ag/AgCl (3M KCl) reference electrode and a platinum wire counter electrode was employed for cyclic voltammetry of ferredoxin. The working electrode of 1.5mm radius was chemically modified with the MPc by the drop-dry method as explained in Section 4.3.4.

Prior to coating with the MPc complex, the glassy carbon electrode (GCE) was polished with alumina on a Buehler felt pad, followed by soaking in dilute nitric acid and rinsing in distilled deionised water. In between cyclic voltammetry scans, a fresh surface of the GCE was obtained by soaking in dilute acid and rinsing of the electrode in water, acetone and DMF.

For bulk electrolysis of ferredoxin, a two compartment cell was employed, with a platinum plate of area 2.2 cm^2 as counter electrode and a Ag/AgCl (3M KCl) reference electrode. The working electrode consisted of a carbon rod (area = 0.2 cm^2) coated with $[CoTSPc]^{4-}$, using the drop dry method. Electrical contact with the working electrode was established via a copper wire.

All other glassware and electrodes used were cleaned as described before, Sections 3.3.2 and 4.3.4.

Required volumes of the ferredoxin was dissolved in the buffer solution and gently bubbled with nitrogen gas for 2 minutes before cyclic voltammetric studies. In all experiments, cyclic voltammograms of a) an unmodified GCE in ferredoxin-buffer solution, b) modified GCE in the buffer without ferredoxin and c) modified GCE in ferredoxin-buffer solution, were performed and a potential range scanned. All potential values quoted are referenced against Ag/AgCl (3M KCl).

6.4 RESULTS AND DISCUSSION*

6.4.1. Catalytic Oxidation of Ferredoxin

Fig. 6.3 a) shows the cyclic voltammogram (CV) of a $[CoTSPc]^{4-}$ chemically modified glassy carbon electrode (CoTSPc-CMGCE) in HEPES buffer solution in the absence of ferredoxin. An anodic peak corresponding to the oxidation of $[Co(II)TSPc]^{4-}$ to $[Co(III)TSPc]^{3-}$ was observed at 0.85 V. This anodic wave was observed at 0.70 V during electrodeposition of $[Co(II)TSPc]^{4-}$ onto glassy carbon electrode (Fig 4.12), and at 0.80 V for the CoTSPc-CMGCE (modified by electrodeposition) in pH 8.5 Tris-HCl buffer (Fig. 4.20 a), in absence of thiol compounds. The higher potential for the anodic wave corresponding to the oxidation of $[Co(II)TSPc]^{4-}$ to $[Co(III)TSPc]^{3-}$ observed at 0.85 V, Fig. 6.3 a) is due to the different method of chemically modifying the electrode with $[Co(II)TSPc]^{4-}$ (by the drop-dry method) and the different buffer solution used (HEPES/KCl).

On addition of ferredoxin to the buffer solution at CoTSPc-CMGCE, an enhancement of the peak assigned to the oxidation of $[Co(II)TSPc]^{4-}$ to $[Co(III)TSPc]^{3-}$ is observed. This indicates a catalytic oxidation of the cysteine component of ferredoxin by $[CoTSPc]^{4-}$. This anodic peak is observed at 0.90 V, a potential shift of 0.05 V, Fig. 6.3 b). No current response is observed on the return scan, in keeping with the one electron irreversible nature of the oxidation of cysteine.

Fig. 6.3 c) shows that no oxidation of ferredoxin was observed at an unmodified glassy carbon electrode.

---

* This work has been accepted for publication and is not further referenced in this chapter. Janice Limson and Tebello Nyokong, Voltammetric studies of spinach ferredoxin on a glassy carbon electrode modified with cobalt(II) tetrasulphophthalocyanine. Submitted March 1998, accepted July 1998. *Electroanalysis*, in press.

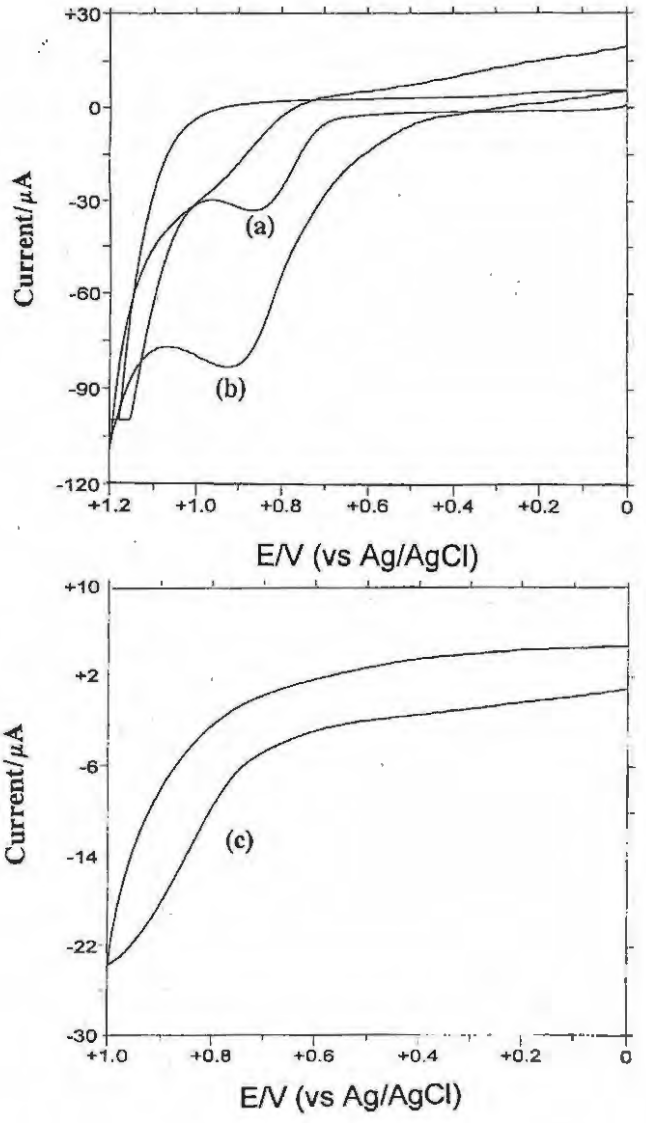

Figure 6.3 Cyclic voltammogram for (a) the buffer solution (blank) on CoTSPc-CMGCE and (b) the oxidation of ferredoxin (44 μg/ml) on CoTSPc-CMGCE. (c) cyclic voltammogram of ferredoxin (44 μg/ml) on unmodified GCE. Electrolyte: 0.01M HEPES buffer (containing 0.1M KCl) pH = 7.4. Scan rate: 20 mV s^{-1}.

The anodic wave in Fig 6.3 b) attributed to the catalytic oxidation of the cysteine component of ferredoxin at CoTSPc-CMGCE increased with increased concentration of ferredoxin, Fig. 6.4.

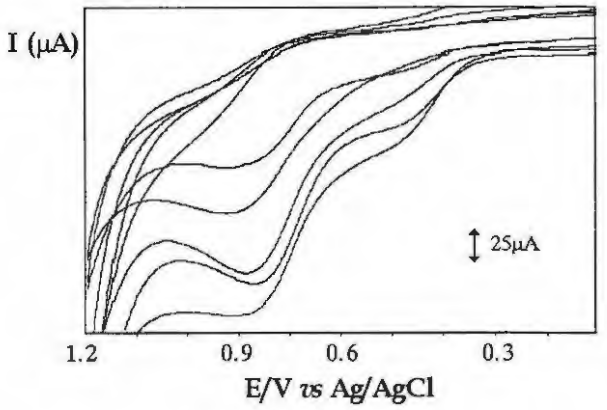

Figure 6.4 Cyclic voltammograms of the oxidation of ferredoxin on CoTSPc-CMGCE showing increasing oxidation waves with ferredoxin concentration. Electrolyte: 0.01M HEPES buffer (containing 0.1M KCl) pH = 7.4. Scan rate: 100 mV s^{-1}.

Catalysis of the oxidation of the cysteine content of ferredoxin by $[CoTSPc]^{4-}$ with increasing ferredoxin concentrations showed a linear current response, Fig. 6.5, in the range 44 to 176μg/ml. The lowest concentration of ferredoxin that could be determined was 20μg/ml.

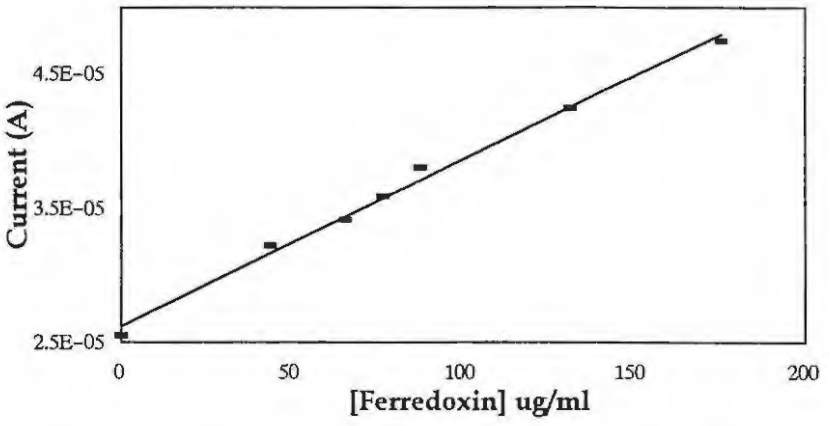

Figure 6.5 The variation of anodic currents (on CoTSPc-CMGCE) with the concentration of ferredoxin. Electrolyte: 0.01M HEPES buffer (containing 0.1M KCl) pH = 7.4. Scan rate: 100 mV s^{-1}.

The electron kinetics of ferredoxin oxidation was examined at increasing scan rates. Fig. 6.6 shows a plot of the square root of the scan rate versus current response. A linear relation (and hence a diffusion controlled oxidation) is observed from 20 mV s^{-1} up to 100 mV s^{-1}. Deviations from linearity were observed above this scan rate. This correlates with

the reported kinetic barrier for electron transfer during the reduction of Fe(III) in spinach ferredoxin at scan rates larger than 100 mV s^{-1}.[171]

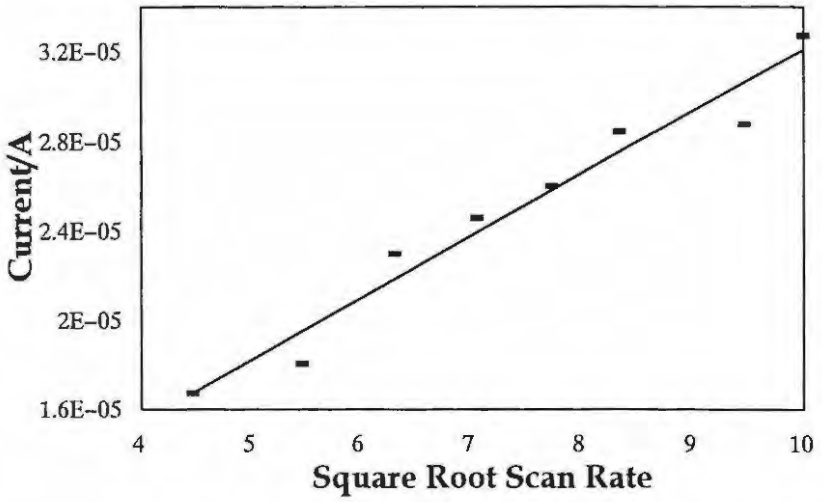

Figure 6.6 The variation of anodic currents for the oxidation of ferredoxin (44 μg/ml) (on CoTSPc-CMGCE) with the square root of the scan rate. Electrolyte: 0.01M HEPES buffer (containing 0.1M KCl) pH = 7.4. Scan rate: 100 mV s^{-1}.

At higher scan rates, above 200 mV s^{-1}, Fig. 6.7 a), a cathodic peak (I) emerged on the return scan in the presence of ferredoxin. This peak increased with increases in scan rate. This peak is thus due to the reversibility of the oxidation wave at 0.90 V (II) with increases in scan rate. This increase in reduction current thus indicates that catalysis of cysteine oxidation is no longer occurring. Fig 6.7 b) shows the CV of CoTSPc-CMGCE in buffer alone at high scan rate. A weaker peak at 0.60 V (III) in Fig. 6.7 a) and Fig. 6.7 b) is the pre-anodic wave observed previously and associated with the splitting due to the stabilisation of mixed valence species, Sections 4.4.6 and 4.4.8. Catalytic oxidation of the cysteine species is thus observed from 20 mV s^{-1} to approximately 200 mV s^{-1} but is diffusion controlled up to 100 mV s^{-1}.

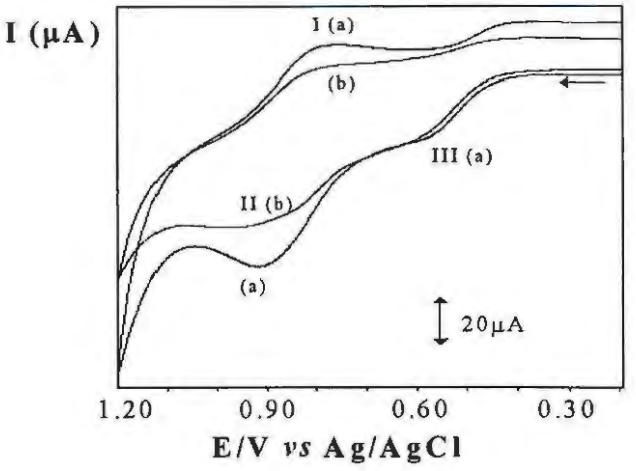

Figure 6.7 Cyclic voltammogram for the oxidation of ferredoxin (44 μg/ml) on CoTSPc-CMGCE at high scan rate (a) and the CV of CoTSPc-CMGCE at high scan rate in absence of ferredoxin, (b). Electrolyte: 0.01M HEPES buffer (containing 0.1M KCl) pH = 7.4. Scan rate: 300 mV s^{-1}.

To investigate the reproducibility of the CoTSPc-CMGCE for ferredoxin oxidation, successive scans were run without recoating nor cleaning of the electrode. The oxidation wave decreases with each scan, Fig. 6.8. This suggests that the electrode was poisoned by adsorption of the oxidation products, as has been observed before[177].

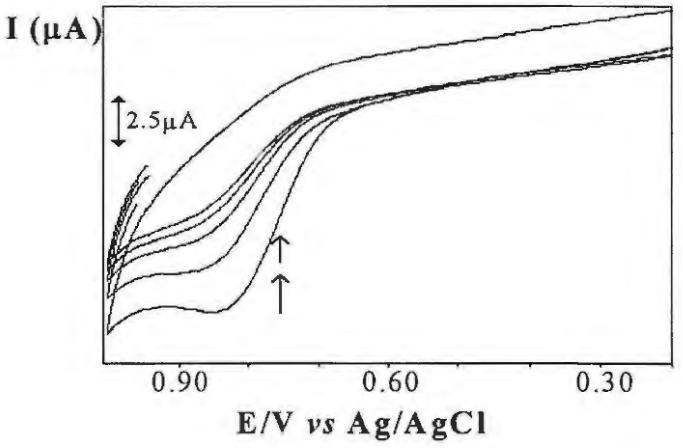

Figure 6.8 Cyclic voltammograms for the oxidation of ferredoxin (20 μg/ml) on CoTSPc-CMGCE, showing decreasing current response with successive scans. Electrolyte: 0.01M HEPES buffer (containing 0.1M KCl) pH = 7.4. Scan rate: 20 mV s^{-1}.

It was found that rinsing the electrode in dilute HNO_3 and then in the buffer solution, reactivated the electrode, probably by dissolving the contaminating oxidation products. A

freshly coated electrode produced reproducible anodic currents; the magnitude of which remained unchanged for ferredoxin that had been stored for several days at 4 °C.

6.4.2 Comparative Studies with different MPc's

Two questions are asked here:
i) How important is the choice of metal in the MPc for catalysis of the oxidation of the cysteine component of ferredoxin? ii) What is the effect of the sulphonation of the MPc ring on catalysis?

To investigate the significance of the central metal and the effects of phthalocyanine ring sulphonation on the catalytic oxidation of ferredoxin by MPc complexes, different metal tetrasulphonated phthalocyanine ($[MTSPc]^{4-}$) complexes and the corresponding MPc complexes were tested as modifiers of the GCE used in determination of cysteine in ferredoxin. The MPc and $[MTSPc]^{4-}$ complexes selected for this study were those of Cu(II), Mo(V), Fe(II) and Ni(II) and CoPc for comparison with $[CoTSPc]^{4-}$. A CV of each of the MPc and $[MTSPc]^{4-}$ complexes deposited on the electrode was first run in the buffer solution without any ferredoxin and then in the ferredoxin-buffer solution. The method of deposition of the MPc and $[MTSPc]^{4-}$ complexes onto the GCE was by the drop-dry method, Section 4.3.4. No leaching of the MPc and $[MTSPc]^{4-}$ complexes adsorbed onto the GCE was observed on placing these CMGCE's into the buffer solution; neither in the absence nor presence of ferredoxin.

Enhancement of the anodic currents on addition of ferredoxin is again associated with the catalytic oxidation of the cysteine component of ferredoxin. This was observed for CuTSPc-CMGCE, CoPc-CMGCE and very weakly for OMo(OH)Pc-CMGCE and in the presence of $[OMo(OH)TSPc]^{4-}$ in solution at an unmodified GCE. The catalytic currents for $[OMo(OH)TSPc]^{4-}$ were more readily observable in aqueous solution than by the drop-dry method with DMF as solvent. Shown in Figs. 6.9 and 6.10 is the catalysis of the oxidation of ferredoxin cysteine on CuTSPc-CMGCE and CoPc-CMGCE, respectively.

These figures show the anodic current due to the metal oxidation in the absence of ferredoxin and the enhancement of this anodic current in the presence of ferredoxin. Again, no ferredoxin cysteine oxidation was observed at a bare glassy carbon electrode.

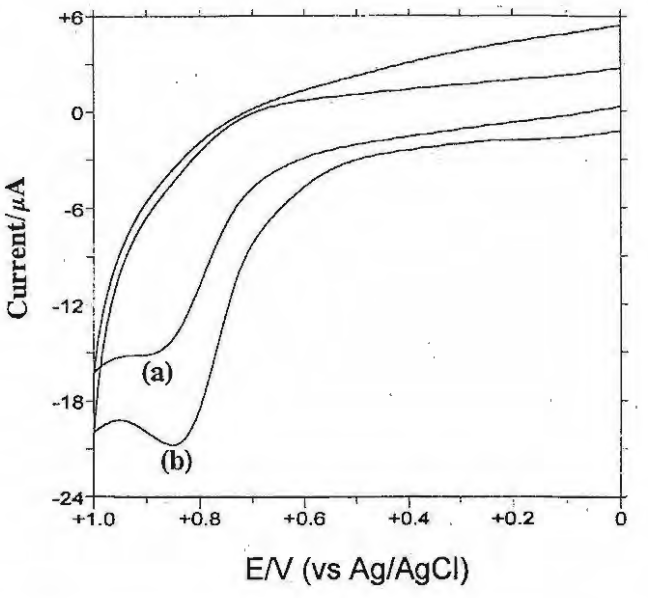

Figure 6.9 Cyclic voltammograms for (a) the buffer solution (blank) on CuTSPc-CMGCE and (b) the oxidation of ferredoxin (44 μg/ml) on CuTSPc-CMGCE. Electrolyte: 0.01M HEPES buffer (containing 0.1M KCl) pH = 7.4. Scan rate: 20mV s^{-1}.

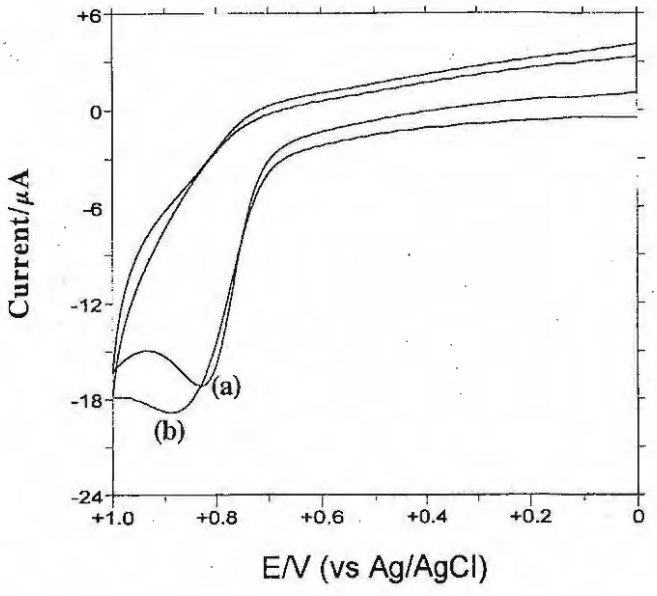

Figure 6.10 Cyclic voltammograms for (a) the buffer solution (blank) on CoPc-CMGCE and (b) the oxidation of ferredoxin (44 μg/ml) on CoPc-CMGCE. Electrolyte: 0.01M HEPES buffer (containing 0.1M KCl) pH = 7.4. Scan rate: 20 mV s^{-1}.

No catalytic oxidation of ferredoxin cysteine was observed for Pc and TSPc complexes of Ni(II) and Fe(II) indicating that there is a metal dependence to the catalysis by the MPc and $[MTSPc]^{4-}$ complexes. For example, Fig 6.11 shows the lowering of the ring oxidation of [Ni(II)TSPc(-2)]/$[Ni(II)TSPc(-1)]^{+}$ (a) on placing the NiTSPc-CMGCE in a ferredoxin-buffer solution (b). The lowered current response in Fig 6.11 b) indicates that the NiTSPc-CMGCE has no catalytic activity for the oxidation of the cysteine component of ferredoxin. The lack of catalytic activity of MPc complexes of Ni(II) for the oxidation of ferredoxin cysteine is in agreement for that observed for free cysteine, while Fe(II)Pc has been shown to catalyse the oxidation of free cysteine[100].

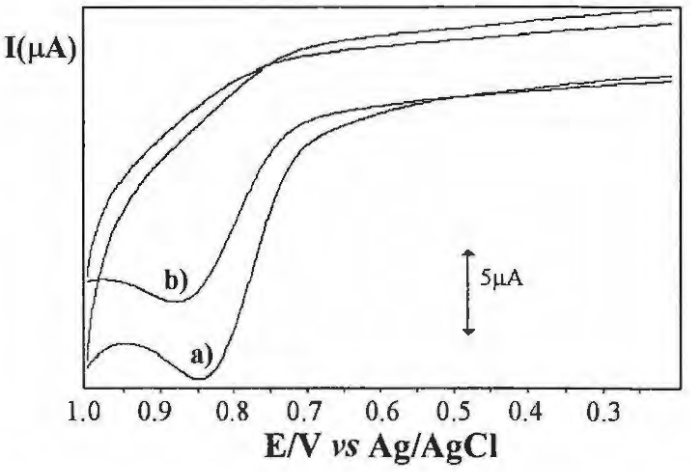

Figure 6.11 Cyclic voltammograms for (a) the buffer solution (blank) on NiTSPc-CMGCE and (b) buffer solution with ferredoxin (44 μg/ml) on NiTSPc-CMGCE. Electrolyte: 0.01M HEPES buffer (containing 0.1M KCl) pH = 7.4. Scan rate: 20 mV s^{-1}.

Of the tetrasulphonated phthalocyanines the highest enhancement in anodic current was observed for the GCE modified with $[CoTSPc]^{4-}$, followed by $[CuTSPc]^{4-}$ and the least response was observed for [OMo(OH)TSPc[in solution at an unmodified GCE. The data for $[CoTSPc]^{4-}$ is also in agreement for that of free cysteine[100] as the best phthalocyanine for catalysis of ferredoxin oxidation.

Of the untetrasulphonated phthalocyanines, only CoPc and OMo(OH)Pc showed catalysis for ferredoxin cysteine oxidation, while CuPc did not. CoPc showed a higher catalytic activity towards ferredoxin oxidation than OMo(OH)Pc. Here it is evident again that the

central metal does confer a role on the catalytic activity of the phthalocyanine, and that the tetrasulphonation of $[CuTSPc]^{4-}$ confers on it a better catalytic role than does CuPc. In addition, CoPc showed a weaker catalytic activity than $[CoTSPc]^{4-}$ towards the oxidation of the ferredoxin cysteine, indicating further that the sulphonated MPc's facilitate better catalysis. This may be because the high negative charge of the sulphate groups attract positive components of the ferredoxin protein, bringing the protein closer to the site of electron transfer with the metal centre. It has indeed been noted that $[MTSPc]^{4-}$ complexes bind proteins prior to electron transfer reactions[183]. It is thus likely that the ferredoxin is bound to the $[MTSPc]^{4-}$ species adsorbed at the electrode prior to electron transfer during the catalytic oxidation of the cysteine component of ferredoxin.

This reasoning may explain why $[CuTSPc]^{4-}$ catalyses ferredoxin cysteine oxidation. Oxidation of cysteine on GCE modified with MPc complexes containing an electroactive central metal is believed to be mediated by one electron oxidation of the central metal[107,100,131]. CoPc, $[CoTSPc]^{4-}$, OMo(OH)Pc and $[OMo(OH)TSPc]^{4-}$ show oxidation at the central metal[110,131,184] whereas oxidation in $[CuTSPc]^{4-}$ is known to occur at the phthalocyanine ring[110]. This suggests that the oxidation of ferredoxin cysteine by $[CuTSPc]^{4-}$ is a ring based catalytic reaction. The mediation of ring-based oxidation processes has also been suggested for the catalytic oxidation of cysteine on GCE modified with Rh, Ru and Os phthalocyanine complexes[185].

As is seen in Figs 6.9 and 6.10, the anodic wave due to ferredoxin cysteine oxidation is accompanied by a potential shift. $[CuTSPc]^{4-}$ showed a marked increase in current response for ferredoxin cysteine oxidation, with a slight potential shift to less positive potentials. CoPc, however, showed a slight enhancement but a shift towards more positive potentials. Potential values at which the various phthalocyanines catalyse ferredoxin cysteine oxidation are shown in Table 6.1. They are slightly different for the various phthalocyanine complexes. The potential at which cysteine oxidation is observed on MPc modified electrodes is not directly related to the potential for the first oxidation in these complexes. The potential value for $[CoTSPc]^{4-}$ catalysis of ferredoxin is, however, close

to that of $[CoTSPc]^{4-}$ catalysis of free cysteine, 0.85 V *vs* Ag/AgCl at neutral pH, as shown in Section 4.4.7. In the presence of $[OMo(OH)TSPc]^{4-}$ the oxidation of free cysteine occurs at 0.28 V[131], a potential lower than that observed for ferredoxin. The large protein environment of the ferredoxin complex may account for this disparity with free cysteine. Table 6.1 also shows that the oxidation of ferredoxin occurs at a higher potential on OMo(OH)Pc-CMGCE than on the other MPc modified electrodes.

Table 6.1 Comparison between half-wave potentials ($E_{½}$) for MPc complexes and peak potentials for the oxidation of ferredoxin on metallophthalocyanine modified GCE. pH = 7.4 HEPES buffer. Scan Rate = 20 mV s^{-1}.

Modifier	$E_{½}$ (V vs SCE)[a]	E_p (V, vs Ag/AgCl)[b]
$[CoTSPc]^{4-}$	0.43 (119)	0.90
$[CuTSPc]^{4-}$	0.87 (119)	0.86
OMo(OH)Pc	0.38 (184)[c]	0.96
$[OMo(OH)TSPc]^{4-}$	0.40 (131)	0.93
CoPc	0.49 (119)	0.87

[a] $E_{½}$ for the MPc complexes in DMF containing tetraethylammonium perchlorate (reference from which data taken in brackets). [b] Potential for ferredoxin oxidation on the GCE modified with various MPc complexes. [c]In dimethylsulphoxide containing tetraethylammonium perchlorate.

6.4.3 pH dependence of the cysteine oxidation of Ferredoxin

pH studies on the electrochemistry of ferredoxin have concentrated on the stability of the protein in terms of potential variation of the ferric/ferrous transition with pH. Generally the ferredoxins are pH independent and thus stable within the pH range 5 to 10. A similar study is shown here in terms of the pH dependence of the cysteine oxidation at varying pH. Choice of buffer solution is of importance in these studies, where the nature of the cation and the ionic strength of the buffer salt is as important as the changes in hydrogen ion concentration. In terms of a broader buffering capacity range, a phosphate buffer was initially selected for the pH studies. At a CoTSPc-CMGCE in a phosphate buffer, pH 7, containing ferredoxin, no oxidation due to ferredoxin was observed. Oxidation of ferredoxin was, however, observed at similar pH's, in HEPES buffer, Section 6.4.1. Phosphate buffers are known to precipitate polyvalent cations, inhibiting certain reactions. This may explain the inhibition of the oxidation of ferredoxin observed using a phosphate buffer. In terms of changing hydrogen ion concentration, the pH studies were thus conducted in a HEPES/KCl buffer. The pH was adjusted accordingly, with 0.1M NaOH in the pH range 5 to 10 and 0.1M HCl in the pH range 2 to 4. Fig. 6.12 shows the oxidation of ferredoxin at CoTSPc-CMGCE in the pH range 6 to 10.

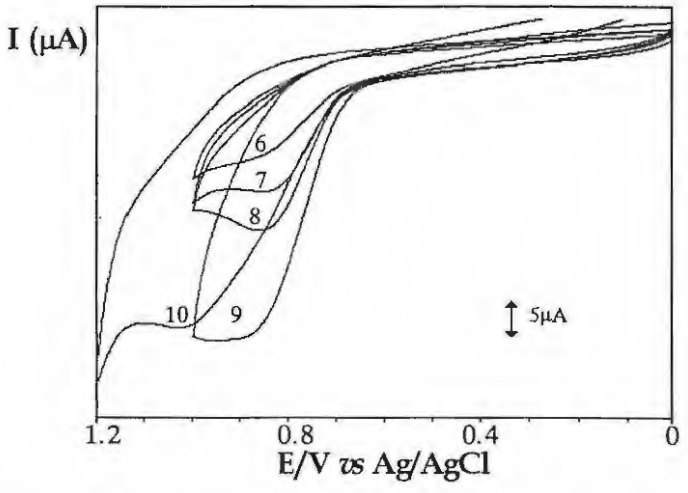

Figure 6.12 Cyclic voltammograms of ferredoxin (88 μg/ml) on CoTSPc-CMGCE. Electrolyte in pH range 6 to 10 : 0.01M HEPES buffer (containing 0.1M KCl) buffered with 0.1M NaOH and 0.1M HCl. Scan rate: 20 mV s^{-1}.

Current response increases with increasing pH, probably due to the favourable conditions for hydrogen ion evolution. The anodic potential shifts towards more positive potentials with increasing pH, and current strength. In the pH range 2 to 4, no ferredoxin oxidation is observed, indicated in Fig 6.13.

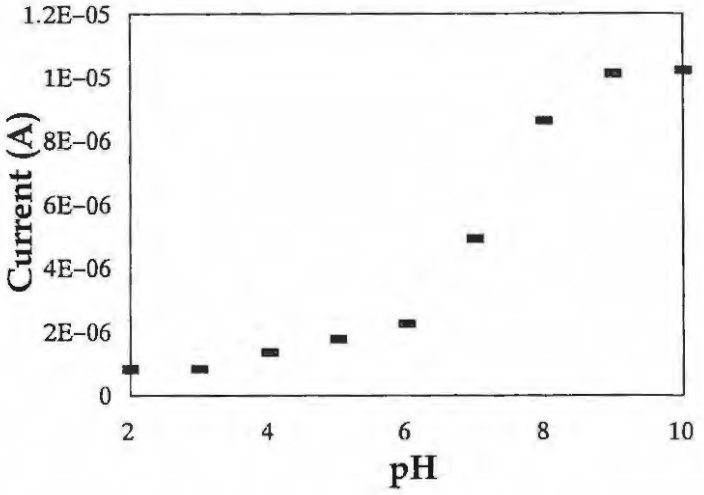

Figure 6.13 Variation of oxidation currents with pH for the cyclic voltammetry of ferredoxin (88 μg/ml) on CoTSPc-CMGCE. Electrolyte: 0.01M HEPES buffer (containing 0.1M KCl) buffered with 0.1M NaOH and 0.1M HCl. Scan rate: 20 mV s^{-1}.

Below pH 4, the protein is positively charged, its isoelectric point (pI) being 4.0. The ferric/ferrous transition in ferredoxin is reported to be pH dependant[157], and unstable at these pH's. This may be due to an unfavourable electrostatic interaction at the electrode due to the positive charge of the ferredoxin and the highly protonated buffer environment, or simply, due to decomposition of the protein at low pH's.

When highly acidic solutions were employed for the oxidation of ferredoxin at CoTSPc-CMGCE, no increase in the anodic wave due to ferredoxin oxidation was observed. An increase in the corresponding cathodic wave on the return scan was observed, Fig 6.14. This indicates that true catalysis of ferredoxin oxidation does not occur at these pH's.

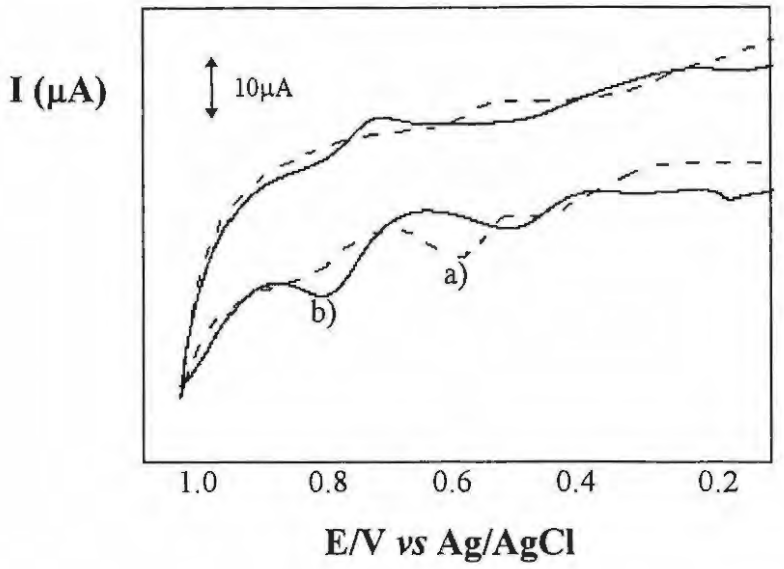

Figure 6.14 Cyclic voltammogram for (a) the buffer solution (blank) on CoTSPc-CMGCE and (b) the oxidation of ferredoxin (44 μg/ml) on CoTSPc-CMGCE. Electrolyte: 0.2M H_2SO_4. Scan rate: 100 mV s^{-1}.

6.4.4 The Effect of Promoters on the Catalytic Oxidation of Ferredoxin Cysteine

A general requirement for protein electrochemistry is that the surface of an electrode is electrostatically compatible with the protein, particularly the binding sites for the biological protein partner[177]. Ferredoxin at neutral pH has an overall negative charge and thus a promoter with positively charged functional groups is required, as discussed in Section 6.1.

$[CoTSPc]^{4-}$ catalyses cysteine oxidation at neutral pH, Section 4.4.7. The combined electrostatic forces of the negatively charged thiols and $[CoTSPc]^{4-}$ are not enough to prevent close interaction between the thiol and the CoTSPc-CMGCE [134,186]. For the highly negatively charged ferredoxin there is expected to be greater electrostatic repulsion.

A stronger catalytic response was observed in HEPES/KCl than in Tris-HCl (without the potassium ions). This may provide evidence for the neutralisation effect of the cation, K^+.

Charge neutralisation is a requirement following oxidation or reduction in cyclic voltammetry. The type of electrolyte is thus of importance[46]. It has been noted[187] that a particular type of electrolyte ion may dominate in maintaining electroneutrality at modified electrodes, such as the redox inactive K^+. However, when an EDTA/ KNO_3 buffer was used, the response was weaker than for the HEPES/KCl buffer. This brings into focus the effect of the buffer salt itself.

Tris buffer is known to block certain biochemical reactions[188]. This may explain why the catalytic oxidation of ferredoxin was not reproducible when Tris-HCl buffer was employed. The electrode appeared irreversibly poisoned after one scan. While the contribution of the K^+ in the HEPES/KCl buffer system is appreciated, the HEPES salt itself may have a role to play in promoting electron transfer. HEPES is a zwitterionic buffer, meaning that it has positive and negative charges. These buffers, designed by Good and co-workers, overcome many of the difficulties associated with buffers in biological systems[188]. It may thus be that its zwitterionic nature promotes closer interaction and electron transfer between ferredoxin and the CoTSPc-CMGCE.

6.4.5 Ultraviolet Spectroscopic Studies of Ferredoxin

Absorption spectra in the near ultra-violet and visible range were studied to observe interaction of ferredoxin with $[CoTSPc]^{4-}$. Shown in Fig. 6.15 a) is the spectra of the ferredoxin in HEPES buffer, pH 7.0. Ferredoxin absorbs in the near ultraviolet range at 280nm. The spectra for $[CoTSPc]^{4-}$ alone in HEPES buffer is shown in Fig. 6.15 b) with a Q band at 740nm and the Soret band at 300nm, as discussed in Sections 4.1.2 and 4.4.4. Addition of ferredoxin to the $[CoTSPc]^{4-}$ did not show marked changes in the shape of the Q band at 740nm. A marked increase was observed in the Soret band region at 300nm, Fig 6.15 c). While this shows interaction, it is unfortunate that these bands overlap. Other studies have, however, shown that co-ordination of bovine serum albumin results in marked changes in the spectra of the $[ClAlTSPc]^{4-}$ species[183].

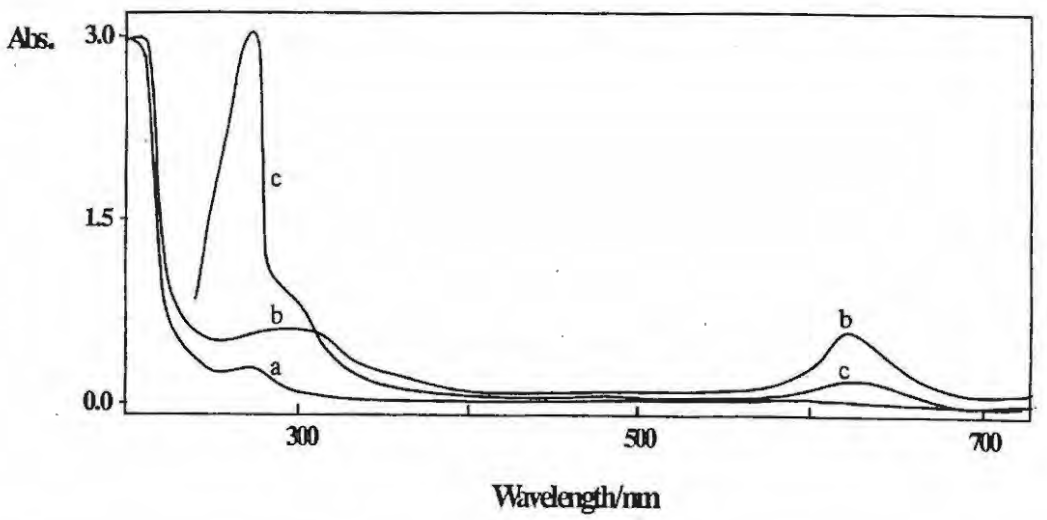

Figure 6.15 The electronic absorption spectra of a) ferredoxin, b) $[CoTSPc]^{4-}$ and c) spectral changes to $[CoTSPc]^{4-}$ on addition of ferredoxin. Ferredoxin concentration: 44 μg/ml; buffer solution: 0.01M HEPES, 0.1M KCl.

Bulk electrolysis of ferredoxin in HEPES buffer on an unmodified carbon electrode and at potentials slightly more positive (0.95 V) than potentials associated with the oxidation of ferredoxin, resulted in the shifting of the ferredoxin spectra to shorter wavelengths, without loss of intensity. Chemical oxidation of the $[2Fe\text{-}2S]^{2+}$ cluster is not known to bleach the ferredoxin absorption peak[171]. When a carbon electrode modified with $[Co(II)TSPc]^{4-}$ was employed for the bulk electrolysis of ferredoxin, a bleaching of the absorption spectra of ferredoxin was observed. This shows that $[Co(II)TSPc]^{4-}$ catalyses the oxidation of ferredoxin, resulting in the degradation of this protein as the cysteine component gets oxidised.

6.4.6 Catalytic Reduction of Ferredoxin

The reduction of Fe^{3+} to Fe^{2+} in spinach ferredoxin has been observed at -605 mV *vs* Ag/AgCl; irreversible at unmodified electrodes and quasi-reversible in the presence of promoters such as neomycin. The potential of this reduction varies slightly with the use of different promoters and different treatment methods of the electrode, in the potential range -605 mV to -628 mV.[157]

MPc complexes are known to catalyse the reduction of many molecules,[100] by lowering the reduction potential of the species of interest. When used as electrode modifiers, MPc complexes lower the reduction potential by transfer of electrons from the reduced MPc species to the species of interest. Both CoPc and $[CoTSPc]^{4-}$ showed a similar promotional effect for ferredoxin reduction. Fig. 6.16 a) shows the CV of the blank (HEPES buffer) at CoPc-CMGCE. With addition of ferredoxin to this solution, a weak reduction couple is observed near -0.2 V *vs* Ag/AgCl, Fig. 6.16 b). The currents for this couple increased with increasing concentration of ferredoxin. The return peak is weak compared to the forward scan but this quasi-reversible couple is an improvement over the irreversible ferredoxin reduction observed at unmodified electrodes. The fact that a reduction peak in the presence of ferredoxin on CoPc-CMGCE was observed at a lower reduction potential than reported in the literature[157] for the Fe^{3+}/Fe^{2+} couple, shows that CoPc lowers the potential for the reduction of ferredoxin.

The CV at a CoTSPc-CMGCE, in absence of ferredoxin, shows an irreversible reduction at -0.23 V, Fig. 6.17 a). This is due to the reduction of the adsorbed $[Co(II)TSPc]^{4-}$ to the $[Co(I)TSPc]^{5-}$ species. Reductions are known to occur at the central metal on Co(II) phthalocyanine complexes[110]. In the presence of ferredoxin, Fig. 6.17 b), this reduction peak is enhanced and shifts to -0.34 V.

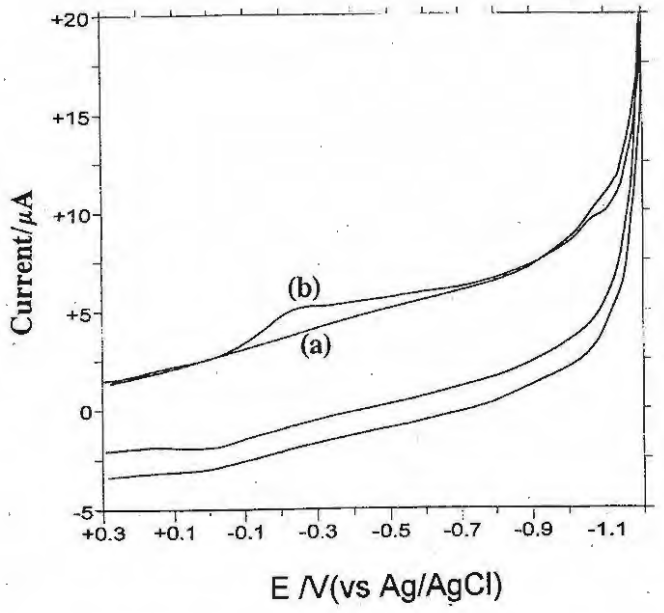

Figure 6.16 Cyclic voltammogram for (a) the buffer (blank) solution on CoPc-CMGCE and (b) the reduction of ferredoxin (44 μg/ml) on CoPc-CMGCE. Electrolyte: 0.01M HEPES buffer (containing 0.1M KCl) pH = 7.4. Scan rate: 20 mV s^{-1}.

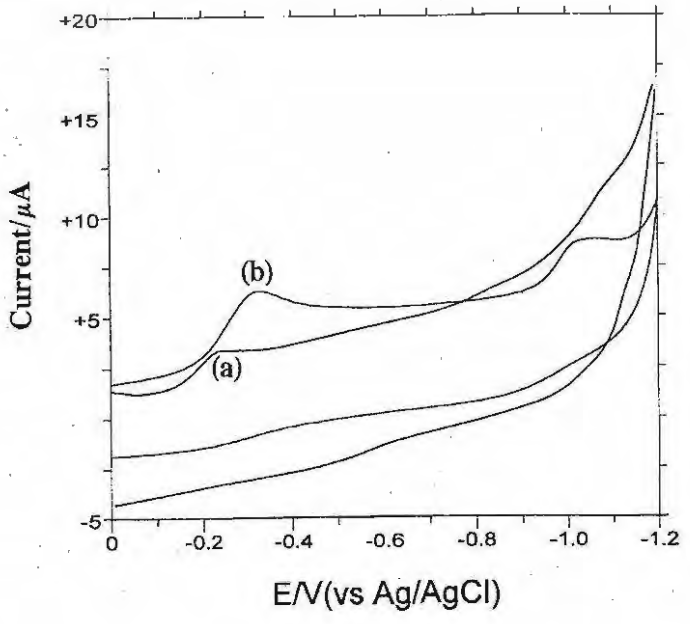

Figure 6.17 Cyclic voltammogram for (a) the buffer (blank) solution on CoTSPc-CMGCE and (b) the reduction of ferredoxin (44 μg/ml) on CoTSPc-CMGCE. Electrolyte: 0.01M HEPES buffer (containing 0.1M KCl) pH = 7.4. Scan rate: 20 mV s^{-1}.

The reduction peak in Fig 6.17 b) increased with increasing concentrations of ferredoxin, Fig. 6.18. This implies that the reduction of Co(II) to Co(I) catalyses the reduction of ferredoxin. In the presence of other mediators, reduction of ferredoxin has been observed

between -605 mV and -628 mV *vs* Ag/AgCl[157] and at poly-L-lysine modified electrodes at -0.59 V;[180] a potential difference of 250 mV from the -0.34 V *vs* Ag/AgCl observed here for ferredoxin reduction. The relatively large shift in potential of the peak assigned to the reduction of ferredoxin compared to the peak due to adsorbed $[Co(II)TSPc]^{4-}$ suggests that interaction occurs between ferredoxin and adsorbed $[Co(II)TSPc]^{4-}$.

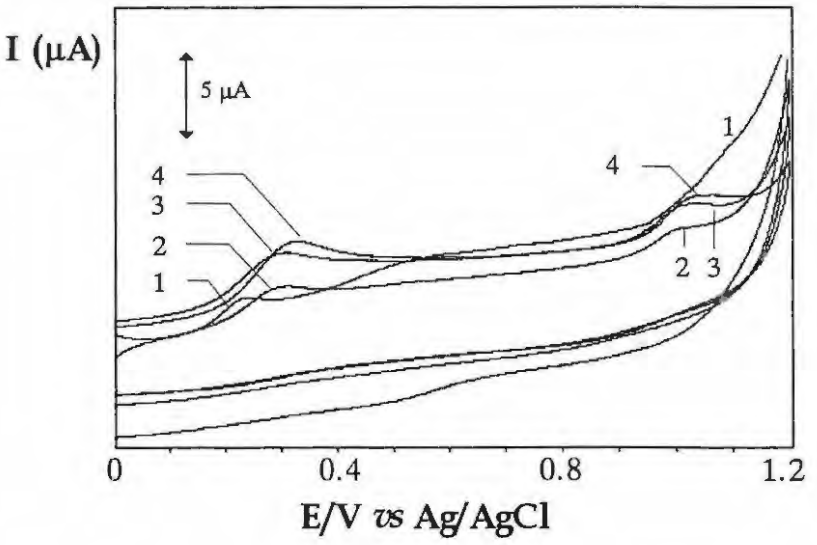

Figure 6.18 Cyclic voltammogram for (1) the buffer (blank) solution on CoTSPc-CMGCE; the reduction of ferredoxin (2) (22 μg/ml), (3) (33 μg/ml) and (4) (44 μg/ml) on CoTSPc-CMGCE. Electrolyte: 0.01M HEPES buffer (containing 0.1M KCl) pH = 7.4. Scan rate: 20 mV s^{-1}.

The reduction of ferredoxin by $[Co(II)TSPc]^{4-}$ may be related to the biological reduction of cobalamin (*in vivo*), from Co(II) to (Co(I) complexes by ferredoxin[168].

A further irreversible reduction peak is observed in Fig. 6.17 at -1.02 V. which also increased with increasing concentrations of ferredoxin, Fig. 6.18. Addition of free Fe^{3+} caused enhancements in this reduction wave. This may thus be associated with the presence of free Fe(III) in the solution possibly as result of some ferredoxin contamination or decomposition. This reduction wave is close to the potential at which the second ferric transition has been observed for the Rieske iron-sulphur protein, an irreversible reduction at -1040 mV *vs* Ag/AgCl. This second reduction wave appears to be pH dependent. A

high current response is observed at acidic pH's, Fig. 6.19, at pH 2 and 3. Beyond pH 4 this peak decreases dramatically but still persists at pH's above 7. This may be related to the overall charge on the protein, as ferredoxin is positively charged below pH 4. The current response decreases with increasing pH and the negative charge on the protein. The reduction peak at -0.34 V is not observed until pH 4 and is observed, though weakly, until pH 10. It can be inferred from the above that the two reduction peaks are dependant on pH, or rather the charge on the protein.

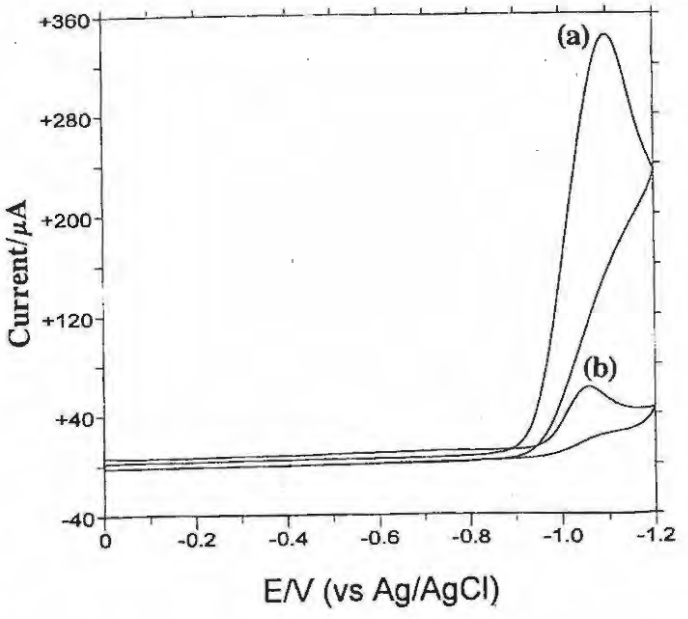

Figure 6.19 Cyclic voltammograms for the reduction of ferredoxin (88 μg/ml) on CoTSPc-CMGCE at (a) pH = 2 and (b) pH = 3. Electrolyte: 0.01M HEPES buffer (containing 0.1 M KCl). Scan rate: 20 mV s^{-1}.

As mentioned in Section 6.1.3, reduction of the second ferric ion in spinach ferredoxin has not been observed. This has been reasoned by consideration that it would be too highly negative and thus out of the biological potential range. It is tempting then to associate this second reduction at -1.02 V with the previously unobserved reduction of the second ferric reduction of spinach ferredoxin. Considering that $[CoTSPc]^{4-}$ lowers the reduction potential of the ferredoxin at -0.34 V as shown in Fig 6.18, it is feasible then that this second reduction potential is also significantly shifted to less negative potentials. The second reduction in the Rieske centre at -1.04 V was due to adsorbed ferredoxin[157]. As suggested before, adsorption of ferredoxin may be occurring in these studies.

However, in Section 6.4.3 it was suggested that true catalysis of the oxidation of the cysteine component does not occur at highly acidic pH's. Furthermore, ferredoxins are not stable below pH 4 and so increases in the current response with decreased pH of this peak, in Fig 6.19 is associated with the decomposition, or destruction of the iron-sulphur active site, yielding free iron.

6.5 CONCLUSIONS

It has been shown that a GCE modified with $[CoTSPc]^{4-}$ catalyses the oxidation of the cysteine component of the spinach ferredoxin protein. The oxidation of ferredoxin on CoTSPc-CMGCE is pH dependent and significant currents were only observed above pH 5. A linear plot for the oxidation current versus ferredoxin concentration was obtained. This plot may be used as a means of quantification of the spinach ferredoxin as the cysteine fragment is known to constitute 11% mass of the protein. The catalytic oxidation is dependant on the type of metal centre in the metallophthalocyanine and on the presence of the sulphonate substituents on the MPc ring. $[MTSPc]^{4-}$ complexes with M = Co(II) or Cu(II) or Mo(V), catalysed the oxidation of ferredoxin cysteine while $[MTSPc]^{4-}$ complexes M = Ni(II) and Fe(II) did not; $[CoTSPc]^{4-}$ producing the higher current response. This may be related to the readiness with which cobalt phthalocyanine form axial ligands with the analyte. Of the untetrasulphonated MPc's only cobalt and molybdenum catalysed the oxidation of spinach ferredoxin and these current responses were weaker than those observed for the corresponding sulphonated MPc. This may be explained in terms of the favourable electrostatic interaction between ferredoxin and the sulphonated MPc's.

The nature of the catalytic oxidation waves was dependant on the buffer solution. Using HEPES buffer with KCl electrolyte, reproducible and strong current responses were observed. This is related to favourable electron transfer kinetics between ferredoxin, the modifier and the electrode, due to charge neutralisation.

Both CoPc and $[CoTSPc]^{4-}$ catalyse the reduction of ferredoxin. Ferredoxin reduction is normally not reversible on carbon electrodes, but on CoPc-CMGCE, the ferredoxin peaks show some reversibility. Thus, chemically modifying the electrodes with cobalt(II) phthalocyanines improves the activity of the GCE for the detection of ferredoxin. This is a pH independent reduction above pH 5 and is observed at -0.34 V in presence of

$[CoTSPc]^{4-}$, a significant lowering of the reduction potentials as reported previously using other modifiers or mediators. This reduction wave is related to the reduction of the first Fe^{3+} centre of ferredoxin. A second reduction wave at high negative potentials, -1.02 V is pH dependant below pH 5. The nature of this reduction wave below pH 5 may be associated with the decomposition of ferredoxin at very low pH's.

Chapter Seven

The Interaction of Melatonin and its Precursors with Metals

7.1 INTRODUCTION

7.1.1 Metals and Neurodegenerative Diseases

There exists a definite link between metals, essential and toxic and the onset of neurodegenerative diseases. Causal or symptomatic, their concentration fluctuations within the central nervous system in diseased states suggests an importance in understanding their role in neurodegenerative disease. These fluctuations can serve as early indicators in prediseased stages, leading towards possible treatment measures. Metals can exist free in the cytosol, in storage vesicles, at the active sites of enzymes or proteins, or bound to ligands which facilitate their transport. The reasons for their imbalances may thus be due to displacement by other metals, toxic or essential, inhibition of the enzyme or protein, ruptured storage vesicles, dietary deficiency or a breakdown in their transport mechanism in the central nervous system (CNS).

Metallothionein is believed to function in the CNS in transport, storage and release of zinc and calcium. Zinc, after calcium and magnesium, is the most abundant cation in the brain. Zinc concentration in the brain is non-uniform, its concentration being highest in the cerebellum, hippocampus (higher in the hilar region and lowest in the fimbria), retina and the pineal gland. Metallothionein has also been identified in the bovine pineal gland[189]. Zinc plays a role in more than 235 metalloenzymes, as a catalyst, structurally and regulatory, professedly participating in neurosecretion, neuromodulation and neurotransmission. The importance of zinc in neural development can be exemplified by

its role in synthesis of pyridoxal phosphate, a precursor of the neurotransmitters dopamine, norepinephrine, serotonin, histamine, and γ-aminobutyric acid (GABA). Thirty to forty percent of all neurons require GABA. While zinc is required for GABA synthesis, high levels of zinc can retard its release, as in Pick's disease. Here higher than normal accumulation of zinc in the hippocampus causes inhibition of GABA transmission. This example highlights the requirement for a steady state concentration of zinc. There are an extensive number of disorders of the CNS where zinc concentration has been shown to be altered. These include alcoholism, Alzheimer type dementia, Down's syndrome, epilepsy, Friedreich's atachia, retinitis pigmentosa, schizophrenia and Wernicke-Korsakoff syndrome[144]. The value of metallothionein in zinc homeostasis is emphasised by findings of a down-regulation of genes coding for thionein production in Alzheimer's Disease[141].

Other examples of metal links with neurodegenerative diseases includes Fhar's calcinosis,[190] where crystalline deposits of calcium coincide with disorders of the CNS, critical copper imbalances in Wilson's (due to congenital absence of copper-binding ceruloplasmin) and Menkes' Diseases,[95] and then the much debated, much disputed, role of aluminium in Alzheimer's disease. The neurotoxicity of lead and mercury is well known.

Lead causes stupor, convulsions and neural damage. Children are more susceptible to this type of poisoning due to incompletely developed metabolic pathways and blood brain barriers (BBB). Lead, being a soft acid, displaces zinc and calcium at the active sites of enzymes. By inhibiting iron uptake into protoporphyrin IX, the biosynthesis of haem is retarded, protoporphyrin IX accumulates in the red blood cells (often the first sign of physiological impairment due to lead toxicity in humans) and Fe^{2+} in the blood. Lead also inhibits the biosynthesis of δ-aminolevulinic acid dehydrogenase (ALAD). This leads to an increase in ALA levels which may be neurotoxic to the brain. 5-ALA could be a weak antagonist to the neurotransmitter GABA and may mimic GABA as a false neurotransmitter. The implication here is that lead may inhibit the metabolism of GABA causing anxiety and hyperactivity [12].

Reportedly, lead incapacitates glial cells in the brain, while manganese toxicity causes inhibition of the uptake of the neurotransmitters, serotonin and dopamine, in certain parts of the brain. This evidence suggests that metal pollution may lead to "violent urges"[191].

The toxicity of mercury depends on the chemical form, alkyl mercury being the most toxic to the CNS. Alkyl mercury causes lysis of brain cells affecting sensory, visual, auditory and co-ordination control. Mercury metal vapours readily cross the BBB and once oxidised in the blood stream, remains in brain tissue whereas the free metal may move out again. The Minamata incident is a case in point, where locals consuming shellfish which had bioaccumulated mercury effluent from a plastics factory, suffered brain damage[12].

7.1.2 Alzheimer's Disease

Alzheimer's Disease (AD), is one of the senile dementias. The first visual symptoms are a striking loss of short term memory, space and time disorientation. Following these symptoms are the impairment of speech, amnesia, muscle twitches, mood changes. AD sufferers show a rapid loss of touch with the real world, becoming bedridden and incontinent. Of importance, is that the first symptoms appear in the limbic regions of the brain associated with speech, memory and personality. In the brain, AD, is associated with the presence of amyloid (or senile) plaques and the proliferation of glial cells which cause astrocytes and neurofibrillary tangles.[190,192]

The association with AD and aluminium was made when it was reported that AD patients show an accumulation of aluminium in localised areas of the brain. Aluminosilicates have been found at the core of senile plaques and aluminium is present in neurons bearing neurofibrillary tangles. In the brains of humans with AD, aluminium concentrations approach 12μg /g of tissue in some regions, in sharp contrast to the values of 3μg /g in "normal" brain tissue.[6]

Aluminium is the third most abundant element in the earth's crust. Humans ingest about 30mg per day, mostly as food contaminant. It is mostly assumed to be a non-essential, non-toxic element, but this view has changed with its intercranial accumulation in AD, Parkinson's and dialysis dementia patients. Aluminium reportedly increases the permeability of BBB, leading to dementia. Intracranial injections of aluminium salts in cats, rabbits and dogs cause neurofibrillary degeneration and the impairment of learning and memory abilities, symptoms associated with AD.[6]

Aluminium is transported in the plasma. In the plasma, aluminium is bound with silicic acid free in solution. Aluminosilicates will form and deposit in focal areas within which aluminium is free as $Al(OH)^{4-}$ or weakly bound to phosphate, in the presence of silicic acid. These conditions may apply at the nucleus of senile plaques in AD. Aluminosilicates at the core of plaques appear to be the result of the transport of aluminium from diseased cells to the extracellular space in which its combination with silicic acid is possible.[6]

Perforations in the CNS protective shield, the blood brain barrier, may also facilitate the influx of metals into the brain[141].

Al^{3+} toxicity can result from the inhibition of Mg^{2+} dependant enzymes as Al^{3+} has a higher affinity for these ligands than Mg^{2+}. Nanomolar concentrations of Al^{3+} will displace millimolar levels of Mg^{2+} from adenosine triphosphate (ATP^{4-}) for example and will not maintain the activity of the enzyme because ligand exchange at Al^{3+} is much slower than at Mg^{2+}. Al^{3+} may also compete with Fe^{3+} and Ca^{2+} [9]. Aluminium toxicity in *chlorella* can be alleviated by increasing the concentrations of calcium[6]. This may be associated with AD, where abnormal levels of free iron[193] and calcium deposits occur in the brain. Other areas where Al^{3+} (a hard acceptor) is potentially destructive, is in its proposed binding to the oxygens of phosphate groups of DNA and the carboxylates of fatty acids[6].

A cause for concern is that acid rain solubilises aluminosilicates so there is an increase in free aluminium in the environment. Certain regions such as Guam and other Pacific areas have higher concentrations of aluminium in their environment and higher rates of occurrence of AD and Parkinson's disease.[6]

Studies to measure total amounts of aluminium in tissues is usually via AAS, the shortcoming of this method being that it does not allow for distinction between free and bound aluminium. Aluminium may also be bound in a non-toxic form. Electrochemical methods are of better analytical value in distinguishing between free and bound aluminium. The interaction of aluminium with biological ligands (fatty acids, amino acids and DNA) has mostly been through the use of ^{27}Al NMR. This technique is complicated by the extensive hydrolysis of aluminium in aqueous solutions to form polymers. These polymers distort NMR data by causing ^{27}Al chemical shifts.[6] Understanding these interactions with biological ligands are of value in defining the toxic role of aluminium.

An important point to remember is that not all of the pathological changes in AD are readily explained by aluminium toxicity and so the debate still continues as to aluminium's causal or symptomatic role in these neurodegenerative disorders[192]. The answer may lie in ascertaining the reason for the accumulation of aluminium in AD.

What causes the imbalances of other metals such as calcium and zinc? While metallothionein functions in the peripheral organs in metal regulation as discussed in Section 4.1, its functional role appears to be curtailed in the central nervous system to that of zinc regulation. Furthermore, considering that the brain is the "power-box" of the mammalian body, how does it cope with toxic metals like cadmium, lead and mercury and maintain the homeostasis of essential elements?

7.1.3 The Pineal Gland and Melatonin

The answer may be sought in the pineal gland, for the role it plays in neuroprotection. The pineal gland, the mysterious organ at the base of the skull, revealed its secrets with the discovery of melatonin, its principal hormone. Melatonin is also produced, to a lesser extent, in the retina and in the gastro-intestinal tract. Fig. 7.1 shows a simplified representation of the synthesis of melatonin.

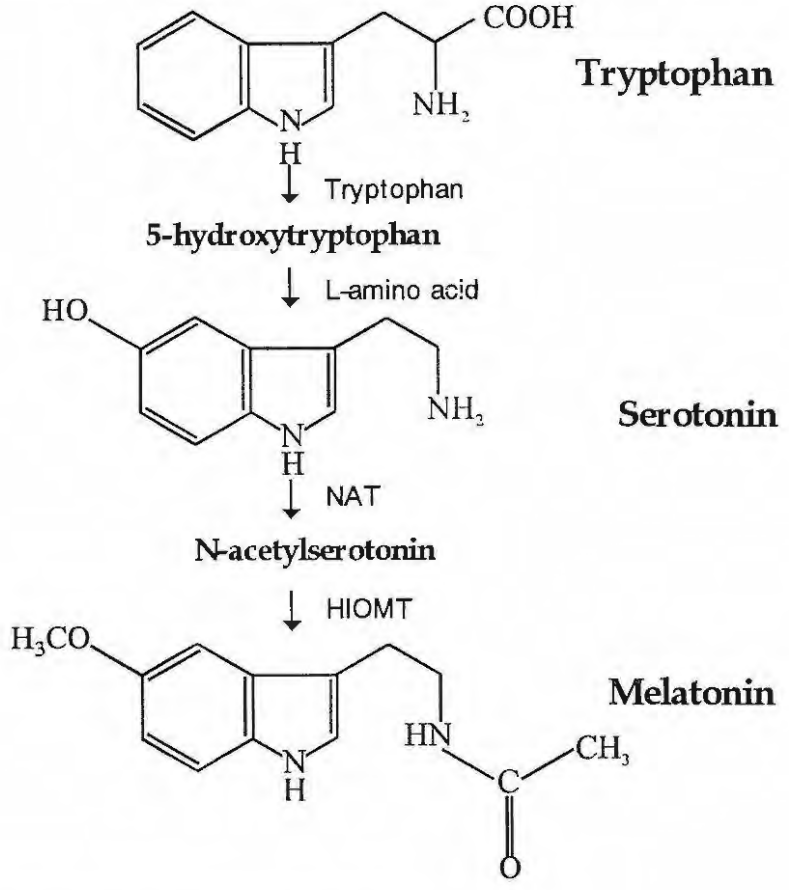

Figure 7.1 Schematic representation of melatonin synthesis.

Melatonin is a product of tryptophan metabolism. Its synthesis begins with the uptake of tryptophan by the endocrine cells of the pineal gland, the pinealocytes. The enzyme tryptophan hydroxylase hydroxylates tryptophan to 5-hydroxytryptophan (5-HT), which is then decarboxylated by L-amino acid decarboxylase, forming serotonin. Serotonin is then N-acetylated by N-acteyltransferase (NAT) to N-acetylserotonin and converted to

melatonin (N-acetyl-5-methoxytryptamine) by hydroxyindole-*O*-methyltransferase (HIOMT). NAT controls the synthesis and amount of melatonin produced. NAT activity in the pineal gland increases almost 100-fold at night. This rise follows stimulation of the intracellular secondary messenger, cyclic adenosine monophosphate (cAMP), which is a result of activation of the *B*-adrenergic receptors in the cell membrane of the pinealocytes by norepinephrine (NE). NE is the catecholaminergic neurotransmitter that is released from the postganglionic sympathetic neurons that innervate the mammalian pineal gland.[194]

Melatonin is not stored by the pineal gland. Once produced in the pinealocytes, it is released into the blood. In this way, blood levels of melatonin follow a circadian pattern: low during the day and high at night. Melatonin is both lipophilic and hydrophilic, crossing all morphophysiological barriers, entering all tissues and cells[194]. Melatonin is not only able to exert its influence on cells possessing membrane and nuclear receptors for melatonin, but has intracellular actions independent of it binding to a receptor molecule[195].

Melatonin is "functionally diverse". The 24 hour rhythmic synthesis and release facilitates a role as a signalling molecule for circadian events[196]. Melatonin has been identified in mammals, non-mammals, invertebrates and even in algae. It is widely accepted that melatonin acts to set and entrain circadian rhythms in all of these organisms. Melatonin is linked with the neuroendocrine system and in particular with the hypothalamo-pituitary-gonadal axis[197]. The seasonal changes in melatonin production (higher in the winter than summer months) is a signal for the annual fluctuations in reproduction of photoperiodic animals. The seasonal fluctuation in melatonin has implicated it in depressive disorders[198], particularly the Seasonal Affective Disorder. The suprachiasmatic nuclei (SCN), the so-called biological clock, also possess receptors for melatonin. It is uncertain whether or not the role of melatonin in circadian rhythms is dependant on these receptors. The theoretical role of the SCN is in transmitting light information (light and dark) from the retina to the pineal gland, stimulating the synthesis and release of melatonin, depending on the information received. It has also been postulated that the role of the receptors on

the SCN may be to switch off melatonin synthesis once peak levels are reached. It is, however, the discovery of melatonin as free radical scavenger[199] and general antioxidant[200] that has generated the most interest in recent years[195,201-204].

Free radicals

Free radicals are chemical species which possess an unpaired electron. The unpaired electron makes them highly reactive towards biological substrates. The utilisation of oxygen in the mitochondrial production of ATP produces the superoxide anion of oxygen, $O_2^{\cdot -}$, a free radical which is converted to relatively harmless hydrogen peroxide by the metalloenzyme superoxide dismutase (SOD), as depicted in Fig 7.2. Mn-SOD generally occur in mitochondria while Cu and Zn-SOD are found in the cytosol and are the major contributors to the dismutating activity of the SOD's. While the major source of the superoxide anion radicals is in the mitochondria, nitric oxide, epinephrine, norepinephrine and several oxygen utilising enzymes, also generate this free radical.

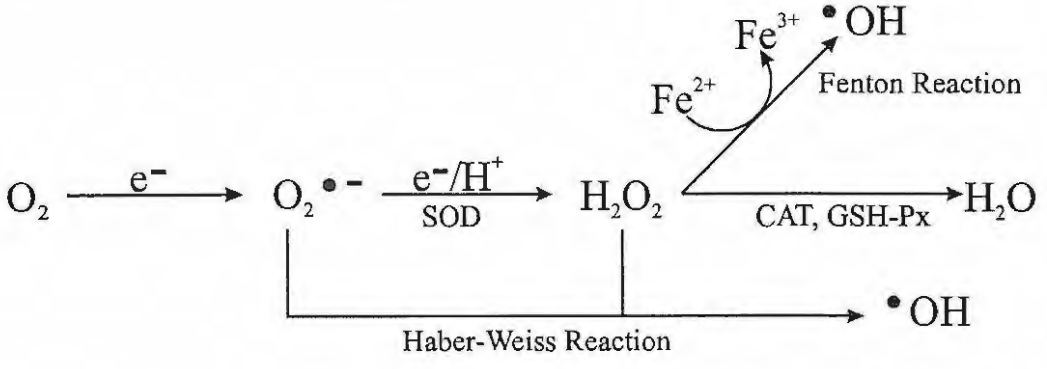

Figure 7.2 The production of free radicals by oxygen utilisation. SOD = superoxide dismutase, CAT = catalase and GSH-Px = Glutathione peroxidase.

H_2O_2 produced from the dismutation of $O_2^{\cdot -}$ is not regarded as a free radical but as a reactive oxygen intermediate which readily crosses cell membranes. In the presence of glutathione peroxidase and catalase enzymes, it is readily converted into harmless water. However, in the presence of Fe^{2+} or Cu^{+}, H_2O_2 is converted into the toxic hydroxyl radical

in the Fenton reaction, shown in Fig. 7.2. The superoxide anion is also capable of generating the hydroxyl radical (•OH). Other enzymes, including L-amino acid oxidase and monoamine oxidase are also capable of generating H_2O_2, increasing the possibility of oxidative damage by formation of •OH.[195]

The hydroxyl radical, the most potent radical, is highly reactive and with a very short half-life, is indiscriminate in its attack on molecules and macromolecules such as DNA, membrane lipids, proteins and carbohydrates. In DNA, •OH attacks the sugar of a base, producing strand breaks, also causing chemical changes in the pyrimidine and purine bases. This DNA damage may be a precursor to cancer. It also initiates lipid peroxidation by abstracting a hydrogen from a polyunsaturated fatty acid (PUFA) side chain in the membrane lipid, generating the peroxyl radical. The peroxyl radical not only has the capacity to damage nearby protein and enzyme receptors in the membrane, but by abstracting hydrogens from a nearby PUFA side chain, can initiate a self-perpetuating lipid peroxidation. Membrane lipids are converted to lipid peroxides which alter the fluidity of the membrane, permitting the leaking of essential ions such as calcium. Lipid hydroperoxides react with iron and copper to produce peroxyl and alkoxyl radicals which may reinitiate lipid peroxidation. The high lipid content of neural tissues predisposes it to hydroxyl damage. Vitamin E, α-tocopherol, concentrated in the hydrophobic interior of cell membranes, acts as a chain breaking antioxidant by donating an electron to the peroxyl radical. Vitamin C recycles the vitamin E radical, but in the presence of free iron, acts as a prooxidant.[195]

Further damage is caused by •OH on amino acids of proteins, causing protein-protein crosslinking, such as disulphide bonds, thereby functionally impairing or disabling these proteins. Proteins most susceptible are those containing the transition metal ions (particularly iron and copper), as they present the most immediate target for the hydroxyl radicals which these metals generate.

The products of oxygen utilisation places the brain at a significant disadvantage when considering that it utilises twenty percent of the body's oxygen intake[195] and moreso considering that the antioxidant system is not perfect.

It is widely accepted that free radicals and their associated damage is partially responsible for the ageing process. This is feasible considering the accumulation of free radical damage to DNA, cell membranes and the impairment of proteins, particularly those involved in antioxidant defence. Indeed, there are a host of ageing and neurodegenerative diseases that can be attributed to free radical damage, such as Parkinson's, Down syndrome, aluminium-induced neuropathy, vitamin E deficiency and AD.[195]

In light of this, the discovery of the antioxidative function of melatonin is a welcome relief. Melatonin has been shown *in vitro* and *in vivo* to scavenge both the hydroxyl radical and the peroxyl radical. It does this by donating an electron to these reactive species and in so doing, being oxidised to the unreactive indolyl cation radical. The latter may then quench a superoxide radical, further reducing the damaging effects of oxidation on brain tissues. Various studies have shown that melatonin is efficient in protecting DNA, proteins and lipid membranes against free radical damage. Melatonin may also interrupt the chain reaction during lipid peroxidation. Its high mobility means that this protection is not localised. Furthermore, melatonin stimulates the activity of the antioxidant glutathione in the brain and inhibits the activity of the enzyme generating nitric oxide. In relation to glutathione as hydroxyl radical scavenger and vitamin E as peroxyl radical scavenger, melatonin has been shown to be five times as efficient as glutathione and nearly twice as efficient as vitamin E.[195]

These discoveries place melatonin in a new role, in neuroprotection and further unfolds the mystery of the pineal gland. Melatonin thus has an important role in ageing and ageing diseases, in terms of the neuroprotection it offers. However, along with a daily and seasonal fluctuation, melatonin also appears to have a life-time clock. At a certain age, its synthesis and release reaches a peak, then declines with age. This depletion has been linked with the deterioration of the pineal gland and the SCN neurons which stimulate the pineal gland synthesis of melatonin. The retinohypothalamic neurons terminating in the SCN are believed to sustain free radical damage, reducing the light signal to the pineal gland. These neurons deteriorate even further with diminished melatonin and the coincident neuroprotection. In patients with neurodegenerative disorders such as AD,

virtually no melatonin is produced. The depletion of melatonin with age has thus been associated with ageing and neurodegenerative diseases such as Parkinson's[205] and AD.[206,207]

7.2 AIM OF RESEARCH

The role of transition metals such as iron and copper in the ageing process; zinc imbalances in neurodegenerative diseases and the toxicity of heavy metals such as lead, cadmium and aluminium, suggests that metals are involved in the degeneration of the CNS. The accumulation of aluminium in AD[208] and onset of neurodegeneration with decreased melatonin synthesis, prompted an investigation into the role of this pineal hormone in metal regulation.

Thus, the aim of this study was to explore the possibility of an interaction between these metals and melatonin in the onset of neurodegenerative disorders.

Any changes in the levels of the essential amino acid, tryptophan or serotonin (the precursors to melatonin), will naturally affect the amount of melatonin synthesised in the pineal gland. This is evident in that melatonin prevents the breakdown of tryptophan in the liver by tryptophan pyrrolase[209]. Tryptophan, an amino acid is known to alleviate depression[198] while serotonin is an important neurotransmitter. The focus is thus extended to explore the interaction of melatonin, tryptophan and serotonin with some metals of biological importance. Metals studied are aluminium, cadmium, copper, iron, lead and zinc.

7.3 TECHNIQUE

For this work, adsorptive cathodic stripping voltammetry (AdCSV), the technique described in Sections 2.5 and 3.3, is used to study the interactions of metals with the ligands. In chapter 3 different ligands were examined for their utility in quantifying metals. In this chapter, the focus is on identifying whether the ligands (melatonin, serotonin and tryptophan) bind metals. The modification of this technique for these purposes also defines a new method for testing metal-ligand bond formation between a metal and a chosen ligand of biological and synthetic origin and as such is discussed in detail below.

Adsorptive cathodic stripping voltammetry for identifying metal-ligand interactions

A metal ion, when reduced at a working electrode, produces a current response equivalent to its concentration in solution, at a fixed potential *vs* a standard reference electrode. In the presence of a ligand which forms a bond with a metal, the metal-ligand complex may form and adsorb to the working electrode, thereby enhancing the preconcentration of the metal. The reduction wave observed will be that of the metal-ligand complex and an enhancement of the current response is expected with a shift in potential commensurate with the reduction of a new species. As discussed in Section 3.3.3, a negative potential shift is indicative of a strong metal-ligand interaction while a large positive shift is associated with a weaker metal-ligand interaction. The absence of enhancement in the current response of the metal ions in the presence of a ligand or a lowering in current response, indicates that no metal-ligand bond formation has occurred. Lowering in current response may also indicate competition by the ligand for binding sites at the electrode. This technique thus provides simple, fast, efficient information on whether a ligand will bind a metal and if so, how strong the bond is, the kinetics of the bond formation, i.e. how easily the ligand will bind the metal and how easily it will release the metal.

7.4 EXPERIMENTAL

7.4.1 Reagents

Solutions of Al^{3+}, Cu^{2+}, Zn^{2+}, Fe^{2+}, Fe^{3+}, Cd^{2+} and Pb^{2+}, were prepared from the salts of $AlCl_3$ (Merck), $CuCl_2$ (Unilab), $ZnCl_2$ (Univar), $FeCl_2$ (Aldrich), $FeCl_3$ (Unilab), $CdSO_4$ (Merck), and $PbSO_4$ (NT Chemicals). Aqueous solutions of melatonin, serotonin and tryptophan were prepared daily. All aqueous solutions were prepared from triply distilled, de-ionised water. Tetraethylammonium perchlorate (TEAP) was synthesised as described in Section 4.3.1.2 and used as the electrolyte for electrochemical experiments in non-aqueous solutions. Acetonitrile was freshly distilled and used as a solvent for experiments in non-aqueous solutions.

Sodium acetate buffer (0.2M) of pH 4.4 was prepared from stock solutions of 0.2M acetic acid and 0.2M sodium acetate and used as the electrolyte solution for aqueous electrochemical experiments. A 1000μg/ml mercury solution was prepared from $HgCl_2$ (PAL Chemicals).

7.4.2 Apparatus

Stripping voltammograms were obtained with the Bio Analytical Systems (BAS) CV-50W voltammetric analyser. An undivided cell was employed for the cathodic adsorptive stripping voltammetry. A 3 mm diameter glassy carbon electrode filmed with mercury *in situ* (MFGCE) was employed as a working electrode. A silver/silver chloride ([NaCl = 3 mol dm^{-3}]) and a platinum wire were employed as reference and auxiliary electrodes, respectively. For non-aqueous solutions, a silver wire coated with silver chloride was employed as a pseudo reference electrode. Prior to use, the glassy carbon electrode was cleaned by polishing with alumina on a Buehler pad, followed by washing in nitric acid and rinsing in water and the buffer solution. In between scans, the electrode was cleaned by immersing the electrode in acid solution and rinsing with water.

7.4.3 Electrochemical Methods

Acetate buffer (pH = 4.4), Hg^{2+} solution (1000 μg ml^{-1}) and appropriate concentrations of the metal ions and of the ligands (melatonin, serotonin or tryptophan) were introduced into an electrochemical cell. The solution was then deaerated with nitrogen for 5 min, after which a flow of nitrogen was maintained over the solution throughout the measurement. The metal complexes of melatonin, serotonin or tryptophan are expected to have formed at this stage. Acetonitrile was used as a solvent for studies involving aluminium. The use of acetonitrile and TEAP as an electrolyte, allowed the observation of the reduction peaks of the *in situ* complexes of aluminium with melatonin, serotonin and tryptophan. The reduction peaks could not be observed in aqueous solvents due to the high negative potential. For studies with iron (III), a 0.05M citric acid buffer was used, to prevent formation of iron hydroxides. An optimum deposition potential was then applied for a known period to effect the formation of the Hg film onto the GCE and the adsorption of the metal complexes onto Hg film. The voltammograms were recorded in the negative direction from the deposition potential to 0.4 V vs Ag/AgCl beyond the metal complex reduction at the scan rate of 200 mV s^{-1} during the stripping step. During the stripping step, the current response due to the reduction of the metal complexes of melatonin, serotonin and tryptophan, were measured as a function of potential. The concentrations of melatonin, serotonin and tryptophan were in the range 1.0×10^{-6} to 1.5×10^{-5} mol dm^{-3}. The metal ion concentrations ranged from 1×10^{-7} to 2×10^{-4} mol dm^{-3}.

7.5 RESULTS AND DISCUSSION*

The accumulation time, deposition potential, and deposition time were optimised for the adsorptive cathodic stripping voltammetry of the metals with the ligands were optimised. These experiments were performed by keeping all the other variables constant and only altering the parameter being optimised. The highest current responses observed was used as the measure in ascertaining the optimum value of the parameter. Optimum deposition potentials found were: -1400 mV for aluminium, 100 mV for copper, 400 mV for cadmium, -350 mV for iron III, 0 mV for iron II, -100 mV for lead and -700 mV for zinc. As in Section 3.4.1, optimum accumulation times found were 5 minutes to achieve formation of the metal-ligand complex and 3 minute deposition times for deposition of the mercury film onto the electrode and the metal-ligand complex onto the mercury film.

The adsorptive cathodic stripping voltammograms (AdCSV) of Al^{3+}, Cd^{2+}, Cu^{2+}, Fe^{3+} Pb^{2+} and Zn^{2+} in the presence of melatonin, serotonin and tryptophan as ligands are shown in Fig. 7.3. AdCSV of metals in the absence of ligand were measured as represented by the dotted lines in Fig. 7.3. AdCSV following addition of small amounts of each of the ligands to each of the metal solutions resulted in the enhancement or lowering of the reduction peaks of the metals. Fig. 7.3 a), b) and c) show the AdCSV of the metals in the presence of melatonin, serotonin and tryptophan, respectively. The enhancements show the metal binding affinity of the ligand for the metal. For Al^{3+}, no defined peak was observed in the absence of the ligands probably due to the masking of the Al^{3+} reduction peak by the onset of solvent reduction. However, a reduction peak was observed on addition of solutions of the ligands to

---

* The following publication resulted from this work and is not further referenced in this chapter: J. Limson, T. Nyokong, S. Daya, The interaction of melatonin, and its precursors, with aluminium, cadmium, copper, lead and zinc: An adsorptive voltammetric study, *Journal of Pineal Research*, **1998**, 15-21.

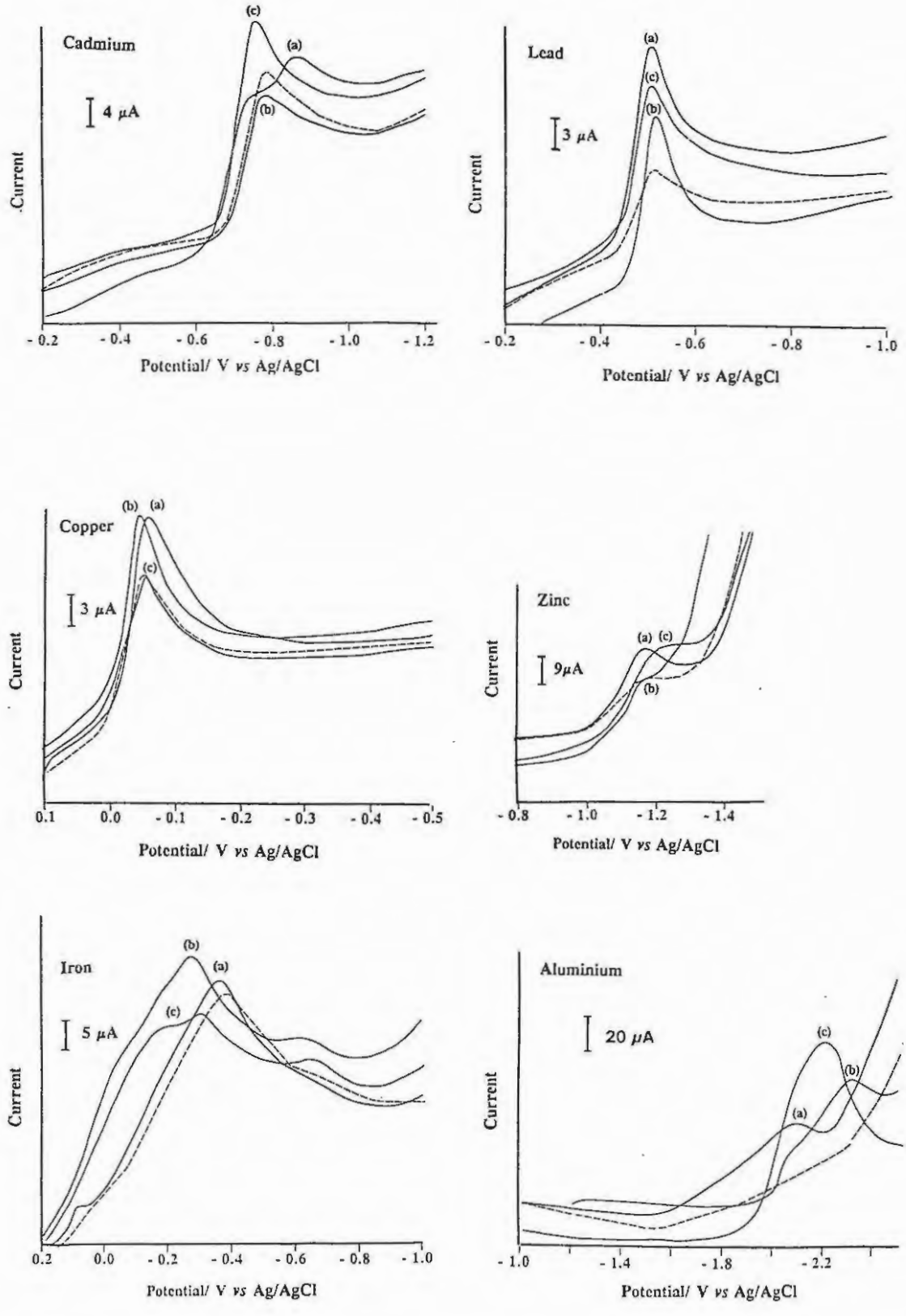

Figure 7.3 Adsorptive cathodic stripping voltammograms obtained for 1 x 10^{-5} mol dm^{-3} of Cd^{2+}, Pb^{2+}, Cu^{2+} and Zn^{2+} and 1 x 10^{-3} mol dm^{-3} Fe^{3+}in the presence of 1.5 x 10^{-5} mol dm^{-3} (6 x 10^{-5} mol dm^{-3} in the case of Fe^{3+}) (a) melatonin (b) serotonin and (c) tryptophan; (d) is the voltammogram of the metal in the absence of the ligand. Electrolyte: pH = 4.4 sodium acetate buffer, for Al^{3+}, acetonitrile containing TEAP was employed as an electrolyte. Scan rate = 200 mV s^{-1}.

solutions of Al^{3+}. No voltammograms were observed for the ligands alone in the absence of the metal ions. The enhancement of the metal reduction peak on addition of the ligands is an indication of the *in situ* formation and deposition of the metal complexes of melatonin, serotonin or tryptophan at the electrode. Where no increases in current responses of the metals were observed on addition of the ligands, it can be assumed that no metal-ligand were formed.

At the concentrations of the metal ion used for Figure 7.3, no increase in current response was observed when serotonin was added to cadmium or zinc, nor when tryptophan was added to copper or ion. At the respective metal-ligand concentrations, the data shows that the following metal-ligand bonds form: aluminium with melatonin, tryptophan and serotonin; cadmium with melatonin and tryptophan; copper with melatonin and serotonin; iron(III) with melatonin and serotonin; lead with melatonin, tryptophan and serotonin; and zinc with melatonin and tryptophan.

As discussed in Section 3.4.3, the extent of the shift in reduction potential of the metal on addition of the ligand is a good measure of the stability of the metal-ligand complex formed *in situ*. Table 7.1 lists the shifts in the peak potentials for the reduction of the metals, ΔE_p, on addition of ligands. An accurate potential shift could not be determined for Al^{3+} due to the lack of a reduction peak for the metal.

For melatonin, a high negative shift in potential was observed for Cd^{2+}. The high negative shift in the reduction potential reflects the difficulty in reducing the Cd-melatonin complex as compared to the reduction of the free metal. Cu^{2+}, Pb^{2+} and Zn^{2+} showed only minor potential shifts on addition of melatonin, implying that the complexes formed between melatonin and these metals are not as strong as complexes formed between melatonin and Cd^{2+}.

Table 7.1. Parameters obtained for the adsorptive cathodic stripping voltammetry of the aluminium, cadmium, copper, iron, lead and zinc in the presence of melatonin, tryptophan and serotonin.

(a) Melatonin

Metal	Slope[a] (A/mol dm^{-3})	E_p (V vs Ag/AgCl)[b]	ΔE_p (mV)[c]
Cadmium	2.18	- 0.857	- 79
Copper	1.23	- 0.057	- 7
Iron		- 0.377	+ 2
Lead	0.99	- 0.504	+ 5
Zinc	0.94	- 1.160	- 2

(b) Tryptophan

Metal	Slope[a] (A/mol dm^{-3})	E_p (V vs Ag/AgCl)[b]	ΔE_p (mV)[c]
Cadmium	2.18	- 0.752	+ 16
Copper	1.19	- 0.051	- 1
Iron		- 0.299	+ 80
Lead	1.11	- 0.504	+ 5
Zinc	0.41	- 1.197	- 39

(c) Serotonin

Metal	Slope[a] (A/mol dm^{-3})	E_p (V vs Ag/AgCl)[b]	ΔE_p (mV)[c]
Cadmium	2.72	- 0.78	0
Copper	1.26	- 0.045	+ 5
Iron		- 0.273	+ 106
Lead	1.31	- 0.509	0
Zinc	0.37	- 1.158	0

[a] Slope of the plots of AdCSV currents (in μA) versus the concentration of the metal in mol dm^{-3}.
[b] For Al^{3+}, a silver wire coated with AgCl was used as a pseudo reference electrode.
[c] The difference between the peak potential of the uncomplexed metal ion and the peak potential of the metal formed *in situ*.

For tryptophan, Table 7.1 shows that the largest negative potential shift was obtained for Zn^{2+}. This observation suggests that tryptophan forms stable complexes with zinc and less stable complexes with the other metal ions; complexes with Cd^{2+} and Fe^{3+} being less stable than with Pb^{2+} and Cu^{2+}. A positive ΔE_p indicates the ease of reduction of the Cd-tryptophan complexes as compared to the Cd-melatonin complex.

Table 7.1 shows that at the relatively low metal and ligand concentrations used, serotonin did not form stable *in situ* complexes with any of the metals. Apart from the large positive potential shift observed for serotonin complexes with Fe^{3+}, insignificant changes between the reduction potentials of the metals and of the metal-serotonin complexes were observed for the other metals studied. Fe^{3+} showed a variable affinity for the ligands. Tryptophan did not cause any enhancement in the Fe^{3+} reduction, while melatonin and serotonin did. A larger positive potential shift for the serotonin-Fe^{3+} reduction than for melatonin-Fe^{3+} suggests that the melatonin-Fe^{3+} bond is more stable.

Plots of the current response of the metal-ligand complexes versus the concentration of the metal ion are shown in Fig.7.4 for melatonin, tryptophan and serotonin. Generally, weak metal-ligand current responses were observed at very low metal concentrations, followed by a linear range at intermediate metal concentrations. Deviations from this linearity were observed at high metal concentrations. This trend was particularly observed for Cd-ligand complexes. The linear range is indicative of the metal concentration range in which the given concentration of ligand would be functional for effective metal binding. For zinc, the current response remained low over a larger range of metal ion concentrations, than for the other metals. However, for cadmium, deviation from linearity was reached sooner than for the other metals. The deviations at high concentration is thus probably due to competition between the metal complex and the free metal ion for the electrode surface. The point of deviation would then be an indication of the concentration of metal ion at which all of the given concentration of ligand is bound to metal ions.

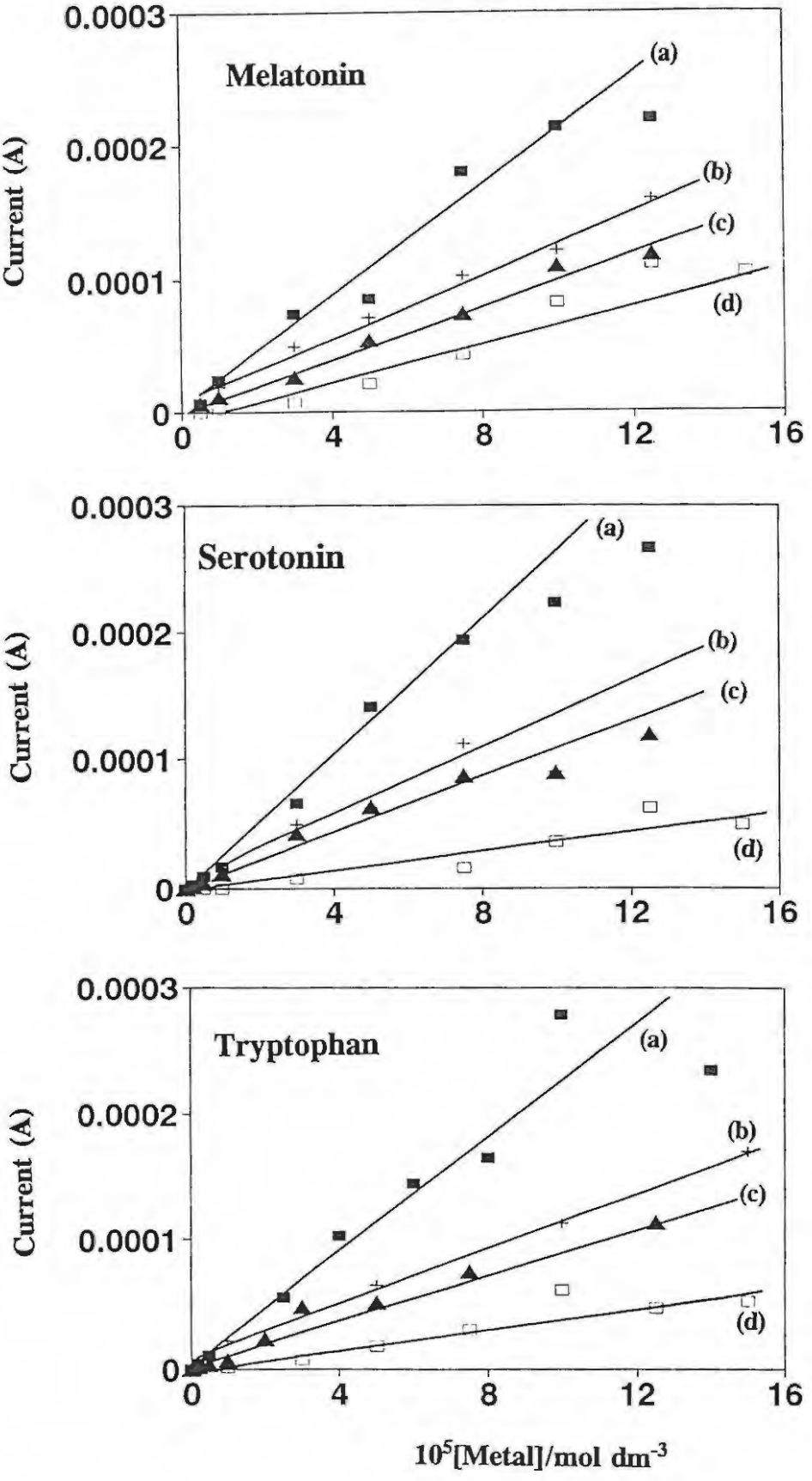

Figure 7.4 The effect of metal ion concentration on the adsorptive cathodic stripping voltammogram currents of 1 x 10^{-6} mol dm^{-3} of (a) melatonin (b) serotonin and (c) tryptophan. (■) Cd^{2+}, (+) Cu^{2+}, (▲) $Pb^{2+}$and (□) Zn^{2+}. Electrolyte: pH = 4.4 sodium acetate buffer. Scan rate = 200 mV s^{-1}.

The slopes of the plots shown in Fig. 7.4 are given in Table 7.1. As discussed before in Section 3.4.4, these slopes may be used as a guide in determining the sensitivities of the ligands for the metal ions. The highest slope was obtained for Cd^{2+} in all cases. The lowest slope was obtained for Zn^{2+}. Thus, as the concentration of the metal ion increases, all the ligands under discussion, melatonin, serotonin and tryptophan, seem to show an affinity for Cd^{2+} with the following trend in the metal ion being obtained: $Cd^{2+} > Cu^{2+} > Pb^{2+} > Zn^{2+}$. Comparing the three ligands, serotonin shows the largest slope for Cd^{2+}, $Cu^{2+}$and Pb^{2+} and hence is more sensitive for these metals than tryptophan and melatonin, at concentrations greater than 2×10^{-5} mol dm^{-3}. The adsorptive cathodic stripping voltammograms for Al^{3+} in the presence of melatonin and tryptophan were very weak and could not be accurately determined. Serotonin was the only ligand of the three that could bind Al^{3+} *in situ* to a significant extent. Thus, serotonin has a larger affinity for Al^{3+} than tryptophan and melatonin. The slopes of current versus the concentration of the Al^{3+} ion may not be compared directly with those of the other metals since non-aqueous conditions were employed for Al^{3+}, whereas the rest of the metal ions were studied in aqueous solutions (pH = 4.4 buffer).

Experiments were also performed to examine the effect of increasing ligand concentrations on the current response. For all the metal ions, AdCSV currents of the metal ion increased linearly with increase in the concentration of the ligand, at low ligand concentrations, as shown in Fig. 7.5. Deviation from linearity at higher ligand concentrations reflects the ligand concentration at which all the metal is bound. The deviations are thus due to the presence of free ligand in solution which competes with metal-ligand complexes for sites at the electrode. Shown in Fig 7.5 are the AdCSV of a) Pb^{2+} in the presence of melatonin, b) Cd^{2+} in the presence of melatonin and c) Pb^{2+} in the presence of serotonin.

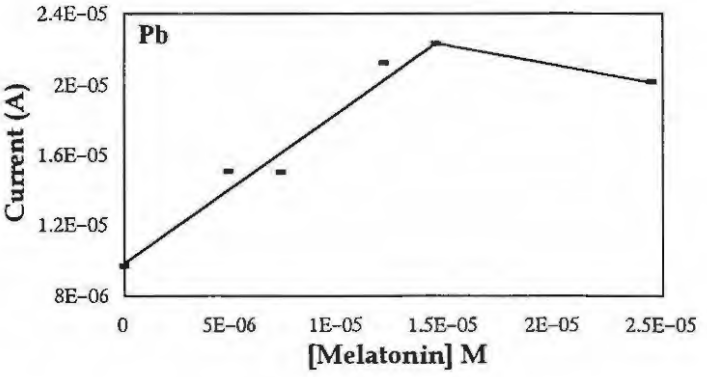

Figure 7.5 a) Plot of the concentration of melatonin versus the adsorptive cathodic stripping voltammogram currents of 1 x 10^{-5} mol dm^{-3} Pb^{2+}. Electrolyte: pH = 4.4 sodium acetate buffer. Scan rate = 200 mV s^{-1}.

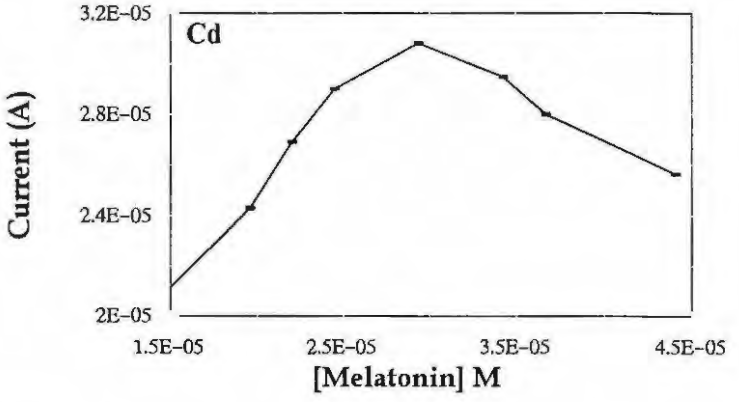

Figure 7.5 b) Plot of the concentration of melatonin versus the adsorptive cathodic stripping voltammogram currents of 1 x 10^{-5} mol dm^{-3} Cd^{2+}. Electrolyte: pH = 4.4 sodium acetate buffer. Scan rate = 200 mV s^{-1}.

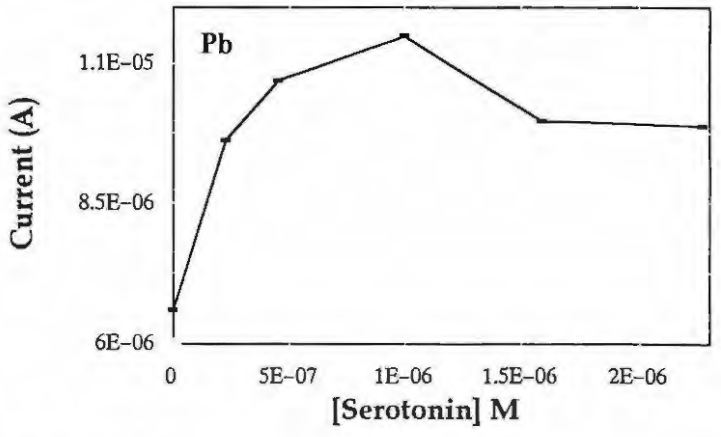

Figure 7.5 c) Plot of the concentration of serotonin versus the adsorptive cathodic stripping voltammogram currents of 1 x 10^{-5} mol dm^{-3} Pb^{2+}. Electrolyte: pH = 4.4 sodium acetate buffer. Scan rate = 200 mV s^{-1}.

The observed interactions may also be explained, as in Section 3.4.6, in terms of the different structural and chemical aspects of the bond formation between the metals and these ligands. Looking at the structural representation of melatonin and its precursors in Fig. 7.1, possible binding sites of the metals may be elucidated in terms of the HSAB theory.

Cadmium is the only metal classified as soft, while both Al^{3+} and Fe^{3+} are hard acids. The other metals studied are borderline acids. The COOH on tryptophan, the OH group on serotonin and the NH_2 group on both are hard acceptors, with a preference for either hard acids or borderline acids. Sterically, the OH group on serotonin is a better binding site than the COOH on tryptophan which may explain the preference of Al^{3+} for serotonin. The carbonyl group on melatonin and the two NH groups are soft bases, which have preferences for soft acids such as radicals. These functional groups may explain the strong preference as observed by cadmium for melatonin. The O-methyl group on melatonin is also a hard base which can also bind hard acids. Melatonin thus has a combination of hard and soft binding base functional groups, meaning that it is capable of binding hard, borderline and soft acids. This would explain why only melatonin showed bond formation with metals from each of these groups. The comparative hardness or softness of the functional groups on serotonin and melatonin may be a factor which defines their relative particular strengths and affinities for metal bond formation.

The AdCSV currents obtained for all metal-ligand complexes showed a linear relation with the square root of the scan rate. Fig 7.6 shows a plot of the AdCSV currents for lead with tryptophan versus the square root of the scan rate. This linearity reflects a diffusion controlled mass transport of the metal-ligand complex to the electrode.

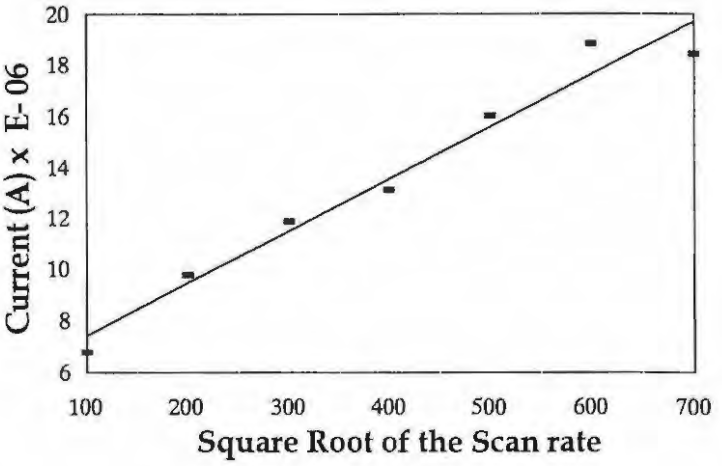

Figure 7.6 The variation of current with the square root of the scan rate for 1.47 x 10^{-5} mol dm^{-3} tryptophan with 1 x 10^{-5} mol dm^{-3} lead in pH 4.4 Sodium acetate buffer.

7.6 CONCLUSIONS

In conclusion, it has been shown in this work that the interaction of copper, cadmium, iron, lead, zinc and aluminium with melatonin and its precursors is concentration dependent. At low concentrations of the ligands or the metals, melatonin forms relatively stable *in situ* complexes with Cd^{2+}. While tryptophan forms relatively stable *in situ* complexes with Zn^{2+}, melatonin and its precursors show very little affinity for Zn^{2+}. The reason for this may be that metallothionein performs this function in zinc homeostasis in the brain. Melatonin, serotonin and tryptophan all showed an affinity for Al^{3+}. Considering the depletion of melatonin and probably serotonin and tryptophan with advancing age, this study may explain the accumulation of aluminium in the brains of Alzheimer's patients.

All three ligands show a binding affinity for lead, but these *in situ* complexes formed showed less stability than the zinc-tryptophan or the cadmium-melatonin complexes. Serotonin and melatonin show a binding affinity for copper, but the complexes formed are relatively unstable. Both lead and cadmium are highly toxic to living systems, mostly because they easily displace softer metals such as zinc at the active sites of proteins and enzymes, thereby inactivating them. This would then confer a role of metal detoxification on melatonin and its precursors. Melatonin was shown to bind iron III but not iron II. This may have relevance to the Fenton reaction, where iron II generates the toxic hydroxyl radical and is oxidised to iron III. The stable oxidation state of iron is Fe^{3+} , difficult to store *in vivo* as it reacts to form an insoluble polymer which is toxic to cells. Ferritin and transferrin[210] have evolved to overcome this difficulty. The fact that melatonin binds iron III may thus suggest that melatonin removes iron III, if unbound to a protein, preventing it from reducing back to iron II, the form in which it generates a free radical. If, however, the iron is bound to a protein such as haemoglobin, which suffered this oxidative attack, melatonin could restore the iron II state by reducing iron III and thereby restoring biological activity to the protein. The proposed mechanism, shown in Fig 7.7 a), is similar

to the reducing action of melatonin on toxic hydroxyl radicals, Fig 7.7 b), as devised by Reiter's[204] group.

Reiter's group showed that, dose dependently, melatonin was twice as potent an antioxidant as glutathione. Glutathione is known to protect haemoglobin by reducing iron (III) back to iron (II). Melatonin, in binding iron III, may thus be displaying a further antioxidative function.

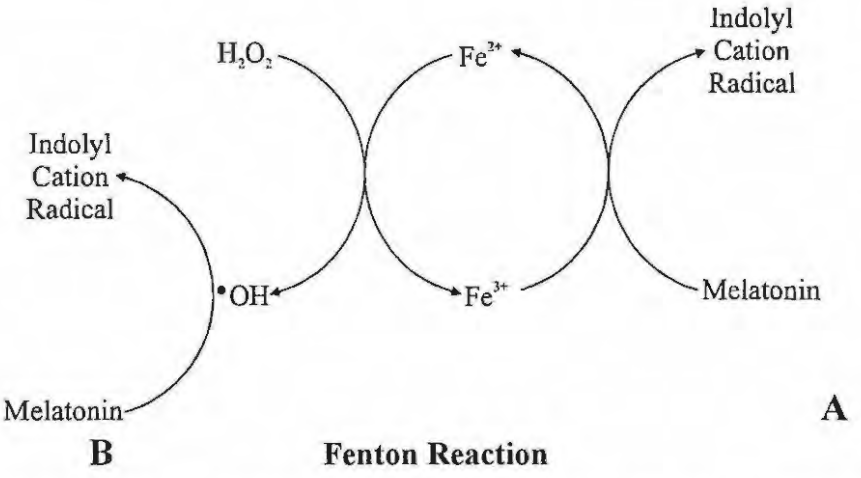

Figure 7.7 A) A possible mechanism for the protective role of melatonin in restoring the iron (II) state generated by the Fenton reaction. B) represents the mechanism[204] by which melatonin scavenges free radicals also generated by the Fenton reaction.

This reasoning would explain the lesser role played by metallothionein in transition metal bonding in the brain, considering that the brain, which constitutes 2% of the body's mass, utilises 20% of its oxygen intake. As metallothionein is a protein, any bonds it may form with the transition metals would predispose this protein to free radical damage, generated by these metals in a Fenton reaction. The most likely damage would be oxidation of its cysteine groups to disulphides, denaturing the protein. It has been suggested that zinc in metallothionein protects the protein from disulphide bonds. This may explain why brain metallothionein is mostly limited to zinc regulation. Melatonin on the other hand counteracts this free radical damage. Another factor favouring a metal binding role for melatonin is its hydrophilic, lipophilic nature. This allows melatonin to move freely across all cellular barriers, facilitating the removal of toxic metals from the CNS.

These studies suggest an important role for melatonin and its precursors in Alzheimer's disease. A depletion of melatonin and its precursors would predispose the build-up of toxic metals and their associated damage. Of most significance is aluminium which is known to cause neurofibrillary tangles associated with AD. Recent studies have shown that disturbances in zinc homeostasis may also be associated with the formation of neurofibrillary tangles during instances of metallothionein down-regulation[141]. If suggestions that the pineal gland exerts control over zinc-metallothionein in the brain[144] are considered in this light, then it may be postulated that any disturbances in the pineal gland functioning could be related to a zinc imbalance, resulting in neurofibrillary tangles. One such disturbance could be the depletion of melatonin, which it seems may have far-reaching consequences in ageing and in AD.

Chapter Eight

Overall Conclusions

These studies have shown how an understanding of metal-ligand chemistry can be used to design techniques for the qualitative and quantitative analysis of metals and proteins, as well as the identification of metal-ligand interactions. These techniques have a ready application in the study of living systems, where the interaction between a metal and a ligand is an integral component of biochemical pathways.

Chapter 2 provided an overview of the basic principles of electroanalytical chemistry, highlighting the benefits of the techniques researched in this thesis. The analytical sensitivity and selectivity of adsorptive cathodic stripping voltammetry for the analysis of metals, is based on the design and application of appropriate ligands, for the effective preconcentration of the analyte at the electrode. Specificity and catalytic activity is afforded by attaching appropriate reagents, by a range of techniques, at electrodes to produce new chemically modified electrodes. Enhanced stability and sensitivity may be achieved through the electrodeposition of modifiers to the electrode surfaces.

In chapter 3, analogs of the naturally occurring catechols were examined as ligands for the adsorptive cathodic stripping voltammetric analysis of physiologically important metals. The current responses and potential shifts of the metals with the various ligands, were used as the criteria in establishing feasible metal-ligand interactions and the utility of these ligands for sensitive analysis of the metals. The best ligand for the quantitative determination of lead, bismuth and copper was found to be resorcinol, and 4-methylcatechol for the analysis of cadmium. The sensitive simultaneous analysis of all four metals achieved, coupled with the simplicity of the mercury film glassy carbon

electrode described, provides a technique which has a ready application to related on-site metal analyses.

The electroanalysis of thiol-containing proteins is hampered by their sluggish electron transfer kinetics, exhibiting large overpotentials at unmodified electrodes. Electrodes modified by metallophthalocyanines (MPc) are known to catalyse the oxidation of cysteine at significantly lowered potentials. MPc complexes are often attached to electrodes in the presence of supports. While methods such as these may provide improved stability, they are countered by a loss of sensitivity and are often limited to the analysis of cysteine at low pH's. In chapter 4, experimental conditions were examined to achieve the direct electrodeposition of various MPc complexes onto a glassy carbon electrode (GCE), in the absence of supports. The research resulted in a technique for achieving the direct electrodeposition of MPc complexes onto GCE for cysteine analysis at lowered potentials. The direct electrodeposition of $[Co(II)TSPc]^{4-}$ onto a GCE produced a chemically modified electrode (CMGCE) which offered improved sensitivity for the analysis of the amino acid cysteine in both acidic and basic media. This technique, therefore, has a ready application to the analysis of cysteine-containing proteins.

A major problem in defining a specific functional role for metallothionein, believed to function in metal regulation in the peripheral organs, is the lack of adequate methods for the analysis of this protein. As metallothionein is composed mainly of 1/3 cysteine residues, the technique for cysteine analysis devised in chapter 4 could be applied to the analysis of this protein An electrode modified by electrodeposition of $[Co(II)TSPc]^{4-}$ catalysed the oxidation of the cysteine component of metallothionein at biological pH's. The linear current response exhibited with metallothionein concentration, provides a new technique for the analysis of metallothionein. Of further significance is that the technique is both non-destructive and highly sensitive, and may thus be of significant value for *in vivo* voltammetric analysis of this protein.

Chapter 6 introduced a new methodology for the analysis of the iron-sulphur protein, ferredoxin. Ferredoxins are vital as electron carriers in electron transport chains in photosynthesis and respiration. Electroanalysis of ferredoxin has focused on its

ferric/ferrous redox transition, in the presence of mediators. An alternative means for the quantification of ferredoxin was introduced in this thesis by the catalytic oxidation of its cysteine component at electrodes modified by drop-dry with MPc complexes. Of the various metal phthalocyanines examined, $[Co(II)TSPc]^{4-}$ showed the best catalytic activity for analysis of the cysteine component of ferredoxin. The phthalocyanines were also examined as possible mediators for the monitoring of the reduction of iron in ferredoxin. Co(II) and Cu(II)TSPc-CMGCEs were found to catalytically reduce the iron in ferredoxin at significantly lower potentials than previously observed.

Complimentary to the techniques designed in this thesis for the analysis of metals and metalloproteins, a new methodology for identifying metal-ligand interactions, based on adsorptive cathodic stripping voltammetry, was introduced and applied in chapter 7.

In chapter 7, the interaction of the pineal hormone, melatonin and its precursors, serotonin and tryptophan, with a group of metals were examined. Using AdCSV, these ligands exhibited a variable affinity and selectivity for different metals studied. Of the three ligands, only melatonin was found to bind all the metals studied. The findings of this research suggest that apart from its role in neuroprotection as a general antioxidant and free radical scavenger, melatonin could be involved in metalloregulation and detoxification in the brain. By binding iron (III) melatonin may be displaying a further antioxidative role. The most important implication is that the depletion of melatonin with advancing age predisposes the brain to the accumulation and toxicity of both free radicals and metals. These findings also suggest a plausible explanation for the accumulation of aluminium in the brains of patients with Alzheimer's disease.

Further Applications and Research Areas Identified

The techniques researched in this thesis may have important applications in the field of bioinorganic chemistry. Bioinorganic chemistry is the study of the role of metals in biological systems. The electrochemical techniques for analysis of metals, thiols, metalloproteins and the identification of metal-binding ligands may be of use in bridging the gap between the disciplines, through the application of electroanalysis to real biological systems.

Micro-electrodes chemically modified with non-toxic metallophthalocyanines may have important applications for *in vivo* voltammetric analysis of a range of biological compounds, for example, thiol-containing amino acids and proteins. As cysteine, metallothionein and metal-free metallothionein oxidise at slightly different potentials at the electrodes discussed, the technique could be used to monitor and determine the conditions under which metallothionein binds or frees a metal, to become the thiol- containing apoform. In addition, micro-electrodes modified with metal-specific ligands could be used to both qualify and quantify the metals involved.

The technique designed for analysis of thiols could be expanded to include the analysis of other thiol containing proteins such as glutathione and thioredoxin.

While preliminary studies suggest that melatonin binds metals *in situ*, further research in this area should be directed at similar studies using *in vivo* voltammetric methods.

Environmental monitoring of heavy metals of biological importance, as suggested, is an obvious application of this research. A ligand such as resorcinol, which may simultaneously determine several metal concentrations, could be used for on-site metal analysis. Nature tends to protect itself, for example, by the evolution of micro-organisms and even certain plants which bind and remove metals from soils and rivers. The techniques designed in this research for identifying metal-binding ligands could be of particular benefit in identifying such metal-binding agents in samples of environmental origin.

References

[1] C.K Mathews, K.E. van Holde, *Biochemistry*, Benjamin/Cummings Publishing Company, California **1990**.

[2] P.M Harrison, R.J. Hoare, *Metals in Biochemistry*, Chapman and Hall, New York **1980**.

[3] E.C. Constable, *Metals and Ligand Reactivity*, Ellis Harwood, New York **1990**.

[4] L.R. Milgrom, *An introduction to the chemistry of porphyrins and related compounds*, Oxford University Press, Oxford **1997**.

[5] A.M. Bond, *Inorganica Chimica Acta* **1994**, *226*, 293.

[6] M.J. Kendrick, M.T. May, M.J. Plishka, K.D. Robinson, *Metals in Biological Systems*, Ellis Harwood, New York **1992**.

[7] R.G. Pearson *J. Chem. Ed.* **1968**, *45*, 643.

[8] J. E. Huheey in *Inorganic Chemistry-Principles of Reactivity and Structure*, 2nd Edition, Harper and Row, New York **1978**.

[9] M.N. Hughes, R.K. Poole in *Metals and Micro-organisms*, Chapman and Hall, New York **1989**.

[10] C.D.C. Salisbury, W. Chan, P.W. Saschenbrecker, *J. Assoc. Off. Anal. Chem.* **1991** *74*, 587.

[11] B. Selinger, *Chemistry in the Marketplace*, 3rd Edition, 423, **1986**.

[12] J.E. Fergusson, *The Heavy Elements: Chemistry, environmental impact and health effects*, Pergamon Press, New York **1990**.

[13] L. Penumarthy, F.W. Oehme, R.H. Hayes, *Arch. Environm. Toxicol.* **1980**, *9*, 193.

[14] M. Mjør-Grimsrud, G. Norheim, *Acta Vet. Scand.* **1980**, *21*, 71.

[15] C. Starr, R. Taggart, *Biology, the unity and diversity of life*, 5th Edition, Wadsworth Publishing Company, California **1989**.

[16] D.A. Phipps, *Metals and metabolism*, Clarendon Press, Oxford **1976**.

[17] P.T Kissinger in *Laboratory Techniques in Electroanalytical Chemistry*, 2nd Edition, (Eds: P.T. Kissinger, W.R. Heineman), Marcel Dekker Inc. New York **1996**.

[18] P.T Kissinger, C.R. Preddy, R.E. Shoup, W.R. Heinemann in *Laboratory Techniques in Electroanalytical Chemistry*, 2nd Edition, (Eds: P.T. Kissinger, W.R. Heineman), Marcel Dekker Inc. New York **1996**.

[19] J. Wang, *Analytical Electrochemistry*, 1st Edition, VCH Publishers, New York **1994**.

[20] A.J. Bard, L.R. Faulkner, *Electrochemical methods, Fundamentals and Applications*, John Wiley and Sons, New York **1980**.

[21] K.C. Sole, *Chemistry of Copper Hydrometallurgy*, Mintek Lecture, Rhodes University **1995**.

[22] F.M Hawkridge in *Laboratory Techniques in Electroanalytical Chemistry*, 2nd Edition, (Eds: P.T. Kissinger, W.R. Heineman), Marcel Dekker Inc. New York **1996**.

[23] G. Dryhurst, D.L. McAllister in *Laboratory Techniques in Electroanalytical Chemistry*, 2nd Edition, (Eds: P.T. Kissinger, W.R. Heineman), Marcel Dekker Inc. New York **1996**.

[24] B.L. Vallee in *Methods in Enzymology*, Vol. 205 (Eds: J.F. Riordan, B.L. Vallee), Academic Press, New York **1991**.

[25] W.R. Heinemann, P.T. Kissinger in *Laboratory Techniques in Electroanalytical Chemistry*, 2nd Edition, (Eds: P.T. Kissinger, W.R. Heineman), Marcel Dekker Inc. New York **1996**.

[26] CV - 27 Manual, Bioanalytical Systems Inc.

[27] C.M.A Brett, A.M.O. Brett, *Electrochemistry: Principles, Methods and applications*, Oxford University Press, New York **1993**.

[28] M. Nicholson, *Anal.Chem.***1965**, *37*, 1351.

[29] Constant M.G. van den Berg, *Anal. Chim. Acta*, **1991**, *250*, 265.

[30] Z.R. Komy, *Mikrochim. Acta*, **1993**, *111*, 239.

[31] L.Chiang, B.D. James, R.J. Magee, *Mikrochim. Acta*, **1989**, *II*, 149.

[32] J. Wang, in *Electroanalytical Chemistry*, Vol. 16 (Ed: A.J. Bard), Wiley, New York **1989**.

[33] M. Nimmo, G. Fones, *Anal. Chim. Acta*, **1994**, *291*, 321.

[34] Z.-Q Zhang, S.-Z Chen, H.-M. Lin, H. Zhang, *Anal. Chim. Acta*, **1993**, *272*, 227.

[35] R.N. Naumann, W. Schmidt, G. Hohl, *Fresenius J. Anal. Chem.* **1992**, *343*, 746.

[36] J. Wang, J. Lu, C. Yarnitzky, *Anal. Chim. Acta*, **1993**, *280*, 61.

[37] S.B.O Adeljou, F. Pablo, *Anal. Chim. Acta*, **1992**, *270*, 143.

[38] Z.-Q. Zhang, Z.-P. Cheng, S.-Z. Cheng, G.-F. Yang, *Talanta*, **1991**, *38*, 1487.

[39] Z.-Q Zhang, *Mikrochim Acta*, **1991**, *I*, 89.

[40] J. Wang, B. Tian, *Anal. Chim. Acta*, **1992**, *270*, 137.

[41] T-G Wu, J.L. Wong, *Anal. Chim.Acta*, **1991**, *246*, 301.

[42] J.Wang, J. Mahmoud, J. Zadeii, *Electroanalysis*, **1989**, *1*, 229.

[43] J. Wang, T. Golden, K. Varughese, I. El-Rayes, *Analytical Chemistry*, **1989**, *61*, 508.

[44] M. D. Imisides, R. John, P.J. Riley, G.C. Wallace, *Electroanalysis*, **1991**, *3*, 879.

[45] C.R. Martin, C.J. Foss Jr, in *Laboratory Techniques in Electroanalytical Chemistry*, 2nd Edition, (Eds: P.T. Kissinger, W.R. Heineman), Marcel Dekker Inc. New York **1996**.

[46] C.R. Martin, L.S. Van Dyke, in *Molecular Design of Electrode Surfaces* (Ed: W. Murray), Wiley, New York **1992**.

[47] X. Huang, W.T. Kok, *Anal. Chim. Acta*, **1993**, *273*, 245.

[48] M.A. Ruiz, M.G. Blazquez, J.M. Pingarron, *Anal. Chim. Acta*, **1995**, *305*, 49.

[49] S. Zecevic, et. al. *J. Electroanal. Chem.* **1985**, *196*, 339.

[50] V. Iliev, *J. Molecular Catalysis*, **1993**, *85*, L269.

[51] J. Andrieux, *J. Electroanal. Chem.* **1978**, *93*, 163.

[52] R. Arraz, M.T. Sevilla, L. Hernandez, *Anal. Chim. Acta*, **1993**, *273*, 205.

[53] I. Turyan, D. Mandler, *Anal. Chem*, **1994**, *66*, 59.
[54] C. Sun, Y. Sun, X. Zhang, H. Xu, J. Shen, *Anal. Chim. Acta*, **1995**, *312*, 207.
[55] R.N. Adams, *Anal. Chem*. **1976**, *48*, 1128A.
[56] C.A. Marsden, M.H. Joseph, Z.L. Kruk, N.T. Maidment, R.D. O'Neill, J.O. Schenk, J.A. Stamford, *Neuroscience*, **1988**, *25* (2), 389.
[57] J.A. Stamford, J.B. Justice Jr., *Analytical Chemistry News and Features*, **1996**, 359A.
[58] A-E. F. Nassar, J.F. Rusling, N. Nakashima, *J.Am.Chem.Soc*. **1996**, *118*, 3043.
[59] W. Lu, H. Zhao, G.G. Wallace, *Anal. Chim. Acta*, **1995**, *315*, 27.
[60] F. Xu, H. Li, S.J. Cross, T. Guarr, *J. Electroanal. Chem*. **1994**, *368*, 221.
[61] Q.-Y Peng, T.F. Guarr, *Electrochimica Acta*, **1994**, *39* (17), 2629.
[62] J. Hayon, A. Raveh, A. Bettelheim, *J. Electroanal. Chem*. **1993**, *359*, 209.
[63] F. Mizutani, S. Yabuki, S. Iijima, *Anal. Chim. Acta*, **1995**, 59.
[64] J.G. De Gao, R.Q. Yu, *Analyst*, **1995**, *120*, 499.
[65] E.Wang, M.E. Meyerhoff, *Anal. Chim. Acta*, **1993**, *283*, 673.
[66] C. Shi, F.C. Anson, *Inorg. Chem*. **1995**, *34*, 4554.
[67] A. Widelov, *Electrochimica Acta*, **1993**, *38* (17), 2493.
[68] T. Malinski, Z. Taha, S. Grunfeld, A. Burewicz, P. Tamboulian, *Anal. Chim. Acta*, **1993**, *279*, 135.
[69] R. Yuan, Y-Q. Chai, G-L. Shen, R-Q. Yin, *Talanta*, **1993**, 1255.
[70] Y-H. Tse, P. Janda, A.B.P. Lever, *Anal. Chem*. **1994**, *66*, 384.
[71] D. Pang, Z. Wang, *J. Electroanal. Chem*. **1993**, *358*, 235.
[72] D-W. Pang, B-H. Deng, Z-L. Wang, *Electrochimica Acta*, **1994**, *39*, 847.
[73] Z. Wang, D. Pang, *J. Electroanal. Chem*. **1990**, *283*, 349.
[74] D-W Pang, Z-L. Wang, C-S. Cha, *Electrochimica Acta*, **1992**, *37* (14), 2591.
[75] J. Nakamura, S. Igarashi, *Anal. Lett*. **1996**, *29* (14), 2453.
[76] T. Aida, H. Sugimoto, M. Kuroki, S. Inque, *J.Phys. Org. Chem*. **1995**, *8*, 249.
[77] J-K. Tie, W-B. Chang, Y-X. Chi, *Anal. Chim. Acta*, **1995**, *300*, 215.
[78] Zasadowski, K. Markiewicz, M. Buszko, *Polish J. of Env. Studies*, **1993**, *2* (1), 39.
[79] CD Salisbury, W. Chan, *J. Assoc. Off. Anal. Chem*. **1985**, *68* (2), 218.
[80] W. Slavin in *Methods in Enzymology*, Vol. 158, Part A, (Eds: J.F. Riordan, B.L. Vallee), Academic Press, New York **1988**.
[81] T.D.B. Lyon, K. McKay, G.S. Fell, R.D. Scott, *J. Atomic Spectrometry*, **1991**, *6*, 559.
[82] J. Versieck, in *Methods in Enzymology*, Vol. 158, Part A, (Eds: J.F. Riordan, B.L. Vallee), Academic Press, New York **1988**.
[83] J. Oysteryoung in *Methods in Enzymology*, Vol. 158, Part A, (Eds: J.F. Riordan, B.L. Vallee), Academic Press, New York **1988**.
[84] D. Jagner, L. Renman, Y. Wang, *Anal. Chim. Acta*, **1992**, *267*, 165.
[85] J. Wang, D. Larson, D. Foster, S. Armalis, J. Lu, X. Rongrong, *Anal. Chem*. **1995**, *67*, 1481.

[86] J. Wang, B. Tian, *Anal. Chim. Acta*, **1994**, *274*, 1.

[87] D.W. Yeager, J. Cholak, E.W. Henderson, *Environmental Science and Technology*, **1971**, *5*, 1020.

[88] J. Wang in *Laboratory Techniques in Electroanalytical Chemistry*, 2nd Edition. (Eds: P.T. Kissinger, W.R. Heineman), Marcel Dekker Inc. New York **1996**.

[89] L. Xiao, W. Jin, *Talanta*, **1992**, *46* (8), 1221.

[90] J. Davies, D.H. Vaughan, M.F. Cardosi, *Electrochimica Acta*, **1998**, *43* (3-4), 291.

[91] C. Bazzicalupi, A. Bencini, A. Bianchi, V. Fusi, C. Giorgi, L. Messori, M. Migliorini, P. Paoletti, B. Valtancoli, *J. Chem. Soc. Dalton Trans.* **1998**, 359.

[92] M. Vašák, in *Methods in Enzymology*, Vol. 205, Part B, (Eds: J.F. Riordan, B.L. Vallee), Academic Press, New York **1991**.

[93] S. Taniguchi, T. Yanase, K. Kobayashi, R. Takayanagi, M. Haji, F. Umeda, H. Nawata, *Endocrine Journal*, **1994**, *41* (6), 605.

[94] J.G. Correa, A.O.M. Stoppani, *Free Radical Research*, **1996**, *24* (4), 311.

[95] M.J. Stillman, *Co-ord. Chem. Rev.* **1995**, *144*, 461.

[96] T. Nedeltcheva, L. Costadinnova, M. Athanassova, *Anal. Chim. Acta*, **1994**, *291*, 75.

[97] J.M. Zen, S.-Y. Huang, *Anal. Chim. Acta*, **1994**, *296*, 77.

[98] G. Pass, H. Sutcliffe, *Practical Inorganic Chemistry*, 77, **1968**.

[99] W.P. Griffith, H.I.S. Nogueira, B.C. Parkin, R.N. Sheppard, A.J.P. White, D.J. Williams, *J. Chem. Soc. Dalton Trans.* **1995**, 1775.

[100] J. H. Zagal, *Co-ord. Chem Reviews*, **1992**, *119*, 89.

[101] *A Concise Dictionary of chemistry*, (Ed: J. Daintith), Oxford University Press, Oxford **1990**.

[102] M. Shimura, F. Hirota, T. Yagi, *Biochimie*, **1994**, *76*, 614.

[103] J. Meyer, J-M Moulis, J. Gaillard, M. Lutz, *Advances in Inorganic Chemistry*, **1992**, *38*, 73.

[104] N.N. Kundo, N.P. Keier, *Russian J. Off. Phys. Chem.* **1968**, *42* (6), 707.

[105] D.J. Cookson, T.D. Smith, J.F. Boas, P.R. Hicks, J.R. Pilbrow, *J. Chem. Soc. Dalton Trans.* **1977**, 109.

[106] J. Zagal, C. Fierro , R. Rozas, *J. Electroanal. Chem.* **1981**, *119*, 403.

[107] M.K. Halbert, R.P. Baldwin, *Anal. Chem*, **1985**, *57*, 591.

[108] I. M. Kolthoff, C. Barnum, *J. Am. Chem. Soc.* **1940**, *62*, 3061.

[109] W. Stricks, I.M. Kolthoff, *J. Am. Chem. Soc.* **1952**, *74*, 4646.

[110] A.B.P. Lever, E.R. Milaeva, G. Speier in *"Phthalocyanines, Properties and Applications"*, Vol. 3 (Eds: A.B.P. Lever, C.C. Leznoff), VCH Publishers, New York **1993**.

[111] S Mho, B. Ortiz, S.M. Park, D. Ingersol, N. Doddapaneni, *J. Electrochem. Soc.* **1995**, *142* (5), 1436.

[112] K. Hanabusa, H. Shirai, in *"Phthalocyanines, Properties and Applications"*, Vol. 2 (Eds: A.B.P. Lever, C.C. Leznoff), VCH, New York **1993**.

[113] H. Aga, A. Aramat, Y. Hisaeda, *J. Electroanal. Chem.* **1997**, *437*, 111.
[114] N. Chebotareva, T. Nyokong, *Electrochim. Acta*, **1997**, *42* (23-24), 3519.
[115] N. Chebotareva, T. Nyokong, *J. App. Electrochem.* **1997**, *27*, 975.
[116] C. Coutanceau, P. Crouigneau, J.M. Leger, C. Lamy, *J. Electraoanal. Chem.* **1994**, 79, 389.
[117] T. Mafatle, T. Nyokong, *Anal. Chim. Acta*, **1997**, *354*, 307.
[118] J. Zagal, R.K. Sen, E. Yeager, *J. Electroanal. Chem.* **1977**, *83*, 207.
[119] J. Zhang, A.B.P. Lever, W.J. Pietro, *Can. J. Chem.* **1995**, *73*, 1072.
[120] F. Bedioui, Y. Bouhier, C. Sorel, J. Devynck, L Coche-Guerente, A. Deronzier, J. C. Moutet, *Electrochimica Acta*, **1993**, *38*, 2485.
[121] T. Pasinszki, M. Aoki, S. Masuda, *J. Phys. Chem.* **1995**, *99*, 12858.
[122] A.B.P. Lever, M.R. Hempstead, C.C. Leznoff, W. Liu, M. Melnik, W.A. Nevin, P. Seymour, *Pure and Applied Chemistry*, **1986**, *58* (11), 1467.
[122] L.C. Gruen, R.J. Blagrove, *Aust. J. Chem.* **1973**, *26*, 319.
[123] J.H. Weber, D.H. Busch, *Inorg. Chem.* **1965**, *4*, 469.
[124] N.P. Farrell, A.J. Murray, J.R. Thornback, D.H. Dolphin, B.R. James, *Inorg. Chim. Acta*, **1978**, *28*, L144.
[125] S.J. Edmondson, P.C.H. Mitchell, *Polyhedron* **1986**, *6*, 315.
[126] T. Nyokong, Z. Gasyna, M.J. Stillman, *Inorg. Chem.* **1987**, *26*, 548.
[127] R.R. Gagne, C.A. Koval, G.C. Lisensky, *Inorg. Chem.* **1980**, *19*, 2854.
[128] D. Dolphin, B.R. James, A.J. Murray, J.R. Thornback, *Can. J. Chem.* **1980**, *58*, 1125.
[129] T. Nyokong, *Polyhedron*, **1993**, *12*, 375.
[130] R. Behnisch, M. Hanack, *Synth. Met.* **1990**, *36*, 387.
[131] T. Mafatle, T. Nyokong, *J. Electroanal. Chem.*, **1996**, *408*, 213.
[132] H.Li, T. Li, E. Wang, *Talanta*, **1995**, *42*, 885.
[133] M. Sekota, T. Nyokong, *Polyhedron*, **1997**, *16*, (19), 3279.
[134] E.T.W.M. Schipper, J.P.A. Heuts, P. Piet, T.P.M. Beelen, A.L. German, Journal of Molecular catalysis, **1994**, *87*, 161.
[135] T. Saji, in *"Phthalocyanines, Properties and Applications"*, Vol. 2 (Eds: A.B.P. Lever, C.C. Leznoff), VCH Publishers, New York **1993**.
[136] J.H.R. Kagi in *Methods in Enzymology*, Vol. 205 (Eds: J.F. Riordan, B.L. Vallee), Academic, New York **1991**.
[137] P.E. Olsson, C. Haux, *Aquatic Toxicology*, **1986**, *9*, 4813.
[138] R.W. Olafson, *Int. J. Peptite Protein Res.* **1984**, *24*, 303.
[139] J.H.R. Kagi, S.R. Himmelhoch, P.D. Whanger, J.L. Bethune, B.L. Vallee, *J. Biol. Chem.* **1973**, *249* (11), 3537.
[140] W. Lu, A.J. Zelazowski, M.J. Stillman, *Inorg.Chem.* **1993**, *32*, 919.
[141] M. Aschner, *FASEB J.* **1996**, *10*, 1129.
[142] M. Nordberg, *Talanta*, **1998**, *46*, 243.

[143] I. Bremner in *Methods in Enzymology*, Vol. 205 (Eds: J.F. Riordan, B.L. Vallee), Academic, New York **1991**.

[144] M. Ebadi, in *Methods in Enzymology*, Vol. 205 (Eds: J.F. Riordan, B.L. Vallee), Academic, New York **1991**.

[145] M. Nordberg, G.F. Nordberg, in *Highlights Mod. Biochem., Proc. Int. Congr. Biochem. 14th*, Vol. 1 (Eds: Kotyk, Arnost), VSP: Zeist, Netherlands **1989**.

[146] D.M. Templeton, G. Cherian, in *Methods in Enzymology*, Vol. 205 (Eds: J.F. Riordan, B.L. Vallee), Academic, New York **1991**.

[147] E. Palecek, Z. Pechan, *Anal. Biochem.* **1971**, *42*, 59.

[148] R.W. Olafson, P.E. Olsson in: *Methods in Enzymology*, Vol. 205 (Eds: J.F. Riordan, B.L. Vallee), Academic, New York **1991**.

[149] K.H. Summer, D. Klein in *Methods in Enzymology*, Vol. 205 (Eds: J.F. Riordan, B.L. Vallee), Academic, New York **1991**.

[150] R. Brdicka, *Collect. Czech. Chem. Comm.* **1933**, *5*, 112.

[151] M. Kuik, K. Krassowski, *Bioelectrochemistry and Bioenergetics*, **1982**, *9*, 419.

[152] J.A.J. Thompson, RP Cosson, *Marine Environ. Research*, **1984**, *11*, 137.

[153] P. Olsson, C. Haux, *Aquatic Toxicology* **1986**, *9*, 231.

[154] I. Šestákova, D. Miholova, H. Vodickova, P. Mader, *Electroanalysis*, **1995**, *7*, 237.

[155] A. Munoz, A.R. Rodriquez, *Electroanalysis* **1995**, *7*, 674.

[156] J. Mendieta, J. Chivot, A. Munoz, A.R. Rodriquez, *Electroanalysis* **1995**, *7*, 663.

[157] M.J.M. Verhagen, T.A. Link, W.R. Hagen, *FEBS Letters*, **1995**, *361*, 75.

[158] H. Sigel, A. Sigel, *Metal ions in biological systems*, Vol 28, Marcel Dekker, Inc. New York **1992**.

[159] L. E. Mortenson, R.C. Valentine, J.E. Carnahan, *Biochemical and Biophysical Research Communications*, **1962**, *7* (6), 448.

[160] W.J. Driscoll, J.L. Omdahl, *The Journal of Biological Chemistry*, **1986**, *261* (9), 4122.

[161] P.W. Andrew, L.J. Rogers, D. Boulter, B.G. Haslett, *European Journal of Biochemistry*, **1976**, *69*, 243.

[162] J.J.G. Moura, A.L. Macedo, P.N. Palma, in: *Methods in Enzymology*, Vol. 243 (Eds: H.D. Peck Jr., J. LeGall), Academic, New York, **1994**.

[163] K. Wada, M. Onda, H. Matsubara, *Plant Cell Physiology*, **1986**, *27* (3), 407.

[164] N. Waki, A. Hiwatashi, Y. Ichikawa, *FEBS Letters*, **1986**, *195* (1-2), 87.

[165] H. Sakai, K. Kamide, S. Morigasaki, Y. Sanada, K. Wada, M. Ihara, *Journal of Plant Research*, **1994**, *107*, 299.

[166] A. Aliverti, W.R. Hagen, G. Zanetti, *FEBS Letters*, **1995**, *368*, 220.

[167] M.J. Therien, M. Selman, H.B. Gray, I-J. Chang, J.R. Winkler, *J. Am. Chem. Soc.* **1990**, *112*, 2420.

[168] F.A. Cotton, G. Wilkinson, P.L. Gaus, *Basic Inorganic Chemistry*, 2nd Edition, Wiley, New York **1987**.

[169] C.D. Crowley, F.M. Hawkridge, *J. Electroanal. Chem.* **1983**, *159*, 313.

[170] B. Shen, L.L. Martin, J.N. Butt, F.A. Armstrong, C.D. Stout, G.M. Jensen, P.J. Stephens, G.N. La Mar, C.M. Gorst, B.K. Burgess, *The Journal of Biological Chemistry*, **1993**, *268* (34), 25928.

[171] T.A. Link, W.R. Hagen, A.J. Pierik, C. Assmann, G.von Jagow, *Eur. J. Biochem*, **1992**, *208*, 685.

[172] P.J.H. Daas, W.R. Hagen, J.T. Keltjens, G.D. Vogels, *FEBS Lett.* **1995**, 361, 75.

[173] L. Calzolai, L. Messori, R. Monnanni, *FEBS Letters*, **1994**, *350*, 41.

[174] K. Tagawa, D.I. Arnon, *Biochim. Biophys. Acta*, **1968**, *153*, 602.

[175] H.A.O. Hill, *Coord. Chem. Rev.* **1996**, *151*, 115.

[176] J.L. Anderson, E.F. Bowden, P.G. Pickup, *Anal.Chem.* **1996**, *68*, 379.

[177] L-H. Guo, H.A.O. Hill, *Adv. Inorg. Chem.* **1991**, *36*, 341.

[178] J. Higgins, H.A.O. Hill in *Essays in Biochemistry*, **1985**, *21*, 119.

[179] K. Nishiyima, H. Ishida, I. Taniguchi, *J. Electroanal. Chem*, **1994**, *373*, 255.

[180] P. Bianco, J. Haladjian, S.G. Derocles, *Electroanalysis*, **1994**, *6*, 67.

[181] J.S. Leigh, M. Erecinska, *Biochim. Biophys. Acta*, **1975**, *387*, 95.

[182] H.A. Heering, Y.B.M. Bulsink, W.F. Hagen, T.E. Meyer, *Eur. J. Biochem.* **1995**, *232*, 811.

[183] K. Lang, D.M. Wagnerova, P. Engst, P. Kubat, *Z. Phys. Chem.* **1994**, *187*, 213.

[184] T. Nyokong, *Polyhedron*, **1994**, *13*, 215.

[185] M. Sekota, T. Nyokong, *Electroanalysis* **1997**, *9*, 1257.

[186] E.T.W.M. Schipper, A.H.C. Roelofs, P. Piet, A.L. German, *Polymer International*, **1994**, *33*, 79.

[187] J. Redepenning, B.R. Miller, S. Burnham, *Anal. Chem.* **1994**, *66*, 1560.

[188] D.J. Plummer, *Introduction to Practical Biochemistry*, 3rd Edition, Mcgraw-Hill, New York **1987**.

[189] A. Awad, P. Govitrapong, Y. Hama, M. Hegazy, M. Ebadi, *J. Neural. Transm.* **1989**, *76*, 129.

[190] *Alzheimer's Disease and Related Conditions*, (Eds: G.E.W. Wolstenholme, M. O'Connor), Churchill, London **1970**.

[191] A. Motluk, *New Scientist*, 31 May, **1997**.

[192] G.D. Fasman, *Co-ord. Chem. Rev.* **1996**, *149*, 125.

[193] L. Gopinath, *Chemistry in Great Britain*, May, **1998**.

[194] R.J. Reiter, L-D Chen, B.H. Poeggeler, L. Barlow-Walden, E. Sewerynek, D. Melchiorri, *Handbook of Antioxidants*, (Eds: E. Cadenas, L. Packer), Marcel Dekker, New York **1996**.

[195] R.J. Reiter, *Frontiers in Neuroendocrinology*, **1995**, *16*, 383.

[196] V.M. Cassone, *Trends Neurosci.* **1990**, *13*, 457.

[197] R.J. Reiter, *Experientia*, **1993**, *49*, 654.

[198] S. Daya, *Specialist Medicine*, September **1994**, 58.

[199] D.X. Tan, L.D. Chen, B. Poeggeler, L.C. Manchester, R.J. Reiter, *Endocrine J.* **1993**, *1*, 57.

[200] R.J. Reiter, D. Melchiorri, E. Sewerynek, B. Poeggeler, L.R. Walden-Barlow, J.I. Chuang, G.G. Ortiz, D. Acuña-Castroviejo, *J. Pineal Res.* **1995**, *18*, 1.

[201] M.I Pablos, M.T. Agapito, R. Gutierrez, J.M. Recio, R.J. Reiter, L. Barlow-Walden, D. Acuña-Castroviejo, A. Menendez-Pelaez, *J. Pineal Res.* **1995**, *19*: 111.

[202] E. Sewerynek, D. Melchiorri, G.G. Ortiz, B. Poeggeler, R.J. Reiter, *J. Pineal Res.* **1995**, *19*, 51.

[203] D. Melchiorri, R.J. Reiter, E. Sewerynek, L.D. Chen, G. Nistico, *FASEB J.* **1995**, *9*, 1205.

[204] R.J Reiter, FASEB J. **1995**, *9*, 526.

[205] D. Acuña-Castroviejo, A. Coto-Montes, M.G. Monti, G.G. Ortiz, R.J. Reiter, *Life Sciences*, **1997**, *60* (2), 23.

[206] R.J. Reiter, *Aging. Clin. Exp. Res.* **1995**, *7*, 340.

[207] R.J. Reiter, Ann. *N.Y. Acad. Sci.* **1996**, *786*, 362-378.

[208] D.J. Skene, *Chemistry & Industry*, September **1996**: 637.

[209] S.Daya, K.O. Nonaka, G.R. Buzzell, R.J.Reiter *J. Neurosci. Res.* **1989**, *23*, 304.

[210] E.I. Solomon, *Co-ord. Chem Rev.* **1995**, *144*, 369.

Appendices

Appendix 1

Results of IR spectral analysis of metallophthalocyanines

RuPc	FeTSPc	CoTSPc	NiTSPc	OMoPc	OMoTSPc	Assignment
	699s	699s	698m	---	688m	υ(S-O)
737vs				729(716)s		π(C-H)
829vw	840m	842s	830m		841s	(C-H)
				973s	967vw	υ(Mo = O)
	1033vs	1031vs	1029vs	1030m	1034vs	δ(C-H)
1172w	1058s	1062s	1054m		1073w	(C-H)
1125vs	1115s	1119m	1118m	1117vs	1125w	(C-C)
1289s				1289w		υ(C-C)
1400s	1400m	1401s	1400m	1410m	1405m	υ(C-C)
1509m	1509m	1509m	1509m	1509m	1509m	υ(C-C)
1618m				1606m		υ(C-C)
1637s	1638s	1638m	1638s	1645s	1636m	υ(C-N)
2067s						υ(Ru-CN)
	3050w	3081w	3050w	3050m	3161w	υ(C-H)
3449m	3449m	3431m	3449m	3450m	3436m	υ(O-H)

υ = stretching vibrations, π = out-of-plane bending vibrations, δ = in-plane bending or deformation, vs = very strong, s = strong, m = medium, w = weak, vw = very weak, frequencies in brackets represent split bands.

Appendix 2

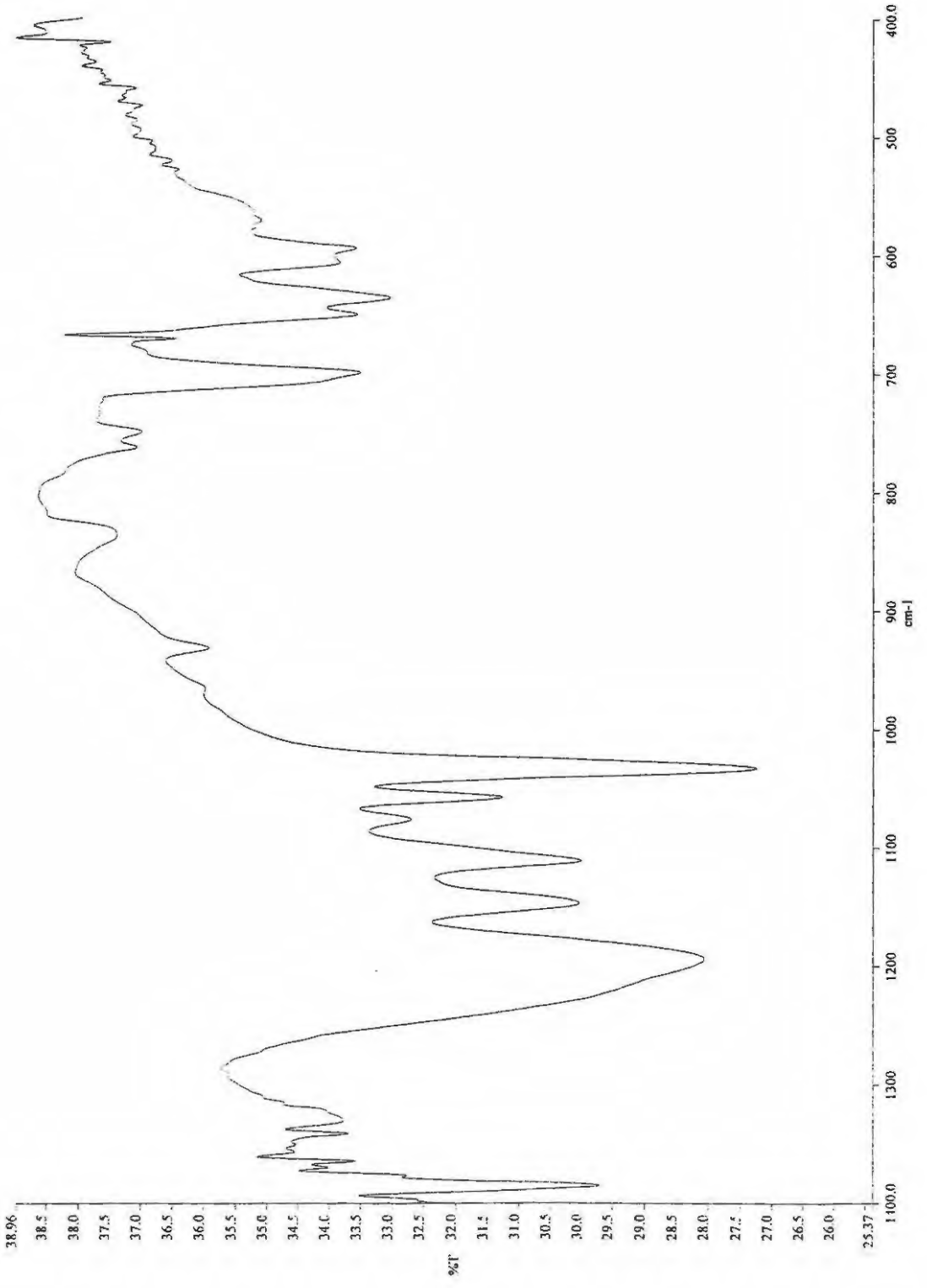

IR Spectra (KBr disks) $[Fe(II)TSPc]^{4-}$

Appendix 3

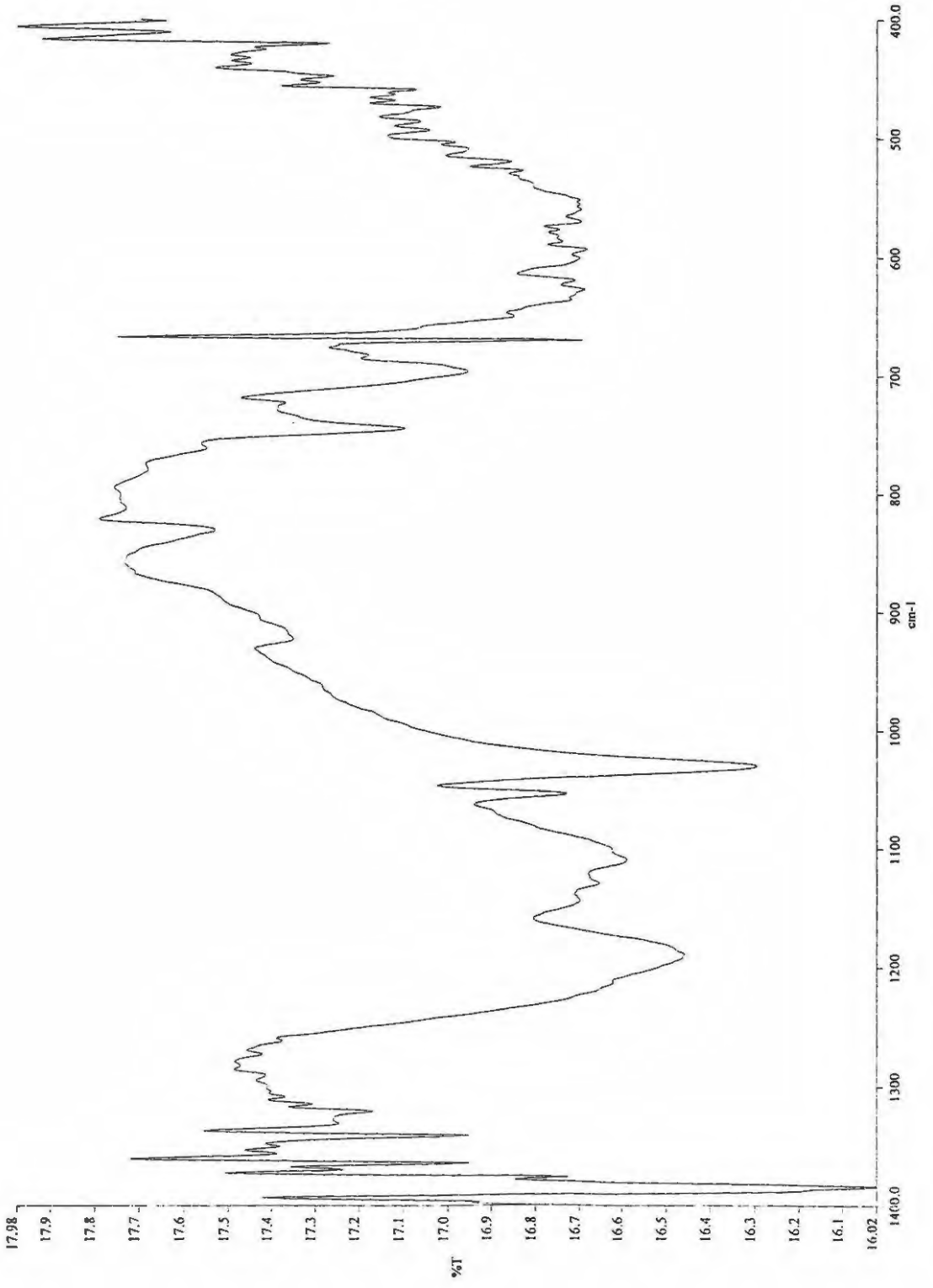

IR Spectra (KBr disks) $[Ni(II)TSPc]^{4-}$